

Library Declaration Form



University of Otago Library

Author's full name and year of birth: ANDRES ADOLFO NAVARRO NEWBALL,
(for cataloguing purposes) 9 April 1971

Title of thesis: Londra, A Dog Facial Animation Model

Degree: Doctor of Philosophy

Department: Department of Computer Science

Permanent Address: Computer Science Department, Pontificia Universidad Javeriana,
Cali, Colombia

I agree that this thesis may be consulted for research and study purposes and that reasonable quotation may be made from it, provided that proper acknowledgement of its use is made.

I consent to this thesis being copied in part or in whole for

- i) a library
- ii) an individual

at the discretion of the University of Otago.

Signature:

Date:

Londra, A Dog Facial Animation
Model

Andrés Adolfo Navarro Newball

a thesis submitted for the degree of
Doctor of Philosophy
at the University of Otago, Dunedin,
New Zealand.

31 May 2010

Abstract

Several human facial animation models have been developed in the last 30 years. In contrast, less attention has been given to animal facial models. Animal facial anatomical features are usually humanised, oversimplified, cartoonised or ignored.

With Londra, our dog facial animation model, we successfully synthesised dog facial expressions such as anger, affection, attention, fear, happiness, yawning and smelling without displaying anthropomorphic features. A preliminary validation suggested that most expressions were recognised consistently.

Our contributions include: a simplified model inspired by anatomy; a new bottom up form of the layered approach for the bone, muscle, complementary, skin and fur layers; a Dog Facial Action Coding System to synthesise the expressions; and the Tabulated Sphere Subsets to provide a fast way to approximate collisions between objects with constrained motion.

Acknowledgements

'Era ya para mí una necesidad tenerla constantemente a mi lado; no perder un solo instante de su existencia abandonada a mi amor ...', (Jorge Isaacs, 'María', 1867)

...To my beloved wife Victoria.

...To my pet Londra.

I would like to thank: my supervisors Professor Geoff Wyvill and Dr. Brendan McCane at the University of Otago for their guidance and patience. Dr. Edmond Prakash at the Manchester Metropolitan University for sharing his wisdom and making a dream come true. Drs. Jorge Estela, Camilo Rueda, Diego Linares, Julián Garcés and Padre Peláez S.J. at the Pontificia Universidad Javeriana for supporting this opportunity. The Universidad Javeriana, Cali; the University of Otago; Colfuturo, Colombia and the Manchester Metropolitan University for their financial and academic support. To my parents and to my siblings (CJ, GM, HE) for all their love and endless support. To my In-laws. To my previous supervisors Dr. Luis Múnera, Mr. Derek Wills, Mr. Alvaro Pachon and Professor Franco Roviello for helping me gain the required knowledge. To Charles Darwin for opening the door for this research. To Mr. Francisco Herrera and Mr. Diego Loaiza for taking care of my matters. To Mr. Danner for all his help. To Dr. Viant (Hull); Dr. Lee, Dr. Costen, Dr. Dancey, Mr. Longshaw and Mr. Topson (Manchester), Dr. Praticizzo (Siena); and Mr. Visser and Dr. Sealy (Dunedin). To my past pets. To the magical city of London. To all those friends. To all those gone. To all those inspiring. To God.

Contents

1	Introduction	1
1.1	Preamble	1
1.2	Motivation	2
1.3	Applications	4
1.4	Contributions	5
1.5	Limit of Scope	6
1.6	Publications and Conferences	8
2	Facial Animation	9
2.1	Overview	9
2.2	Discussion	14
3	Facial Expressions in Dogs	21
3.1	Darwin’s Observations	21
3.2	Video Observation	23
3.3	Facial Expressions in Artificial Pets	26
3.4	Discussion	26
4	Dog head anatomy overview	29
4.1	Anatomical Directions	29
4.2	Osteotomy	29
4.3	Teeth	33
4.4	Main articulations in the dog head	34
4.5	Jaw biomechanics	34
4.6	Miology	36
4.7	Ears	37
4.8	Eyes	38
4.9	Nose	40
4.10	Tongue	40
4.11	Discussion	41
5	Dog facial coding	43
5.1	Facial measurement systems	43
5.2	From FACS to DFACS	44
5.3	EMFACS	44
5.4	DFACS	44

5.5	Discussion	52
6	Efficient Mesh Generation Using Subdivision Surfaces	54
6.1	Overview	54
6.2	Triangular meshes	55
6.2.1	Data structures for triangular meshes	56
6.3	Subdivision surfaces	58
6.3.1	Subdivision techniques for triangular meshes	58
6.4	$\sqrt{3}$ subdivision using the Direct Edges data structure	60
6.4.1	Memory allocation	60
6.4.2	Assigning halfedges and counting	61
6.4.3	Splitting	64
6.4.4	Swapping faces.	64
6.4.5	Detecting boundaries and subdividable faces	65
6.4.6	Calculating a neighbourhood	65
6.5	Results	66
6.6	Discussion	67
7	Superquadrics: simplifying generalised cylinders	69
7.1	Generalised cylinders	69
7.2	Superquadrics: a solution with the same idea	70
7.2.1	Bending the superellipsoids	73
7.3	Discussion	74
8	Object Interaction Using Tabulated Spheres Subsets	75
8.1	Overview	75
8.2	Tabulated Spheres Subsets	76
8.2.1	Spheres generation	77
8.2.2	Colliding spheres search	78
8.2.3	Spheres' reduction and tabulation	79
8.3	Results	79
8.4	Discussion	80
9	System overview	83
9.1	Setting up	83
9.2	Processing	84
9.3	Output	85
9.4	Discussion	85
10	Bone layer	87
10.1	The rôle of the bone layer	87
10.1.1	Analysis	88
10.2	Importing the skull	89
10.3	The need for subdivision surfaces	90
10.4	Reshaping the Head	90
10.4.1	Applying Anatomical indices to the Skull	90

10.4.2	Evaluation	90
10.5	Jaw motion with TSSs	91
10.5.1	Evaluation	93
10.6	Head motion	95
10.7	Discussion	95
11	Muscle layer	97
11.1	Previous work	97
11.1.1	Muscles and cylinders	98
11.2	Muscles modelling with superquadrics	99
11.3	Discussion	101
12	Complementary layer	102
12.1	Tongue	102
12.1.1	Previous work	102
12.1.2	Analysis	103
12.1.3	A dog tongue model	104
12.1.4	Tongue motion with TSSs	107
12.2	Eyes	109
12.2.1	Previous work	109
12.2.2	Analysis	110
12.2.3	A dog eye model	111
12.3	Nose	111
12.3.1	Previous work	111
12.3.2	Analysis	113
12.3.3	A dog nose model	113
12.3.4	Nostril dilation	113
12.4	A note about the ears	114
12.5	Discussion	115
13	Skin layer	117
13.1	Previous work	117
13.1.1	Analysis	118
13.2	Skin generation	119
13.2.1	Interpolation	120
13.2.2	Bottom up generation of the skin	121
13.2.3	Lips	122
13.2.4	About feature point generation	124
13.3	Skin deformation	124
13.3.1	Keeping track of the original shape	127
13.3.2	Obtaining forces	127
13.3.3	Particle-particle interaction	128
13.3.4	Elasticity, viscosity and plasticity	131
13.3.5	Integration and stability	131
13.4	Muscles-skin interaction with TSSs	132
13.5	Regions	136

13.6	Thickness	136
13.7	Discussion	138
14	Fur layer	140
14.1	Previous work	140
14.1.1	Coat pattern for mammalian models	141
14.1.2	Fur	141
14.1.3	Analysis	143
14.2	Adding fur	143
14.3	Discussion	145
15	Validation	147
15.1	optical flow	147
15.2	Surveying	149
15.2.1	Session 1	150
15.2.2	Session 2	151
15.2.3	Session 3	153
15.2.4	Consolidated result	155
15.2.5	Changing the model	157
15.3	Visual comparison and sequence of events	159
15.4	Beyond real dog expressions	159
15.5	Model Performance	161
15.6	Discussion	162
16	Conclusions	165
	References	170
A	Artificial Pets	190
A.0.1	Tamagotchi (Allison (2006))	191
A.0.2	Cypet (Warren (2004))	191
A.0.3	Furry Paws (Furry Paws LLC (2007))	191
A.0.4	AIBO (Allison (2006))	193
A.0.5	HOMIE (Kriglstein and Wallner (2005))	193
A.0.6	eMuu (Bartneck and Okada (2001a,b))	194
A.0.7	Alpha wolves (Tomlinson <i>et al.</i> (2002))	194
A.0.8	PETZ (Stern <i>et al.</i> (1998); Stern (1999))	194
A.0.9	Nintendogs (Wixon (2006); Wikimedia Foundation (2009h))	195
B	Special Effects	196
C	Original Parke and Waters parameters	198
D	Additional Observations	201

E	Subdivision algorithms	206
E.1	Step1: finding new vertices	206
E.2	Step2: flipping edges	207
E.3	Step 3: old vertices re positioning	207
E.4	Neighbourhood calculation	207
F	Halfedge elements implementation	208
G	The 3DS file format	209
H	Applying subdivision surfaces to Londra’s skull.	212
I	Barycentric coordinates	214
J	Survey format	217
K	Videos	219
L	Glossary	220

List of Tables

2.1	Brief story of digital facial animation	10
4.1	Dog classification according to head osteotomy	31
5.1	EMFACS	45
5.2	Universal human expression, from Noh and Neumann (1998) p.4	45
5.3	DFACS	47
5.4	Extending AUs to body postures	51
5.5	Expressions in Londra. A preceding '2' refers to the counter AU	51
6.1	Swapping face number F and face number M. Half edge number obtained according to (6.1)	65
13.1	Tests and spheres per muscle pair per time step	135
13.2	Total tests per AU	136
13.3	Basic operations required	136
15.1	Results from session 1. Rows: participants' choice. Columns: video groups. Columns' sub-indices: expression displayed (e.g. An = anger). The number of dog people is indicated in parentheses.	152
15.2	Results from session 2. Rows: participants' choice. Columns: video groups. Columns' sub-indices: expression displayed (e.g. An = anger). The number of dog people is indicated in parentheses.	154
15.3	Results from session 3. Rows: participants' choice. Columns: video groups. Columns' sub-indices: expression displayed (e.g. An = anger). The number of dog people is indicated in parentheses.	156
15.4	Final result. Rows: participants' choice. Columns: video groups. Columns' sub-indices: expression displayed (e.g. An = anger). The number of dog people is indicated in parentheses.	158
16.1	Animation parameters for Londra	168
C.1	Parke's Facial Animation Parameters	199
C.2	Water's muscle based parameterisation.	200
F.1	Halfedge elements implementation	208
G.1	Fields of a 3DS chunk	209
G.2	Important 3DS chunks	211

I.1	Barycentric coordinates for the vertices in a triangle	214
J.1	Dog expression survey	218

List of Figures

1.1	Expressions through time. A) Senufo mask (African Art Museum (2009)). B) Noh theatre mask (Wikimedia Foundation (2009i)). C) Tumatauenga (New Zealand’s National Education Monitoring (2009)). D) Faunus (Wikimedia Foundation (2009e)). E) Quetzalcoatl (Wikimedia Foundation (2009k)). F) Horus (Wikimedia Foundation (2009g)). G) Caiman man (Yurany (2008)). H) Peter Rabbit (Wikimedia Foundation (2009a)). I) Felix the cat (Wikimedia Foundation (2009f)). J) Rin Rin the tadpole (Wikimedia Foundation (2009l)). K) Donald Duck (Wikimedia Foundation (2009m)). L) Puss ’n Boots (Dreamworks (2009)).	3
1.2	Different dog shapes. A) Greyhound (FreeDigitalPhotos.net (2009)). B) The real Londra. Staffordshire Terrier. C) Boxer (Wikimedia Foundation (2009b)).	7
2.1	Bottom up layered approach.	16
3.1	Occurrences of face related organs in expressions described by Darwin .	22
3.2	Hostile intention. Drawn for Darwin by Briton Riviere	22
3.3	Nostril movement. Appendix K, ONostril.avi	23
3.4	Attention. Appendix K, OAttention.avi	24
3.5	Fear. Appendix K, OFear.avi	25
3.6	Anger. Appendix K, OAnger.avi	25
3.7	Affection. Appendix K, OAffection.avi	26
3.8	Facial Organs in artificial Pets	27
3.9	Artificial Pet Features	27
4.1	Anatomical directions	30
4.2	Dog head osteotomy	30
4.3	Anatomical proportions in the head. A)Length. B)Breadth. C)In red the distance between nuchal crest and the frontonasal suture. In green the distance between the frontonasal suture and the nasal notch. D) Brachycephalic dog (Sisson <i>et al.</i> (1975), p. 1543).	32
4.4	Occlusion in dogs. The main contact occurs between superior premolar 4 and inferior molar 1.	35
4.5	Joints and muscles. A)Joint to the first vertebra. B)Dog miology. . . .	37
4.6	Ear anatomy. Adapted from Sisson <i>et al.</i> (1975), p. 1769.	38

4.7	Anatomy of subsidiary organs. A)Eyes and nose. B)Eyelids. C)Tongue. D)Human tongue (adapted from Wikimedia Foundation (2009n)). Here, some important lines of muscular actions are highlighted. Genioglossus (red line); styloglossus (yellow line); hyoglossus (green line).	39
5.1	Coding expressions. A)Human facial muscles (Wikimedia Foundation (2009d)). B)Anger in dogs.	46
5.2	AUs in DFACS. Refer to Appendix K for videos.	48
5.3	Expressions in Londra. Anger and Affection I. Refer to Appendix K for videos.	49
5.4	Expressions in Londra. Affection II, Attention, Fear, Happiness. Refer to Appendix K for videos.	50
5.5	Expressions in Londra. Yawn and Smell. Refer to Appendix K for videos.	51
5.6	Displaying Londra. A) Dialog box for AUs, expressions and visualisation options. B) Puppet controls.	53
6.1	Subdivision with the Direct Edges data structure. A) Non subdivided face and edges. B) New vertices at boundary. C) Subdividing a regular face. D) Subdividing a boundary face in odd step. E)Flipping edges. F)Neighbourhood. G) Original mesh. H) Middle point. I) Split triangles. J) Flipping edges	57
6.2	Opposite halfedges O_0 , O_1 and O_2 for halfedges 0, 1 and 2 in face G	63
6.3	Subdivision of arbitrary surfaces. A) Mesh with boundaries and 1 non-subdividable face (7 levels). B) Limit and control surface of a cube (4 Levels). C) Big plane with boundaries (2 levels). D) Spaceship (2 levels). E) Element increase in $\sqrt{3}$ subdivision. F) Subdivision dialog box.	67
7.1	Generalised cylinders. A) Orientation of the cross section. B)Cylinder along a path. C)Problematic case.	71
7.2	Superquadrics. A) Superellipsoids with different squaredness and resolution. B)Supertoroid. C)Bent superellipsoids (the squaredness factor of the leftmost one has been changed producing sharper edges)	72
8.1	TSSs. A)B)C)D) n is the number of spheres in a , m is the number of spheres in b . Note that TSSs perform T_{TSS} tests which is lower than $m \times n$. Also, $M_{ss} \subset M_{sm} \subset M_{sc} \subset M_s$. A) a and b approximated with volumetric spheres. B) The non colliding spheres are removed. C) The typical subset of spheres found (a few redundancies remain). D) Minimal subset with no redundancies. E) a and b approximated with surface spheres.	77
8.2	Spheres generation. A) The growth of a line between points m_i and m_{i+1} can be obtained from the parametric equation of a line in 3D space $m_i + T_i \times (m_{i+1} - m_i)$ by varying T_i by some δt . B) Growing radius (searching for the second point). C) Growing radius (searching for the third point). D) Growing radius (searching for the fourth point).	78

8.3	Parameters in sphere generation. A) Generating spheres for narrow regions (spheres tend to group in the edges). B) Generating spheres for wide regions (more spheres fill the mesh). C) Mesh distortion. D) Dialog box for sphere generation. E) Dialog box for colliding spheres search and spheres reduction.	81
9.1	Londra's system overview. Dotted lines are optional depending on the chosen task or expression.	86
10.1	Londra's bone layer. A) Approximation to spheres. Mandible: 812 spheres, skull: 1158 Spheres. B) Reduced subset. Mandible: 22 spheres, skull: 9 spheres. C) Skull and Mandible, imported from Turbo Squid, Inc (2008). D) Dialog box for reshaping.	89
10.2	Reshaping the skull. The red dotted line crosses zygomatic and the fronto nasal suture. The region below the line belongs to the snout (real skulls from Will (2008)). A) indices FI , CI and CI , obtained as width / height (represented in the blue lines) . B) Brachycephalic. C) Dolichocephalic.	92
10.3	Evaluating TSSs in the bone layer. A) Problematic region. B) Two levels of a sphere tree. C) Tight sphere tree. D) The collision region is $(T-\tau)$, assume that the skull has n spheres and the mandible m . E) Performance (tests) of a sphere tree versus that of TSSs.	94
11.1	Muscle layer. A) Mirroring. B) Dialog box for muscle construction. C) Muscles in the muscle layer. D) Fibres. E) Bone and muscle layer. . . .	100
12.1	Tongue model. A) Regions and skeleton. B) Common expressive shapes . C) Expansion up to the middle. MT is the maximum allowable expansion for the tip. Interacting spheres are emphasised. D) Expansion up to the back. $MTM - MT$ is the maximum allowable expansion for the middle. Interacting spheres are emphasised.	105
12.2	Tongue volume and mesh. A) Original dimensions in a tongue region $A \times B \times C$ with a radius R . B) Changing dimensions and preserving volume. C) Generating vertices. D) Alternative for tongue motion. $E1$ and $E2$ limit expansion for tip and middle regions. E) Vertices in the tongue. F) Textured triangulation.	106
12.3	Bending the tongue. A) Bending the tip and the middle. Interacting spheres are emphasised. B) Bending the tip. Interacting spheres are emphasised. C) Rolling the tongue. Interacting spheres are emphasised. D) Unnatural bend. E) Enhanced bend.	107
12.4	Eye and nose models. A) Layered eye model base on spheres. B) Gaze. D is the distance to a point P . α is the orientation. C) Londra's eyes. D) Dilating Nostrils. E) Nose before and after nostril dilation. F) Nose and the complementary layer. G) Bone, muscle and complementary layers.	112
12.5	Complementary layer GUI and ear markers. A) Dialog box for tongue model. B) Dialog box for eyes model. C) Dialog box for ear markers. D) Ear markers.	114

13.1	Skin interpolation. A) A big mesh inscribes the underlying anatomy. B) Characteristic points in the facial mesh. C) Blue points are counterparts of yellow characteristic points. D) Triangulation of characteristic points in the facial mesh. Remaining vertices are interpolated with barycentric coordinates. E) Facial mesh shrunk to make characteristic points coincide with their counterparts. Remaining vertices are interpolated with barycentric coordinates. F) Interpolated skin.	121
13.2	Skin generation. A) Feature point generation. B) 2D triangulation. C) Inflating the skin. D) Deflating the skin. E) Skin with lips. F) Bone, muscle, complementary and skin layers.	123
13.3	Feature points generation. A) Generating feature points at a distance $R + d$ from the centre of a sphere at an angle α . R is the radius of the sphere. B) Generating points along the main axis of a sphere. $D_0 \neq D_1 \neq D_2$ are distances from the main axis. C) Dialog box for skin generation.	125
13.4	Forces calculation. A) Instant forces applied by the muscles. B) Reaction force. C) Reaction force from neighbours.	129
13.5	An elastic piece of skin. Vertices have spheres associated. A) 5×5 patch with the back region under the action of gravity. B) 13×13 patch under the action of an instant force applied by the superquadric muscle. Some regions are under the action of gravity. C) 13×13 patch under the action of an instant force. Related spheres are displayed. D) Deformation caused by an instant force in the control mesh. E) Smoothed limit surface obtained from the control mesh in Figure <i>D</i> . F) Lower resolution deformation (Appendix K, LowDeform.avi). G) Full smoothing of deformation. H) Localised smoothing of deformation. . .	130
13.6	Muscle-skin interaction with TSSs. A) Skin surface approximated with 1426 spheres. B) Frontalis approximated with 280 spheres. C) 70 spheres chosen in the skin. D) 190 chosen spheres in the Frontalis. E) $\sqrt{3}$ smoothing localised on the region affected by the Frontalis. F) Sample deformation show some wrinkles between the ears. G) Final selection of spheres in Londra's skin. H) Final selection of spheres in Londra's muscles.	134
13.7	TSSs generation and regions. A) Dialog box for muscle-skin TSSs generation. The numbers shown are related to the parameters of the superellipsoids representing the muscles. B) Skin regions.	137
14.1	Fur Approximation. A) Fur model. B) Paralel displaced layers approximating fur. C) Opacity maps. D) Shadow approximation.	144
14.2	Londra's fur. A) Different texture maps. B) Finally, all layers. C) Fur orientation. D) Longer fur. E) Longer fur, fewer layers.	145
14.3	Fur direction. A) Real Londra's fur orientation. B) Approximating fur orientation according to real Londra. C) Fur oriented in the direction of the normal.	146

15.1	optical flow in facial expression. A) optical flow in HFAMs (Prakash (2009), Slide 24). B) optical flow in real Londra (Attention). C) optical flow in virtual Londra (Attention).	149
15.2	optical flow around nostrils. Left, real Londra. Right, virtual Londra. .	150
15.3	Similarities and differences between real and virtual Londra. A) Lateral view. B) Jaw Opening. C) Back view. D) Wrinkles between the ears. E) Expression of fear. F) Lips contraction. G) Tongue and nose.	160
15.4	A) Exaggerating AUs. B) A random unknown expression.	161
15.5	Frames per second (FPS) Vs. number of collision tests. SL= subdivision level.	162
16.1	Left, Londra as a puppet. Right, rendering with Blender.	169
A.1	artificial Pets. A) Tamagotchy (Allison (2006), p. 171). B) Tamagotchy personalities (Allison (2006), p. 173). C) Cypet (Warren (2004)). D) Furry Paws (Furry Paws LLC (2007)). E) AIBO (Friedman <i>et al.</i> (2003), p. 274). F) HOMIE (Kriglstein and Wallner (2005), p. 2097). G) eMuu (Bartneck and Okada (2001b), p. 1). H) Alpha wolves (Tomlinson <i>et al.</i> (2002), p. 7). I) PETZ (Wikimedia Foundation (2009j)). J) Nintendogs (Wikimedia Foundation (2009h)).	192
D.1	Nostril movement. Appendix K, ONostril1.avi	202
D.2	Attention. A) Common attention (Appendix K, OAttention1a.avi). B) Attention with ears (Appendix K, OAttention1b.avi). C) Attention with previous lateral head motion (Appendix K, OAttention1c.avi)	203
D.3	Fear. A) forward - backward ear and open close mouth patterns (Appendix K, OFear.avi). B) Light fear (Appendix K, OFear1.avi)	204
D.4	Another form of anger. (Appendix K, OAnger1.avi)	205
H.1	Subdivision of the skull in Londra. A) B) C) Levels 0, 1, 2 of subdivision for the simplest control mesh. D) E) F) Levels 0, 1, 2 of subdivision for the intermediate control mesh. G) H) I) Levels 0, 1, 2 of subdivision for the original control mesh.	213
I.1	Barycentric coordinates.	215

Chapter 1

Introduction

1.1 Preamble

Over the ages, human beings have been charmed by expressions. From ancient rituals, through theatre to animated movies, expressions have been used to convey information. In particular, human facial expressions have been present in all kinds of rites. For example, Figure 1.1A shows the African Senufo mask representing tranquillity. Figure 1.1B shows a Japanese Noh theatre mask which changes its expression with a tilt of the head. Figure 1.1C shows the Maori god of war, Tumatauenga, with a facial expression which is still common in the Haka dance. Probably because of the desire to give animal supernatural powers to gods and monsters, human expressions have been animalised. Indeed, anthropomorphic creatures are as ancient as human kind. For example, Figure 1.1D shows Faunus, the roman version of Pan, the Greek god of nature which mixes a human with a goat. Figure 1.1E shows Quetzalcoatl a humanised serpent deity present in the Aztec mythology. Figure 1.1F shows Horus, the Egyptian god of war and the sky who is a mixture of human and falcon. Figure 1.1G shows the Colombian Caiman man, a legendary creature half man, half alligator which chases women in the Magdalena river. These kind of supernatural powers seem to have been transferred to modern super hero comic art in the same anthropomorphic manner. Also, probably because of the desire to communicate and understand other creatures, animals have been given human features and expressions since Aesope's fables. For example, Figure 1.1H shows Beatrix Potter's Peter Rabbit and his mother in a very human situation. Figure 1.1I shows Otto Mesmer's Felix the cat waking angry. Figure 1.1J shows Rafael Pombo's Rin Rin the tadpole in a festive mood. Figure 1.1K shows an angry Walt Disney's Donald Duck. Figure 1.1L shows the more recent digital Puss 'n Boots displaying

tenderness.

From ancient rituals to the present, the interest in expressions goes on supported by technology. For example today, expressive artificial pets are a whole technological trend (Appendix A) and facial animation is an area of relevance to computer graphics and has gained interest in other fields such as psychology, medicine and art. Computer animated faces have a wide range of application which include video conferencing, perception research, tele-presence, movies and games. Characters such as Puss 'n Boots and the digital version of Scooby Doo represent the state of the art in animated animals. However, history shows an interest mainly in human expressions, human animalised expressions and humanised animal expression. Pure animal expressions have been ignored. Pioneer works by Disney are the result of deep animal observation to produce a humanised cartoon. At the same time, understanding of the anatomy and the underlying mechanism of expression were rarely done before the digital era. Charles Darwin (1890) was the first to formally approach the problem of real animal expression. In his book 'The Expressions of Emotions in Man and Animals', he describes several animal and human expressions and uses his observations to support his evolution theory claiming that some expressions are inherited. Later, the introduction of the Facial Action Coding System (FACS) by Ekman and Friesen (1978) contributed to the understanding on how human expressions are produced. The FACS has been widely used in anatomically based digital human facial animation models displaying expressions. In contrast, even with the long and valuable relationship of human and dogs and the long historical human fascination with expressions, models of real dog expression do not exist. Moreover, we have not found evidence of animal models for real anatomically inspired animal facial expressions.

1.2 Motivation

Londra comes from the Italian name for London and owes its name to my pet dog, named after that fascinating city. Since the first day we got Londra, we were fascinated by her speechless communication ability. We managed to learn her 'I want to lay on your bed', 'I want to play the ball' and 'I do not care' faces and postures. This, plus the desire to better understand her expressions and how they are produced; the fact that we miss her in the distance and; the excellent descriptions from Darwin (1890) were an initial motivation to propose Londra, our model for a dog facial animation system. Other motivators were:



Figure 1.1: Expressions through time. A) Senufo mask (African Art Museum (2009)). B) Noh theatre mask (Wikimedia Foundation (2009i)). C) Tumatauenga (New Zealand's National Education Monitoring (2009)). D) Faunus (Wikimedia Foundation (2009e)). E) Quetzalcoatl (Wikimedia Foundation (2009k)). F) Horus (Wikimedia Foundation (2009g)). G) Caiman man (Yurany (2008)). H) Peter Rabbit (Wikimedia Foundation (2009a)). I) Felix the cat (Wikimedia Foundation (2009f)). J) Rin Rin the tadpole (Wikimedia Foundation (2009l)). K) Donald Duck (Wikimedia Foundation (2009m)). L) Puss 'n Boots (Dreamworks (2009)).

- Most existing systems attempt to give human-like expressions to animals. Indeed, digital facial animation continues to focus on human or humanised facial expressions. This is probably because of the desire to create human like creatures and the scarcity of accurate animal data. The literature on artificial pets and facial animation shows only a few works using anatomically based animal facial simulation. We found that Sagar (2006) maps motion capture data from a human actor to an expression space, a Gorilla specific superset of FACS. However, muscle motion relies on the captured data set. Moreover, this techniques takes advantage of the anatomical similarities between humans and gorillas but is not adequate for other creatures such as Londra.
- There is not a particular focus on the face in digital animal animation. For example, in video games such as Nintendogs from Nintendo (2005), dog faces are oversimplified.
- Newer trends such as procedural animation ignore the underlying anatomy and the way facial expressions are produced in reality. While realistic results are produced with this technique, these are limited to the captured sets and are not suitable for animals.

Londra is the first documented dog facial animation system which is anatomically inspired. It required the use and creation of advanced computer graphic techniques; simulation; geometric modelling; identification of animation parameters; the development of a GUI and the development of a computational workflow and an architecture to support the system.

1.3 Applications

In animals, applications are similar to those of human facial animation systems. Additionally, there are potential applications such as:

- A full virtual pet system or a synthetic dog actor in a virtual world.
- Virtual biology. In particular, dog zoology and anatomy studies.
- Girl's video games.

- Dog psychology. For example, communication between dogs and humans lacks returning speech from the animal. Dogs communicate with barking, corporal postures and facial expression. Dogs' facial expression understanding could enhance pet-human communication.
- The Londra model could be expanded to other real or non real non human creatures.
- Techniques proposed could be either used in human facial animation systems or included in other kind of environments.
- A dog facial animation plug-in.

1.4 Contributions

Londra is the first documented dog facial animation system which is anatomically inspired. It uses a layered model intuitively following the layered nature of anatomy. We followed a bottom up approach. Taking the skull as a base, we placed muscles and generated skin and fur. We complemented the model with subsidiary eyes, nose and tongue. Our main contributions are (Navarro Newball *et al.* (2009b)):

- We demonstrate that the dog face plays an important rôle in expression.
- A Dog Facial Action Coding System (DFACS) adapted from a human FACS and anatomy. We identified anatomical features which provide a method of parameterisation and we propose an anatomically based coding system to organise these parameters.
- A new muscle model based on geometry and super quadrics.
- New tongue, eye and nose models.
- A semi automatic iterative skin generation algorithm capable of producing ears and holes based on anatomical features. This method does not require pre-existing skin data.
- An efficient implementation of $\sqrt{3}$ subdivision surfaces based on counting used to smooth the skin.

- The Tabulated Spheres Subsets (TSSs) technique which is used for jaw motion, muscle-skin interaction and tongue motion.
- Novel use of spheres for model construction and working. Approximations to spheres such as Longshaw *et al.* (2009) have been used before in the field of Discrete Element Modelling. Here, we use such approximations to define geometrical interaction among layers.
- A layered facial model of a dog head which represents and manipulates expression based on the geometrical characteristics of the skin, tissue and muscles and considers some physical characteristics of the skin. Our control system is somewhere in the middle between parametric and physically based models. Here, animation of the model is mainly guided by an approximation of the geometry of the anatomical components, but simplified elastic properties are included.
- Successful use of the pure bottom up approach, quite uncommon in facial models.

In the process of building Londra, we faced some interesting challenges such as (Navarro Newball *et al.* (2009b)):

- Understanding previous human facial animation systems in order to follow previous approaches in a new animal context while introducing new techniques.
- Anatomical differences between humans and dogs. In dogs, elements such as ears, nose and tongue play a more important rôle, while eyebrows are not visible and colouration changes are not important.
- Scarcity of 3D digitised data, anatomical and biometric information for dogs. There was no such thing as FACS for dogs; we did not find statistical information about the thickness of different dog's skin regions and we found only a few basic studies on dog jaw motion and head proportions.

1.5 Limit of Scope

Dogs come in many breeds and shapes. There are different types of snout, fur or ears. Figure 1.2A shows a dog with long head. Figure 1.2B shows the real Londra, a dog with average proportions. Figure 1.2C shows a dog with short head. While the anatomical underlying mechanism in all of them is similar, the automatic generation of a different

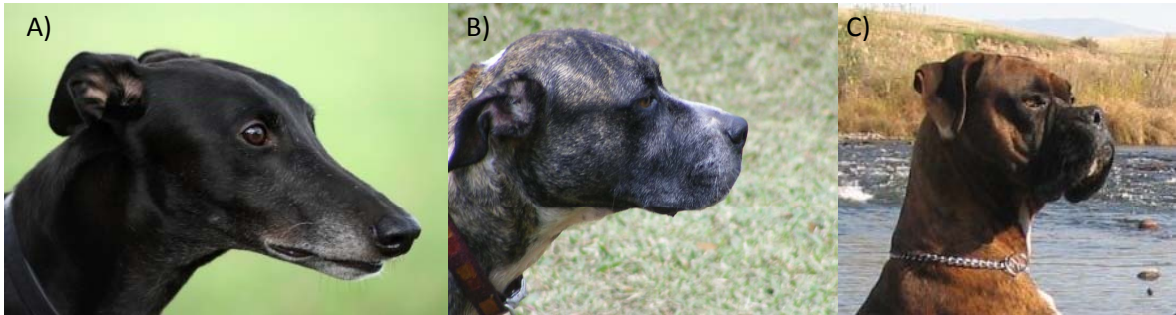


Figure 1.2: Different dog shapes. A) Greyhound (FreeDigitalPhotos.net (2009)). B) The real Londra. Staffordshire Terrier. C) Boxer (Wikimedia Foundation (2009b)).

shape proved to be difficult and requires further research. In order to have more breeds, we would require more source skull meshes or to study dog anatomy in collaboration with zoology in order to find good conformational parameters. This is out of the scope of this project. Actually, it is possible to reshape Londra's base skull. However, correct anatomical proportions are not maintained leading to cartoonish results. For this reason, Londra displays only one dog similar to 1.2B.

Darwin (1890) provides evidence of the importance of the face as an expressive organ in dogs. For example, he emphasises that the whole appearance of the face is altered when a particular dog changes the position of its ears and, this causes the movement of many facial muscles. Also, he describes the 'hot-house' face of disappointment of a dog when it perceived that the master (Darwin himself) was going to end a nice walk in order to do research in the hot house. Darwin also describes the important rôle that the body plays in dog expression. In Londra, facial expressions are not complemented with body postures. This makes some expressions more difficult to understand. Including a body is out of the scope of this project. However, we explain how the body could be included in the system.

The complexity related to replicating every anatomical component in a digital facial model, makes simplification a must. Facial animation systems use the organs more relevant in facial expression. In Londra, the skin is idealised as a surface. The skin's multiple layers and fat are simplified as the threshold distance between the skin and the underlying anatomy. Finally, in Londra ears are assumed to be cropped ears. The dog is assumed to have short fur. Saliva and internal texturing of the mouth are not present.

Londra is neither a full artificial pet (Appendix A) nor a special effect (Appendix

B). Londra is intended neither for breeding nor for an emotional connection with the user. However, the underlying developments may be useful for a full virtual pet system. It contains an advanced expression mechanism. It is inspired by a natural coding and anatomy. Unlike many pets, Londra does not rely on texturing and humanisation of features. There is a strong relationship among special effects, animation and character development (Falk *et al.* (2004)). In this context, Londra is related to special effects. Londra is mostly the development of a meaningful expressive character.

1.6 Publications and Conferences

Londra's advances and results have been published and/or presented in the following journals or events:

- Navarro Newball *et al.* (2008b) New Zealand Computer Science Research Student Conference, NZCSRSC 2008 Proceedings. This paper describe Londra's project proposal and includes literature review in the field of Facial Animation.
- Navarro Newball *et al.* (2008a) Engineering Faculty journal from the ICESI University in Colombia. Here, our implementation and use of subdivision surfaces is explained. This is our second most important paper to date.
- Navarro Newball *et al.* (2009c) Theory and Practice of Computer Graphics: Eurographics UK chapter proceedings 2009. Our most important paper and presentation to date. Here, we introduce the Tabulate Spheres Subsets concept to the world.
- Navarro Newball *et al.* (2009a) British Machine Vision Association and Society for Pattern Recognition. Facial Analysis and Animation Symposium 09 proceedings. Here we discuss facial animation in dogs.
- Navarro Newball *et al.* (2009b) Workshop on Face Behaviour and Interaction (FBI 2009) Proceedings. Here we present Londra's challenges and architecture.

Additionally, during my PhD study period, I was invited as a visiting research fellow in the Computing and Mathematics Department at the Manchester Metropolitan University, UK. There, I had the chance to get insight on Face Alive (Zhang *et al.* (2004a)) among other important tasks.

Chapter 2

Facial Animation

In section 2.1 we present our summary of facial animation history, techniques and methods. In section 2.2 we discuss different facial animation approaches and show how they are different from Londra. Also, we show how we discarded performance driven and purely geometric models because they ignore most of the anatomy.

2.1 Overview

Note: some portions of this section were taken from my own published work at Navarro Newball *et al.* (2008b)

Animation aims to create the illusion of life for artificial characters. From the works of Darwin (1890) to the present, facial expressions have been an important research field. Particularly, digital facial animation techniques have been approached during the last 40 years (Haber and Terzopoulos (2004); Terzopoulos *et al.* (1997)). During the 70s, work by Parke (1974) displayed the first parameterised human faces and Ekman and Friesen (1978) developed the FACS to describe expressions. During the 80s, Platt and Badler (1981) developed the first human muscle based model. Lately, digital film production has been the birthplace for many interesting characters such as the expressive Puss 'n Boots from Shrek (Falk *et al.* (2004)). Table 2.1 shows a brief history of digital facial animation.

Facial animation has been addressed in different ways such as models based on interpolation, parameterised models, pseudo-muscle models, physically based models, layered models and performance driven models. A well constructed model should display typical expressions (e.g. anger, fear, surprise, disgust, happiness, sadness). Expressions are physiological responses which are reflected in muscle tension affecting

Table 2.1: Brief story of digital facial animation

Year	Event	Author
1971	2D Faces	Chernoff (1973)
1972	3D facial animation	Parke (1972)
1973	Interactive line drawn faces	Gillenson (1974)
1974	Parameterized facial model	Parke (1972)
1978	FACS	Ekman and Friesen (1978)
1981	Physically based muscle controlled face	Platt and Badler (1981)
1984	Facial caricature	Brennan (1984)
1985	Facial expressions and speech animation	Lachapelle <i>et al.</i> (1985)
1987	New muscle model	Waters (1987)
1987	Automatic speech synchronization	Lewis and Parke (1987)
1988	Abstract muscle action model	Magenat-Thalmann <i>et al.</i> (1988)
1988	Animated speech	Hill <i>et al.</i> (1988)
1990	Performance-driven facial animation	Williams (1990)
1995	Toy Story	Henne and Hickel (1996)
1998	Subdivision surfaces in character animation	DeRose <i>et al.</i> (1998)
2001	Enhanced speech with dynamic phonemes	King (2001)
2004	Non linear multi layer model	Zhang <i>et al.</i> (2004b)
2004	Shrek	Falk <i>et al.</i> (2004)
2005	Universal capture of faces	Borshukov <i>et al.</i> (2005)
2008	Benjamin Button: realistic illumination	Caulkin (2009)
2010	Alice in Wonderland: mostly humanised, but shows some real animal expression. Probably no underlying anatomy	Mouroux (2010)
2010	Londra: real animal expressions	Navarro Newball <i>et al.</i> (2009b)

the display of the face (Haber and Terzopoulos (2004)). Sometimes, due to their complexity, regions such as the mouth and the tongue are considered separately from the face or oversimplified (Simmons *et al.* (2002); Noh and Neumann (1998)). Facial modelling requires understanding of the face anatomy. The more realism required, the more precisely the anatomy is simulated. In the simplest case, knowledge about the shape structure and position and interaction of facial components is required (Haber and Terzopoulos (2004)). Performance based techniques rely on motion capture. They are a trend in the entertainment industry, but are limited to the captured data sets, ignore most of the anatomy and are usually costly. Other approaches recreate several anatomical components but rely on a more complex model. However, if a model flexible enough is created, then, it can produce an endless range of expressions.

The creation of models suitable for facial animation is a difficult task. The idea is finding a method to capture the facial geometry and represent it in a generic topological facial mesh that can be adjusted according to the data obtained from digitalisation, drawing or image processing. Sources of geometric data go from graph paper and direct surface measurement to the use of 3D design packages and 3D laser scans. Scanning requires the subject to stay static for a reasonable period of time and motion capture technologies may produce inaccuracies. Modelling primitives go from polygonal surfaces to subdivision surfaces (Haber and Terzopoulos (2004)). An explanation of some facial model construction techniques follows (Noh and Neumann (1998)):

- Bilinear interpolation: Assumes that a large variety of faces can be represented from variations of a single topology previously created.
- Radial basis functions: Facial shapes are closely approximated or interpolated from smooth hyper-surfaces.
- Laser scanning and stereo images: Acquire detailed geometry and fine textures. However, often miss occluded regions and perimeter artefacts must be touched up by hand.
- Anthropometry: For applications where absolute appearance is not important and facial variations are desirable. In these systems, quality depends on the quantity of input samples. For example, in Zhang and Prakash (2009) the system learnt a facial model from 3D scans using principal component analysis. Then, the example meshes are parameterised into a measurement space using anthropometric measurements. This information is used to interpolate new face shapes in real time.

Control systems specify how an object is animated. They can be geometric, physical or behavioural (O'Brien *et al.* (2000); Thalmann and Thalmann (2002)). The dynamics of motion (temporal domain) deals with feature point coordinates, muscle contractions and action units. Then, surface deformation (spatial domain) deals with high resolution mesh vertices displacement, wrinkles generation and, may be solved statically at each moment (Haber and Terzopoulos (2004)). An explanation of the basic control systems follows:

- Geometric: Replicate traditional film production and use key framing techniques which consist of interpolating frames between key frames. They go from shape interpolation to deformable facial rigs (Haber and Terzopoulos (2004)).
- Physical: Physically based models were created for representing and manipulating expressions based on the physical characteristics of skin tissue and muscles. They can be used as a base for models such as the layered one and can be approached in several ways such as mass-spring methods, vector approaches and finite element methods. In mass-spring methods an elastic spring mesh which models the skin is used to propagate muscle forces. In vector approaches motion fields in delineated regions of influence are used to deform the facial mesh. In finite element methods the physics is approximated through a numerical approach (Noh and Neumann (1998)).
- Behavioural: They specify motion in terms of character's behaviour. They are based on the way humans or animals act. These systems are less formalised than the other two. Here, actions can be produced from the connection of the character's behaviour and perception.

Some facial animation control technologies are shape interpolation, direct parameterisation, muscle based parameterisation, viseme level parameterisation, dynamic simulation, facial rigs. The aim is to have a scripted or interactive control of the interpolation coefficients, parameter values, dynamic forces and facial rig handles. All facial control systems can be seen as parameterisations where the functional mapping consists of interpolations, affine transformations and generative procedures. Here, expressive parameters are higher level parameters which allow specifications and control of expressions. Conformational parameters are lower level parameters which are implemented with surface control points and alter face attributes (Haber and Terzopoulos (2004)). An explanation of some control technologies follows:

- Model-based: Match feature points describing a target face by deforming the geometry of a generic face. It can be done with an interpolation function (Simmons *et al.* (2002); Noh and Neumann (1998)).
- Interpolation: Specifies smooth motion between two key-frames at extreme positions, over a normalized time interval. It is restricted to some facial configurations (Noh and Neumann (1998)).
- Parameterisation: Direct parameterisation was developed for performing facial animation using a set of control parameters to manipulate local regions. It specifies any possible face and expression by a combination of independent parameter values. Often, the parameter set depends on its topology and may not be general. It can be enhanced if conformational parameters are used and positional and scale values included. In muscle based parameterisations, the face is controlled by parameter functions which emulate or simulate muscle actions. Appendix C shows the original parameters defined by Parke and Water's muscle based parameterisation.
- Layered models: Layered models represent an anatomical structure with several connected mesh layers (e.g. extend a physically based structure into several connected mesh layers). Usually, they contain a skeleton layer, intermediate layers simulating the physical behaviour of muscles, bones, fat and tissue and, a skin layer. Motions or expressions are produced by the activation of muscles. Here, changes in the underlying muscles deform the skin (Simmons *et al.* (2002); Noh and Neumann (1998)). A layered model itself can be complex and require high processing depending on how the layers are modelled (Simmons *et al.* (2002); Noh and Neumann (1998); Thalmann (1996)).
- Learning based: Measures movement of real faces reproducing only the shape and ignoring underlying mechanisms. A face model is derived from a set of 3D face models which are transformed in texture and shape to produce a vector representation (Haber and Terzopoulos (2004); Noh and Neumann (1998); Blanz and Vetter (1999)).
- Performance driven: Used to transfer performance of a human actor to a synthetic model (Haber and Terzopoulos (2004)).
- Synthetic motion: From text, audio or defined by an artist (Haber and Terzopoulos (2004)).

Mixed parameterised physically based and layered models are amongst the most popular. For example, Wu *et al.* (1994) model expressive wrinkles with a plastic-visco-elastic model supported by a layered and physically based model which simulates the fat tissue of the skin. Zhang *et al.* (2004b) introduce a non linear multi layered model of the skin where the skin is built as a mass spring network.

Enhancing realism complements the facial model. An explanation of some techniques for facial rendering follows.

- Photograph texturing: Extraction and application of additional texture information. It is a cheap means of conveying realism. Texture synthesis and texture mapping can be used with a parameterisation of the 2D texture space, a texture resampling method and, a radial texture synthesis approach (Simmons *et al.* (2002); Tarini *et al.* (2002)).
- Colouration: Colouration provides clues to the interpretation of particular signals from the human face (Noh and Neumann (1998); Patel (1995)). For example, it could be used for blushing, which is based on colour changes.
- Lighting models: Use advanced reflectance models of the skin.

Nowadays, facial animation aims to be realistic, efficient, adaptable to individual faces and as automated as possible (Noh and Neumann (1998)). For example, Lee *et al.* (1995) use a feature matching algorithm to adapt a subject's face to a generic face using a Laplacian operator. Then, the model is converted to a physically based model using feature points. Weyrich (2009) uses a multi layered, heterogeneous spectral reflectance model and a thin absorbing layer to enhance human skin appearance. Xiang *et al.* (2009) present an automated mechanism for transferring facial expressions from a generic facial model to individual faces. Here, feature landmarks are automatically detected. Chen (2006) generates personalised face shapes using radial basis functions and the MPEG-4 standard. Zhang *et al.* (2003a, 2004a) explain an adaptive simulation algorithm to speed up the animation. The appearance of GPUs is also influencing facial animation (Chen and Prakash (2006)).

2.2 Discussion

Facial animation of expressions and the creation of animatable models are both complex tasks. For example, in some cases physical accuracy is sacrificed for speed and some

other times speed is sacrificed in search of anatomical accuracy. There is evidence that the combination of physically based models and layered models is amongst the most popular in facial modelling (e.g. Terzopoulos and Waters (1990); Wu *et al.* (1994); Zhang *et al.* (2004a); Haber and Terzopoulos (2004)).

Performance driven approaches are limited by the set of postures and shapes that have been captured. Motion capture is also limited by the difficulties to produce the desired behaviour or posture in real animals (because you can't just ask animals to do what you want them to). Indeed, the data sets for Sagar (2006) were obtained from a human actor. Pure geometric parametric models ignore anatomy claiming that physical models of such anatomy do not bring any advantage in the final result (Watt and Policarpo (2001)). Instead, we built a layered model which replicates the layered nature of anatomy. Layered models bring advantages such as:

- They are layered as is anatomy. Here, it is possible to get insight into the anatomy of the entity being modelled as the interaction of the layers plays a very important part in the final result.
- With some work layered models can be generalised to other faces.
- They allow the study and testing of novel ways for object to object or layer interaction.
- We can have a better control of the resulting unlimited set of postures/shapes, as opposed to the fixed set of performance driven approaches or the tedious interaction required in pure geometric parameterisations.

However, there are some disadvantages too:

- They require good anatomical knowledge.
- Calculations are more expensive.
- Visual realism is more difficult to achieve.

Many human facial animation models (HFAMs) use a layered model (Zhang *et al.* (2004b); Kähler *et al.* (2003); Wu *et al.* (1994)). However, different models implement different layers. For example, several HFAMs ignore the skull layer as it is not visible (e.g. Yao *et al.* (2005); Wu *et al.* (1994); Xiang *et al.* (2009)). In contrast, King (2001); Kähler *et al.* (2003); Zhang *et al.* (2004a) and Londra, include the skull as an important component of the model. Indeed, the use of a skull in Londra guides the

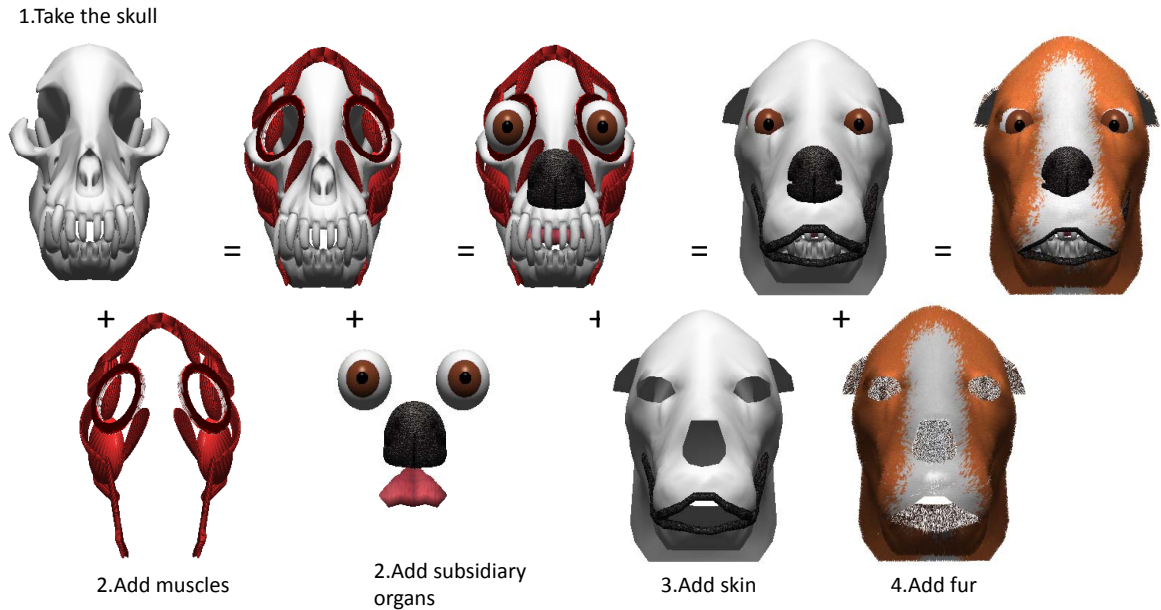


Figure 2.1: Bottom up layered approach.

construction of the whole model and allowed us to implement one major contribution to the layered model approach: we are able to follow a pure bottom up approach which starts with the skull and ends with the fur (Figure 2.1). Here, we do not need to start with a facial mesh. Instead, Londra’s facial mesh is generated from the underlying anatomy. The skull plays an important rôle in the final shape. It is true that HFAMs such as Kähler *et al.* (2003) follow a facial reconstruction approach starting from the skull. However, at the end, they rely on the existence of a generic facial mesh which is fitted to the skull. Moreover, most HFAMs using a skull, fit it to a facial mesh (e.g. Lee *et al.* (1995); Tarini *et al.* (2002); Zhang *et al.* (2004b)). Our pure bottom up approach gives more generality to skin generation. In contrast, many HFAMs give generality to the model by scanning new faces that are then adapted to a template facial mesh (e.g. Tarini *et al.* (2002); Zhang *et al.* (2004a); Chen (2006); Xiang *et al.* (2009); Zhang and Prakash (2009)). While the problem of giving generality to our base skull is a proposed future research problem, we find our bottom up approach and our skin generation method are closer to animal anatomy.

Muscles also play an important rôle in Londra’s skin shape. Indeed, our bottom up approach required the underlying muscle geometry. Many HFAMs ignore muscle geometry as it is not visible (e.g. Waters (1987); Watt and Policarpo (2001); King (2001); Zhang *et al.* (2004b)). Some HFAMs included muscle geometry (Wu *et al.* (1994); Chen and Prakash (2006)) to aid muscle contraction, but muscles are not visualised

or require many parameters. Apart from supporting our pure bottom up approach; muscular geometry and some ideas from Müller *et al.* (2005) allowed us to propose a skin deformation mechanism where forces and the direction of deformation are obtained geometrically. Here, the area and volume of influence of a muscle is implicit in the muscle's geometry (muscular influence is determined by the shape of the muscle itself). In contrast, in HFAMs such as Zhang *et al.* (2004a), muscles are represented as physical equations which affect nearby skin vertices which sometimes include non linear components for more realistic results. Their only visual representation is a line which is placed interactively. That makes muscle placement easier but calculations more complex and natural visualisation of muscles' shape infeasible. In Londra, muscles were positioned according to anatomy literature and verified by observation only. Cylindrical projection can be used to ease muscle insertion and to automatically adapt the whole model to a new input face (Zhang *et al.* (2004a)). There are even HFAMs which automatically detect feature points (Xiang *et al.* (2009)) but ignore muscles. In Londra, muscle insertion would be still a bottleneck in the generalisation of the model generation. Here, we use 3D interaction to be able to define muscles' curvature properly. Additionally, we take advantage of head symmetry and mirror half of the muscles. It can be claimed that 2D interaction or a mixture of multiple views is easier for non experts. However, using mirroring eased 3D interaction considerably. We are not aware of much use of mirroring in HFAMs. This is probably because heads are not exactly symmetric. However, the idea of simplifying to a symmetric model, especially when the differences are not perceptible is nice. In the future, one could even consider mirroring the computations.

In some HFAMs (e.g. Lee *et al.* (1995); Zhang *et al.* (2004b)) the layered model is extended so that the skin has several layers. This brings a better volumetric effect during deformation. Also, it helps to represent the non-homogeneity of soft tissue. In contrast, in Londra, the skin was idealised as a surface, requiring fewer calculations. Even though we lack the volumetric effect, the introduction of multi-layered fur helps to enhance the look of the final result. The fur layer is not required in HFAMs but brings advantages in creatures such as Londra. At the moment the non homogeneity of the soft tissue has not been considered in Londra but we think it could be related to the radii of spheres used in the model.

In Londra, mirroring is also used during skin generation. Here, from a set of landmarks and from the underlying anatomy we generate one side of the skin. Then, we triangulate it considering some restrictions for the required holes. Finally, we mirror

and smooth the mesh. Skin is a direct consequence of the underlying anatomy and definitely the most generic layer in our model. Londra’s model generation can be more suitable for those who do not have scanning capability; for creatures which are difficult to scan; and for users with the required knowledge to decide the location of anatomical landmarks.

Londra’s control system is somewhere in between pure geometric parametric models and physically based models. Some HFAMs (e.g. King (2001); Chen (2006); Xiang *et al.* (2009)) and Londra associate vertices on the skin to anatomical regions, use some anatomical landmarks and move some regions with kinematics. While pure physical models such as Zhang *et al.* (2004b) reach an equilibrium state, models such as Londra reach a smoothed state. In some HFAMs (Lee *et al.* (1995); Zhang *et al.* (2004b); Chen (2006)), layers are connected with springs and the positions of the muscles are indicated with markers. In Londra, we propose a simpler system where muscles are placed in anatomical positions and layers are lightly connected and interact with spheres. The novel use of spheres is present throughout Londra. We use spheres for shape generation, deformation, collision detection, motion control and thickness. In particular, we introduce our Tabulated Spheres Subsets (TSSs) for layer to layer interaction (Navarro Newball *et al.* (2009c)). In some HFAMs (e.g. King (2001); Breton *et al.* (2001); Zhang *et al.* (2004a)) and in Londra the mandible is moved with simple geometric transformations. Jaw biomechanics can usually be simplified to this kind of operation. In Londra jaw motion is constrained using TSSs. Londra’s simpler calculations make it more suitable for gaming applications, while more complex pure physical models are more accurate and more suitable for surgical simulation.

HFAMs and Londra aim to produce skin deformation to replicate facial expressions. Both consider the skin as an elastic entity. However, elastic properties in Londra were simplified assuming a template equilibrium state (in Londra the undeformed vertices in the control mesh are in equilibrium). Producing deformations increases the complexity of models in general. In HFAMs such as Zhang *et al.* (2004a), after deformation, the equilibrium state of the mass-spring network representing the skin is reached using numerical integration. Muscular forces are obtained using a physical model. Instead, Londra uses forces obtained geometrically from the distance between the centres of interacting spheres (TSSs in the muscle and TSSs in the skin). When a vertex in the control mesh is moved, its new position is obtained using Euler integration. Here, thanks to Hookes law, the deformed node will tend to go back to its original position. For instance, physical calculations are done only for the nodes affected directly and only

to return them to their assumed equilibrium position. However, moving one vertex in the control mesh of the skin affects several vertices in the limit surface, emulating the effect of a mass spring network. A simplified system such as Londra is not likely to be affected by inaccuracies caused by Euler integration because of the small time steps and the fewer calculations.

Some HFAMs (e.g. Chen (2006); Blanz and Vetter (1999); Zhang *et al.* (2004a)) use regions and sub-regions so that deformation can be adaptively or locally calculated. While regions can be pre-computed in an offline process, high storage and managing of the data structure could be still required. Adaptive refinement based on the amount of deformation (Zhang *et al.* (2004a)) is done to smooth the resulting surface. In Londra, we use localised refinement. The fact that Londra’s refinement is localised but not adaptive can produce unnecessary extra triangles or lack of detail if little refinement is done in the deformed regions. However, Londra does not require additional structures to store a region’s information. Here, affected regions are directly related to the geometry of the acting underlying muscles. We believe this is consistent with anatomy.

The use of coding systems such as FACS (Waters (1987); King (2001); Haber and Terzopoulos (2004)) or MPEG-4 (Chen (2006)) is common in HFAMs. Londra uses our Dog FACS (DFACS) which is an adaptation of FACS. This sort of parameterisation helps to gain an understanding of the expression production mechanism. It considers important dog facial actions that were obtained from dog anatomy study.

In many HFAMs (e.g. King (2001); Breton *et al.* (2001); Kähler *et al.* (2002); Simmons *et al.* (2002); Zhang *et al.* (2004b,a); Haber and Terzopoulos (2004); Sifakis *et al.* (2006)) and in Londra a sensibly realistic model is achieved using texturing. Other models (Weyrich (2009)) develop very advanced lighting models. The disadvantage of simple texturing is that realism is limited because the texture does not respond to lighting. However, textures are rendered very efficiently. Using data sets scanned from real people and individual face measurements limits the model to the existing data sets. But in Londra, the search for realism also relies on the fact that a model is completely built upon the underlying anatomy.

Optimisation is possible using regions (Zhang *et al.* (2004a)). As explained, in Londra, skin is changed only in those regions affected by the underlying muscles. However, there are some other major facial regions (e.g. neck, ears, mandible) which initially move with kinematics. Because of the differences between dog and human anatomy, the number of regions in HFAMs and Londra differs. In Zhang *et al.* (2004b) each facial region (or sub-region) contains a group of muscles that are responsible for the

motion of the skin in this area. In Londra, muscles are not directly related to regions. However, their effect is implicit thanks to the geometrical model: each muscle affects the region of skin it touches. In Londra, regions are detected in 3D. Here, a portion of the skin belongs to a particular region if it is touched by a sphere generated from the underlying anatomy. In summary Londra:

- Is anatomically inspired and uses geometrically based modelling with some physics. Thus, it is somewhere in between geometric parametric facial models and physically based models.
- Lowers the use of complex elements and requires fewer calculations than physical models and less user interaction than pure geometric parameterisations.
- Proves that a dog face with some basic expressions can be modelled following some basic anatomical principles and a simplified anatomical model: the face anatomy is layered so that muscles control the shape and behaviour of the skin.

Chapter 3

Facial Expressions in Dogs

Notice: some portions of this section were taken from my own published work at Navarro Newball *et al.* (2008b)

3.1 Darwin's Observations

Dogs and other creatures have typical expressions. Darwin (1890) was one of the first to study animal expression and to show the importance of the dog's face as an expressive organ. He highlighted that the appearance of a dog is altered when the position of its ears is changed due to the movement of many facial muscles. Also, he described the 'hot-house' face of disappointment of his dog when it perceived that he was going to end a walk in order to do research in the hot house. Darwin described dog expressive actions such as anger, happiness, affection, attention, hostile intention, fear, disappointment, delight, discomfort and friendliness. Charles Darwin's descriptions served as a starting point and an inspiration for this project. We analysed 26 of his descriptions. Figure 3.1 shows the expressive use of facial organs in dogs. We found that the ears, the head, the eyes, the eyelids, the teeth, the upper lip and the tongue are necessary organs for showing expressions. In dogs, the face and the body postures and gestures play an important rôle in expression display. However, dogs express very differently from humans. That is why six of the expressions for Londra were chosen for the number of facial organs involved in the development of the expression. Additionally, there are two forms of affection and we added two physiological expressions (smell, yawn). Figure 3.2, shows Darwin's hostile intention.

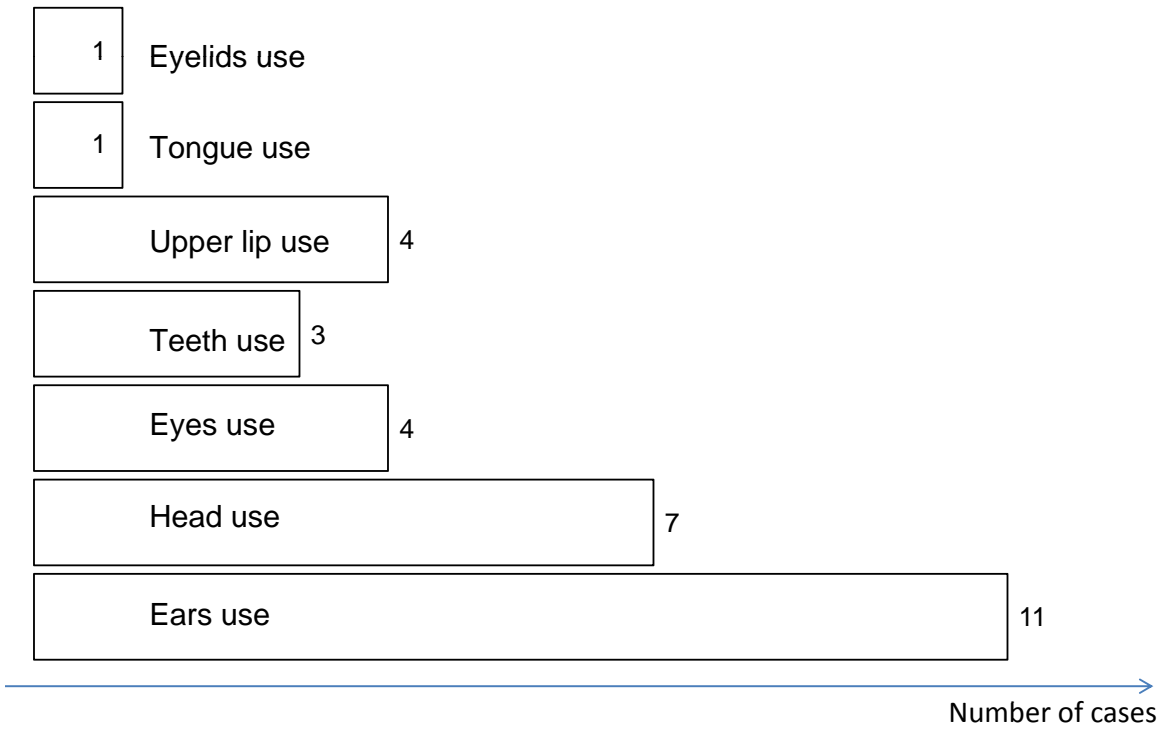


Figure 3.1: Occurrences of face related organs in expressions described by Darwin

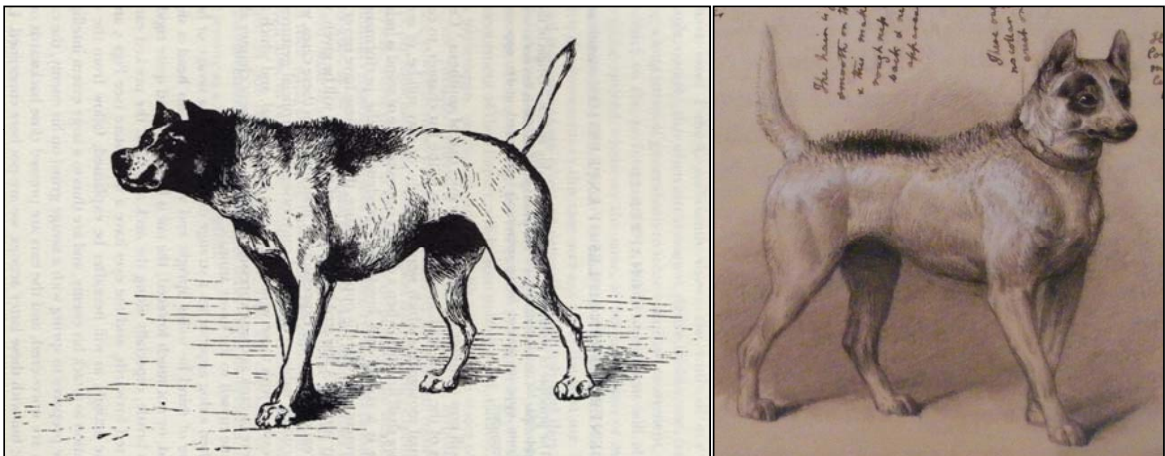


Figure 3.2: Hostile intention. Drawn for Darwin by Briton Riviere

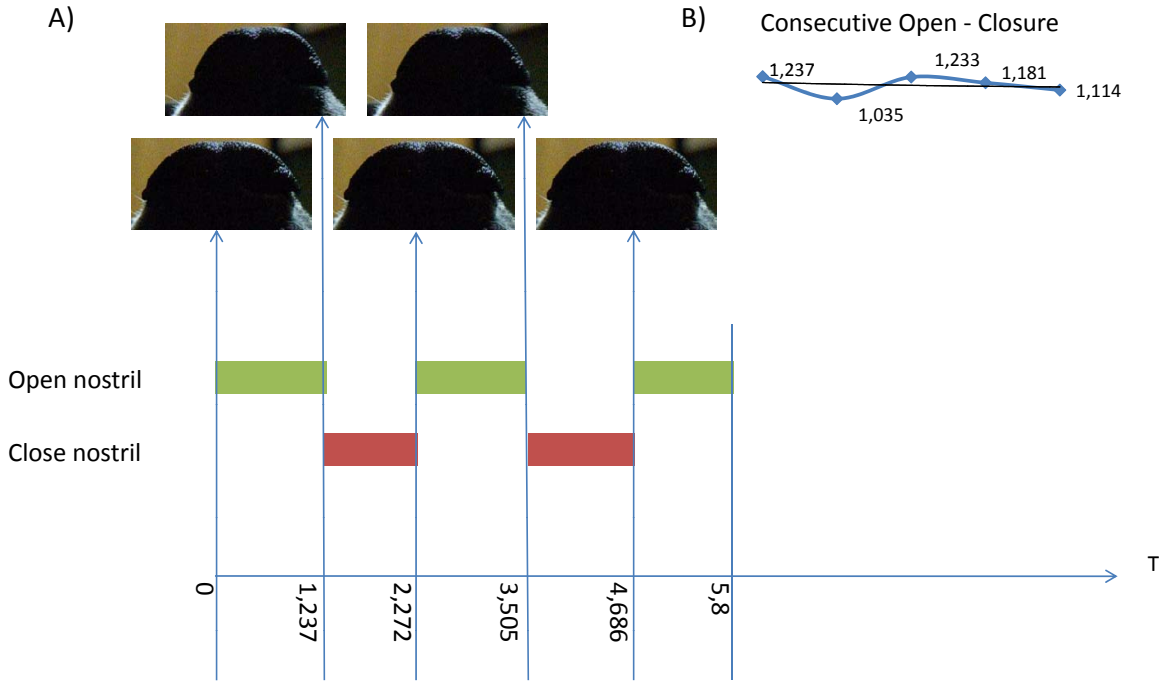


Figure 3.3: Nostril movement. Appendix K, ONostril.avi

3.2 Video Observation

Darwin’s descriptions are static and depict the most characteristic instant of some dog expressions accurately. However, dog expressions are more complex. For example, they can come mixed and they evolve through time with different intensities. As expected, observation plays an important rôle in animal expression modelling in general. Thus, using the software, Observer, at the Gaming laboratory at the Manchester Metropolitan University (UK), we were able to complement some of Darwin’s observations by analysing 11 dog videos. 5 videos are explained here, 6 are detailed in Appendix D. ‘The Observer is the professional and user-friendly event logging software for the collection, analysis, and presentation of observational data’ (Noldus Information Technology (2009)). We observed 7 different dogs at the Dunedin dog park. However, The videos were chosen from videos taken to the real Londra and two angry dog videos obtained from YouTube. Particularly, we observed the real Londra during two different one month periods, one in 2007 and one in 2009.

Figure 3.3A shows that Londra used similar time slots to keep the nostrils open and closed. The behaviour of the values of the time slots used in each action was nearly linear (3.3B).

Figure 3.4 shows that in attention, the ears are raised before anything else and all

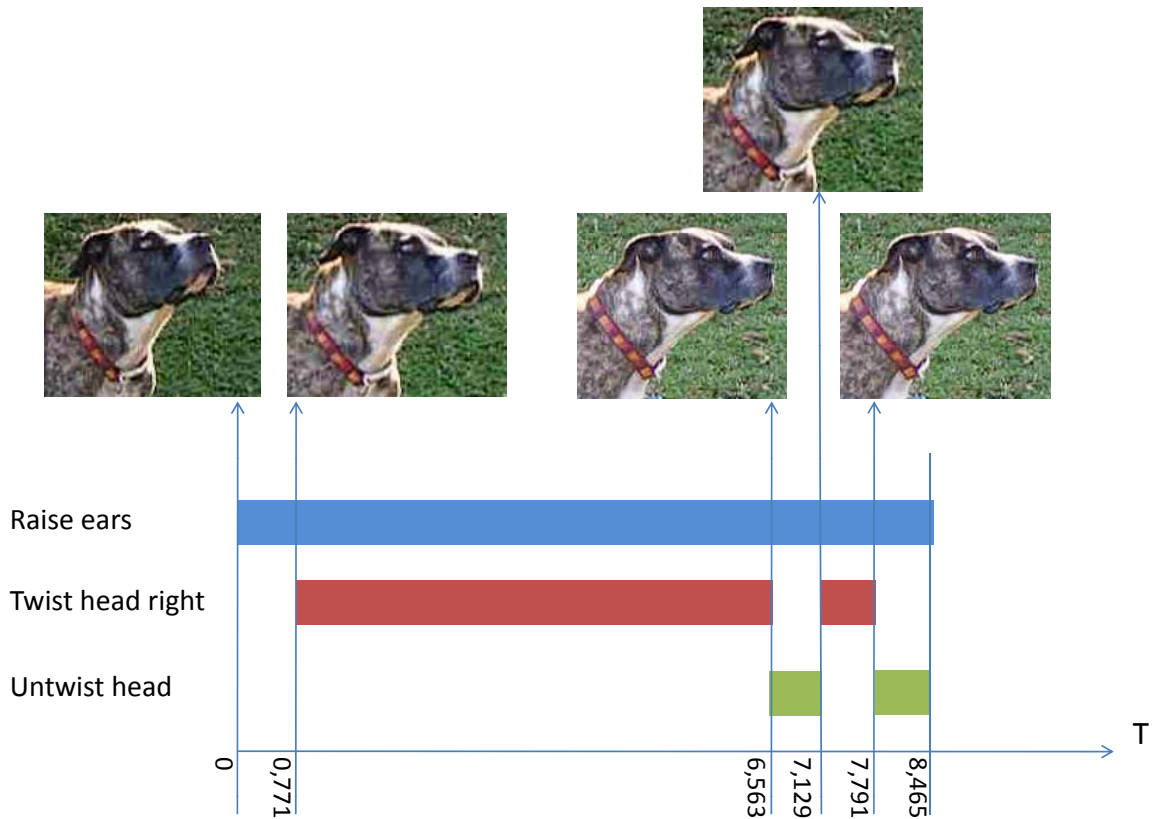


Figure 3.4: Attention. Appendix K, OAttention.avi

the time. It is common to have long periods of head twisting that can be followed by short periods of head untwisting.

Figure 3.5 shows that a common action in fear is moving the ears backward. This action can be followed by moving the ears forward during short periods of time. In cases of stronger fear, ear movement is accompanied by head lowering actions. Also, consecutive small mouth opening closures could occur. Eye blinking may occur any time.

Making a sweet dog such as Londra angry was a non doable task. Thus, we decided to download some angry dog videos from YouTube LLC (2009). Figure 3.6 shows the sequence of actions to display anger. All of them occur almost simultaneously but first the mouth was slightly opened; then the lips were raised; then the ears were moved forward. The tongue was shown for a short period of time. Note that these actions may vary in intensity through time and / or depending on the intensity of anger.

Figure 3.7 shows affection. In this video we decided to observe mainly head motion and assumed that Londra could open the mouth and lick at any time. We observed completely random motion of the head in all directions. However, the direction of head

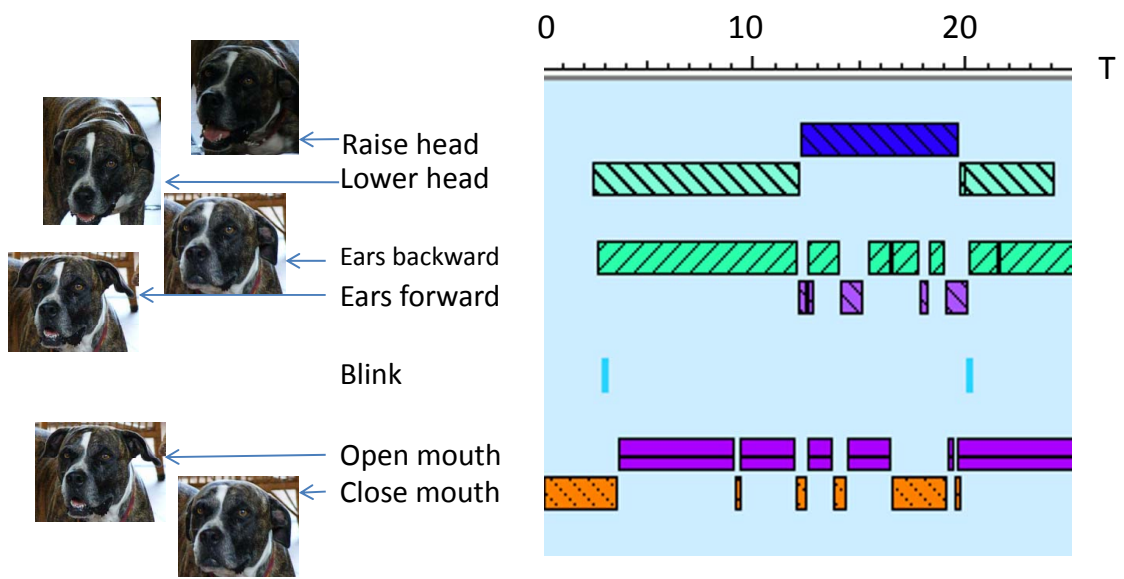


Figure 3.5: Fear. Appendix K, OFear.avi

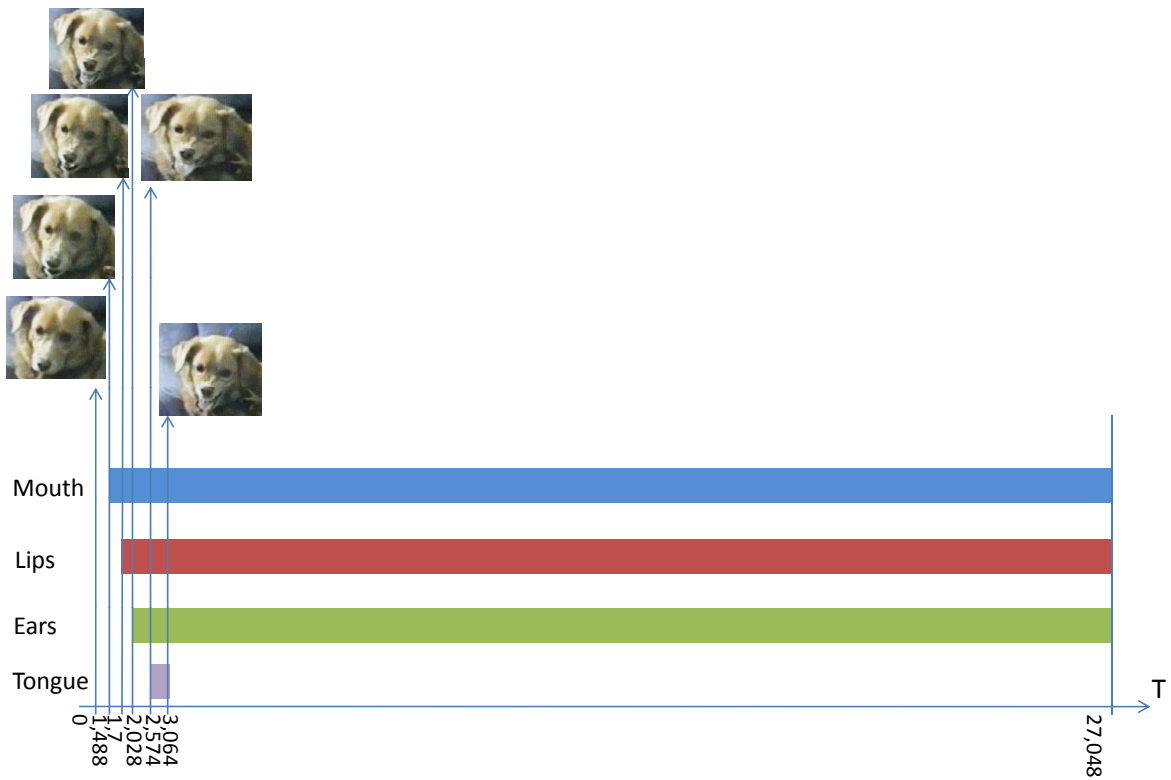


Figure 3.6: Anger. Appendix K, OAnger.avi

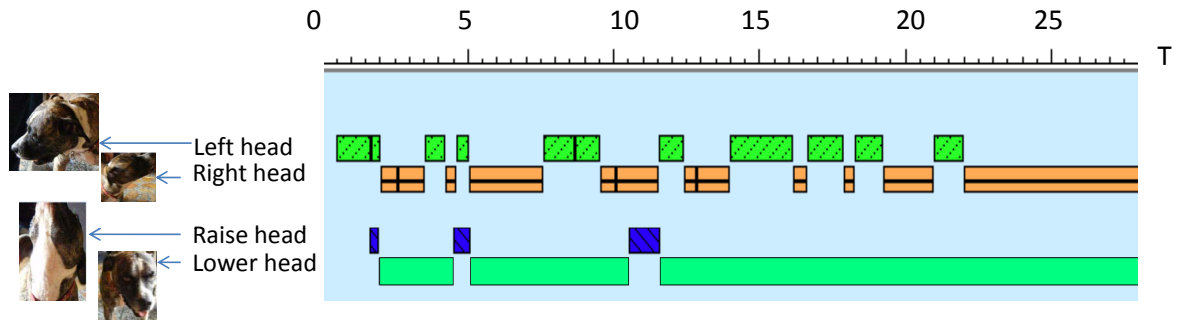


Figure 3.7: Affection. Appendix K, OAffection.avi

motion could depend on what the human interacting with Londra is doing at the time. The degrees of intensity of each action could be annotated to enhance the chart. In essence this chart only provides a good example of timing of actions in one particular event of Londra's affection. Of course head raising and lowering and head right / left movements cannot occur at the same time.

3.3 Facial Expressions in Artificial Pets

An artificial pet is a robotic or software toy intended to provide a companion to its owner and to behave like a pet. We analysed a selected group of representative artificial pets comparing them with Londra from the computer science point of view. Here, artificial pets were chosen in some cases for their popularity and in some others for their use of specific expressive mechanisms. We analysed a group of 10 representative artificial pets. The chosen pets were Tamagotchi, Cypet, Furry Paws, AIBO, HOMIE, eMuu, the alphawolves, Petz, Nintendogs and Londra. Appendix A summarises them. Figure 3.8 shows the expressive use of facial organs in artificial pets. Figure 3.9 shows features from artificial pets. We found that artificial pets had movable facial organs such as the eyes, the mouth, the ears, the head and the tongue. Also, we found that only Londra is based on a natural coding system, proposed skin movements and emphasised the face.

3.4 Discussion

We demonstrated that animals and in particular dogs have facial expressions. These expressions play an important rôle in emotion display. Indeed, not only real dogs display facial expressions, but several modern artificial pets have some kind of expressive

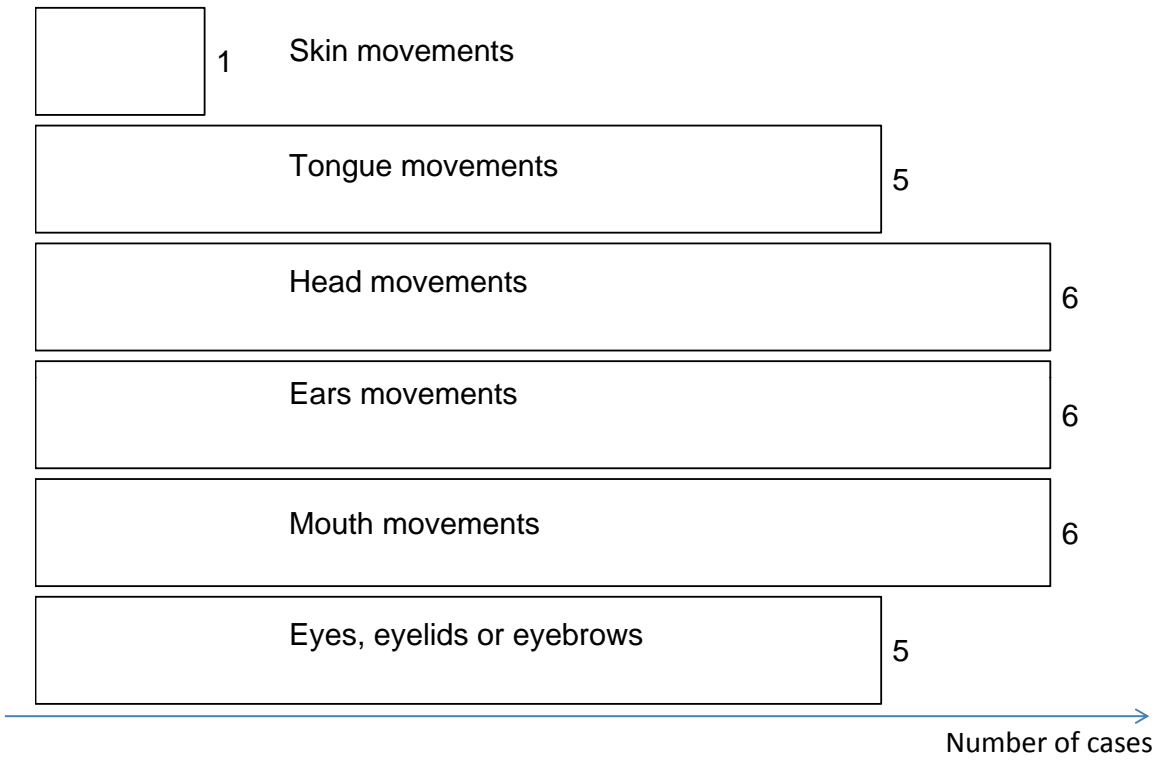


Figure 3.8: Facial Organs in artificial Pets

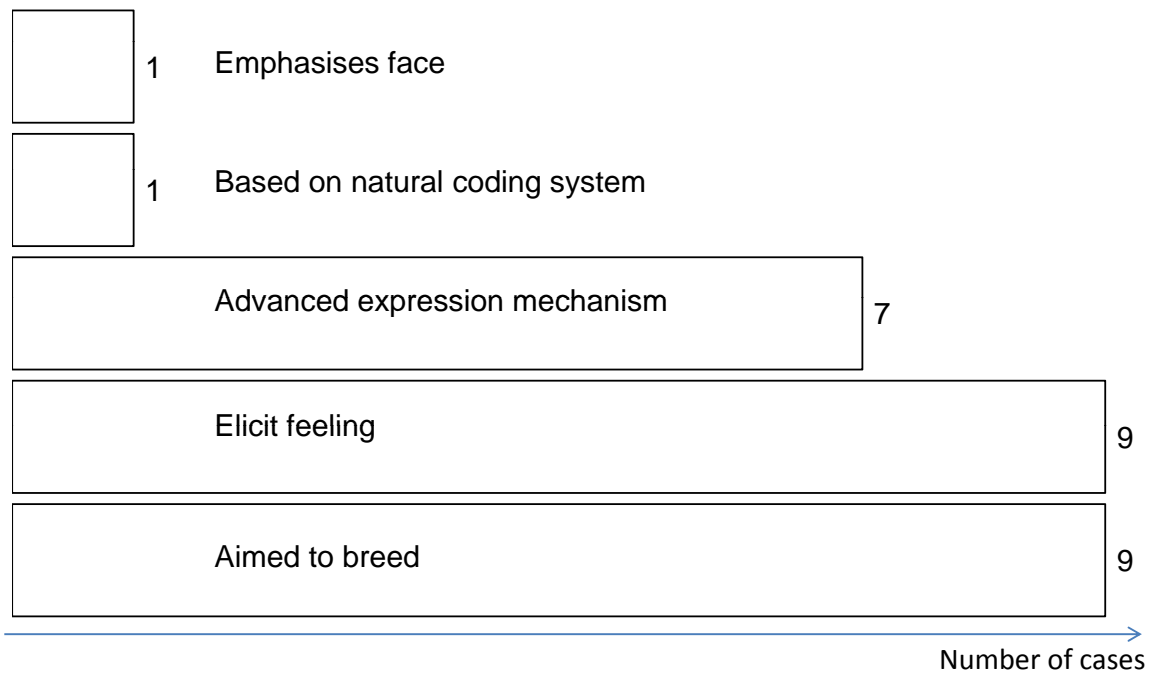


Figure 3.9: Artificial Pet Features

mechanism which includes facial expressions.

Chapter 4

Dog head anatomy overview

In this chapter we summarise the most relevant dog head anatomy for Londra. Our Londra is a mesaticephalic (see Table 4.1). All figures using Londra are based on this sort of dog. For an excellent description refer to Sisson *et al.* (1975).

4.1 Anatomical Directions

Frequently, it is necessary to gain a sense of position and direction in anatomy. Anatomical terms for position and direction are shown in Figure 4.1. The median plane divides anatomy in two halves. The frontal plane divides the anatomy in the dorsal (upper) and ventral (lower) regions. The term Caudal refers to the back and Rostral or Cranial to the front (Sisson *et al.* (1975)).

4.2 Osteotomy

Figure 4.2 shows some relevant features in the skull and the mandible. They are explained next (Sisson *et al.* (1975)):

- Occipital bone: contains the nuchal crest and the occipital condyles. Junction points for the neck.
- Parietal bones: form the sagittal crest and the temporal fossa.
- Temporal bones: contain the mandibular notch and condyle.
- Frontal Bones: have a zygomatic process and form an incomplete supraorbital margin.

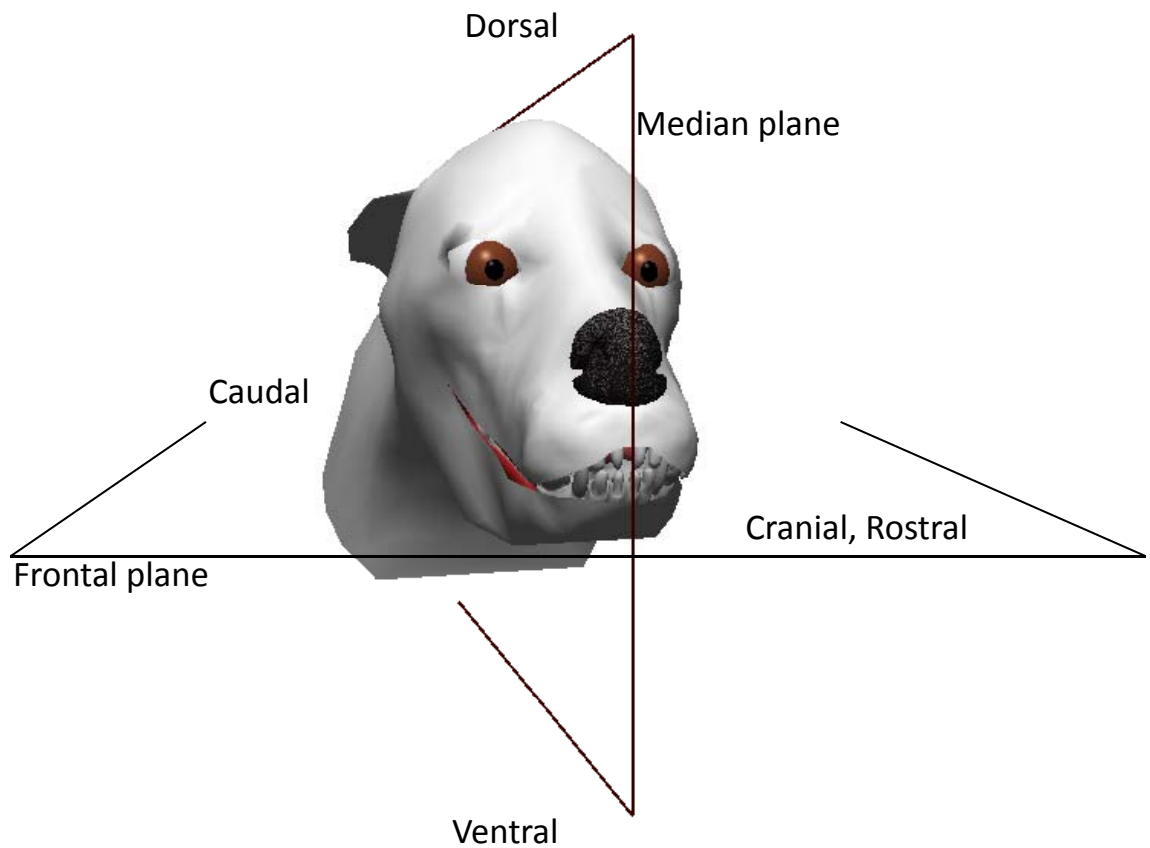


Figure 4.1: Anatomical directions

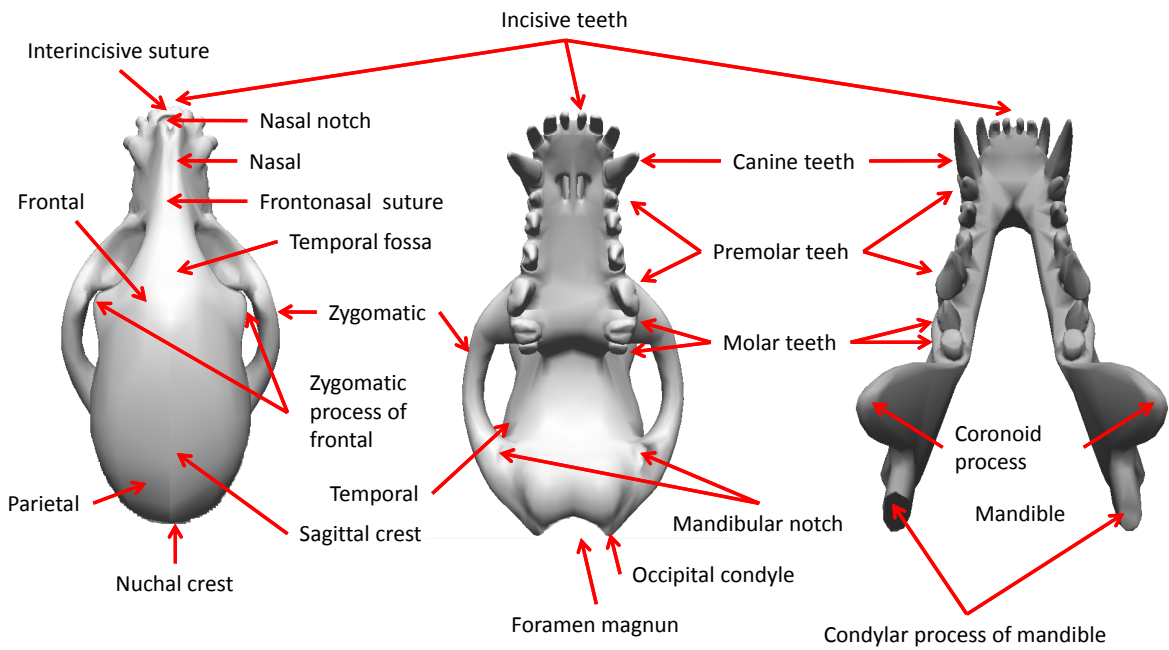


Figure 4.2: Dog head osteotomy

Table 4.1: Dog classification according to head osteotomy

Head type	Description	Cephalic index	Craniofacial index
Dolichocephalic	Long , narrow skull	50	10:7
Brachycephalic	Broad, short skulls	90	10:3
Mesaticephalic	Intermediate	70 ... 75	

- Zygomatic bones: form part of the orbital margin.
- Nasal bones: long and wider rostrally than caudally.
- Mandible: movable, contains several alveoli.
- Frontonasal suture: nasal and frontal bones' junction.
- Mandibular notch: receives the condylar process of the Mandible.
- Incisive bones: keep three alveoli for the incisor teeth. Contains the incisive suture.

The length of the skull can be measured from the nuchal crest to the rostral end of the interincisive suture (Figure 4.3A). The breadth is measured between the summits of the zygomatic arches (Figure 4.3B). Also, there are two basic indices to measure the dog head's proportions (Sisson *et al.* (1975)). The cephalic index is the relation of the breadth to the length (4.1). The craniofacial index (Figure 4.3C) is the relationship of the distance between the nuchal crest and the frontonasal suture, L_1 (4.2); to that between the frontonasal suture, and the nasal notch, L_2 (located just behind the interincisive suture). Table 4.1 shows the value of the cephalic and craniofacial indices for the main kinds of dog (Sisson *et al.* (1975)). Figure 4.3D shows an example of a brachycephalic dog.

$$Cephalic = (Breadth \times 100) \div Length \quad (4.1)$$

$$Cranio\ Facial = \frac{L_1}{L_2} \quad (4.2)$$

There are anatomical differences among breeds in the skull and mandible. In contrast, the size of the orbit is similar among breeds. Some differences are (Sisson *et al.* (1975)):

- The sagittal crest is more prominent in large breeds.

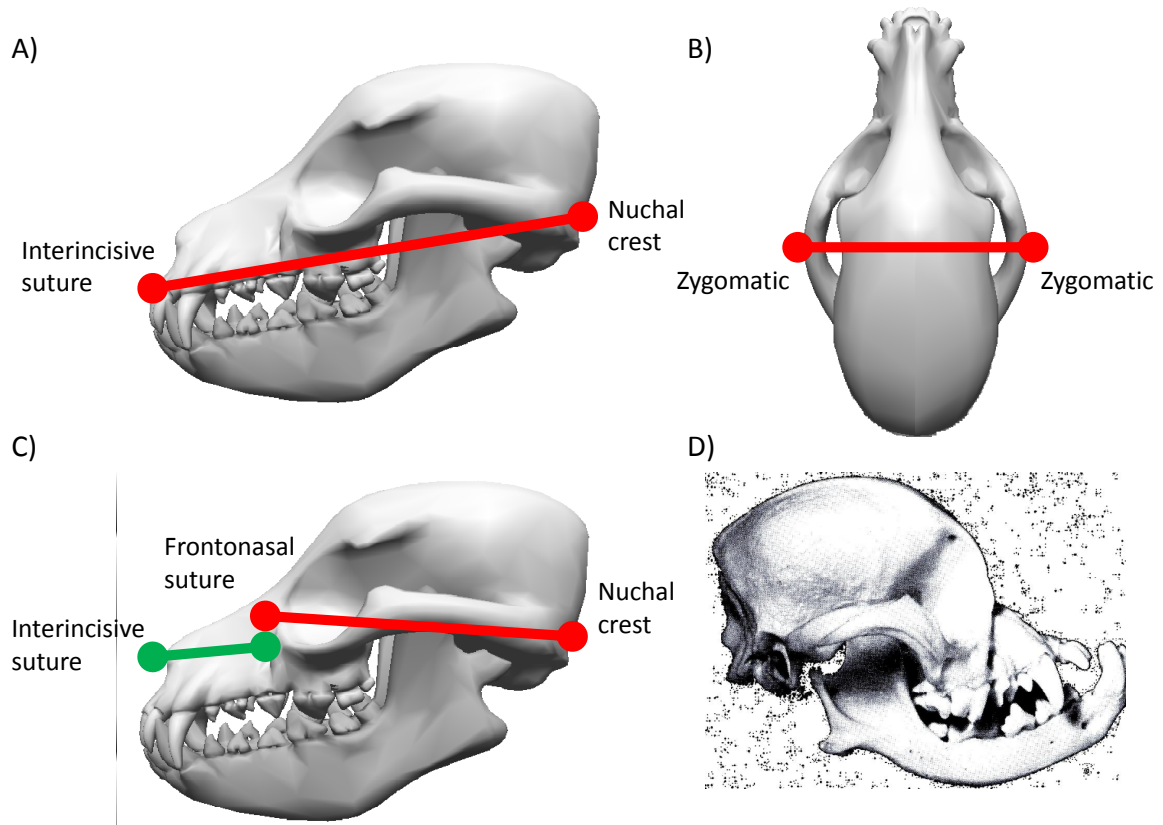


Figure 4.3: Anatomical proportions in the head. A)Length. B)Breadth. C)In red the distance between nuchal crest and the frontonasal suture. In green the distance between the frontonasal suture and the nasal notch. D) Brachycephalic dog (Sisson *et al.* (1975), p. 1543).

- The jaw protrudes beyond the upper face (prognathism); or, upper face protrudes beyond the jaw (brachygnathism).
- The angle of divergence of the mandible vary from 25 to 30 degrees and is larger in brachycephalic dogs.
- The nuchal crest is more prominent caudally in large breeds.
- In large breeds the temporal fossa is wider.
- There is a depression at the frontonasal suture in brachycephalics.

4.3 Teeth

Adult dogs have 42 permanent teeth. Most of the teeth are adapted to cutting, shearing and holding objects. The teeth shown in Figure 4.2 are briefly explained below (Sisson *et al.* (1975)).

- Incisives: their contact surface lie in a horizontal plane.
- Canines: the upper and lower ones lie next in occlusion but do not wear against each other.
- Cheek: these are the molar and the premolar. The more rostral premolars do not contact those of the opposing jaw. Upper cheek teeth are lateral to those of lower jaw. The upper teeth shear past the lateral surfaces of the lowers. The medial portions of the upper oppose to the lower teeth.

There are some differences in teeth among breeds too. Some are listed below:

- In medium length heads, the upper incisor set protrudes slightly rostrally to the lower. The opposite happens in small skulls
- In brachycephalic occlusion canine teeth do not wear against each other.
- In brachycephalic skulls, upper and lower premolars do not alternate in position. Here, the upper jaw is displaced upwards rostrally from a pivot point which is between the most rostral molar and the most caudal premolar. The teeth move laterally from this point; look turned and crowded; and the lower jaw turns upwards rostrally.

4.4 Main articulations in the dog head

There are three major articulations related to the head:

- Temporomandibular articulation: Main head articulation. It does not present transverse or gliding movement.
- Joint to the vertebrae: It is supported by the nuchal ligament. Includes the axis, the atlas and involves the atlanto-occipital and atlantoaxial joints (Figure 4.5A). It is related to neck movement. The occipital condyles face the atlas vertebra.
- Ear articulation: Formed by the set of cartilages and ligaments which allow ear movement.

4.5 Jaw biomechanics

Most biomechanical studies refer to the human mandible (e.g. Leader *et al.* (2003); Koolstra and van Eijden (2004); Hannam (2008)). A few studies refer to animals such as sheep (De Jongh *et al.* (1989)) and pigs (Allen and Athanasiou (2006)). We found only two studies related to dog's mandible (Ashman *et al.* (1985); Sisson *et al.* (1975)). In average dogs (Sisson *et al.* (1975)):

- Jaw biomechanics can be complex. However, because Londra's expressions required simpler mandible openings, we decided to see it as a beam, hinged at the temporomandibular joint.
- The lower jaw is kept in a momentary position by the masticatory muscles (e.g. masseter, temporal).
- The acting forces are the weight of the mandible (which can be ignored) and the reaction of the elements of the upper dentition upon the lower.
- The contact area includes 6 teeth and occlusion surfaces are inclined (Figure 4.4).
- The effective blade of the shear occurs in the inner side of the fourth upper premolar and the outer side of the first lower molar (Figure 4.4).
- The shearing mechanism is mostly influenced by the forces from the temporal muscle.

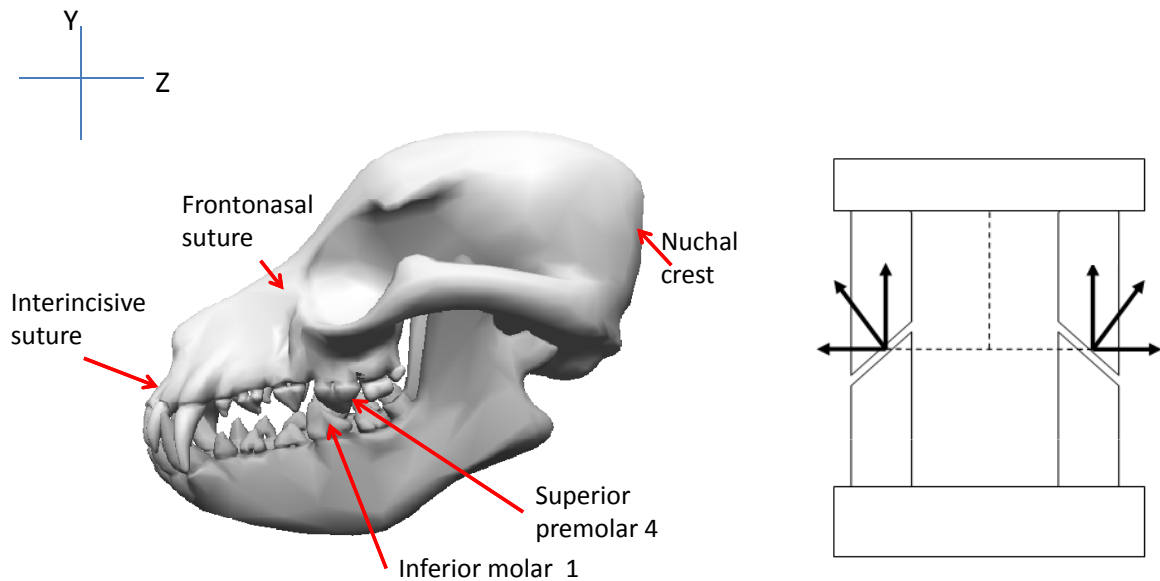


Figure 4.4: Occlusion in dogs. The main contact occurs between superior premolar 4 and inferior molar 1.

- Shortening of the jaw causes the partial loss of the shearing effect due to a lateral gap (in consequence, greater lateral mobility of the mandible is required).
- Mandibular tissue is elastically isotropic and homogeneous (Ashman *et al.* (1985)).

Amongst the techniques used for the biomechanical model of the jaw are:

- Finite elements modelling (De Jongh *et al.* (1989)).
- Dental arches (Weijs (1989)). An arch is connected by a bar to the condyles.
- Muscle activation patterns.
- Planar and curvilinear surface restrictions (Koolstra and van Eijden (2001)).

Methods to represent joint kinematics include:

- Roll, pitch and jaw angles and displacements (King (2001); Zhang *et al.* (2004a)).
- Path of a point. For example, mandible rotation is represented by the chin (Breton *et al.* (2001)) or by the lower incisor (Koolstra and van Eijden (2001)) and a centre of rotation is defined (kinematics centre). After parametric animation is performed, muscular animation is applied.

- Cartesian coordinate systems mixed rotations and translations (Koolstra and van Eijden (1997); Osborn (1996)). For example, one Cartesian coordinate system is attached to the skull and one to the mandible. At the start of each movement these coordinates coincide with their origins located at the centre of gravity of the mandible.
- Non orthogonal floating axis systems (Leader *et al.* (2003)). The non orthogonal floating axis has been recommended by the International Society of Biomechanics to represent relative orientation between two bodies.
- Action screws (Gal *et al.* (2004)). Muscle forces are represented as action screws stating that tracing a single point does not reveal the true nature of motion.

4.6 Miology

There are several muscle layers in the dog head. The most superficial layer includes the 'cutaneous' muscles of the head and the muscles in the neck. In order to simplify the model and to be able to produce finer detail deformations on the skin we implemented 11 pair of muscles and the Frontalis which lay underneath the 'cutaneous' facial muscles. Also, we ignored the muscles from the neck, the tongue and the eyes as we were concerned with those muscle producing more evident deformations on the skin. Figure 4.5B shows the chosen muscles, they were located according to anatomical books (Sisson *et al.* (1975)). They are described next:

- Frontalis: fixes and pulls skin of upper head
- Temporalis: close jaw.
- Auricularis (Dorsales, Rostrales): move ears.
- Levator: dilate nostril and raise upper lip
- Levator oculis: lifts medial portion of upper eyelid.
- Orbicularis oculis: sphincter of the eyelids.
- Zygomaticus: moves mouth corner.
- Digastricus: depresses mandible.
- Masseter: close jaw.

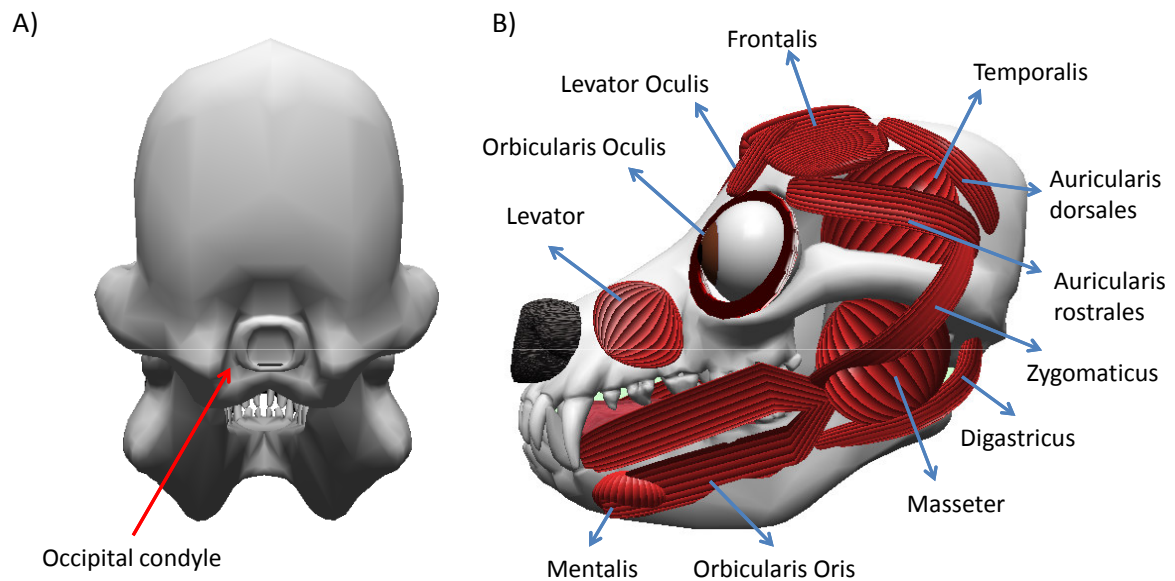


Figure 4.5: Joints and muscles. A) Joint to the first vertebra. B) Dog miology.

- Mentalis: stiffens the lower lip.
- Orbicularis Oris: sphincter muscle of the mouth.

4.7 Ears

Ears are very mobile and each ear can be independently controlled. They are formed by two skin covered cartilages, the auricular and the anular and by the ear canal. The Auricle, formed by the auricular cartilage, is the projecting part of the ear and varies considerably in shape (Sisson *et al.* (1975), Figure 4.6). The main shapes are (Wikimedia Foundation (2009c)):

- Bat ear: It is erect and broad next to the head and rounded at the tip (e.g. Chihuahua).
- Button ear: it is a small ear. Here, the tip folds forward nearly to the skull and forms a V shape (e.g. Jack Russell Terrier).
- Drop or pendant ear: ear that folds and droops close to the head (e.g. hound).
- Rose ear: it is a small drop ear that folds back (e.g. Bulldog).

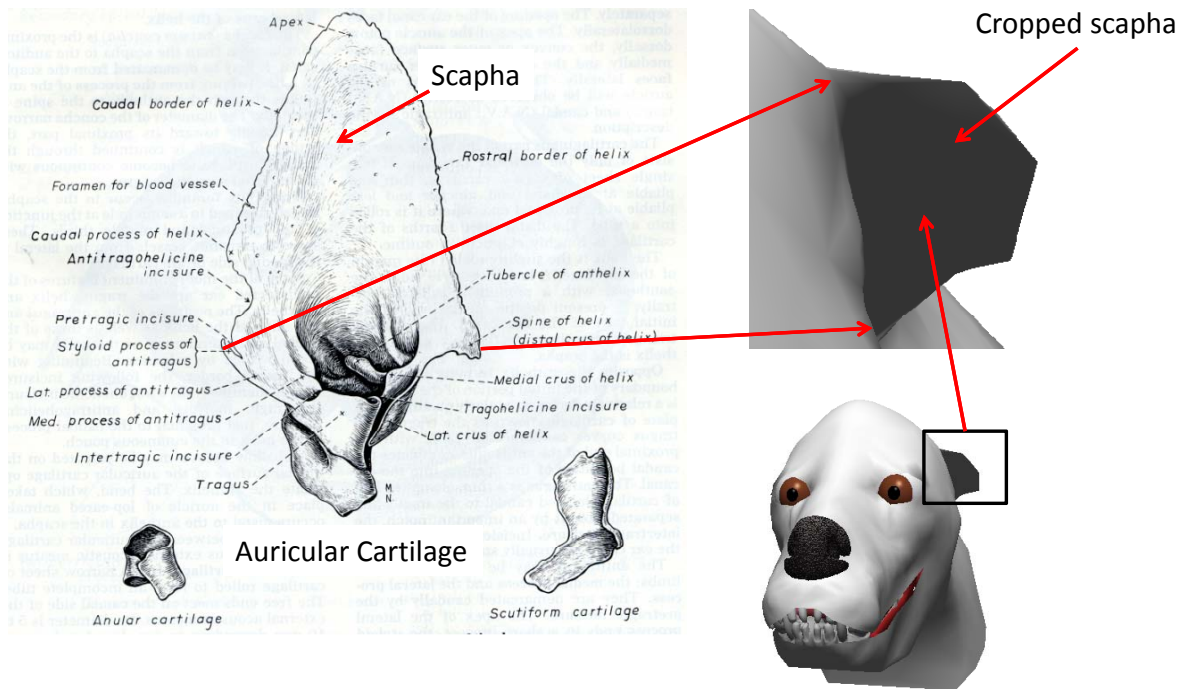


Figure 4.6: Ear anatomy. Adapted from Sisson *et al.* (1975), p. 1769.

- Natural: it is similar to that of a wolf.
- Prick ear: it is an erect and pointed ear.
- Semipricket ear: it is a prick ear where the tip slightly begins to fold forward (e.g. Rough Collie).
- Cropped ear: It is shaped by cutting.

4.8 Eyes

The eye orbit is defined between the Zygomatic process of the Frontal bone and the Zygomatic bone. The eyes are located here. Dog's eye orbit and eye ball present little size and shape changes among different breeds. The visible organs of the eye are explained below (Sisson *et al.* (1975), Figure 4.7A).

- Sclera: it is opaque and fibrous with variable thickness. It is composed of collagenous and elastic fibres and may have pigmentation. Extra ocular muscles attach to it to provide mobility

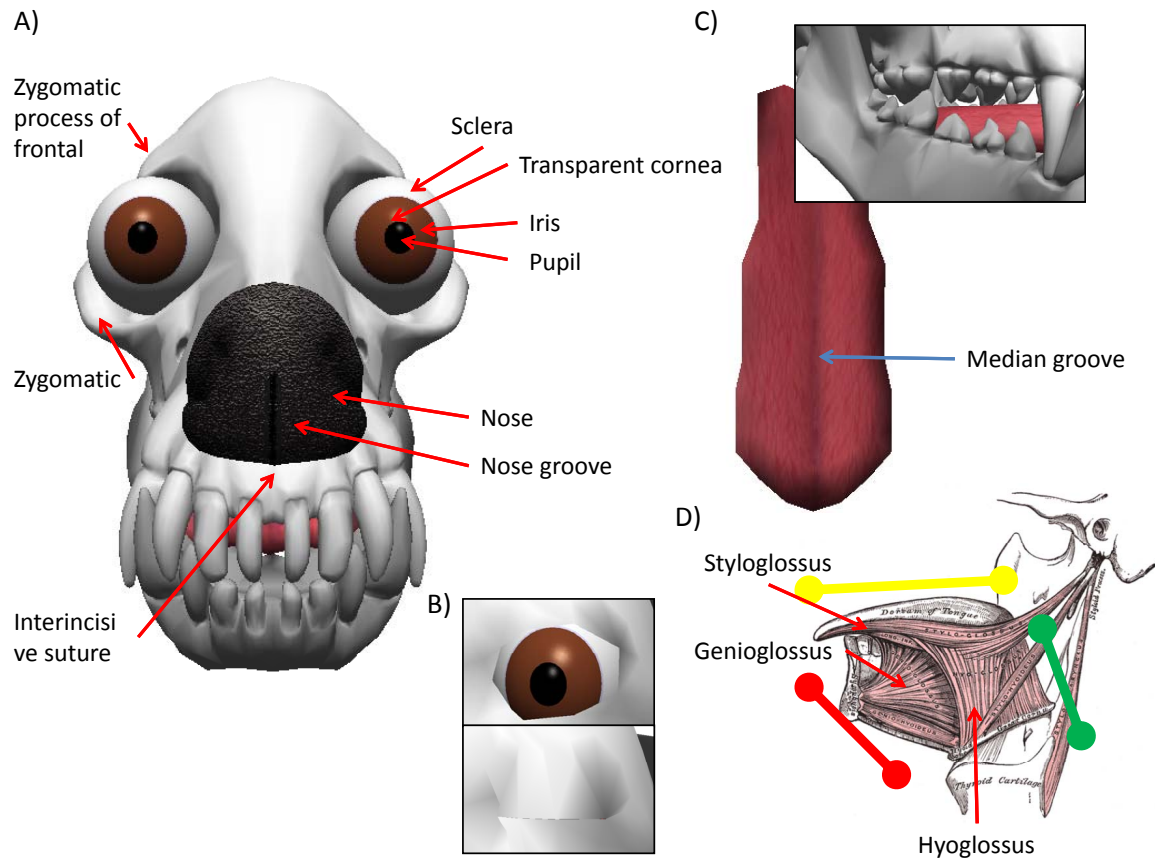


Figure 4.7: Anatomy of subsidiary organs. A) Eyes and nose. B) Eyelids. C) Tongue. D) Human tongue (adapted from Wikimedia Foundation (2009n)). Here, some important lines of muscular actions are highlighted. Genioglossus (red line); styloglossus (yellow line); hyoglossus (green line).

- Cornea: Formed by several layers, its posterior surface (endothelium) continues on the anterior surface of the iris. It is transparent and gives the shininess to the eyes.
- Iris: it is round and controls the passage of light through an opening called Pupil. In order to do this, it has sphincter muscle fibres that extend from the margin of the pupil toward the base of the iris
- Eyelids: regions of the skin which protect the eyes (Figure 4.7B).

In humans, the oculomotor system includes 3 types of movements (Haber and Terzopoulos (2004)):

- Gaze: sum of head and eye position.

- Holding movements: which compensate for the movement of the head
- Gaze shifting movements (saccades): which shift the direction of the eye to the target (the eyes must converge onto the target)
- Fixation movements: with micro shifts.

4.9 Nose

The nose and the nostrils are supported by a cartilaginous skeleton and their mobility is very limited, since the responsible muscles are poorly developed. Also, the median groove which divides the upper lip extends into the nasal plane and divides it partially. In some breeds the groove is very deep and looks like a double nose (Sisson *et al.* (1975), Figure 4.7A).

4.10 Tongue

The tongue is wide and thin rostrally and thicker caudally. It is bright red coloured and very mobile. Also, it is marked by a median groove. It is a flexible organ with very articulated and irregular movements. It has a fixed volume which can be redistributed. Its shape is related to its position. The tongue is the large bundle of skeletal muscles on the floor of the mouth (Sisson *et al.* (1975), Figure 4.7C and D). The tongue has many functions. In terms of expressions the most important are:

- Helps reduce body temperature.
- It is an Affection Giving Tool. Dogs kiss their owners and provide affection with their tongue (Pet Comfort Newsletter (2009)).
- Yawning, for example, in laziness.

In general, tongues have many muscles to alter their shape by: lengthening and shortening it; curling and uncurling it; and flattening its surface. Also, some of them assist the tip, others influence the middle regions of the tongue. The action of some is not visible from outside. Figure 4.7D shows a human tongue with the muscles acting in different sections.

4.11 Discussion

Even though most organs have similar function in all dogs, dog head anatomy is very diverse. A good way to make the Londra model generic to other dog breeds would be using conformational parameters to reshape the skull, the mandible and to relocate the teeth, according to that. Apart from the basic Cephalic and Craniofacial indices, parameters to go from long to short head can include a measure for all the differences among breeds explained in the above sections (Sections 4.2 and 4.3). For example:

- sagittal crest prominence.
- Prognathism-Brachygnathism index.
- Mandible divergence angle.
- Nuchal crest prominence.
- Temporal fossa width.
- Frontonasal suture angle.
- Relative position of teeth.

Other facial organs could be extended to have some generality. Some additional conformational parameters could be:

- Eyeball radius. Note that the eye orbit and eye ball presents little size and shape changes among different breeds (Sisson *et al.* (1975)). Probably, that is why small breeds look as though they have very big eyes.
- Nose groove length.
- Ear type.
- Parameters related to colour.

Movement of the articulations in the head can be modelled with biomechanics. However, in dogs, jaw movements are similar to those of a hinge and can be simplified with simple geometric transformations (e.g. rotations of the mandible with respect to a centre). In Londra, kinematic jaw motion is performed first and deformation of the skin due to the muscles is obtained next. Transformations are performed uniformly as the mandible is rigid and homogeneous.

Section 4.5 explains the points of contact in occlusion for an average dog. However, in extreme breeds (e.g. Boxer, Greyhound) this can vary a lot. Londra's mechanism involved kinematics knowledge. As a consequence, the technique easily adapts the points of contact to any shape making it suitable for conformational generalisation and simplifying jaw motion.

Londra includes a selection of organs which are important for facial expression display in the dog model created from one source skull. As expected, accuracy and complexity of the model can be enhanced or simplified depending of the number of organs and movements and the techniques used. For example, we chose 23 representative muscles which allowed us to generate a skin and several typical skin deformations. Some muscles with a less evident effect on the facial skin were ignored and the movement was performed with kinematics only (e.g. eyes, tongue). Also, some techniques (e.g. jaw motion, skin generation, skin deformation) are ready for a generic model. Other techniques require further work (e.g. Skull reshape). Overall, we demonstrate that it is possible to generate typical dog expressions with the chosen subset of organs. Also, we show some potential for generalisation.

The tongue is a complex organ formed by several muscles (Section 4.10). However, we see that these muscles act in different tongue regions (e.g. tip, middle, back). For instance, to simplify the model, we decided to divide the tongue into a number of interacting regions and to limit its kinematics to a number of expressive postures. However, tongue motion can be easily extended. Other not very visible organs were not included and the lips were simplified. In the future these could be included to enhance Londra's appearance (e.g. Palate, internal glandules).

Chapter 5

Dog facial coding

5.1 Facial measurement systems

Facial measurement systems measure spontaneous facial expression in humans. Next, we briefly describe some of them:

- The Facial Action Coding System (FACS): It is comprehensive and applicable to all observable expression in human faces (Ekman and Rosenberg (1998)). It is anatomically derived.
- Maximally Discriminative Facial Movement Coding System (MAX): It is selective and only recognizes the universal expressions in infants (Knudsen *et al.* (2002)). It is theoretically derived.
- EMFACS, emotional FACS: It is a selective subset of FACS and scoring the expression of simple human emotions only. It is anatomically derived (Ekman and Rosenberg (1998)).
- Facial electromyography (EMG): It is comprehensive and capable to detect muscular activity not observable by the naked eye (Ekman and Friesen (1978)). However, it is obtrusive and can suffer from interference, leading to other interpretations. It is anatomically derived by measuring electrical potentials from facial muscles to infer muscular contraction.
- MPEG-4 facial animation parameters: It is comprehensive and suitable for realistic human face animation and for cartoon-like animation. It is theoretically derived and defines facial definition parameters to encode the face geometry and

facial animation parameters to deform the face (Chen (2006)). Here, a neutral face and a set of facial features (FPs) are specified. A set of facial actions (FAPs) deform the neutral face. FAPs are defined in face animation parameter units (FAPUs) which are computed from spacial distances between major facial features. FAPs are suitable for web applications and only consider the spatial control (Chen (2006)).

Coding systems describe expressions in terms of constitutive components (action units, AUs, in the case of FACS and MPEG-4).

5.2 From FACS to DFACS

EMFACS, commonly referred as FACS, was the most suitable coding system to inspire our Dog FACS (DFACS). Even though it was designed for scoring expressions, it has been widely used for expression synthesis in HFAMs. The way EMFACS was built allows easy extension to other live beings once the facial anatomy of the creature is understood. For example, it is clear which muscles are responsible for specific AUs making it closer to anatomy. Additionally, we only need AUs for a selection of expressions and we will use them for synthesising expressions. The main differences are that we focused on dog expressions and that we derived DFACS theoretically to avoid the use of real animals. Other coding systems such as MPEG-4 and MAX are more difficult to adapt to the animal context. For example, MPEG-4 is tightly integrated to human face proportions.

5.3 EMFACS

Table 5.1 shows the 16 EMFACS' AUs (Ekman and Friesen (1978)). Table 5.2 shows the AU based description for the human universal expressions. Figure 5.1A shows the basic human anatomy.

5.4 DFACS

Table 5.3 shows the 19 DFACS' AUs and 17 counter AUs. In DFACS several AUs were implemented with muscle actuations. However, AUs where no significant skin deformation was produced by the muscle were implemented with kinematics or with a

Table 5.1: EMFACS

AU	FACS name	Muscle
1	Inner Brow Raiser	Frontalis
2	Outer Bow Raiser	Frontalis
4	Brow Lower	Depressors Glabellae and Supercilli, Corrugator
5	Upper Lid Raiser	Levator Palpebrae Superioris
6	Cheek raiser	Orbicularis Oculi
7	Lid tightener	Orbicularis Oculi
9	Nose wrinkler	Levator Labii Superioris, Alaeque Nasi
10	Upper lid raiser	Levator Labii Superioris, Caput Infraorbitalis
12	Lid Corner puller	Zygomatic
14	Dimpler	Buccinator
15	Lip corner depressor	Triangularis
16	Lower lip depressor	Depressor Labii
17	Chin raiser	Mentalis
20	Lip stretcher	Risorius
23	Lip tightener	Orbicularis Oris
26	Jaw drop	Maseter, Temporalis and Pterygoid

Table 5.2: Universal human expression, from Noh and Neumann (1998) p.4

Expression	Involved AUs
Surprise	AU1,2,5,15,16,20,26
Fear	AU1,2,4,5,15,20,26
Disgust	AU2,4,9,15,17
Anger	AU2,4,7,9,10,20,26
Happiness	AU1,6,12,14
Sadness	AU1,4,15,23

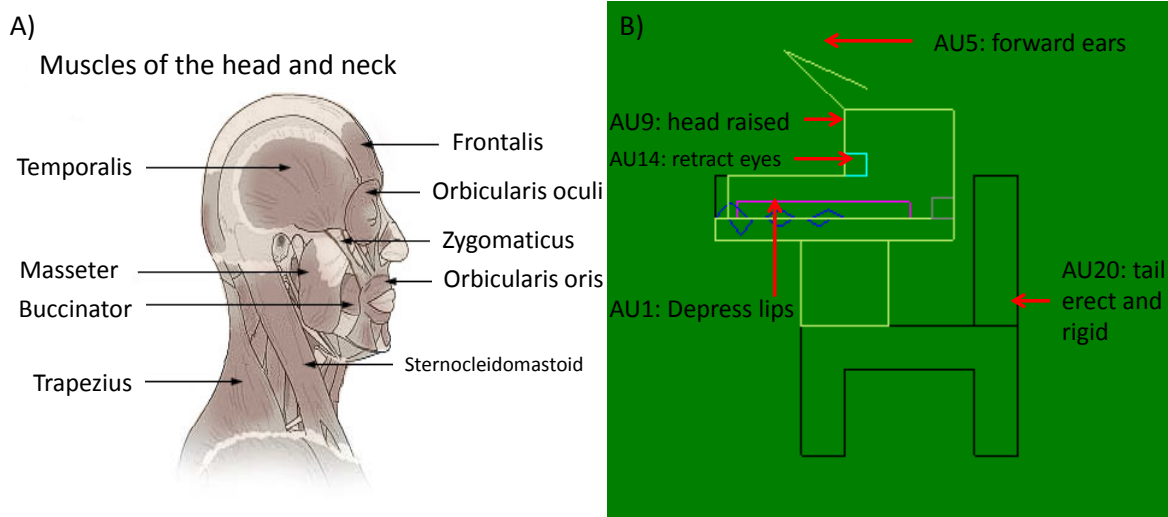


Figure 5.1: Coding expressions. A) Human facial muscles (Wikimedia Foundation (2009d)). B) Anger in dogs.

mixture of kinematics and muscle actuations. For instance, some muscles were ignored and are not explained (e.g. Buccinator in AU2; Malaris in AU4; Auriculares Caudales and Ventrals in AU 5 and 6; Pterigoyd in AU 7 and 8; muscles of the neck eyes and tongue). Refer to Figure 4.5B and Section 4.6 for an explanation of the muscles used.

One natural way to connect Londra to a body and include complete expressions with facial movement and body posture is to extend DFACS to include AUs that alter the body. Some of the potential AUs are shown in Table 5.4. Of course, this approach requires more detailed study for a proper implementation.

We adapted descriptions from Darwin (1890) and our video observations to Londra. For example, our anger takes the original hostile intention description, and mixes it with the anger description by raising the lips. Then, according to our video observations displays the tongue for a moment. We implemented two forms of affection which are very similar. The main difference is that the second form is enhanced with licking. Also, we included Darwin’s fear, happiness and attention and added two expressions, yawning and smelling. Figure 5.1B shows the use of DFACS’ AUs to display one version of anger. Here our first version of Londra is used to illustrate the expression.

Table 5.5 shows one AU based description for Londra’s expressions.

Figure 5.2 shows DFACS’ action units. Figures 5.3, 5.4, 5.5 show Londra’s expressions.

Figure 5.6A shows the dialog box to display expressions and AUs. It contains parameters such as U and V to indicate eye direction of sight (if it is important in the

Table 5.3: DFACS

AU	Description	Muscle	Counter AU
1	Depress Lip	Orbicularis Oris, Levator Mentalis	Relax lip
2	Contract Mouth Corner	Zygomaticus	Relax mouth corner
3	Dilate Nostril	Levator, kinematics	Relax Nostril
4	Depress Eyelids	Levator oculis, frontalis orbicularis oculis	Relax Eyelids
5	Forward ears	Auriculares rostrales and dorsales Frontalis, Ear's kinematics	Backward ear
6	Raise ears	Auriculares rostrales Frontalis, Ears' kinematics	Lower ears Lower ears
7	Open Mandible	Masseter, Temporalis, Digastricus Orbicularis Oris, Jaw kinematics	Close mandible
8	Left Mandible	Masseter, Temporalis, Digastricus Orbicularis Oris, Jaw kinematics	Right Mandible
9	Raise head	Head kinematics	Lower head
10	Left head	Head kinematics	Right head
11	Twist head	Head kinematics	Untwist head
12	Left eyes	Eyes and gaze kinematics	Right eyes
13	Raise eyes	Eyes and gaze kinematics	Lower eyes
14	Retract eyes	Eyes and gaze kinematics	Relax eyes
15	Blink eyelid	eyelid kinematics	N/A
16	Lick	Tongue kinematics	N/A
17	Roll tongue	Tongue kinematics	Unroll
18	Show tongue tip	Tongue kinematics	Hide tongue tip
19	Draw tongue	Tongue kinematics	Hide tongue



Figure 5.2: AUs in DFACS. Refer to Appendix K for videos.



Figure 5.3: Expressions in Londra. Anger and Affection I. Refer to Appendix K for videos.



Figure 5.4: Expressions in Londra. Affection II, Attention, Fear, Happiness. Refer to Appendix K for videos.

Table 5.4: Extending AUs to body postures

AU	Description	Counter AU
20	Raise tail	Lower tail
21	Roll tail	Unroll tail
22	Raise paw	Lower paw

Table 5.5: Expressions in Londra. A preceding '-' refers to the counter AU

Expression	Involved AUs
Anger	AU14,4,1,2,5,7,18
Affection I	AU-14,9,-9,9,-9,10,-10,10,-10,9
Affection II	AU-14,-9,9,7,16
Attention	AU12,13,6,11,9
Fear	AU-14,-5,-9
Happiness	AU6,9
Yawning	AU17,7,-17,19
Smelling	AU3,-3



Figure 5.5: Expressions in Londra. Yawn and Smell. Refer to Appendix K for videos.

expression or AU); and iterations for AUs that can be repeated. To the right of this box we find Londra's different visualisation options. Figure 5.6B shows a set of sliders to 'puppet' basic Londra movements.

5.5 Discussion

Sometimes there are some analogies among different species [6]. However, by looking at the EMFACS and DFACS, it is evident that frequently, muscles with the same name perform a different function. Some muscles are just different. Londra is mainly based on Darwinian expressions. However, we complemented some from our video observations.

DFACS is a selective model used to model dog expressions. It has been built theoretically from the knowledge gained from dog anatomy books. It is built upon AUs. It is specific for dogs. Here, AUs can vary in intensity, can be repeated or organised in different ways as expressions are not absolute and are not necessarily reached the same way.

DFACS introduces new action units such as those related to ear movements, which are not useful in human expressions. DFACS could be a comprehensive model for dog faces by including a few more muscles and adding more AUs which could include body postures. Also, it could be further verified by a zoologist in order to look for potential simplifications and inaccuracies. However, it actually offers a first set of parameters for Londra which produces a nice set of recognisable expressions (Chapter 15).

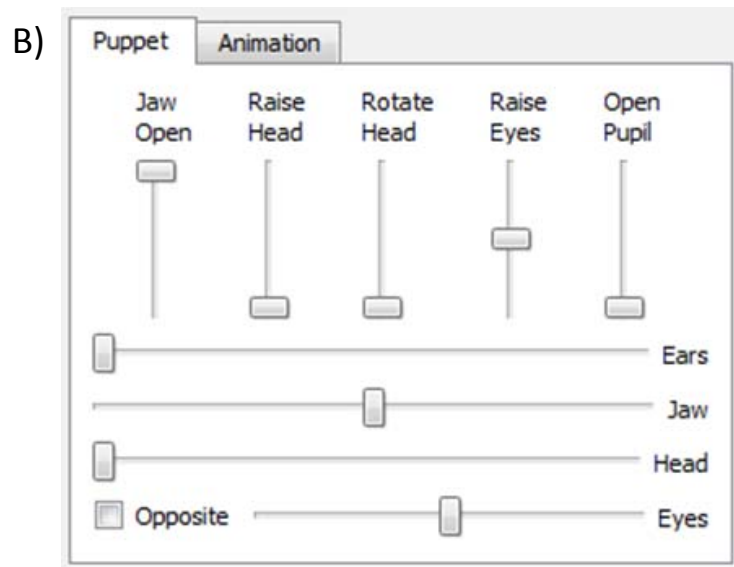
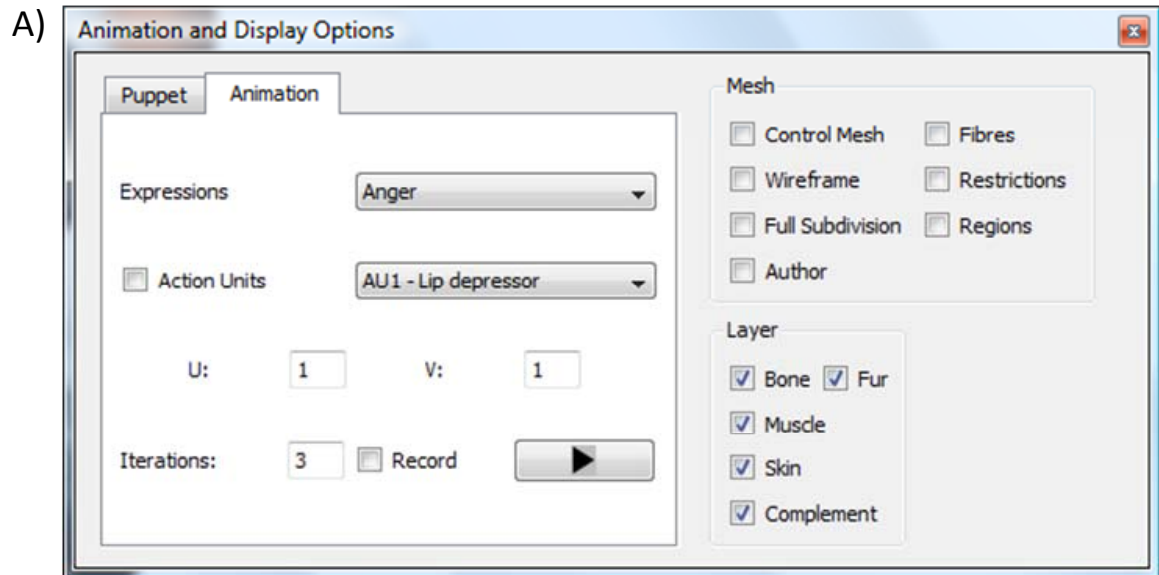


Figure 5.6: Displaying Londra. A) Dialog box for AUs, expressions and visualisation options. B) Puppet controls.

Chapter 6

Efficient Mesh Generation Using Subdivision Surfaces

Note: much of the text of this chapter comes from my own published work at Navarro Newball *et al.* (2008a). Some information was updated.

Polygonal meshes are commonly used for defining the shape of an object. In Londra, they are used for modelling organs such as the skull and the skin. We implemented a method to create and smooth polygonal meshes. This is particularly important in Londra's skin, where a polygonal mesh is created from the underlying anatomy and a smoothing phase takes place after deformation.

6.1 Overview

In order to generate a mathematical surface we need to establish continuity and neighbourhood relation between samples. Complex shapes require piecewise representations and are split into sub-regions each one of which is defined by an individual function. These representations are just approximations of the surface. In order to decrease the error one can use more segments or sub-regions. Operations required by surfaces include evaluation, query and modification. Evaluation refers to the sampling of the surface and its attributes. Query identifies if a given point $p \in R^3$ is inside or outside the solid bounded by the surface. Modification refers to geometry changes such as surface deformations or topology changes. There are two major classes of representation (Botsch *et al.* (2007)). Parametric representations are defined by a vector valued parameterization function. Implicit representations are defined by a zero set of a scalar valued function. Parametric representations are better for evaluation and modification,

implicit representations are better for query (Botsch *et al.* (2007)).

Polygonal meshes approximate a surface by a mesh of planar polygonal facets. They are low complexity representations more efficient for rendering. Triangular meshes remain the most used structure for 3D modelling. In DeRose *et al.* (1998) they argue that quadrilaterals are better than triangles capturing the symmetries of objects and that they are compatible with bi cubic patches used in commercial software. However, in Botsch *et al.* (2007) they state that triangles are increasingly popular because they allow more flexible and efficient processing and avoid conversion errors. We decided to follow the approach from Botsch *et al.* (2007) and use triangular meshes. Additionally, we found that subdivision surfaces are an appropriate way to generate and create parametric polygonal meshes. They reduce the representation of a complex surface to a simpler control mesh that is able to generate refined surfaces.

6.2 Triangular meshes

Frequently, triangular meshes are considered as a coarse collection without a mathematical representation. Problems arising from a coarse mesh include little connectivity information (triangle soups), inconsistent normal orientations, gaps, intersecting patches and degenerate elements such as triangles with zero area. However, an acquired coarse mesh can be used as an input to produce an enhanced one (i.e. using subdivision surfaces) (Botsch *et al.* (2007); Watt and Policarpo (2001); Doo (1978)). A parametric triangular mesh M can be described as $M(P, K)$, where $P = \text{Set of } N \text{ positions } p_i(x_i, y_i, z_i) \in R^3$ and K contains the description of the topology. Triangular meshes are the most simple and flexible continuous surface representation where only C^0 continuity is required (Botsch *et al.* (2007)). Here, complex surfaces are formed by triangular pieces with a linear parameterisation function with an approximation error of $O(h^2)$, where h is the maximum edge length. The valence of a vertex is the number of vertices in its neighbourhood (vertices connected to it by edges). In semi-regular triangular meshes, most of the vertices have a valence of 6. Vertices with a different valence are called extraordinary vertices. An important topological quality of a surface is whether or not it is two-manifold, which is the case if for each point the surface is locally homeomorphic to a disk (or a half disk at boundaries). A triangle mesh is two-manifold, if it does neither contain non-manifold edges or non-manifold vertices, nor self-intersections. A non-manifold edge has more than two incident triangles and a non-manifold vertex is generated by pinching two surface sheets together at that

vertex, such that the vertex is incident to two fans of triangles' (Botsch *et al.* (2007), p.19).

6.2.1 Data structures for triangular meshes

Efficient data structures allow local and global traversal of a mesh (Botsch *et al.* (2007)):

- Access and enumeration of individual vertices, edges, faces.
- Oriented traversal of edges of a face (next edge in a face).
- Access to at least one face attached to a given vertex.

The Direct Edges data structure is the most efficient to deal with triangular meshes (Botsch *et al.* (2007)). Here, each edge is represented as two opposing halfedges consistently oriented counter clockwise, (Figure 6.1A). It is based on indices as references to each element where indexing follow rules to implicitly encode connectivity information. indices and references are explained below:

- f : Index of a face.
- $H(f, i)$: Get halfedge (f, i) from face number.

$$H(f, i) = 3f + i, \text{ with } i \in \{0, 1, 2\} \quad (6.1)$$

- h : Index of a halfedge.
- $A(h)$: Adjacent face from halfedge. $A(h) = h \div 3$
- $N(h)$: Next halfedge . $N(h) = (h + 1) \bmod 3$

This data structure is only useful for triangular meshes and provides no explicit representation of edges (though it can be specialised to other polygons). It groups the three halfedges belonging to a common triangle. Additional information is explicitly stored in arrays. For instance, for each vertex, the index of an outgoing halfedge is stored and; for each halfedge, the index of its opposite half edge and the index of the vertex the halfedge points to are stored. Boundaries are managed with special negative indices that indicate that the edge vertex is invalid.

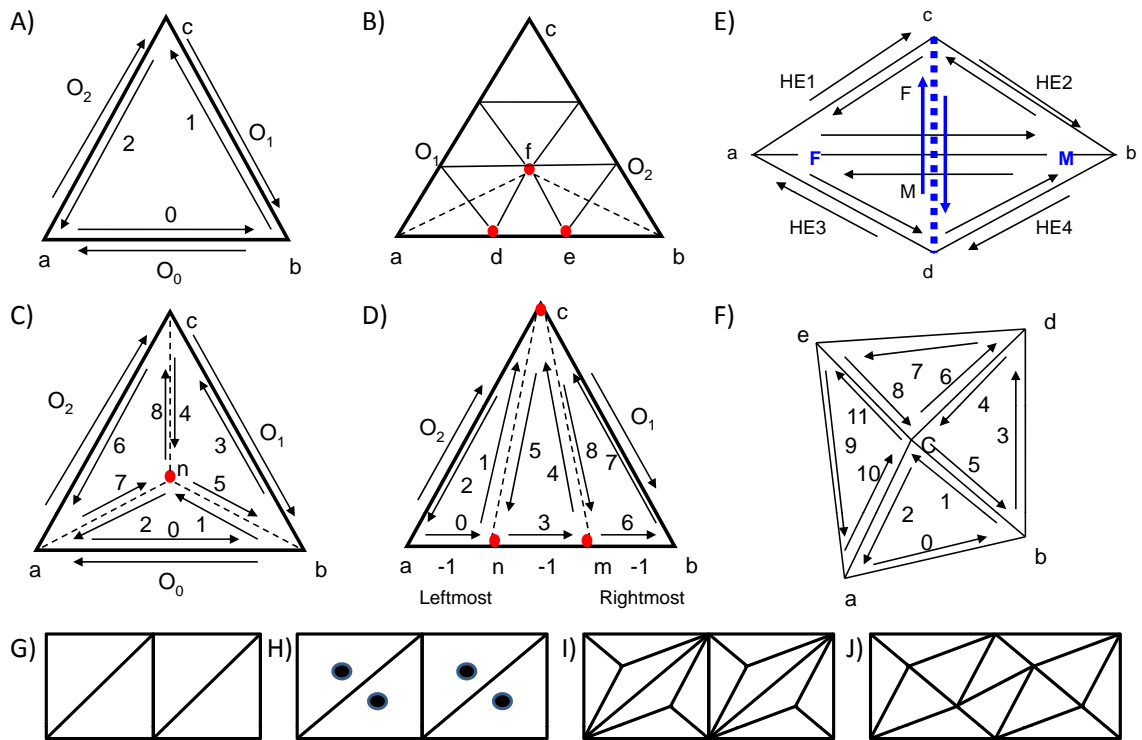


Figure 6.1: Subdivision with the Direct Edges data structure. A) Non subdivided face and edges. B) New vertices at boundary. C) Subdividing a regular face. D) Subdividing a boundary face in odd step. E) Flipping edges. F) Neighbourhood. G) Original mesh. H) Middle point. I) Split triangles. J) Flipping edges

6.3 Subdivision surfaces

Subdivision surfaces help in the creation and refinement of 3D mesh models. They are capable of representing an arbitrary geometrically unrestricted topology. They produce an efficient hierarchical structure and an object can be modelled as a low resolution control mesh from which we can generate new meshes by refining the previous one. Some subdivision methods such as Catmull and Clark (Watt and Policarpo (2001)) work on quadrilaterals or extend subdivision to a n-sided problem and are not restricted to triangles such as Doo (1978); Doo and Sabin (1978). Others such as butterfly (Watt and Policarpo (2001)), $\sqrt{3}$ Subdivision (Kobbelt (2000)) and Loop (1987) are specialised on triangles. Loop (1987) Has been widely used (Zorin (1998); Lee *et al.* (1998, 2000)).

One can define: $M^0(P^0, K^0)$ as the original coarse mesh (which can be used as the control mesh) and $M^j(P^j, K^j)$ as the j times subdivided mesh. Here, P^j are the mesh points at level j of subdivision and K^j contains the description of the topology at level j . M^j , with $j \rightarrow \alpha$ is the approximation of a B spline limit surface. A subdivision scheme S takes the vertices from level j to level $j+1$ so that $S(K^j) = K^{j+1}$. A subdivision matrix or stencil SM maps a mesh M^j to a topologically equivalent refined mesh M^{j+1} . Eigenvalues or characteristic roots are a special set of scalars associated with linear systems of equations such as matrix equations. In a subdivision scheme S , the eigenvalues of the subdivision matrix are important to determine if the method converges to a limit smooth surface. For instance, all subdivision schemes must guarantee adequate design of the SM stencil such that eigenvalues have a certain distribution and a continuous surface approximating the limit surface can be generated (Kobbelt (2000); Zorin (1998)). In SM , every row is a rule to compute the position of a new vertex and every column tells how one old vertex contributes to the vertex positions in the refined mesh (Botsch *et al.* (2007)). In stationary methods the refinement functions are the same for every subdivision level. However, different rules are applied to define sharp features, creases or to deal with extraordinary vertices (Zorin (1998)). Also, stop conditions can be used for adaptive refinement (Kobbelt (2000)). In some methods old vertices are re positioned for smoothing (Kobbelt (2000)).

6.3.1 Subdivision techniques for triangular meshes

Butterfly subdivision (Watt and Policarpo (2001); Zorin (1998)) converts each face into four using edge vertices. Artefacts and discontinuities are produced in vertices with

valence different from 6. It never produces smooth surfaces on extraordinary vertices and incorrect smooth regions can appear near high valence vertices due to eigenclustering (more than one eigenvalue per matrix). It is based on dyadic split (divide every edge in two) and does not produce C^2 continuity. The modified butterfly deals with artefacts of the original butterfly (Watt and Policarpo (2001)). It approximates the behaviour of a C^2 surface based on dyadic split. Here, eigenclustering is avoided. Loop subdivision (Zorin (1998)) is one of the simplest C^1 subdivision schemes. Here, stencils are smaller and convergence rate is better than in modified butterfly. It is based on dyadic split and is not C^2 at extraordinary vertices. The scheme does not look smooth for large valences, due to eigenclustering. The modified Loop (Zorin (1998); Stam (1998)) increases the stencil in a minimal way around a vertex and avoids eigenclustering. Here, vertices have better structure at extraordinary points. However, ripples appear. The ternary Loop subdivision (Loop (2002)) uses three stencils. It achieves bounded curvature, manifold support, and convex hull. It is C^2 continuous. However, No rules have been defined to deal with boundaries or with sharp features.

$\sqrt{3}$ Subdivision (Kobbelt (2000)) is a stationary subdivision scheme with slower topological refinement with trisection of every original edge (two new vertices are introduced for every original edge every two steps). It inserts a new vertex at the centre of every face (figures 6.1G and H). Then, it creates the new faces (Figure 6.1I) and flips every original edge (Figure 6.1J). To do that, it uses simple stencils of minimum size and maximum symmetry. Here, a new vertex is calculated as the average of the three old ones (a new vertex only affects one face). Then, the old ones are relaxed using (6.2). Relaxation occurs so that 'the eigenvalues of the subdivision matrix have a certain distribution and a local regular parameterization exists in the vicinity of every vertex on the limit surface' (Kobbelt (2000), p. 104). The scheme uses a generation index to perform adaptive refinement and allows sharp feature lines. It is C^2 continuous except at extraordinary points. All new vertices have valence 6 and the valence of the old ones is not changed. We chose this method because it produces more levels of subdivision with lower number of triangles and simpler rules.

$$\begin{aligned}
 S(p) &= (1 - \alpha_n)p + \alpha_n \frac{1}{n} \sum_{i=0}^{n-1} p_i, \text{ where} \\
 \alpha_n &= \frac{4 - 2 \cos(\frac{2\pi}{n})}{9} \\
 n &= \text{valence} \\
 S(p) &= \text{relaxation stencil}
 \end{aligned}
 \tag{6.2}$$

6.4 $\sqrt{3}$ subdivision using the Direct Edges data structure

In our implementation, a main subdivision cycle calculates the subdivision surface until it reaches the number of levels defined by the user. In each level, the algorithm performs three tasks. First, it calculates the new vertices in each face. Here, if it is a non-boundary subdividable face or a boundary face in an even level (6.1C), the mid point is obtained and three faces are created. If the face is not subdividable then one face is recreated (6.1A). If the face is a boundary face and the level of subdivision is odd, two new vertices are calculated and three faces are created (6.1D). After the faces have been subdivided a mesh similar to that shown in Figure 6.1I is produced. The next task is to flip the edges in each face of the new subdivided mesh. Here, the edges are flipped only if the face and its mate are sub dividable and non-boundary or, when the face belongs to a boundary at an odd level of subdivision. After the edges have been flipped a mesh similar to that shown in Figure 6.1J is produced. The final task is to re-position the three old vertices in each face. Calculations are done taking care of avoiding boundary vertices, because these can cause visible discontinuities. Here, the calculation of the vertex's neighbourhood is required. Appendix E shows the algorithms for the previous steps.

6.4.1 Memory allocation

Every time the calculations for a new level of subdivision start, the memory is allocated according to the new needs. At level 0, memory for the control mesh is allocated according to the number of vertices, faces and halfedges, see Appendix F. Memory for subsequent levels of subdivisions is calculated according to (6.3), (6.4) and (6.5). Here:

- NV = Number of vertices.
- NF = Number of faces.
- NHE = Number of halfedges. 3 halfedges per face.
- OVN = Old number of vertices.
- NSF = Number of subdividable faces. One new vertex per face.
- NBF = Number of boundary faces. Two new vertices per face.

- ONF = Old number of faces (each subdividable one produce 3 new ones).
- NNF = Number of non subdividable faces.

$$NV = OVN + NSF + 2NBF \quad (6.3)$$

$$NF = (ONF - NNF)3 + NNF \quad (6.4)$$

$$NHE = ((ONF - NNF).3.3) + 3NNF \quad (6.5)$$

6.4.2 Assigning halfedges and counting

Our main challenge was to keep track of the halfedges after each task. Assigning correct halfedges numbers is very important before flipping, otherwise the mesh will be corrupted. The naive solution is to create costly loops to find and assign halfedge numbers. However, counting helps to use the Direct Edges data structure efficiently.

The first and easiest thing is to calculate the interior halfedges using (6.1). For example, a face F has three interior halfedges. These are assigned counter clock wise starting from vertex a . For instance:

- Halfedge 0 goes from a to b .
- Halfedge 1 goes from b to c .
- Halfedge 2 goes from c to a .

Figure 6.1A shows the halfedge numbers for face $F = 0$. In the regular case (Figure 6.1C) an old face produces 9 new halfedges. Assuming face $[a, b, n]$ as Face 0; $[b, c, n]$ as Face 1 and $[c, a, n]$ as Face 2, the halfedge values are easily obtained with (6.1). At boundaries (Figure 6.1D) faces are created differently. Here, we assumed the leftmost face as Face 0, the middle one as Face 1 and the rightmost as Face 2.

Finding the values for the opposite halfedges (exterior) is more difficult. Let $G = 0$ be our face. Finding the values for the exterior halfedges for Face G requires counting. Let us suppose that before subdivision (Figure 6.2):

- Face F_0 is the neighbour face that contains Halfedge O_0 which is opposite to Halfedge 0 from face G .

- Face F_1 is the neighbour face that contains Halfedge O_1 which is opposite to Halfedge 1 from face G .
- Face F_2 is the neighbour face that contains Halfedge O_2 which is opposite to Halfedge 1 from face G .

The index for the 0 halfedge (HEZERO) of face F_0, F_1 or F_2 can be obtained from (6.6). Here:

- $HEZERO$ = Halfedge number.
- F = Current face number.
- N = Number of non subdividable faces before F .

$$HEZERO = ((F - N)9) + 3N \quad (6.6)$$

However, we need to identify if halfedges O_0, O_1, O_2 correspond to the halfedges 0, 1 or 2 from faces F_0, F_1, F_2 . For example, for Face F_0 (faces F_1 and F_2 use similar calculations):

- If $O_0 = 3F_0$ then the O_0 is F_0 's halfedge number 0.
- If $O_0 = 3F_0 + 1$ then the O_0 is F_0 's halfedge number 1.
- If $O_0 = 3F_0 + 2$ then the O_0 is F_0 's halfedge number 2.

Now we know if O_0 corresponds to the 0, 1, or 2 halfedge from face F_0 before subdivision. As new halfedges will be created, we need to identify what will be the new halfedge number for O_0 after F_0 has been subdivided. There are several cases:

- F_0 is a subdividable face or F_0 is a boundary face in even level of subdivision: if O_0 before subdivision is F_0 's 0 halfedge, then its new value is $O_0 = HEZERO$. If O_0 before subdivision is F_0 's 1 halfedge, then its new value is $O_0 = HEZERO + 3$. If O_0 before subdivision is F_0 's 2 halfedge, then its new value is $O_0 = HEZERO + 6$.
- F_0 is a non subdividable face: if O_0 before subdivision is F_0 's 0 halfedge, then its new value is $O_0 = HEZERO$. If O_0 before subdivision is F_0 's 1 halfedge, then its new value is $O_0 = HEZERO + 1$. If O_0 before subdivision is F_0 's 2 halfedge, then its new value is $O_0 = HEZERO + 2$.

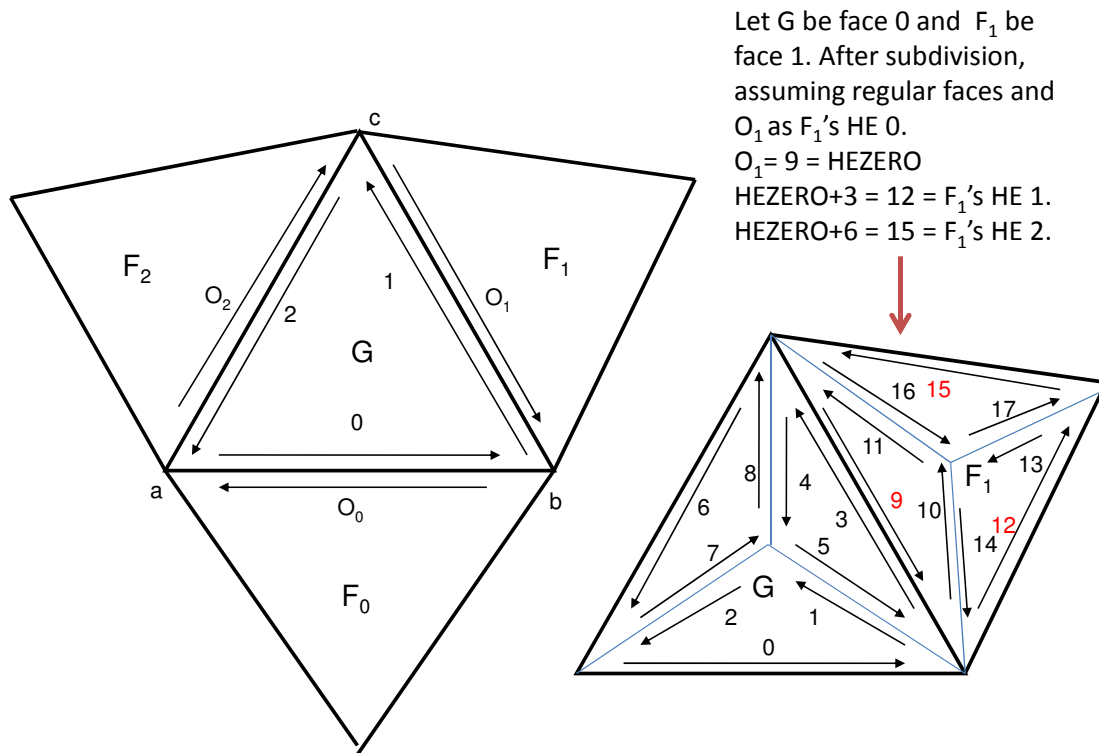


Figure 6.2: Opposite halfedges O_0 , O_1 and O_2 for halfedges 0, 1 and 2 in face G .

- F_0 is a subdividable boundary face in odd level of subdivision: here, the new three triangles are arranged differently from the regular case (figures 6.1C and D), this affects the way we count. Here, if O_0 before subdivision is F_0 's 0 halfedge, then its new value is $O_0 = \text{HEZERO}$. If O_0 before subdivision is F_0 's 1 halfedge, then its new value is $O_0 = \text{HEZERO} + 6$. If O_0 before subdivision is F_0 's 2 halfedge, then its new value is $O_0 = \text{HEZERO} + 2$.

Calculating the new interior opposite halfedges (1, 5, 4, 8, 7, 2 in Figure 6.1C and 1, 5, 4, 8 in Figure 6.1D) is straightforward. Here, Halfedge 1 of one new face is next to Halfedge 2 of the other one (6.7). Opposite halfedges to the 0 halfedge of new boundary faces are assigned -1 (non existent).

$$\text{OppositeOf}(3F + 1) = (3(F + 1)) + 2, \text{ with } F = \text{face number} \quad (6.7)$$

6.4.3 Splitting

A new vertex n in a regular face (Figure 6.1C) is obtained from (6.8)(Kobbelt (2000)). At boundaries (figures 6.1B and D), every odd subdivision level two new vertices are calculated in the edge of the boundary and the centre of the boundary triangle is displaced as in (6.9), (6.10) and (6.11)(Kobbelt (2000)).

$$n = 1/3(a + b + c) \quad (6.8)$$

$$d = 1/27(16a + f + 10b) \quad (6.9)$$

$$e = 1/27(10a + f + 16b) \quad (6.10)$$

$$f = 1/27(4a + 19f + 4b) \quad (6.11)$$

Sub triangles from $[a, b, c]$ are built counter clock wise as $[a, b, n]$, $[b, c, n]$ and $[c, a, n]$ (Figure 6.1C), leaving their 0 halfedge to coincide with an old edge in the subdivided face. Sub triangles at a boundary face in an odd level of subdivision are arranged from left to right (Figure 6.1D). Here $[a, b, c]$ is refined with $[a, n, c]$, $[n, m, c]$ and $[m, b, c]$. Note that the halfedge 0 of each new face is made to face the border.

6.4.4 Swapping faces.

The idea of swapping is to implement the “flipping edges” stage of the $\sqrt{3}$ subdivision method. here, the idea is to get better formed triangles. In Figure 6.1E, face $F[a, b, c]$ is going to be swapped with face $M[b, a, d]$. Let us assume that F is a regular face. Swapping cannot be achieved if:

- M has already been swapped in the current subdivision level.
- M is a boundary face.
- M is a non subdividable face.

If swapping is possible the old opposite halfedge values $HE1$, $HE2$, $HE3$ and $HE4$ have to be stored and reassigned in order to keep consistency and connectivity. Then, the two faces are swapped as shown with the dotted line and the new 0 halfedge is

Table 6.1: Swapping face number F and face number M . Half edge number obtained according to (6.1)

$F[d, c, a]$ halfedges	Opposite	$M[c, d, b]$ halfedges	Opposite
0: $F3$	$M3$	0: $M3$	$F3$
1: $(F3) + 1$	$HE1$	1: $(M3) + 1$	$HE4$
2: $(F3) + 2$	$HE3$	2: $(M3) + 2$	$HE2$

assigned along this line for each face in this new arrangement. The new faces are described in Table 6.1.

A boundary face in an odd level is swapped only if the same conditions for regular swapping are met (except that M could have been swapped). Only the leftmost and rightmost faces (Figure 6.1D) are candidates for swapping, the middle face remains the same. Here (Figure 6.1B) flipping requires the re-arrangement of triangles $[a, f, O_1]$ and $[a, d, f]$ to triangles $[O_1, d, f]$ and $[d, O_1, a]$ and triangles $[f, b, O_2]$ to $[e, b, f]$ to triangles $[e, O_2, f]$ and $[O_2, e, b]$ producing a boundary strip of five triangles (in this example O_1 and O_2 are points).

6.4.5 Detecting boundaries and subdividable faces

A boundary face is detected by checking if it contains at least one -1 valued opposite halfedge. A flag is assigned to each boundary vertex. In Figure 6.1A:

- a is a boundary vertex if the opposite of halfedge 0 or 2 is next to a boundary face.
- b is a boundary vertex if the opposite of halfedge 0 or 1 is next to a boundary face.
- c is a boundary vertex if the opposite of halfedge 1 or 2 is next to a boundary face.

Not keeping track of the boundary vertices may produce distortion. The detection of a subdividable face was not implemented. Under certain flatness criteria (based on differential geometry) a face could be tagged as non-subdividable.

6.4.6 Calculating a neighbourhood

This calculation returns the number of neighbours of a vertex and their average coordinate value. In Figure 6.1F vertex C has four neighbours (a, b, e, d) and their average

is obtained with (6.12). Our implementation deals with closed manifolds, boundaries and distorted polygons. Let us assume that the first detected outgoing halfedge in Figure 6.1F is $HE2$. First, we add vertex a to the average and increment the number of neighbours. Then, we find the opposite halfedge (in this case 10). If it is the 2 halfedge of the next face we subtract 2 in order to find the halfedge which points to the next vertex. If it is the 0 or 1 halfedge of the next face we add 1 in order to find the halfedge which points to the next vertex. Then, we add this vertex to the average and increment the number of neighbours. The algorithm continues until the halfedge pointing to the next vertex is equal to the first halfedge or until an edge or a distortion is detected (see Appendix E).

$$A(C) = (a + b + e + d)/4, \text{ where } A(C) = \text{Average of the neighbours of vertex } C \quad (6.12)$$

6.5 Results

The size of one vertex, one polygon and one halfedge can be easily calculated according to the data in Appendix F. According to (6.3), (6.4) and (6.5) for a mesh object in a subdivision step the size in bytes can be found from (6.13). The complexity $O(n)$ for the main subdivision routine can be approximated by (6.14), because all values can be approximated in terms of F with the Euler formulas (Botsch *et al.* (2007)). It estimates time for the three main procedures (e.g. splitting, flipping and repositioning). The number of elements growth is shown in Figure 6.3E. Here, it can be seen that the number of regular faces and the number vertices have an exponential growth, while the growth of the number of boundary faces is much slower and behaves linearly. The number of non-subdividable faces remains constant. Meshes produced are shown in figure 6.3A, B, C and D. Figure 6.3F shows a dialog box to choose the mesh to subdivide, indicate the number of subdivision levels and visualise the number of elements in the output.

$$Size = (160NV + 224NF + 64NHE)/8 \quad (6.13)$$

$$\begin{aligned}
O(n) &= O(LFI), \text{ where} \\
L &= \text{Subdivision levels number} \\
F &= \text{Faces number} \\
I &= \text{Neighbourhood size (insignificant in big meshes)}
\end{aligned} \quad (6.14)$$

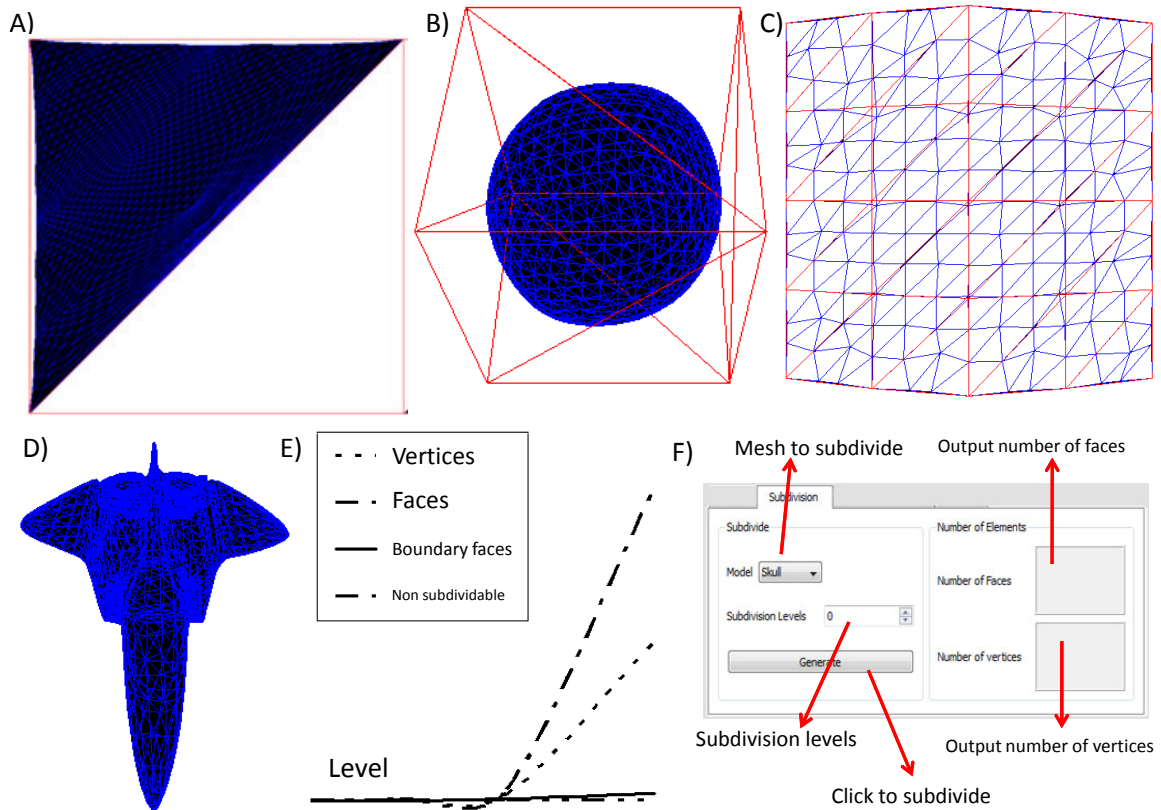


Figure 6.3: Subdivision of arbitrary surfaces. A) Mesh with boundaries and 1 non-subdividable face (7 levels). B) Limit and control surface of a cube (4 Levels). C) Big plane with boundaries (2 levels). D) Spaceship (2 levels). E) Element increase in $\sqrt{3}$ subdivision. F) Subdivision dialog box.

6.6 Discussion

Parametric triangular meshes allow efficient validation (used for display) and modification (especially when defined with subdivision surfaces). We used them, because due to their popularity, many methods for processing them have been developed. Coarse meshes may bring distorted triangles and edges. However, we manage them with the definition of proper stop conditions. Our implementation can be applied to an arbitrary mesh. The understanding of the Direct Edges data structure allowed efficient implementation. Here, counting was essential in memory allocation and in keeping track of the halfedges for each new face. It allowed the effective implementation of the basic operations required by the subdivision algorithm.

Subdivision surfaces provide a control mesh (which facilitates deformation) and

a refined triangular mesh (which eases display). Their use brings C^2 continuity to most regions of the mesh, producing a more natural look. $\sqrt{3}$ subdivision is a better and newer subdivision scheme which is supported by less complex stencils. Here, subdivision growth is slower than in other subdivision techniques. Our inclusion of non-subdividable faces lowers the number of new generated faces. Apart from boundary faces, the growth is still exponential.

Initially, we believed that $\sqrt{3}$ subdivision surfaces were an appropriate modelling technique for the skull. This is true only for re-shaping. However, as we decided to implement one dog only, we also found them useful for skin generation and deformation. Still, the skull can be re-shaped with cartoonish results.

Chapter 7

Superquadrics: simplifying generalised cylinders

Dog's facial muscles can be thought as generalised cylinders which are placed on the skull. However, creating, positioning and deforming generalised cylinders require many parameters. A simpler alternative which can be used to approximate the behaviour of generalised cylinders are superquadrics. In particular, superellipsoids were very important for modelling Londra's muscles.

7.1 Generalised cylinders

Cylinders are an attractive way to model geometry for several reasons. They are simple primitives and volume preservation after deformation is straight forward. Generalised cylinders extend the basic cylinder so that it can have any kind of cross section which is repeated several times. This cross section can vary in size across an arbitrary path which can be closed or open (Aguado *et al.* (1999); Bloomenthal (1985)). Several works use generalised cylinders. For example, Simmons *et al.* (2002) and Semwal *et al.* (2008) use them for modelling muscles. Aguado *et al.* (1999) and Bloomenthal (1985) use them for modelling trees and plants.

We implemented a form of generalised cylinders. First, we used the parametric equation of an ellipse in 3D space for the cross section. Then, we defined the orientation of each elliptical cross section according to the main direction of the cylinder's axis (path). Let us suppose that in the case of Figure 7.1A the cylinder's axis runs mainly along the Z axis. The orientation of the ellipse's normal at P_i is obtained as:

- Orientation: $O(n) = ((P_{i+1} - P_i) + (P_i - P_{i-1}))/2$ (average of green vectors).

- If there was no change in the path along the Y axis, ellipse's minor axis remains $(0,1,0)$.
- If there was no change in the path along the X axis, ellipse's major axis remains $(1,0,0)$.
- If there was change in the path along X or Y , the orientations of the ellipse's axis are obtained as cross product, $O(n) \times (0, 1, 0)$ or $O(n) \times (1, 0, 0)$ or both, depending on the case.
- Analogous calculations are done when the main path runs along Y or Z .

The length of the generalised cylinder is the sum of all line segments joining the path. We obtained promising shapes (Figure 7.1B). However, problems arose in the orientation of the cross section when there was a big change of orientation in the path (Figure 7.1C). Indeed, constructing generalised cylinders can become tedious requiring the definition of many interactive parameters such as:

- Key points along the generation path.
- Number of cross section per length unit.
- 2D dimensions and equations of the cross sections.
- Orientation of the cross section along the path. Commonly implemented with Frenet Frames (Bloomenthal (1985)) or interpolations (Aguado *et al.* (1999)) to achieve smoothness.

7.2 Superquadrics: a solution with the same idea

Barr (1981) defined a parametric representation for superquadrics. Here, superquadrics are obtained raising each trigonometric function of a quadric surface (e.g. ellipsoid, hyperboloid, torus) to an exponent, and calculating the spherical product of pairs of these. The exponents are used to create shapes somewhat squared, somewhat pinched or somewhat rounded. Superquadrics divide the 3D space in the inside, outside and boundary regions (Barr (1981)). We studied superquadrics and found that:

- Superellipsoids (Figure 7.2A) can follow the idea of ellipses along a path and its resolution (number of ellipses) and other parameters are easily controllable.

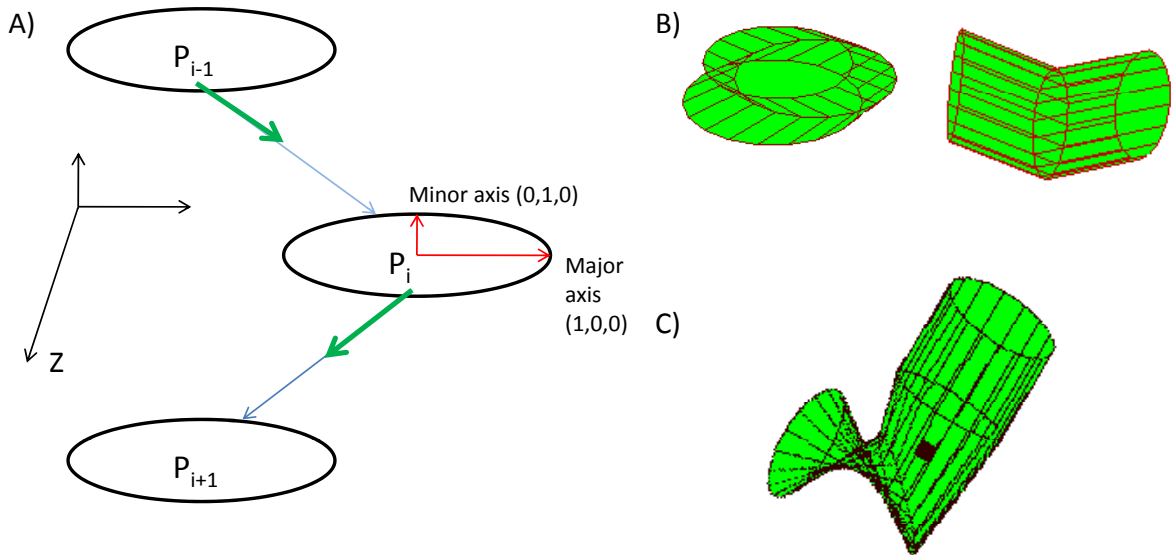


Figure 7.1: Generalised cylinders. A) Orientation of the cross section. B) Cylinder along a path. C) Problematic case.

- Shaping the extremes is unnecessary as superellipsoids naturally close the extremes.
- Continuity and smoothness of the surface is not an issue.
- Volume preservation can be reduced to a simple formula.
- Contraction and stretching of the shape is done naturally by altering its radii. Here, if some of the radii a_1 , a_2 , or a_3 is changed; the other two are recalculated according to (7.2) or (7.6) preserving volume. For example if we change a_3 in a superellipsoid by a factor F ; a_2 and a_1 have to be changed by a factor of $1/\sqrt{F}$; or at least one of them has to be changed by a factor of $1/F$ in order to preserve volume.
- The definition of key points along a path is not required.
- Supertoroids (Figure 7.2B) can be seen as closed generalised cylinder.

The canonical surface of a superellipsoid can be described with (7.1), its volume with (7.2), its normal with (7.3) and its inside / outside function with (7.4) (Barr (1981)). The canonical surface of a supertoroid can be described with (7.5) its volume with (7.6), its normal with (7.3) and its inside / outside function with (7.7) (Barr (1981)). Here:

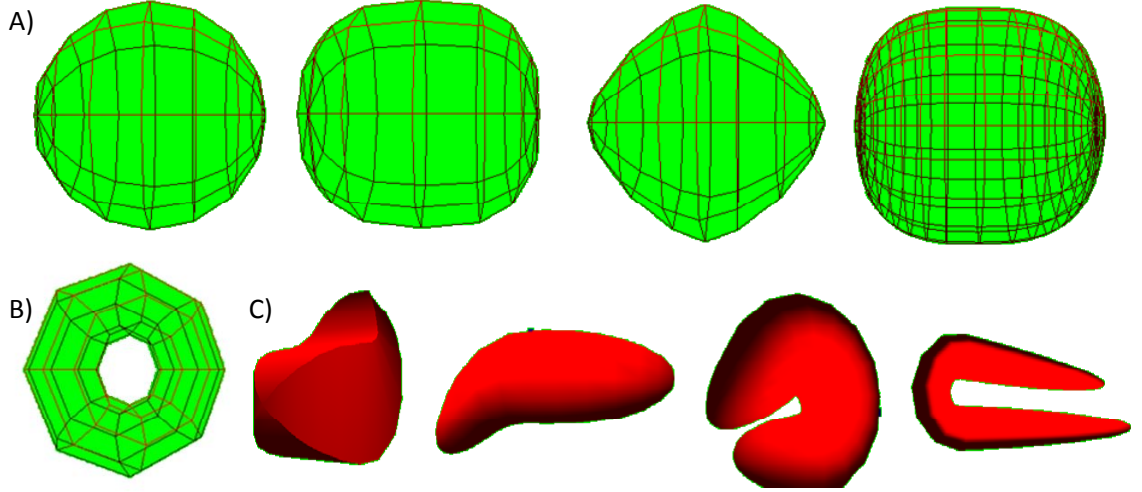


Figure 7.2: Superquadrics. A) Superellipsoids with different squaredness and resolution. B) Supertoroid. C) Bent superellipsoids (the squaredness factor of the leftmost one has been changed producing sharper edges)

- a_1, a_2, a_3 are the radii for the X, Y and Z axes.
- ϵ_1 is the squareness in the north-south direction.
- ϵ_2 is the squareness in the east-west direction.
- α is the torus inner radius.
- η is the latitude (north-south) parameter.
- ω is the longitude (east-west) parameter.

$$x(\eta, \omega) = \begin{bmatrix} a_1 \cos(\eta)^{\epsilon_1} \cos(\omega)^{\epsilon_2} \\ a_2 \cos(\eta)^{\epsilon_1} \sin(\omega)^{\epsilon_2} \\ a_3 \sin(\eta)^{\epsilon_1} \end{bmatrix}, \quad -\frac{\pi}{2} \leq \eta \leq \frac{\pi}{2}, \quad -\pi \leq \omega \leq \pi \quad (7.1)$$

$$Volume = \frac{4}{3}\pi \times a_1 a_2 a_3 \quad (7.2)$$

$$n(\eta, \omega) = \begin{bmatrix} \frac{1}{a_1} \cos(\eta)^{2-\epsilon_1} \cos(\omega)^{2-\epsilon_2} \\ \frac{1}{a_2} \cos(\eta)^{2-\epsilon_1} \sin(\omega)^{2-\epsilon_2} \\ \frac{1}{a_3} \sin(\eta)^{2-\epsilon_1} \end{bmatrix} \quad (7.3)$$

$$f(x, y, z) = \left(\left(\frac{x}{a_1} \right)^{\frac{2}{\epsilon_2}} + \left(\frac{y}{a_2} \right)^{\frac{2}{\epsilon_2}} \right)^{\frac{\epsilon_2}{\epsilon_1}} + \left(\frac{z}{a_3} \right)^{\frac{2}{\epsilon_1}} \quad (7.4)$$

$$x(\eta, \omega) = \begin{bmatrix} a_1 & a_4 + \cos(\eta)^{\epsilon_1} & \cos(\omega)^{\epsilon_2} \\ a_2 & a_4 + \cos(\eta)^{\epsilon_1} & \sin(\omega)^{\epsilon_2} \\ a_3 & \sin(\eta)^{\epsilon_1} & \end{bmatrix}, \quad -\pi \leq \eta \leq \pi, \quad -\pi \leq \omega \leq \pi, \quad a_4 = \frac{\alpha}{\sqrt{a_1^2 + a_2^2}} \quad (7.5)$$

$$Volume = 2\pi^2 \times a_1 \alpha \quad (7.6)$$

$$f(x, y, z) = \left(\left(\left(\frac{x}{a_1} \right)^{\frac{2}{\epsilon_2}} + \left(\frac{y}{a_2} \right)^{\frac{2}{\epsilon_2}} \right)^{\frac{\epsilon_2}{2}} - a_4 \right)^{\frac{\epsilon_2}{\epsilon_1}} + \left(\frac{z}{a_3} \right)^{\frac{2}{\epsilon_1}} \quad (7.7)$$

In order to rotate and translate superquadrics to desired configurations, the canonical surface x must be modified with (7.8). The normal n with (7.9) and the new inside / outside function requires inverting the transformation and substituting into the original inside / outside function. Here:

- M is the rotation matrix.
- b is the displacement vector.

$$\hat{x} = Mx + b \quad (7.8)$$

$$\hat{n} = Mn \quad (7.9)$$

7.2.1 Bending the superellipsoids

Barr (1987) proposed a way of deforming solid primitives. Among the proposed deformations are: tapering, twisting and bending. Bending allows defining superellipsoids on semi-curved paths. We implemented bending along the Z axis for the superellipsoids according to (7.10, 7.11, 7.12, 7.13, 7.14) (Barr (1987)). Figure 7.2C shows the results (Appendix K, BentSuperellipsoid.avi). Here:

- θ is the bending angle.

- k is the bending rate.
- $[Z_{min}, Z_{max}]$ is the range of the bending deformation.
- $1/k$ is the bending radius of curvature.
- (x, y, z) is the original point.
- (X, Y, Z) is the bent point.

$$\theta = k(\hat{z} - z_0) \quad (7.10)$$

$$\hat{z} = \begin{cases} z_{min}, & z \leq z_{min} \\ z, & z_{min} < z < z_{max} \\ z_{max}, & z \geq z_{max} \end{cases} \quad (7.11)$$

$$X = x \quad (7.12)$$

$$Z = \begin{cases} -\sin(\theta) \left(y - \frac{1}{k} \right) + z_0, & z_{min} \leq z \leq z_{max} \\ -\sin(\theta) \left(y - \frac{1}{k} \right) + z_0 + \cos(\theta)(z - z_{min}), & z < z_{min} \\ -\sin(\theta) \left(y - \frac{1}{k} \right) + z_0 + \cos(\theta)(z - z_{max}), & z > z_{max} \end{cases} \quad (7.13)$$

$$Y = \begin{cases} \cos(\theta) \left(y - \frac{1}{k} \right) + \frac{1}{k}, & z_{min} \leq z \leq z_{max} \\ \cos(\theta) \left(y - \frac{1}{k} \right) + \frac{1}{k} + \sin(\theta)(z - z_{min}), & z < z_{min} \\ \cos(\theta) \left(y - \frac{1}{k} \right) + \frac{1}{k} + \sin(\theta)(z - z_{max}), & z > z_{max} \end{cases} \quad (7.14)$$

7.3 Discussion

Muscles are similar to an elliptical cross section running along a path. This fact made us think about the suitability of generalised cylinders for facial muscle modelling. However, superellipsoids and supertoroids retain the main idea (e.g. ellipse along a path) while reducing the required parameters; and, providing simpler muscle geometry representation, contraction, stretching and bending. We took the implementation by Metzgar (2000). Then, we added volume preserving contraction - stretching and bending capabilities to model Londra's muscles. Bending was useful to adapt muscles to the underlying curved surface of the skull.

Chapter 8

Object Interaction Using Tabulated Spheres Subsets

Note: much of the text of this chapter comes from my own published work at Navarro Newball *et al.* (2009c). Some information was updated.

In Computer Graphics, collision detection is important for object interaction. In Londra we required efficient interaction between different layers and organs. We introduce TSSs, a technique which was used to implement jaw and tongue motion, and muscle skin interaction.

8.1 Overview

Object interaction often implies collision detection. Collision detection is important in computer graphics. In games, it needs to be fast. The most used strategies for collision detection in polygonal meshes are hierarchical bounding volumes and axis aligned bounding volumes (Hadap *et al.* (2004)). It has been suggested that methods based on boxes bound the geometry more tightly implying fewer hierarchical levels and faster performance (Gottschalk *et al.* (1996)).

However, the intersection test between spheres is simple and an object can be approximated with spheres successfully (Hubbard (1996)). O'Rourke and Badler (1979) present an algorithm to tightly approximate an object with spheres by anchoring big spheres to points on the object and shrinking the spheres until they just fit inside. Hubbard (1996) and Bradshaw and O'Sullivan (2002) use automatically generated sphere hierarchies for an effective search structure which tightly approximates the mesh. They approximate the medial axis to guide spheres' placement (according to Bradshaw and

O’Sullivan (2002), medial axes are more accurate than spatial subdivision). The medial axis can be approximated using Voronoi diagrams (Sud *et al.* (2005)). Construction of one sphere can be done in several ways. Welzl (1991) offers a permutation technique to find optimal spheres from a set of points. Hierarchies require the construction of the spheres surrounding a set of spheres for merging adjacent spheres (Bradshaw and O’Sullivan (2002)). Fischer and Gartner (2003) use rational arithmetic and Kumar *et al.* (2003) use core sets to find minimal spheres from other spheres. In a sphere hierarchy, an initial bounding volume test is followed by rejection of non colliding objects or identification of regions of potential collisions using a sphere tree which approximates the geometry. Then, the actual geometry of the object is tested in the regions identified.

We introduce Tabulated Spheres Subsets (TSSs), a technique for constrained interacting bodies which has the advantages of: 1) reducing the number of tests and computations; 2) relying on a simple operation; 3) using a simple data structure; 4) providing flexibility. It has three phases: spheres generation; colliding spheres search; spheres reduction and tabulation.

8.2 Tabulated Spheres Subsets

TSSs are a tabulated selection of the colliding spheres from the spheres’ approximation of two interacting meshes with constrained degrees of freedom (DOF). A TSS indicates which spheres from one mesh must be tested for collision with which spheres from another mesh:

- Figure 8.1A shows objects a and b with 1 DOF (horizontal motion). Here, M_s is the spheres’ approximation of a mesh.
- Figure 8.1B shows the subset M_{sc} of spheres which collide on motion.
- Figure 8.1C shows the smallest subset found, M_{sm} (several redundant colliding spheres were removed).
- Figure 8.1D shows the minimal subset M_{ss} (only non redundant colliding spheres).
- The typical TSS of the two objects is the table $TSS_{ab} = M_{sm}^a \times M_{sm}^b$.
- M_s can be volumetric (Figure 8.1A) or surface (Figure 8.1E).

The steps for generating a TSS are described next.

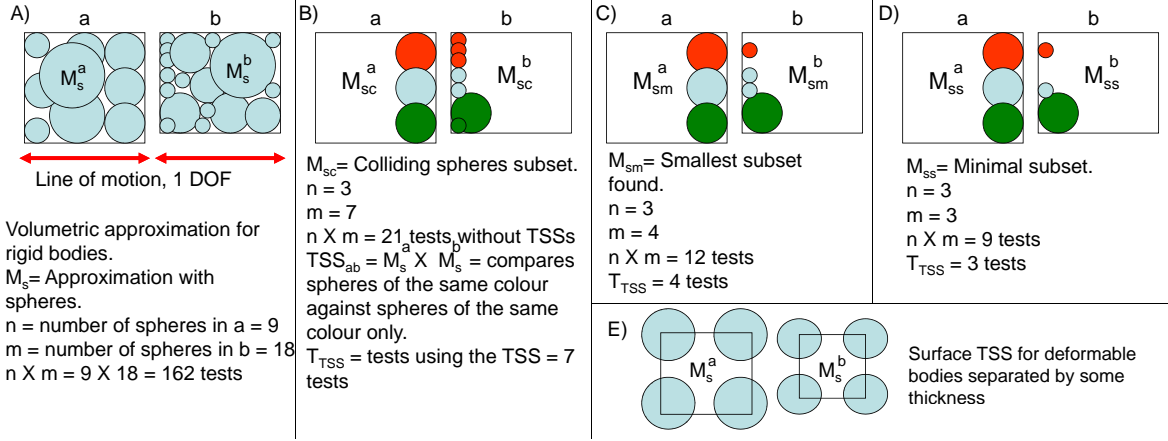


Figure 8.1: TSSs. A)B)C)D) n is the number of spheres in a , m is the number of spheres in b . Note that TSSs perform T_{TSS} tests which is lower than $m \times n$. Also, $M_{ss} \subset M_{sm} \subset M_{sc} \subset M_s$. A) a and b approximated with volumetric spheres. B) The non colliding spheres are removed. C) The typical subset of spheres found (a few redundancies remain). D) Minimal subset with no redundancies. E) a and b approximated with surface spheres.

8.2.1 Spheres generation

We input a mesh representing the boundary of the object. For a volumetric M_s we want the mesh to enclose the spheres. For a surface M_s , every vertex is the centre of a sphere. Sphere generation can be done in many ways (O'Rourke and Badler (1979); Welzl (1991); Bradshaw and O'Sullivan (2002); Sud *et al.* (2005)). We use a simple algorithm. For a volumetric M_s we use a heuristic method to avoid inside / outside tests and random number generation required by other methods (Bradshaw and O'Sullivan (2002); Sud *et al.* (2005)). Here:

- Radius growth is calculated along a line as in Figure 8.2A. Here, δt is found heuristically.
- In Figure 8.2B, we take the first point as a middle point from a triangle in the mesh (m_1) and grow the radius (r) towards a direction opposite to the normal of the triangle (N).
- In Figure 8.2C, once we find the second point (m_2 , middle point in other triangle), we obtain the middle point (m_L) between m_1 and m_2 and grow the sphere in a direction which goes from m_L to the centre of the old sphere (c).

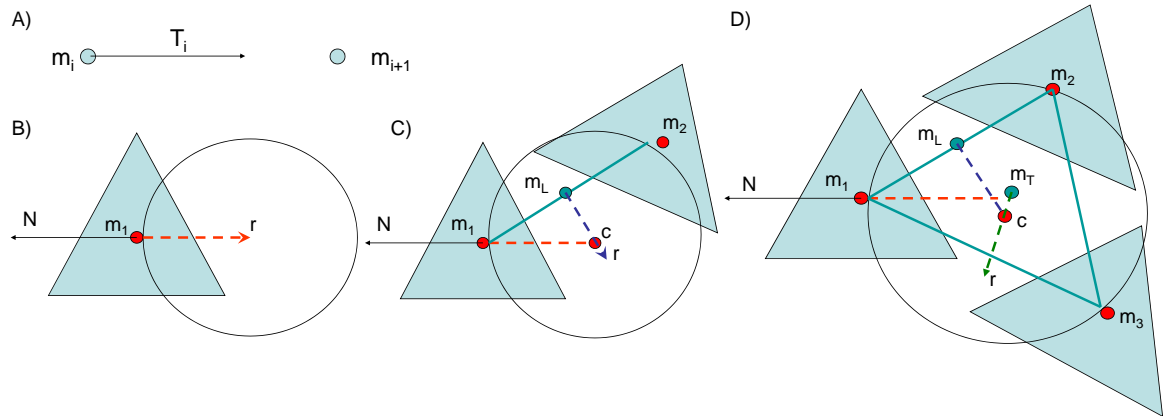


Figure 8.2: Spheres generation. A) The growth of a line between points m_i and m_{i+1} can be obtained from the parametric equation of a line in 3D space $m_i + T_i \times (m_{i+1} - m_i)$ by varying T_i by some δt . B) Growing radius (searching for the second point). C) Growing radius (searching for the third point). D) Growing radius (searching for the fourth point).

- In Figure 8.2D, once we find the third point (m_3 , middle point in other triangle), we obtain the middle point (m_T) of the triangle formed by m_1 , m_2 and m_3 and grow the sphere in a direction which goes from m_T to the centre of the old sphere (c).
- The algorithm stops when a fourth point or a threshold radius is reached. For a surface M_s we associate each vertex of the mesh with a sphere.
- Figure 8.3D shows the dialog box for spheres generation. It allows the definition of all parameters (e.g. δt , s , threshold radius) in the chosen mesh.

8.2.2 Colliding spheres search

This phase requires knowledge of the kinematics of the interacting objects to explore the space of motion and creates a table with all the collisions that occurred. For example, in the case of the dog skull - mandible complex, kinematics can be implemented with two angles which consider opening / closing and lateral motion. The space is explored from many directions to diminish unexplored holes. In the case of the skin - muscle interaction, kinematics can be implemented contracting and expanding the muscle in

all anatomically possible directions. Figure 8.3E shows the dialog box for searching the space of motion. It allows the definition of a step size.

8.2.3 Spheres' reduction and tabulation

After discarding the non colliding spheres, we create a collision table (T_c). It indicates for each sphere in object a , which spheres in object b need to be tested. There are two cases: 1) spheres' positions remain constant with respect to the meshes (rigid objects). 2) spheres' positions are changed and interacting objects are deformed. For the latter, T_c is the TSS. For the former:

- If N_s spheres collided in object b , we create a $N_s \times N_s$ table (T_a).
- Then, we search in T_c how many times a sphere from object b is present and how many times every other sphere from object b is present at the same time.
- Results are counted and stored in T_a while T_c is searched.
- Once this is done, T_a contains all the information about the number of times that the spheres from object b have appeared.
- In T_a a sphere S_i is removed if the number of times it appears is the same as the number of times it appears together with some other sphere S_j (The number of times S_i appeared is stored in $T_a[S_i][S_i]$ and the number of times that S_i appeared together with S_j is stored in $T_a[S_j][S_i]$).
- Finally, we remove the redundant spheres from object a by searching in T_c for rows containing exactly the same spheres from object b . Results are stored in a TSS.

Figure 8.3E shows the dialog box for choosing the colliding spheres. When the check boxes are ticked, the algorithm avoids redundancy.

8.3 Results

We applied our spheres approximation algorithm to a simple mesh. First, we used $\delta t = 0.01$ in the interval $[0.01, 0.101]$ and a threshold radius of 0.035. Then, we used

$\delta t = 0.001$ in the interval $[0.01, 1.101]$ and no threshold radius. The first parameterisation was appropriate for filling the narrow regions of the mesh with spheres (Figure 8.3A), while the second one worked better for wide regions (Figure 8.3B).

Badly formed meshes can produce undesired spheres. Figure 8.3C shows an undesired feature in the source mesh which produces an undesired sphere. The solution to this is to delete the undesired feature in the source mesh or to interactively delete the extra sphere.

Spheres produced can protrude slightly from the meshes (figures 8.3A and B). This can cause problems. For example, if two interactive meshes are very close to each other (e.g. mandible - skull) protruding spheres could cause a default collision state which would impede motion. We found a simple solution to this problem adding an extra parameter, a shrink factor (s) applied to the spheres. In contrast, using the technique by Welzl (1991) it was difficult to maintain a consistent inner direction of sphere growth. Here, more spheres appeared outside the mesh as the centre (c) is lost (Figure 8.2).

In Londra, we applied TSSs to jaw motion, tongue motion and skin/muscle interaction and measured the number of spheres generated and the number of calculations needed for collision tests. In these cases, as we will show in later chapters TSSs outperformed alternative techniques.

8.4 Discussion

TSSs are fast and appropriate for constrained object interaction. Applications include: articulated bodies (e.g. jaw) and relatively fixed deformable bodies (e.g. muscle, tongue). They rely on a simple test; only consider spheres and regions of the mesh which will collide and only test a sphere with the spheres with which it is most likely to collide. They use significantly fewer spheres than other approaches; and no hierarchy is required. TSSs are intended for approximate collision tests and do not deal with polygon to polygon tests. Exact polygon / polygon tests take much longer.

Our sphere generation algorithm is simple. It creates good enough approximations to spheres which can overlap and vary in size. It brings advantages such as:

- Avoids random point generation.
- Allows interaction.

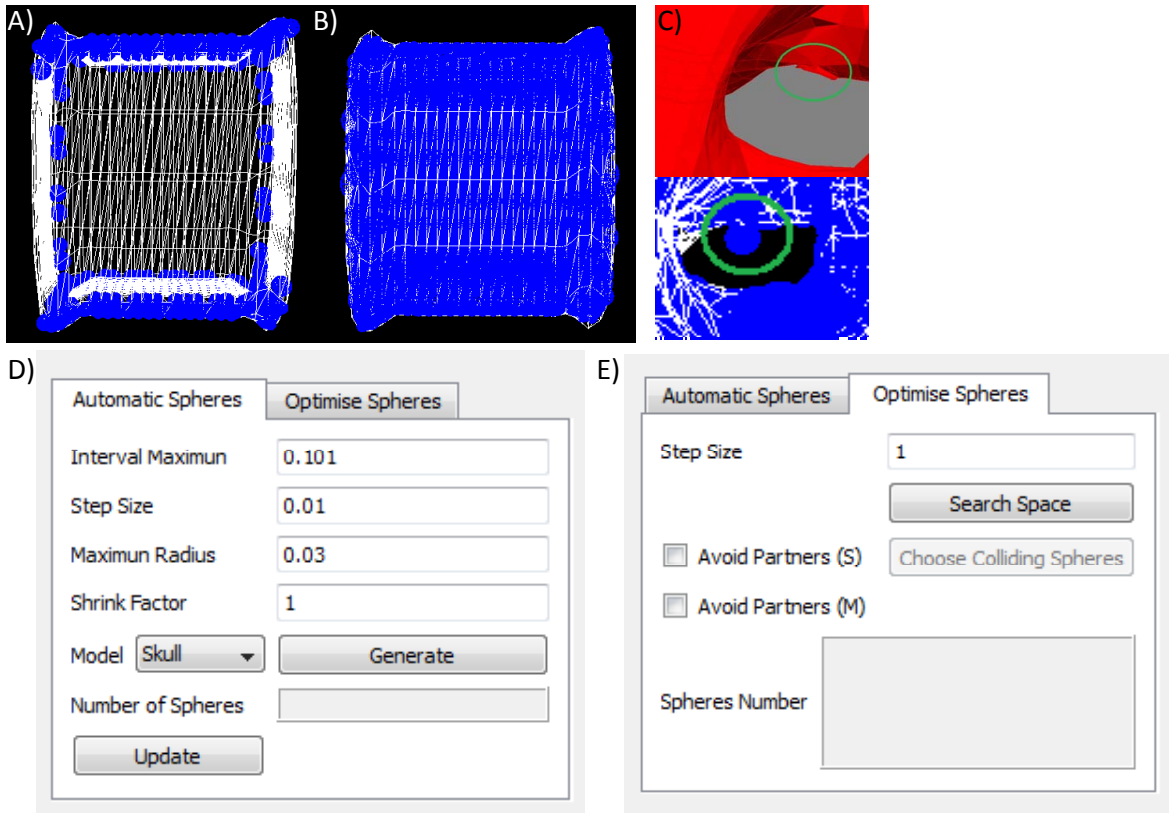


Figure 8.3: Parameters in sphere generation. A) Generating spheres for narrow regions (spheres tend to group in the edges). B) Generating spheres for wide regions (more spheres fill the mesh). C) Mesh distortion. D) Dialog box for sphere generation. E) Dialog box for colliding spheres search and spheres reduction.

- Is an alternative to more complex methods. However, as such methods can be more accurate the approximation to spheres is independent from the other steps in TSSs generation. This means that we could use an approximation generated with any other technique.
- The use of middle points and normals made most of the spheres remain inside.
- It can be adjusted for narrow or wide regions.

Possible enhancements could include the creation of a fully adaptive algorithm and finding a mechanism to measure accuracy.

Searching the space requires knowledge of the kinematics of the object modelled. In general, this can be easily implemented with geometric transformations. It is also a precomputed process. As it is related to the way the interacting objects behave, it is very general. For example, with our technique it would be simple to find the spheres at the contact points between the skull and the mandible for any kind of dog head (e.g. dolichocephalic, brachycephalic), assuming that we already have the mesh for both.

Even though (Figure 8.1) sphere reduction does not necessarily find the minimal subset M_{ss} , it lowers the number of spheres required for object interaction by finding a good M_{sm} and diminishes redundancy. Remaining redundancy means that on some occasions some spheres from object a will always be colliding at the same time with a corresponding sphere from object b (when a collision occurs). Some redundancy is more probable when two deformable objects are interacting than when two rigid bodies are interacting.

TSSs are precomputed. Here, deformations require simple updating of the positions of the chosen spheres. We found that volumetric TSSs were suitable for rigid objects, while surface TSSs were suitable for deformable objects separated by some thickness. An alternative would be the use of volumetric TSSs and extra layers, where one layer, and not the protrusion of the spheres from the surface, represents the thickness. Surface TSSs simplify the idea.

Chapter 9

System overview

Figure 9.1 shows Londra’s system architecture and workflow. Numbers (1) to (18) refer to different stages in the model. Here:

- **Setting up:** refers to the mathematical and geometrical creation of anatomical components and TSSs generation.
- **Processing:** refers to the deformation of skin due to kinematics or muscle movements; deformation of tongue; eyes and nose motion. Here, motion is constrained by TSSs.
- **Output:** refers to adding realism with textures and fur and displaying the animation.

9.1 Setting up

An imported dog skull with mandible mesh is our starting point (1). Optionally (2), it can be reshaped with basic anatomy (equations 4.1, 4.2; Figure 4.3C). However, the result is still cartoonish. Once the skull and mandible are ready, we generate TSSs according to the dog’s jaw kinematics (3).

Next, we interactively place the muscles on the skull surface in the 3D space using a geometric muscle model based on bent super ellipsoids (4). Muscle placement requires anatomical knowledge and takes advantage of head’s symmetry mirroring half of the muscles. Muscles can be consistently modified (e.g. contract, relax, bend) with a few parameters.

We model subsidiary organs too (5). Eyes contain four spheres each (e.g. sclera, cornea, iris, pupil) and look at some particular point using a gaze formula. The nose

is an imported mesh. It can be rotated across its centre and its nostrils can be dilated with a couple of spheres centred at the middle of each nostril. The tongue (6) is formed by a skeleton of three regions with a number of spheres each, and a triangulation of the surface (10, 7). We obtain TSSs for tongue-mouth interaction (8).

Having the skull, the muscles and the subsidiary organs, we generate feature points for half of the face (9). Feature points are generated semiautomatically from the underlying anatomy and are a key element to generate the skin shape. We consider ears and eyelids as part of the skin. We project the feature points on a 2D mirror plane and join them using Delaunay (Cheng *et al.* (2007)) triangulation (10). We defined anatomical restrictions so that the triangulation allows the creation of holes (e.g. mouth, eyelids, ears). Next, we put the meshed feature points back in the 3D space and mirror them to complete a skin’s control mesh (11). This mesh is inflated and then iteratively deflated until the skin surface is at a threshold distance from the underlying anatomy (11). At this stage, we smooth the skin’s control mesh using $\sqrt{3}$ subdivision (12). Then, we use DFACS, the skin’s control mesh and the muscles to produce the TSSs for muscle-skin interaction (13). DFACS’ AUs intensity is pre-programmed for each expression.

Some skin regions obey first kinematics (e.g. ears, eyelids, mandible). With skin region detection we determine to which region a portion of the skin mesh belongs (14). This is done by automatically measuring in 3D space to which part of the underlying anatomy a portion of the skin is closest. Optionally, fur regions can be defined so that fur points in different directions in different skin regions (15).

9.2 Processing

Using DFACS we perform the required actions in the following order: move the skin with kinematics (16); stretch and contract muscles (17); alter eyes, nose (18) and tongue (19). With the deformed skin and muscles (16, 17) and the TSSs for skin-muscle interaction, we perform Euler integration. Here, the skin’s control mesh is assumed to be in equilibrium and each deformed vertex tends to go back to its original position avoiding the need for inter-node interaction. Then, to get the limit surface of the skin, we perform localised $\sqrt{3}$ subdivision (20). This way, the effect of affecting the nearby skin regions is achieved. As a result, we get a deformed skin with underlying organs changed accordingly (21). DFACS’ AUs intensity is pre programmed for each expression.

9.3 Output

We use a layered texture approach and opacity maps to add fur and realism to each frame, (22). Then, we display the animated expression (23). The sequence of events displayed was programmed according to our dog expression observations and analysis (see Chapter 3).

9.4 Discussion

Figure 9.1 reflects our novel, purely bottom-up approach for model creation, which is inspired by dog anatomy. Also, it summarises our expression synthesis mechanism. In the following chapters we explain each layer.

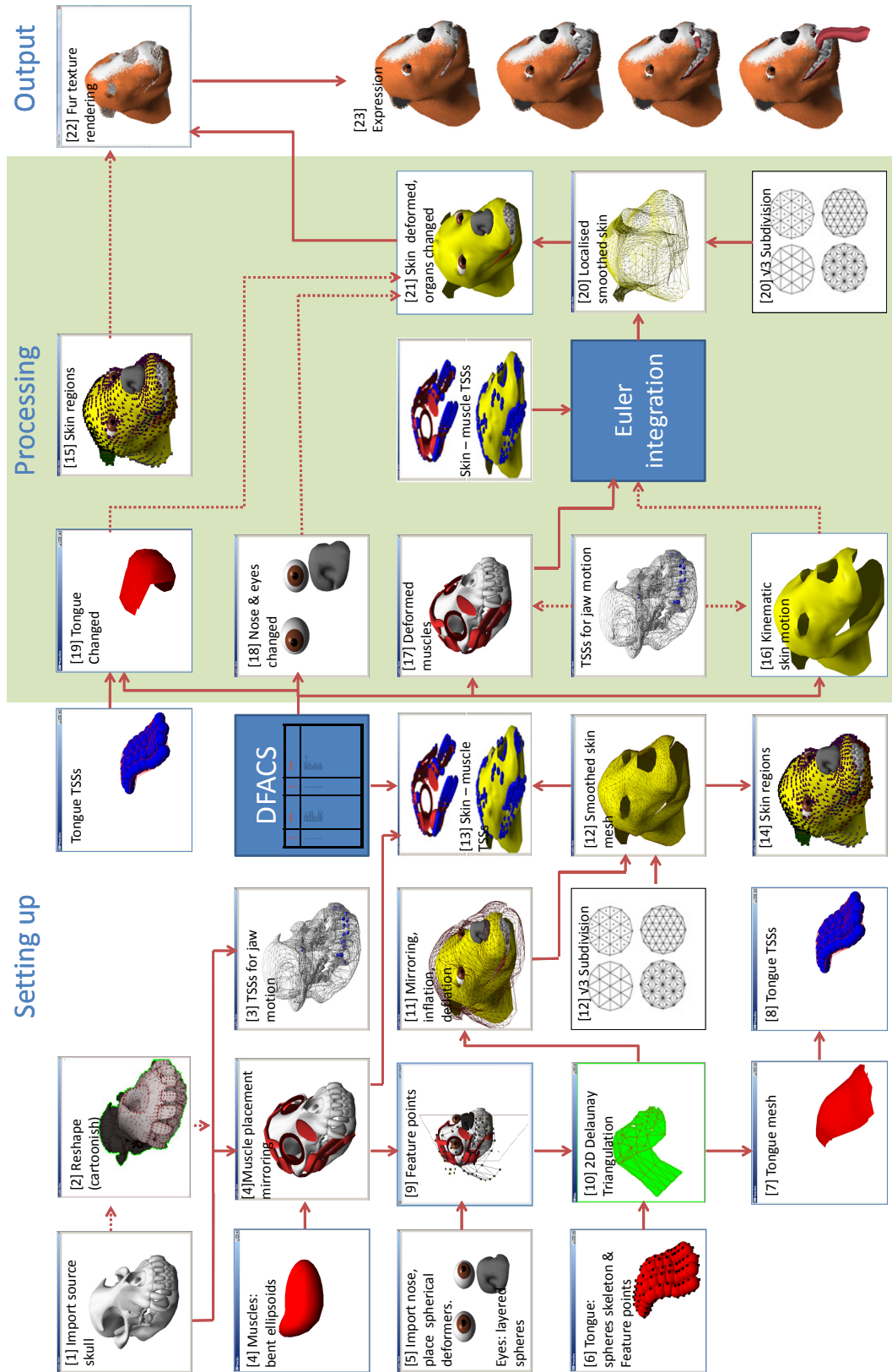


Figure 9.1: Londra’s system overview. Dotted lines are optional depending on the chosen task or expression.

Chapter 10

Bone layer

10.1 The rôle of the bone layer

We analysed the rôle of the skull and the teeth in facial animation. Many authors recognize the rôle of the skull in affecting the face (in medical applications this is even more important, Däuber *et al.* (2003)). In most cases the skull is used only for initialisation and muscle insertion (e.g. Lee *et al.* (1995); Tarini *et al.* (2002); Kähler *et al.* (2002); Däuber *et al.* (2003)). A few times (e.g. King (2001); Zhang *et al.* (2004b)), it is used through all the animation.

In general (Lee *et al.* (1995); Tarini *et al.* (2002); Zhang *et al.* (2004a)), the skull is modelled with polygonal meshes (a few cases describe iterative decimation, Däuber *et al.* (2003), or smoothing for mesh generation, King (2001)) and geometric transformations are used for jaw kinematics. Frequently, the skull mesh is digitised (e.g. CT scan in King (2001); Däuber *et al.* (2003); tomography in Zachow *et al.* (2003)). Some systems make the skull fit a facial model (Lee *et al.* (1995); Tarini *et al.* (2002); Zhang *et al.* (2004b)). A few systems refer to biomechanical analysis (e.g. Zhang *et al.* (2003a)). Some systems use an alternative model for collision detection (e.g. constraint functions, Zhang *et al.* (2003a), implicit functions, King (2001)) and; in some cases the facial model is deformed to fit the skull (Michael and Chen (1996); Archer (1997); Kähler *et al.* (2003)).

Similarly, several authors recognize the rôle of the teeth in facial animation (particularly in speech driven facial animation, King (2001)). In general (e.g. Breton *et al.* (2001); Kähler *et al.* (2002); Zhang *et al.* (2003a); Hyneman *et al.* (2005)), teeth are modelled with polygonal meshes (other techniques include NURBS, Lee *et al.* (1995), and Bezier curves, Waters (1987)) which are enhanced with textures (Guenter *et al.*

(1998)); motion of teeth is linked to that of the jaw and; teeth are modelled separately and then made to fit the skull or jaw model. In some cases, the teeth are not separated from the head or the mouth mesh (Kähler *et al.* (2003)) and; alternative representations can be used for collision detection (e.g. cylindrical arc, King (2001)).

10.1.1 Analysis

In Londra, the skull is not reshaped to fit a facial model. Instead, in our model, all other layers fit the skull shape. We think that generating a triangular mesh takes advantage of the ease of processing triangles. According to biomechanics and dog occlusion (Section 4.5), most dog jaw movements can be represented with a kinematics matrix with two degrees of freedom (one for lateral motion and one for opening and closing) and Cartesian coordinate systems. We believe in the simplicity of collisions between spheres and that a few spherical restrictions can limit motion reasonably. Londra's skull and mandible play an important rôle in expression animation. We decided to leave the teeth in the skull to avoid repositioning. Teeth play a major rôle in occlusion and are very visible in dog expression (unlike humans where teeth are mostly modelled when speech is present).

We consider the bone layer important because the shape of the skull directly affects the way a dog looks. It offers attachment points for the muscles which are the components whose motion drives skin animation. Also, biomechanical properties of the skull affect the way a dog moves its face. With Londra's bone layer we propose a skull suitable for expressive parameterisation and with potential for reshaping. Expressive parameterisation facilitates animation while reshaping may allow approximation of other breeds. Our skull model includes:

- Teeth and a movable jaw.
- A parametric triangular mesh representation with $\sqrt{3}$ subdivision surfaces capability.
- A kinematics model.
- A mechanism to allow basic reshaping (still with cartoonish results).
- TSSs for jaw motion.

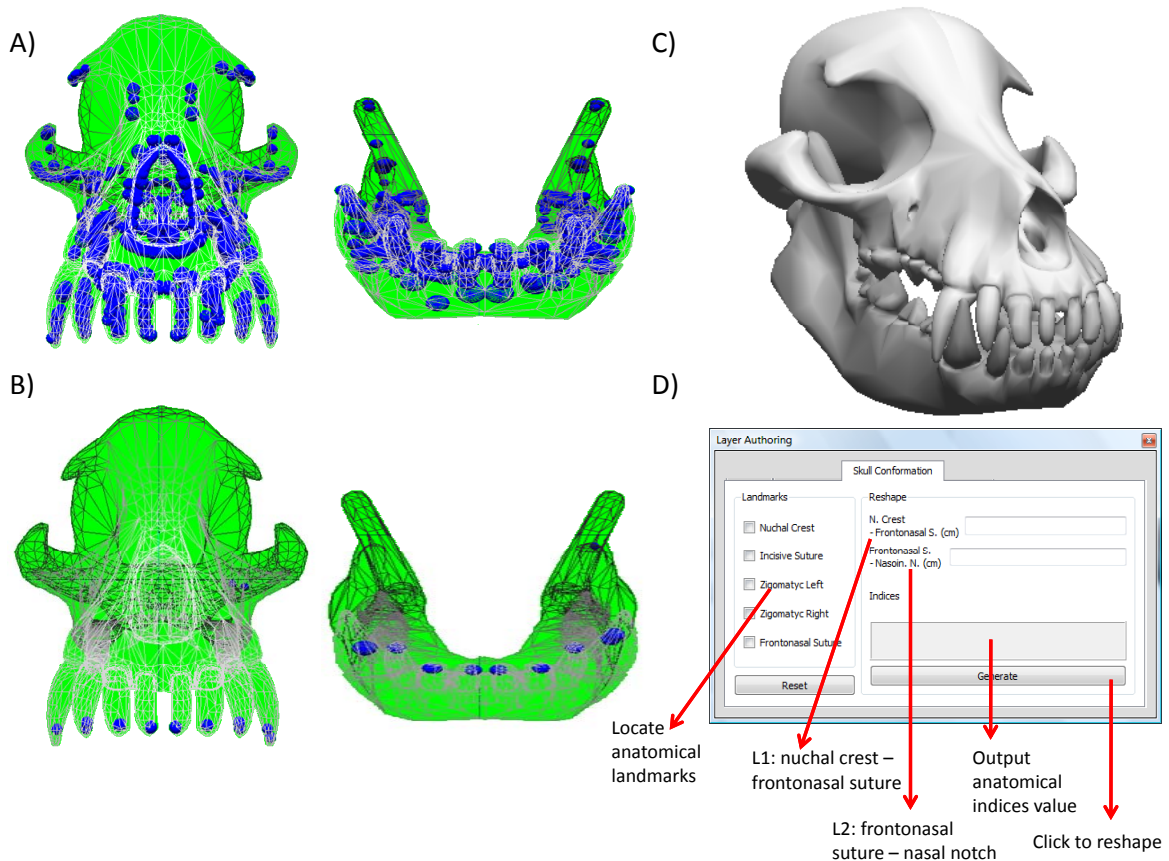


Figure 10.1: Londra's bone layer. A) Approximation to spheres. Mandible: 812 spheres, skull: 1158 Spheres. B) Reduced subset. Mandible: 22 spheres, skull: 9 spheres. C) Skull and Mandible, imported from Turbo Squid, Inc (2008). D) Dialog box for reshaping.

10.2 Importing the skull

Using a 3DS format loader (Vitulli (2005), Appendix G) we created an algorithm that converts a 3DS mesh into a Direct Edges data structure (Section 6.2.1). In our algorithm, only the vertex list and faces descriptions were processed. Our application opens the 3DS file. Next, it reads the vertices and adds them to a vertices list. Then, it reads the faces and adds them to a face list assigning the proper vertex indices. It creates the halfedges list from the faces list. For each one it assigns the vertex it points to and, for each vertex it assigns the outgoing halfedge. Next, for each halfedge it finds and assigns its opposite. Finally, it detects boundary vertices and saves the data. Figure 10.1C shows Londra's skull and mandible.

10.3 The need for subdivision surfaces

$\sqrt{3}$ subdivision is not necessary for enhancing the appearance of our imported skull and mandible meshes (see Appendix H) . Indeed, the use of a coarse mesh is more efficient and does not really require the use of the Direct Edges data structure either. We decided to keep the feature only when the skull is reshaped.

10.4 Reshaping the Head

In dogs, the skull can vary from long and narrow(dolichocephalic) to broad and short (brachycephalic). According to Sisson *et al.* (1975), the shape of the skull is described with two anatomical indices (formulas 4.1, 4.2; Figure 4.3C).

10.4.1 Applying Anatomical indices to the Skull

Figure 10.1D shows the dialog box for reshaping the skull and the mandible. First, the user defines some anatomical landmarks which represent conformational parameters (nuchal crest; incisive suture; frontonasal suture; zygomatic left and right). Then, he introduces L_1 and L_2 (right ((4.2). Then, the craniofacial index is calculated and if it is anatomically correct (between $10/3$ and $10/7$, Table 4.1), we obtain the proportion of how dolichocephalic or brachycephalic is the dog. With this proportion we obtain the cephalic index. Having the cephalic index, getting the width is straightforward. Reshaping of the skull follows. Here (Figure 4.4), vertices to the left (Z coordinate) of the fronto nasal suture are scaled according to the proportion of growth of L_2 . Vertices to the right (Z coordinate) of the fronto nasal suture are scaled according to the proportion of growth of L_1 . The proportion of growth of L_i is obtained calculating how bigger / smaller it is with respect to the equivalent in a generic mesh. The width (X coordinate) is changed uniformly through all the mesh. Once the skull and mandible are reshaped we smooth them with $\sqrt{3}$ subdivision.

10.4.2 Evaluation

Figures 10.2 shows the results of reshaping. Here, the real skulls were obtained from pictures of skulls of a boxer (brachycephalic) and a greyhound (dolichocephalic) and Londra's skulls were obtained by reshaping. In both cases the images were treated to identify the edges using Adobe Photoshop taking care to avoid shape distortion.

Figure 10.2A explains the FI , CI and SI indices, which are obtained as width/height for every case. In the frontal views of figures 10.2B and 10.2C, a distortion appears due to reshaping that makes the skull lose some height in 10.2B ($1 - (1.64/2.1) = 22\%$ error for FI) and lose some width in 10.2C ($1 - (0.71/1.67) = 57\%$ error for FI). On the other hand, in the lateral view, the cranium is longer than required in figures 10.2B ($1 - (2/2.83) = 29\%$ error for CI) and 10.2C ($1 - (2.91/3.75) = 22\%$ error for CI). Meanwhile, the snout is also longer than required in figures 10.2B ($1 - (1.56/2.98) = 48\%$ error for SI) and 10.2C ($1 - (1.83/4.01) = 54\%$ error for SI). Changes from short snout (Figure 10.2B lateral) to long snout (Figure 10.2B lateral) are evident in Londra's skull reshape. However, the proportions are not correctly maintained. Even though the results are not anatomically accurate, they show the potential of Londra to produce more breeds. Further study in conjunction with zoology could bring better results. Formulas (4.1) and (4.2) do not seem to take account of all skull dimensions.

10.5 Jaw motion with TSSs

Notice: much of the text of this section comes from my own published work at Navarro Newball *et al.* (2009c). Some information was updated.

In dogs the mandible behaves like a hinged jaw performing mainly opening and closing movements (Section 4.5). In some cases, lateral movement is performed. We defined the kinematics for jaw motion taking into account these two degrees of freedom (10.1). Here, α is the angle of the lateral rotation and θ is the angle of opening. Animation parameters for jaw motion include (Table 5.3): AU7, AU8 and their counter actions.

$$Kinematics = \begin{pmatrix} \cos \alpha & 0 & \sin \alpha \\ \sin \theta \sin \alpha & \cos \theta & -\sin \theta \cos \alpha \\ -\sin \alpha \cos \theta & \sin \theta & \cos \theta \cos \alpha \end{pmatrix} \quad (10.1)$$

We tested several techniques and chose TSSs to limit motion (Appendix K, skullTSS.avi). For instance, we generated an approximation with spheres for the mandible and the skull. Here, we generated volumetric spheres using the following parameters (see Figure 8.2): $\delta t = 0.01$ for $0.01 \leq T_i \leq 0.101$ and a threshold radius of 0.02 (the use of a threshold value for the radii focused sphere generation on narrow regions). Then, we covered the space of motion of the interacting bodies using dog's jaw kinematics (Appendix K, searchSpace.avi)(10.1). Here, we used a step of 0.1 for space exploration. Finally, for

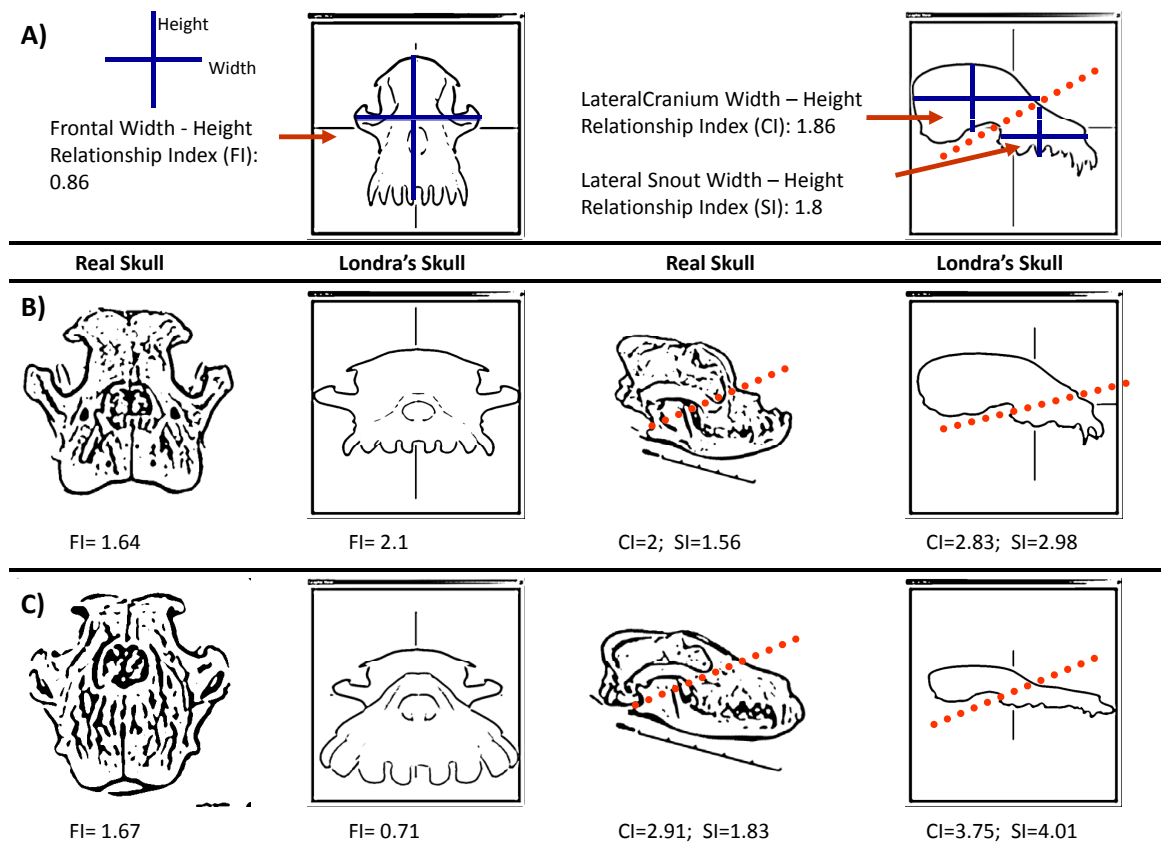


Figure 10.2: Reshaping the skull. The red dotted line crosses zygomatic and the fronto nasal suture. The region below the line belongs to the snout (real skulls from Will (2008)). A) indices FI , CI and SI , obtained as width / height (represented in the blue lines). B) Brachycephalic. C) Dolichocephalic.

each sphere, we identified with which ones it collides and created a TSS. Figure 10.1A shows the initial set of spheres (Mandible: 812 spheres, skull: 1158 Spheres). and Figure 10.1B the reduced subset (Mandible: 22 spheres, skull: 9 spheres). There was a significant decrease in the number of spheres. The resulting TSSs made the collisions test very efficient requiring 22 sphere-sphere intersection tests per time step for jaw motion. In contrast, the initial approximation requires $812 \times 1158 = 940296$ tests and the reduced subset requires $22 \times 9 = 198$ tests, if TSSs are not used.

10.5.1 Evaluation

TSSs take advantage of inherent motion constraints from interacting bodies and reduce the number of collision tests. TSSs can be compared with sphere trees; constrained angles of motion or; allowed motion paths. Sphere trees are better for general collision detection; however, we evaluated them in a constrained environment. Constrained angles are not appropriate for a number of reasons. For example, using 2DOF kinematics with the model in Figure 10.3A can cause problems in the highlighted region because rotation along Y can produce teeth interpenetration. However, one solution can be to define one angular region of collision testing and one free of collisions (Figure 10.3D). Finally, pre definition of allowed paths is limited and every possible path of motion should be stored.

TSSs vs. Sphere trees: in a TSS the number of collision tests T_{tss} is $\sum_n^{i=1} k_i \leq n \times m$ (n = number of spheres in object A ; m = number of spheres in object B ; k_i = number of spheres from B that need to be tested against a sphere i from A) and is constant at every time step. The number of collision tests in a sphere tree varies every time step. Sphere trees require a tight approximation at each level and enhance colliding sphere search by focusing tests only on the colliding branches. However, higher memory storage is required. Excellent sphere trees studies can be found in Bradshaw and O’Sullivan (2002). We analysed two cases:

- A sphere tree is obtained from the low level mesh’s spheres approximation. Even at Level 1 the number of spheres is high (e.g. Fig 1 from Bradshaw and O’Sullivan (2002) or, Figure Figure 10.3B). In a sphere tree, Level 0 encloses all spheres at Level 1. In a complex constrained pair, where meshes are very close to each other, these root spheres are likely to collide every time step. This enforces a full collision test at Level 1. Let N_1 and M_1 be the number of spheres at Level 1 for meshes A and B . It is likely that $N_1 \times M_1 \geq T_{tss}$ and the sphere tree will

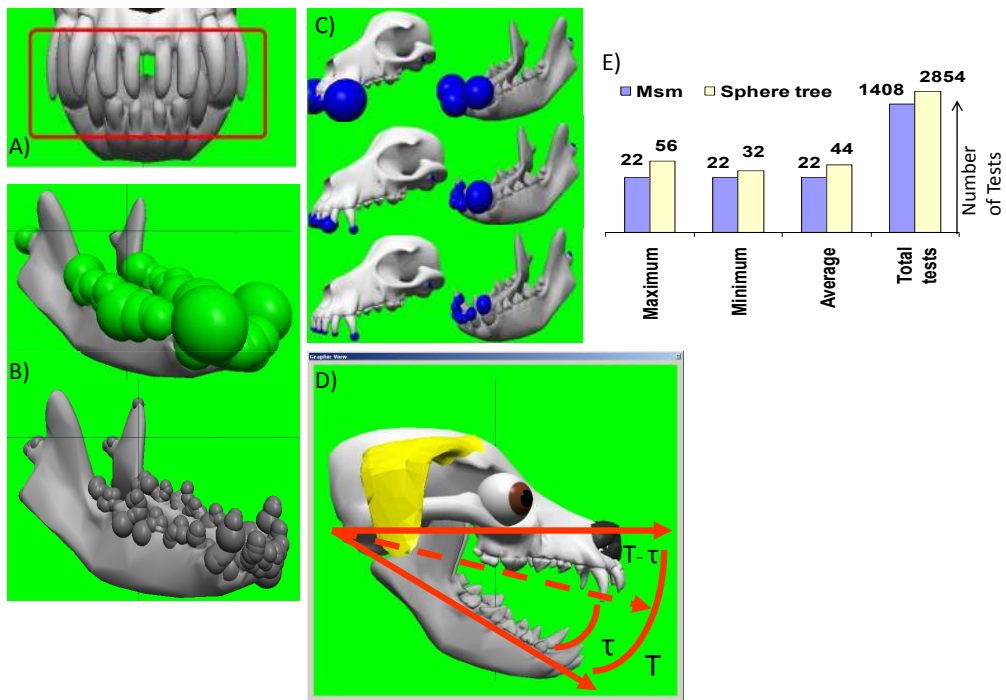


Figure 10.3: Evaluating TSSs in the bone layer. A) Problematic region. B) Two levels of a sphere tree. C) Tight sphere tree. D) The collision region is $(T-\tau)$, assume that the skull has n spheres and the mandible m . E) Performance (tests) of a sphere tree versus that of TSSs.

perform worse. In general, in a sphere tree the number of collision tests T_{st} is $\sum_{L=1}^{i-1} G_i$ (L = number of levels in the tree; G_i = number of spheres colliding at Level i). Whenever $T_{st} \geq T_{tss}$, TSSs will behave better.

- A tight sphere tree is obtained using M_{sm} (figures 8.1C and 10.3C). Figure 10.3E shows the comparison of the performance of this tree with that from the TSS. Here, M_{sm}^A has 9 spheres, and M_{sm}^B has 22 spheres.

TSSs vs. Angular region of collision: in Figure 10.3D; T is the jaw’s opening angle; τ is the non collision region; n is the number of spheres in the skull and m is the number of spheres in the mandible. Using TSSs, the total number of collision tests is $T \times T_{tss}$ and; using angular regions of collisions, it is $(T - \tau)(n \times m)$. In general T_{tss} is much lower than $n \times m$. For example, in the dog’s mandible skull using M_{sm} , T_{tss} is 22. Using angular regions, in order for $(T - \tau)(n \times m)$ to be equal to 22, we would require that $(T - \tau) = 0.111$. In consequence, to achieve $(T - \tau)(n \times m) = 0.111 \times T(n \times m)$; we require that $\tau = 0.89$, leaving 11% of time steps falling in the collision region. In practice we got about 22% of time steps falling in the collision region. Thus, TSSs behave better.

10.6 Head motion

We decided to implement head motion at the Joints in the vertebrae (Section 4.4) with kinematics. Animation parameters include (Table 5.3): AU9, AU10, AU11 and their counter actions.

10.7 Discussion

The shape of the skull directly affects the way a dog looks. It offers attachment points for the muscles which are the components whose motion drives skin animation. Also, biomechanical properties of the skull affect the way a dog moves its face. In our bone layer, teeth are considered part of the skull and the mandible.

We have created a working bone layer for Londra. However, we found that: 1) reshaping requires more complex equations in order to produce additional realistic breeds; 2) it is better to use the original skull or the intermediate simplified control mesh unless a better simplification of the control mesh is produced. 1 and 2 are out of the scope of Londra. However, we believe that the tests done here demonstrate the

potential of the system to produce more dogs and the potential of subdivision surfaces to smooth the new shapes. The measurement of the *FI*, *CI*, and *SI* are approximations to 2D but we consider they give good idea of the level of approximation of the skull to other shapes.

TSSs perform better than sphere trees, angular regions and intersection calculations for the example applications we have shown here. One big advantage is that TSSs are ready for any kind of skull-mandible shape. The process for TSSs generation for other breeds can be replicated easily. Here, the chosen spheres will automatically be in the points of contact of the new shape.

We are relying on a source skull drawn by an artist (Turbo Squid, Inc (2008)). Our bone layer is as anatomically accurate as the source 3DS mesh is. As explained, our TSSs adapt to the existing skull-mandible shape and spheres appear in their points of contact. If some spheres always collide simultaneously, redundant spheres are removed. In our case, most remaining spheres are in the incisive teeth. As expected, other spheres are in the Temporomandibular articulation. The source mesh is good enough to support our concept and our dog model. The TSSs agree with the anatomy of the skull-mandible we are using. Additionally, we are relying on the natural anatomical jaw kinematics for colliding sphere search (Step 2 in TSSs generation).

We identified and used a preliminary set of skull-mandible parameters:

- Conformational: nuchal crest; incisive suture; frontonasal suture; zygomatic left and right
- Expressive: AU7, AU8, AU9, AU10, AU11 and their counter actions.

Chapter 11

Muscle layer

11.1 Previous work

Muscles are groups of fibres operating together (Wu *et al.* (1994)). In muscle based facial animation the number of muscles involved in expressions is greater than in body animation (Radovan and Pretorius (2006)). Facial expressions based on muscles started with Platt and Badler (1981) (simplified muscles), continued with Waters (1987) (linear, parallel and sphincter muscles) and Magnenat-Thalmann *et al.* (1988) (abstract muscle action) and Terzopoulos and Waters (1990) (muscle contraction estimated from video sequences).

A muscle model simulates and understands the motivators of skin deformation in order to produce more realistic results. In many models a subset of major facial muscles is chosen to parameterise expressions based on coding systems (e.g. Waters (1987); Lee *et al.* (1995); King (2001); Bondy *et al.* (2001); Zhang *et al.* (2003a)). At a lower level, parameterisation is achieved with displacement of skin vertices. In facial animation models, muscles have attachment points (fixed attachment muscle-skull) and insertion points (movable attachment muscle-skin).

Physics Based Muscle Modelling simulates muscles and muscle actions in a way consistent with anatomy (Radovan and Pretorius (2006)). They can be implemented with vector fields which cause deformation on a region of influence (Radovan and Pretorius (2006)); mass-spring networks where forces are elastically propagated (Noh and Neumann (1998); Kähler *et al.* (2003)); finite element modelling (Radovan and Pretorius (2006)) and; muscle mask which includes a set of geometric parameters which use parametric representations (Wu *et al.* (1994)).

Pseudo muscles simulate the effect but not the muscles themselves (Watt and Poli-

carpo (2001); Radovan and Pretorius (2006)). Usually, they are implemented with free form deformers where an embedded object is deformed according to the deformation of a control box or line. There are several approaches for muscle generation automation, which rely on the definition of feature points.

In some performance based models Hyneman *et al.* (2005); Kubo *et al.* (2006); Sifakis *et al.* (2006), a physical muscle model can be used to fit the captured image. Here, individual muscle shapes are modelled with anatomically based linear interpolation targets modelling the actions of individual muscles. For each frame the model of the head is oriented and positioned to correspond to a muscle model. Generic muscles are posed to match expressions.

Automation facilitates facial muscle construction (Zhang *et al.* (2004)). Techniques used include: muscle mapping using cylindrical projection (Zhang *et al.* (2003a)); landmark specification (Zhang *et al.* (2003a)); matching scanned data to a virtual muscle layer (Lee *et al.* (1995)); adaptation and minimization of difference between video and mesh (Kubo *et al.* (2006)).

Water's model (Waters (1987)) which has influenced several models (e.g. Lee *et al.* (1995); Breton *et al.* (2001); Zhang *et al.* (2004b)), proposes three kind of muscles: Linear muscles are a bundle of fibres sharing an emergence point and pulling in an angular direction; Sheet muscles are broad flat parallel fibre strands without an emergence point and; Sphincter muscles are fibres looping around a facial orifice and draw to a virtual centre. It is based on geometrical muscle tensions. Zhang *et al.* (2004b) adds external forces. Breton *et al.* (2001) enhances the effect of muscles acting in conjunction. Lee *et al.* (1995) generalise and enhance sphincter muscle fibres to piecewise linear functions. In the case of speech oriented facial animation muscle activation and kinematics can be associated with phonemes (Sifakis *et al.* (2006)), or with muscle displacements along a vector (King (2001)).

11.1.1 Muscles and cylinders

Semwal *et al.* (2008) and Simmons *et al.* (2002) use generalised cylinders to represent body muscles which deform in a volume preserving manner in response to bone motion. In Simmons *et al.* (2002) the cylinders have a variable number of octagonal cross-section. End slices are attached to bones and intermediate slices are attached by anchors. To interpolate smoothly between end slices and maintain a good shape, intermediate slices are automatically adjusted in orientation. The main limitation is the amount of interaction required to create each muscle.

Wu *et al.* (1994) facial muscles' surfaces are parametric representations based on revolution surfaces (e.g. cylinders, cones and ellipsoids). The model includes muscle kinematics. Fat is simulated with a displacement and a spring. Muscle contraction is simulated affecting the parameters of the revolution surface. Springs connecting the skin to the muscles are used to deform the skin.

Simmons *et al.* (2002); Semwal *et al.* (2008) and Wu *et al.* (1994) follow a geometrical muscle deformation approach based on simple primitives. However, in Simmons *et al.* (2002); Semwal *et al.* (2008) the skin is deformed geometrically and in Wu *et al.* (1994) with a physically based approach using springs.

11.2 Muscles modelling with superquadrics

We propose a muscle model based on bent superquadrics (Section 7.2) which considers muscular geometry as an important component. We found that super ellipsoids simulate the effect of muscular geometry while volume preservation and contraction relaxation can be managed with simple parameters. From our DFACS we chose 23 muscles to aid skin generation and 21 to aid expression synthesis (the Orbicularis Oris are used for skin generation only). There are 11 symmetric pairs of muscles and the Frontalis (Section 4.6, Figure 4.5B).

In order to ease muscle construction and taking advantage of symmetry we implemented a mirroring function that recreates a muscle at the other side of the head (Figure 11.1A). Mirroring is done with respect to the Y axis by reflecting the position about the X axis and the rotation angles around the Y and Z axis. Attachment points are not used. Instead, muscles are placed in a fixed position relative to the skull and the mandible. For each muscle, contraction and relaxation occur along the curved axis of the bent superquadric representing it.

Figure 11.1B shows the interface for muscle construction. It includes all the parameters required for building (Group 'Shape') and bending (Group 'Bending') superellipsoids and for building supertoroids (Checkbox 'Closed' in Group 'Shape'). Additionally, it allows correct positioning and saving / loading / editing muscles (Group 'Position'). Parameters in this dialog box are conformational and come from equations 7.1, 7.5 and 7.8. The expressive animation parameter is length, which is altered with the contraction and stretching superellipsoid functions (Section 7.2). Altering muscle length is the basis for AUs 1 to 8 (Table 5.3). Altering curvature is important in AUs 7 and 8.

Muscles' fibres produce a sense of orientation and add realism. Fibres can be

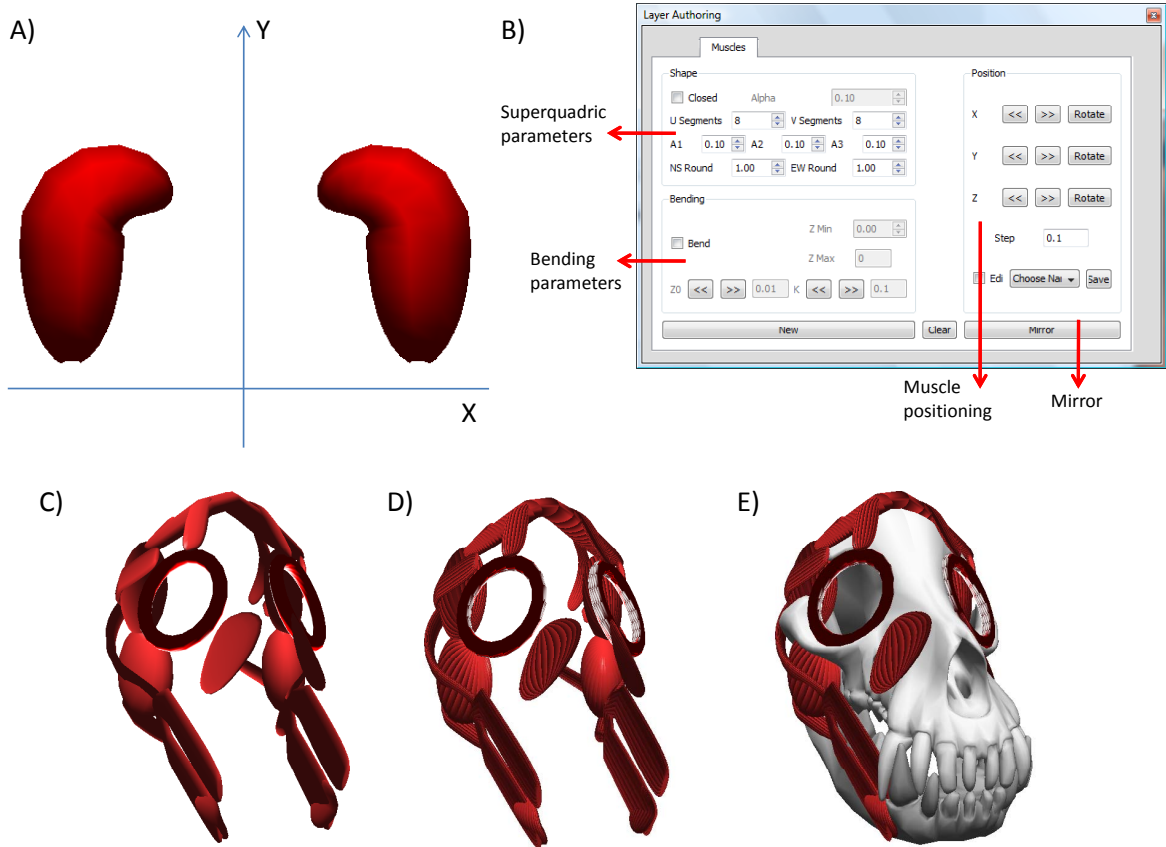


Figure 11.1: Muscle layer. A) Mirroring. B) Dialog box for muscle construction. C) Muscles in the muscle layer. D) Fibres. E) Bone and muscle layer.

directed along or across the direction of the muscle's main axis. One way to visualise them is using bump mapping along the lines joining the superquadrics's cross-sections or along the perimeter of the cross-sections depending on the desired orientation. Bump mapping (Blinn (1978)) is a technique which alters the surface normal of the object being rendered in order to produce more detail through illumination without altering the geometry. For Londra, we changed the normal using simple rotations. Here, the required sine and cosine were pre-calculated. Figure 11.1C shows the muscle in the muscle layer. Figure 11.1D shows muscles enhanced with fibres. Figure 11.1E shows the Bone and Muscle layer together.

11.3 Discussion

Many facial muscles are similar to an elliptical cross section running along a path. Superellipsoids and supertoroids can be seen as generalised cylinders where the number of required parameters is reduced. They provide simpler muscle geometry representation, contraction, stretching and bending. Bending is useful to adapt muscles to the underlying curved surface of the skull.

We identified and used a preliminary set of muscle parameters:

- Conformational: closed or open; a_1 , a_2 , or a_3 radii; squaredness in the north-south and in the east-west direction; torus inner radius; latitude; longitude; bending angle; bending rate; bending range; position; rotation (Section 7.2, Figure 11.1B).
- Expressive (per muscle): muscle's length. Length is related to the a_1 , a_2 , or a_3 radii. For instance changing length affects these conformational parameters. This makes sense as the muscle is being deformed. In AU7, AU8 the muscle curvature is also changed (involving the bending range, $[Z_{min}, Z_{max}]$ and the bending rate, k as defined in Section 7.2).
- Expressive (involving all muscles): AU1, 2, 3, 4, 5, 6, 7, 8 and their counter actions are higher level parameters used in expression synthesis.

We identified the 23 most important muscles affecting dog's facial shape and expression. More realism can be achieved by including more muscles. However, our selection was adequate for Londra. Superquadrics worked fine for the chosen muscles. The introduction of more complex muscles with more complex shapes could require techniques such as generalised cylinders (or arrays of superquadrics). However, one big advantage of our muscle model is the reduced number of parameters which facilitates their construction, deformation and their interaction with the skin. Thanks to mirroring, muscle placement is less tedious than in other systems (e.g. Simmons *et al.* (2002)). The system could be enhanced by automating muscle placement, especially for generalisation to other breeds (this is out of the scope of this thesis).

Muscles are not visible in facial expressions. However, we provide the optional display of fibres using bump mapping to enhance the view of the muscle layer. This feature could be useful in applications related to zoology.

Muscles' shape play an important rôle in skin generation and deformation (e.g. direction and region of deformation)(Section 13.4).

Chapter 12

Complementary layer

This layer is related to the development of organs with a particular or complex behaviour that have to be animated separately. Such organs are commonly referred to as subsidiary organs in HFAMs and sometimes are ignored or oversimplified. Our complementary layer includes: tongue; eyes; nose. We decided to leave the ears as part of the skin layer.

12.1 Tongue

12.1.1 Previous work

Some facial animation systems include a simple subsidiary model of the tongue (e.g. Noh and Neumann (1998); Haber and Terzopoulos (2004); Hyneman *et al.* (2005)). The first works used a solid tongue with some parameters such as width and thickness (Parke (1974)). Some works use texturing approaches. They map the tongue on polygons which are part of the inner mouth representation (Guenter *et al.* (1998)) or on a generic mesh of the tongue (Tarini *et al.* (2002)) when the mouth is opened. According to King (2001), p.63, 'a realistic tongue model should be capable of approximating the shape of any tongue in any natural position. For applications that need a faithful representation of the tongue, this is extremely important. For facial animation, that restriction can be relaxed somewhat. It is only important for those parts of the tongue that are clearly visible to be accurate'. Tongue modelling is important for realistic speech / mouth animation (Noh and Neumann (1998); King (2001); Wampler *et al.* (2007)). In this context, the tongue has been modelled as:

- A blobby object with a pseudo-skeleton with 9 triangles that serve as a mechanism

for charge distribution for a potential field (Pelachaud *et al.* (1994)). Using 18 parameters (e.g. lengths, angles), it is volume preserving, allows asymmetry and its motion is based on FACs.

- Pre-designed key tongue shapes for phonemes (Deng *et al.* (2006)).
- A teardrop shaped collection of 12 bi-cubic patches (Reeves (1990))
- Interpolation from key phonemic portions (Kleiser (1989)).
- With 5×5 functional segments that can be crosswise and lengthwise (Stone (1991)). Here, four classes of symmetric tongue shape are needed to classify the sounds produced (front raising, complete groove, back raising, two-point displacement).
- Finite element models that can be used for biomechanical studies Gerard *et al.* (2003).
- A B-spline surface composed of an 8×13 grid of bi-cubic patches over 60 control points. Symmetric, highly deformable with a parameterisation of 6 parameters (King and Parent (2000)). Geometry defines the surface and the parameters define the possible tongue shapes. Supporting collision detection between the tongue and the rest of the oral cavity, it is volume preserving.
- Images from real time Magnetic Resonance Imaging (Engwall (2000)) used to sustain Swedish articulations with 6 linear parameters that affect the sagittal plane. This model is extrapolated to 3D using articulatory inversion, Engwall (2004).

12.1.2 Analysis

The tongue can be parameterised based on FACS (Pelachaud *et al.* (1994)). Volume preservation can be approximated by extending one dimension and shortening another, (Pelachaud *et al.* (1994); King and Parent (2000)). It is possible to use collision detection based on implicit functions (King and Parent (2000)). Definition of key tongue shapes limit tongue motion but simplify the problem. Advanced tongue models are related to tongue shape during human speech. This reduces the number of required shapes (e.g. 4 key shapes summarise the important tongue movements during English speech). Engwall (2000, 2004) treats the tongue as one piece but most models divide the

tongue in different regions or segments. Each region can move differently but in relation to the other regions. The more segments used, the more allowed degrees of freedom, but the more parameters required. The tongue can produce asymmetric shapes, but not all models implement asymmetry.

12.1.3 A dog tongue model

In dogs, the tongue is very visible. It is not used for speech but it is still very expressive. However, there are some anatomical similarities between the human and the Dog's tongue. Indeed, dog tongues can be divided according to which muscles are in control (similar to Figure 4.7D).

Londra's tongue (Figure 12.1A) consist of three regions built upon a skeleton of spheres. Each tongue region includes $4 \times 5 = 20$ spheres. Though this number was chosen arbitrarily, we believe it is a good number to have enough deformation while keeping the number of spheres low. Here, the back region contains bigger spheres closer to each other; the tip region contains smaller spheres more separated from each other; the middle region is somewhere in between. We created a skeleton with spheres so it was possible to use TSSs in tongue motion. We found that spheres provided flexibility. While an alternative was to use a model equal to that of the muscles. Superellipsoids did not provide the desired results for more than one bend.

We divided the tongue in three regions because many common dog tongue shapes imply one or two main bends (Figure 12.1B). Having the skeleton, we automatically generated vertices at a threshold from the centre of each sphere (figures 12.2C and E) and made a textured Delaunay (Cheng *et al.* (2007)) triangulation (Figure 12.2D).

Londra's tongue rest position is its minimum length. The back region can be expanded until it reaches the incisive teeth (Figure 12.1D) or until the middle region reaches the incisive teeth (Figure 12.1C). Then, the middle and/or the tip regions can be expanded until a maximum length is reached. During contraction and expansion volume preservation is approximated by extending one dimension and shortening another and adjusting the radii of the spheres in the skeleton (figures 12.2A and B).

In our tongue model. The back region never bends. The middle region bends with respect to the back region. The tip region bends with respect to the middle region. However, a bend is not done equally for all spheres in one region as this would bring sharp unnatural results. In Figure 12.3D the middle region is bent an angle α with respect to the back. Then, the tip region is bent an angle β with respect to the middle. In contrast, in Figure 12.3E, we distribute the bent angle among the rows of spheres

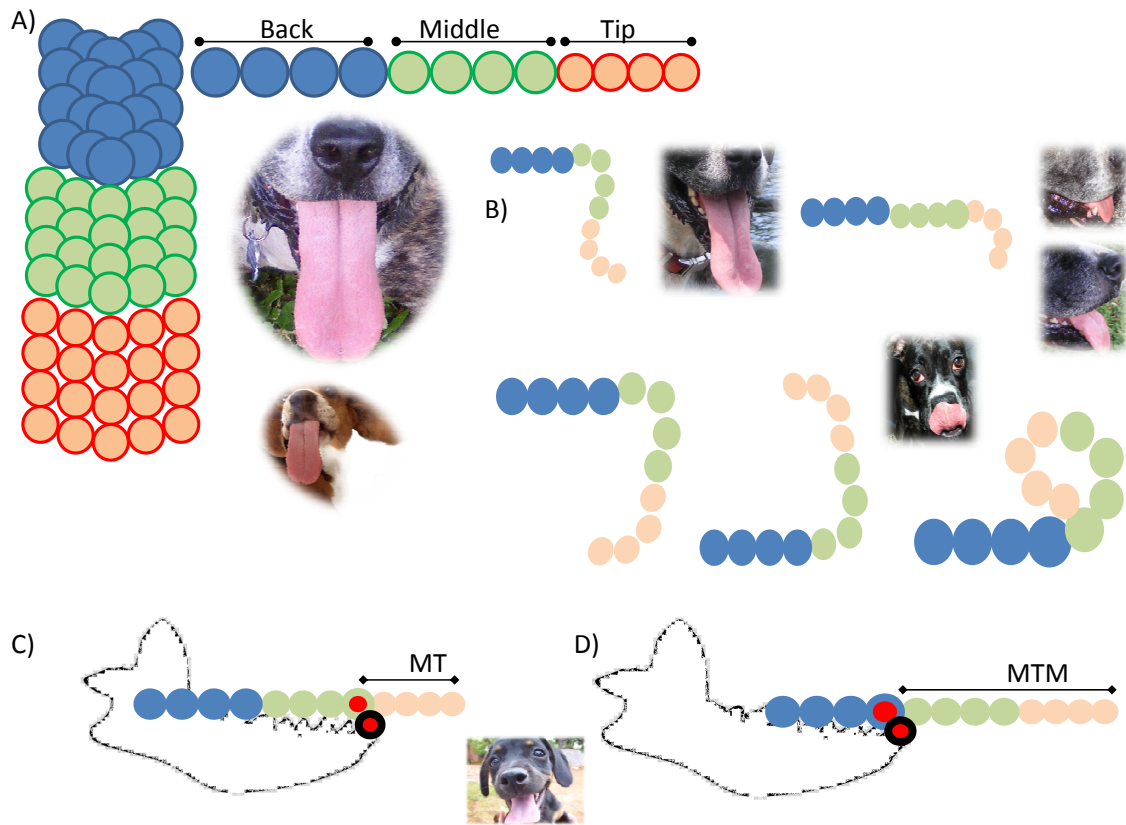


Figure 12.1: Tongue model. A) Regions and skeleton. B) Common expressive shapes . C) Expansion up to the middle. MT is the maximum allowable expansion for the tip. Interacting spheres are emphasised. D) Expansion up to the back. $MTM - MT$ is the maximum allowable expansion for the middle. Interacting spheres are emphasised.

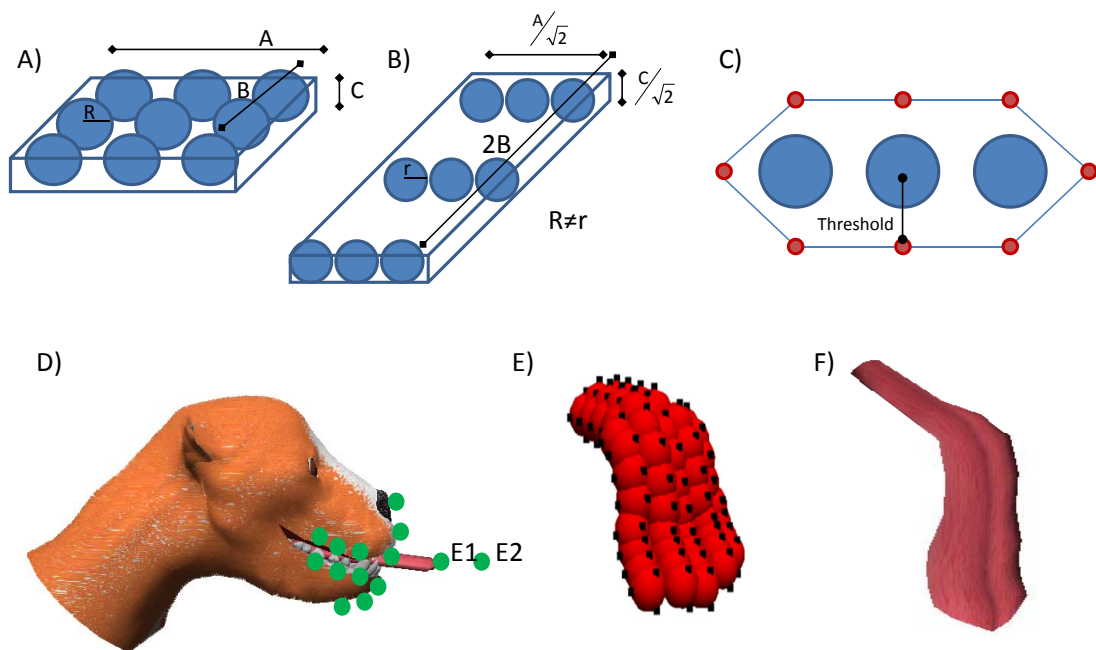


Figure 12.2: Tongue volume and mesh. A) Original dimensions in a tongue region $A \times B \times C$ with a radius R . B) Changing dimensions and preserving volume. C) Generating vertices. D) Alternative for tongue motion. $E1$ and $E2$ limit expansion for tip and middle regions. E) Vertices in the tongue. F) Textured triangulation.

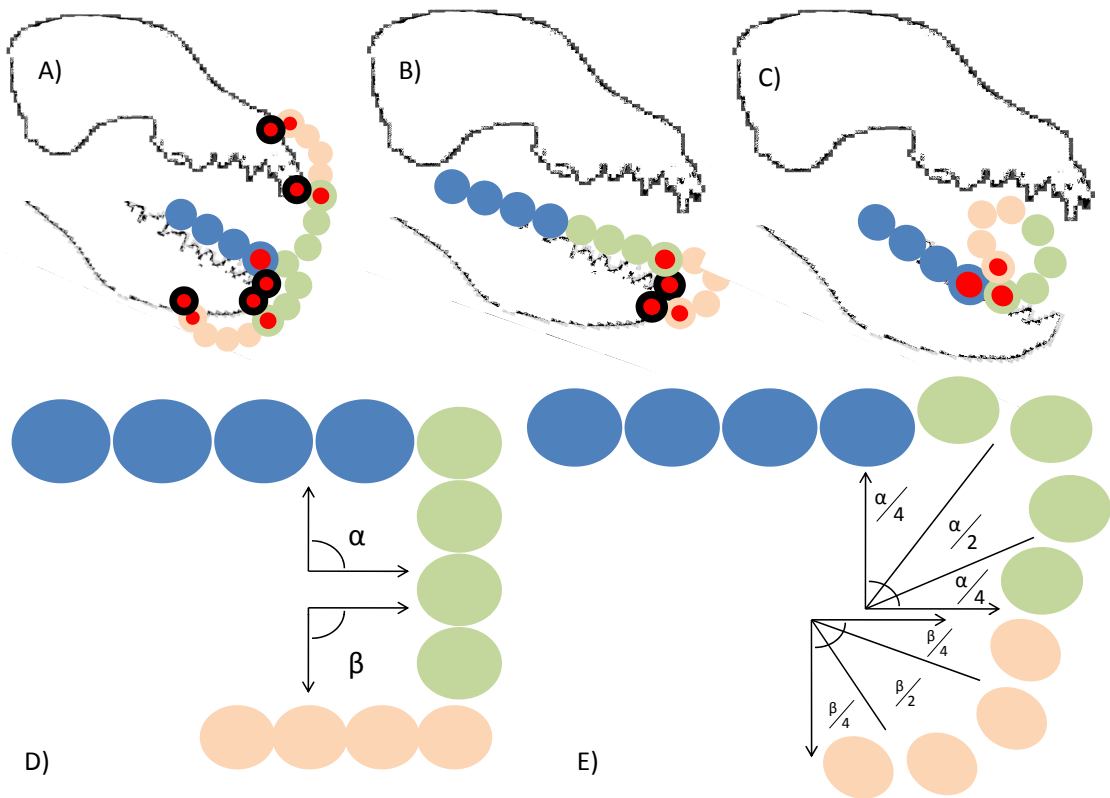


Figure 12.3: Bending the tongue. A) Bending the tip and the middle. Interacting spheres are emphasised. B) Bending the tip. Interacting spheres are emphasised. C) Rolling the tongue. Interacting spheres are emphasised. D) Unnatural bend. E) Enhanced bend.

forming the skeleton of the region and get a more natural result. For example. The first row of spheres in the middle region is bent by an angle $\alpha/4$ with respect to the back. Then, the two following rows are bent by an angle $\alpha/2$ with respect to the first row in the middle. Finally, the last row in the middle region is bent by an angle $\alpha/4$ with respect to the previous row. In order to get a natural result, something similar is done for bending the tip (angle β).

12.1.4 Tongue motion with TSSs

A dog's tongue is complex, can be moved to form many shapes and has many degrees of freedom. However, it is always fixed at the inner part of the mouth and its visible interaction happens on the region just outside the dog's mouth. It can only be expanded to a maximum and contracted to a minimum length. Moreover, the shapes required for

expressions can be limited. All this made us think about extending the idea of TSSs to tongue motion. One solution could be creating an exoskeleton built with spheres around the snout region of the model, Figure 12.2D. What we did was to find, from the underlying anatomy, the colliding spheres that can limit the tongue movement.

In our model, the tongue interacts with spheres from the mandible and the Skull (instead, the skin could be used). Also, each tongue region can interact with each other. For instance, with the tongue, we expanded our TSSs to include:

- The use of a more freely moving object such as the tongue.
- A flexible object interacting with more than one object (e.g. skull, mandible, tongue regions). Though, we could have interacted with one skin or one exoskeleton.
- The use of an object which has been divided in several regions which need to interact with each other.
- Some extraordinary cases where some collisions need to be ignored.

The process of creation of the TSS is the same as in previous cases. However, the approximation of the tongue by spheres is implicit in the tongue skeleton. Thus, we start moving the tongue through all its space of motion. Then, we identify the colliding spheres and tabulate them. To simplify the problem we chose the subspace of symmetric tongue movements which was relevant to Londra's expressions. However, our results suggest that it is neither difficult nor costly to provide more degrees of freedom. Contrary to what was expected the size of the TSSs was small. The explanation of the main cases follows.

- Figure 12.1C shows expansion to the point where only the tip is displayed. Here, one sphere in the middle region is interacting with one incisor. In Figure 12.1D, the first collision is ignored and the expansion occurs so that the tip and middle regions are both displayed. Here, one sphere in the back is interacting with one incisor. For instance, if we want a long tongue expansion, we need to ignore the collision in Figure 12.1C. MT is the maximum allowable expansion for the tip and $MTM - MT$ is the maximum allowable expansion for the Middle. Both, MTM and MT can be an anatomical proportion.
- Once the tongue is drawn. The middle and tip regions can be rotated. In Figure 12.3A, the back region is colliding with one incisor to limit maximum expansion

(collision of the middle region and the incisor was ignored). Then, the tongue can be rotated downwards or upwards. Here, the middle and tip regions collide with spheres in the mandible or in the skull. In Figure 12.3B, the middle region is colliding with one incisor as we only want to display the tongue’s tip. Then, it is rotated downwards. Here, the tip region collides with spheres in the mandible. Figure 12.3C shows tongue rolling. Here, the tip region collides with the middle and back region to avoid interpenetration.

After space exploration, we generated three TSSs for the movement of the tongue. The Tongue-Mandible TSS performs 5 sphere - sphere collision tests per time step. The Tongue-Skull TSS performs 2 sphere - sphere tests per time step. The Tip-Middle and Back region TSS performs 2 sphere-sphere tests per time steps. The TSS used is chosen according to the chosen AU. for instance, all TSSs are not executed at the same time. Additionally, depending on the AU (length of the expansion), one of the 5 tests from the Tongue Mandible TSS is ignored.

AU16 implements consecutive downwards and upwards rotations of the middle and tip regions, mostly used in the expression of affection. AU17 rolls the tongue regions against each other. This shape is common before yawning or hanging out the tongue on tiredness. AU18 display and rotates the tip only. It is an optional AU which can accompany expressions such as anger and fear. AU19 implements drawing. The middle region is rotated downwards and the tip region is rotated upwards. This shape is common in yawning and tiredness. AU16, 17, 18 and 19 are high level expressive parameters; while MT , MTM , α , β are conformational parameters which support the AUs (figures 12.1C and D; figures 12.3D and E). Figure 12.5A shows the dialog box used to locate the tongue and generate its TSSs.

12.2 Eyes

12.2.1 Previous work

Eyes are important for realistic modelling (Byun and Badler (2002); Haber and Terzopoulos (2004)) and can be accompanied by eyebrows (Cazedevals *et al.* (1993); Zhang *et al.* (2004a); Zalewski and Gong (2005)). Misused eyes can produce incorrect perception of faces. For this reason, some works do not include eyes (Curio *et al.* (2006)). Eyes can be represented by additional geometric models that enhance realism (Waters (1987); Breton *et al.* (2001); King (2001); Kähler *et al.* (2002); Tarini *et al.* (2002);

Zhang *et al.* (2003a); Yao *et al.* (2005)). Eyes are important in the parameterisation of facial animation and require believable motion. Realism can be achieved with the inclusion of eye blink (with eyelids), proper eye gaze (direction of eye in space) and the inclusion of head-eye-gaze kinematics or dynamics (Haber and Terzopoulos (2004)).

Amongst the techniques used for eye modelling are polygonal meshes (Breton *et al.* (2001)); layered model of polygonal meshes with animated pupil (Navarro Newball *et al.* (2003)); swept revolution surfaces (Waters (1987)); spheres (King (2001)) with adjustable irises and pupils (Lee *et al.* (1995)); Markov set based texture generation on a generic mesh with animated texture for pupil dilation (Tarini *et al.* (2002)); image processing (Cazedevais *et al.* (1993); Kähler *et al.* (2003)).

Eye movements follow the direction of movement of the face to facilitate visual target localisation,(Haber and Terzopoulos (2004)). Amongst the techniques used to animate the eyes are :

- A few simple parameters (Breton *et al.* (2001); King (2001)).
- Eye kinematics which makes them converge on a fixation point in 3D space (Lee *et al.* (1995)).
- Statistical movements to include saccadic movements (Kähler *et al.* (2002)).
- Interpolation using training sets of capture data (Haber and Terzopoulos (2004)).
- By hand, Radford (2006).
- Mapping 2D animated features of the eyes to a 3D mesh (Williams (1990); Guenter *et al.* (1998)).
- Euler angles which parameterise gaze direction (Pighin *et al.* (2005)).

Additionally, it is possible to model pupil dilation according to the amount of light entering (Lee *et al.* (1995)). Frequently the eye model is complemented with the eyelids and eyebrows. For example, eyelids are modelled with a polygonal mesh with a defined kinematics for blinking (Lee *et al.* (1995)); curves from the vertices of the face (Waters (1987)); image processing (Cazedevais *et al.* (1993)).

12.2.2 Analysis

Eyes are important in facial expression. In general, eyes imply the use of eyelids and eyebrows. Eyelids can be part of the facial mesh or separate meshes. Usually, eyes are

represented as additional geometric models. However, sometimes they are textured on the facial mesh. The iris can be modelled so that the pupil is dilated. Eye and gaze kinematics add realism to the model. Dog’s eyes are spherical (Section 4.8). Even though we did not find information on dog eye kinematics, we assumed it to be similar to that of human eyes. Dogs’ eyebrows are obscured by fur and we did not include them.

12.2.3 A dog eye model

In Londra, eyes are modelled with four layered spheres each (Figure 12.4A). The sclera, the cornea, the iris and the pupil. Spheres are not located in the same centre in order to achieve a slight protrusion in the iris. The use of a transparent cornea adds glistening to the eyeball enhancing realism. The pupil was implemented with the innermost sphere. It dilates by moving its sphere slightly forward through the Z axis. Londra’s eyes include gaze kinematics. They can be made to look at some particular point using a gaze formula (12.1, Figure 12.4A). Figure 12.4C shows Londra’s eyes with and without a dilated pupil.

$$\alpha = \sin^{-1} \left(\frac{\text{Eyes distance}}{2D} \right) \quad (12.1)$$

We decided to implement eye motion with kinematics because muscles moving the eyes do not affect the shape of the facial skin. The eyes include two degrees of freedom and can rotate about the X and Y axis and can rotate in the same or in opposite direction. AU12, 13 and 14 represent high level expressive parameters which alter the eyes’ direction of sight and gaze. Eyes’ radii and the position of the sphere representing the pupil are conformational parameters. Figure 12.5B shows the dialog box used to locate and define the eye radius. Also, it includes buttons to make the eyes closer or farther and a button to generate the eyelids. In Londra, eyelids are part of the skin layer and will be explained later.

12.3 Nose

12.3.1 Previous work

King (2001); Chen (2006) talk about the difficulties in scanning the nose. During a 3D scan of the head it is common to miss nose geometry that has then to be adapted or

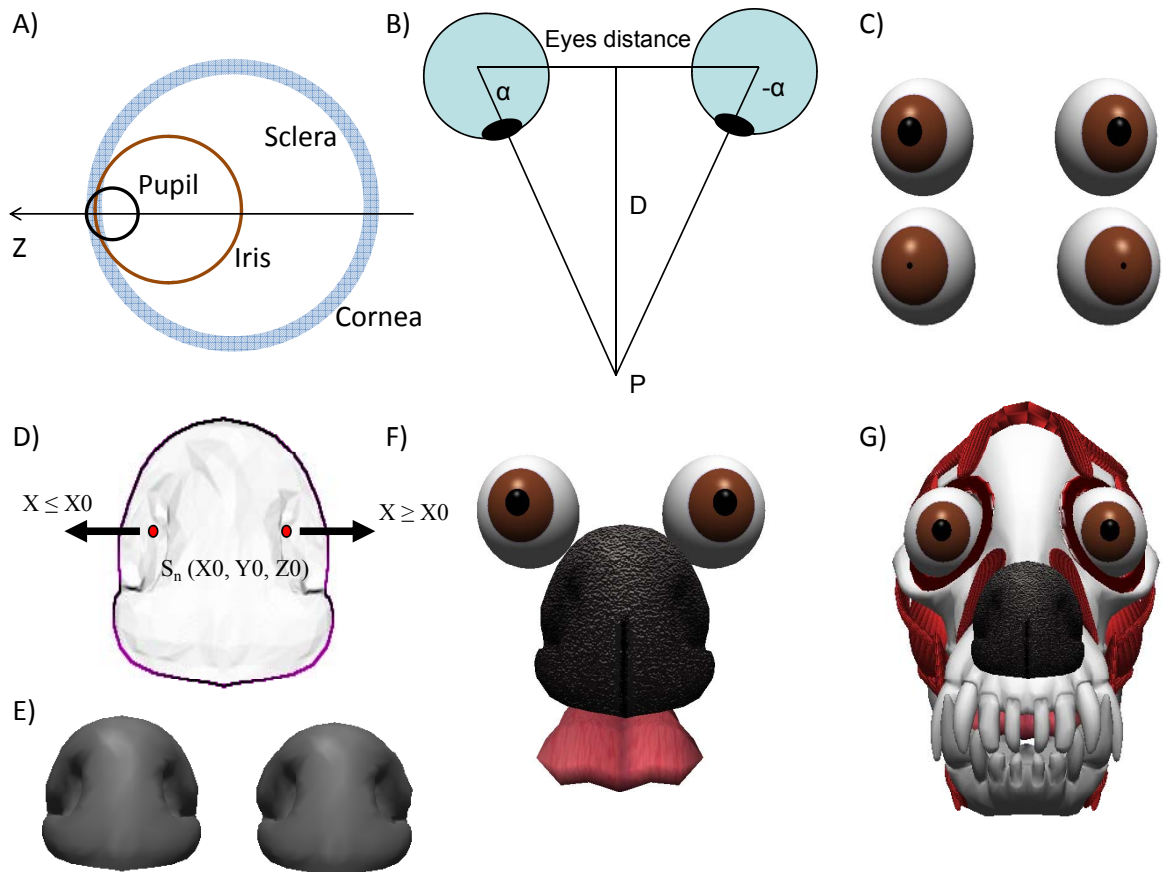


Figure 12.4: Eye and nose models. A) Layered eye model base on spheres. B) Gaze. D is the distance to a point P . α is the orientation. C) Londra's eyes. D) Dilating Nostrils. E) Nose before and after nostril dilation. F) Nose and the complementary layer. G) Bone, muscle and complementary layers.

corrected. The nose is usually included in HFAMs through FACS' AU9, nose wrinkler (King (2001); Zhang *et al.* (2004a)). Also, in some models the shape of the nose plays an important rôle. For example, Parke (1974) describes conformational parameters such as nose length, width of nose bridge and nostril width. Blanz and Vetter (1999) propose a morphable model for synthesis of 3D faces. Here, they include nose shapes such as 'hook' nose. Kähler *et al.* (2003) uses heuristics for nose shaping in facial reconstruction.

12.3.2 Analysis

Nose mobility is limited. However, there are some nose movements that are important and can be coded in FACS. In dogs, we are concerned with nostril dilation; snout wrinkling caused by nostril dilation and some slight rotation. Nose shapes are diverse and some HFAMs include conformational parameters and heuristics to produce the right model. In dogs (Section 4.9), the nose is visible in a different colour and texture. It includes a medial groove and can vary in width and length. For Londra we required one nose only.

12.3.3 A dog nose model

Londra's nose is imported from an artist's 3DS mesh (Artist-3D (2008)) and located in the Nasal Notch (Figure 4.2). The appearance and the median groove are achieved applying a 2D texture to the mesh (Figure 12.4F).

12.3.4 Nostril dilation

Angelidis (2004) introduced swirling sweepers. A virtual sculpting tool where "the artist describes a deformation by dragging a point along a path" (Angelidis *et al.* (2004), p.1). For nostril dilation we followed a similar idea. However, instead of moving the point along a path, nostril dilation is done by placing one sphere at a convenient location in each nostril. When the nostril is dilating, the radius of these spheres is increased. The sphere is intercepted with the vertices of mesh representing the nose. Then, vertices in contact with the spheres are displaced linearly in a direction outwards from the centre of the spheres. In Figure 12.4D, the centre of the sphere in a nostril, S_0 , is located at (X_0, Y_0, Z_0) . For the left nostril, only intercepting vertices, where the position of the vertex $X \leq X_0$ are displaced. For the right nostril, only intercepting vertices, where the position of the vertex $X \geq X_0$ are displaced. From

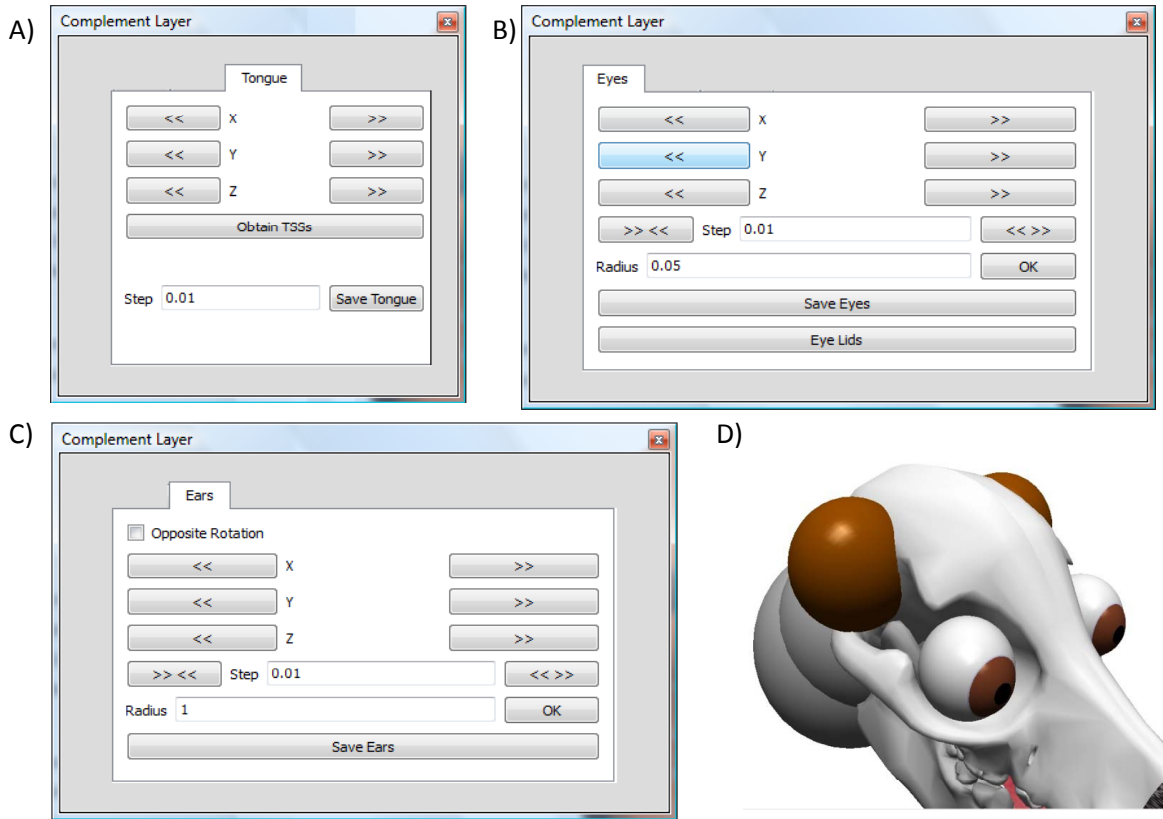


Figure 12.5: Complementary layer GUI and ear markers. A) Dialog box for tongue model. B) Dialog box for eyes model. C) Dialog box for ear markers. D) Ear markers.

our observations (Appendix D, Figure D.1), we decided to accompany nostril dilation with a slight rotation around the X axis (under nose motion). Figure 12.4E shows the nose before and after nostril dilation. Figure 12.4G shows the bone, muscle and complementary layers. AU3 is a high level expressive parameter. The radius of the spheres affecting the nostrils are conformational parameters.

12.4 A note about the ears

Ears could be part of the complementary layer but to maintain skin continuity we decided to model them in the skin layer. However, the position of the ears is defined in the complementary layer. Here, using the dialog box shown in Figure 12.5C we can define the radius and position of two spherical markers that indicate ear position (12.5D).

12.5 Discussion

Londra's tongue collides with the bone layer, and approximates volume preservation. We identified typical dog expressive shapes (e.g. licking) and focused our modelling on those. Our tongue has potential for asymmetric deformation and for parameters that run across and not along it. However, we did not implement those features. Our choice of two bends is good enough for Londra's expression, the addition of more regions would add complexity to the problem. Our implemented tongue shapes give ideas on how to implement human expressions such as 'sticking the tongue' which are not common in current HFAMs. Our model could be enhanced with the addition of interacting forces.

Generalising the TSSs to more degrees of freedom or to include some asymmetric motion is possible while keeping the number of required tests low. However, to implement this, we require the implementation of an asymmetric bend. One idea to explore the whole space of motion during TSS generation would be to:

- Continuously expand and contract the tongue to MTM in all regions of the mouth opening (defining a discrete step size).
- Then, continuously bend the tongue upwards and downwards.
- Repeat the process expanding the tongue to MT only.
- Roll and unroll the tongue.

We identified and used a preliminary set of tongue parameters:

- Conformational: MT, MTM, α, β .
- Expressive: AU16 (which can be iterated), AU17, AU18, AU19 and their counter actions.

Our model successfully approximates dogs' eyes. In the search for realism we added a transparent cornea and a gaze formula which was taken from human eye gaze. The pupil is simulated with an extra sphere. Although the pupil is in reality a hole in the iris, we achieved a nice dilation effect with our implementation. The surfaces of the eyes are anatomically correct because dogs' eyes are spherical. The fact that the layered spheres are not located in the same centre helps achieving the slight protrusion in the iris. In this case we decided to ignore eyes' inner anatomy. Londra's eyes anticipate the expression where they are important. For example, in attention, they move first towards the object of interest.

We used a spherical model of the eyes which requires a few parameters. Our preliminary set of eye parameters include:

- Conformational: radii, pupil position.
- AU12, AU13, AU14 and their counter actions; gaze.

Our nose model can be expanded to allow reshape for other breeds. This is out of the scope of the project and requires further anatomical study. We only affect the nose surrounding region with the Levator. More realism can be achieved by including more muscles (e.g. to produce wrinkles under the nose). Londra's nose is as anatomically accurate as the 3D mesh we used is. It is placed correctly on the skull. However, the nose and the skull were obtained from different sources and do not necessarily belong to the same kind of dog. We identified and used a preliminary set of nose parameters:

- Conformational: Nostril's spheres radius.
- Expressive: AU3 and counter action; rotation around X .

Chapter 13

Skin layer

13.1 Previous work

Skin is anisotropic, has nonlinear stress-strain, visco-elastic behaviour (King (2001); Zhang *et al.* (2004b)). It has three layers (Epidermis, Dermis, Hypodermis); in low stress offers low resistance; in high stress there is a sharp increase in resistance (Haber and Terzopoulos (2004)). Viscosity causes a time dependent deformation; plasticity causes an irreversible deformation (Noh and Neumann (1998)). The skin returns to its rest shape when load is removed. Skin's elastic properties are similar to a spring; skin's viscous properties are similar to a damper-dashpot (King (2001); Haber and Terzopoulos (2004)). Skin deformation highly depends on muscle actions (Byun and Badler (2002); Radovan and Pretorius (2006)). A model can consider the skin as a surface (King (2001)) or to be more accurate as a volume (e.g. Zhang *et al.* (2004a); Chen and Prakash (2006)). Some models mix parametric geometric animation with physically based approaches. Here, some movements are performed with kinematics and muscular animation is performed in a second phase (e.g. Breton *et al.* (2001)). Additionally, colouration caused by vascular changes (Radovan and Pretorius (2006)) or scattered illumination models specialised in faces (Weyrich (2009)) can be used to enhance realism.

Amongst the factors that can be considered are: tensile strength of muscle and skin; proximity to muscle attachment; depth of tissue; proximity to the bone; elastic bounds; interaction of multiple muscles. Real skin can produce thousands of movement combinations based on the interaction with muscles and bone; however, it is required to find a simpler subset of parameters (Waters (1987)). Some previous skin models in facial animation are:

- Lee *et al.* (1995) create a dynamic model from the skin mesh. It has four mass spring layers assembled as triangular prisms according to histology. It has non penetration constraints for the skull and is solved using Euler integration.
- King (2001) uses characteristic points and barycentric coordinates to deform the facial surface. These points are arranged in a control network where the movement of a point represents the movement of a region.
- Kähler *et al.* (2002, 2003) use mass spring mesh of the skin and springs to interact with other layers. Here, radial basis interpolation is used to match the new position to the original skin mesh.
- Zhang *et al.* (2004a) use a multilayer skin with non linear springs and edge repulsion springs (to avoid collapse). They consider skin regions, landmarks, mass, damping and stiffness between nodes. The model is solved with Lagrangian dynamics and semi-implicit integration and uses an adaptive simulation algorithm to concentrate processing on the deformed region.
- Wrinkles can be modelled with bump mapping (Kähler *et al.* (2002); Radovan and Pretorius (2006)); image base techniques (e.g. texture, shadowing) (King (2001); Radford (2006); Bickel *et al.* (2007)); or non linear springs (Wu *et al.* (1994)).
- Geometric approaches (e.g. DeRose *et al.* (1998); Watt and Policarpo (2001)) use some kind of free form deformation; wires; control networks of characteristic points (King (2001)). Some state that geometric approaches are not substantially inferior to more complex models (Watt and Policarpo (2001)).

13.1.1 Analysis

Skin modelling is related to muscle modelling. Deformation of the skin depends on muscles' actions which are able to slightly change the skin's shape. The model can consider the skin as a surface or to be more accurate as a volume which includes multiple sub layers. In geometrical models, the response of the skin to muscle actions can be modelled with free form deformers. Here, displacing a control point is analogous to actuating a muscle. In physical models it is common that skin movement affects its neighbour the same way as a network of springs which sometimes includes non linearity. Some models mix parametric geometric animation with physically based approaches.

Skin nodes can be assigned to some region of the face and some movements can be performed with kinematics (e.g. jaw) and muscular animation can be performed in a second phase. In some models, characteristic points reduce skin complexity. Here, the movement of a simple point can represent the movement of a whole region. Wrinkles represent an additional challenge which sometimes is solved with image based or lighting techniques. Skin rendering has required the development of specialised illumination schemes and the use of specially created textures.

Londra's skin is able to produce wrinkles and does not include sublayers. Due to elasticity, wrinkles are not permanent and vertices go back to the default position. Vascular changes are not important. Instead, the skin is covered with fur. Depth of tissue and fat are approximated by the threshold distance between the skin and the underlying structures. For example, muscles touch the skin through spheres protruding the surface of both. The radii of these spheres can vary in different facial regions. The skin is deformed with kinematics, muscle actuations or both. Deformation is only performed in the regions covering the geometry of the acting muscles (using TSSs) or in regions where kinematics is applied first (e.g. mandible). Muscles' geometry influence Londra's skin geometry and deformation. Indeed, we follow a unique bottom up approach to generate the facial skin mesh which does not rely on a pre-existing mesh.

13.2 Skin generation

In typical skinning (Mohr and Gleicher (2003); James and Twigg (2005); Kavan *et al.* (2007)), vertices are weighted with respect to a skeleton. Frequently, a skin mesh is designed in a reference position and is bound to one or more joints. While this technique has been widely used, the addition of more detail relies on including fake anatomically incorrect joints or bones. Also, the technique can produce artefacts. In model reconstruction (Simmons *et al.* (2002); Kähler *et al.* (2003)), feature points are used to deform or generate a reference skin mesh. Here, a skin reference model is interpolated using radial basis functions. However, feature points need to be defined interactively and generalised tissue must be used to represent bulks. In voxelization (Wilhelms and Van Gelder (1997); Karabassi *et al.* (1999)), a body hierarchy in rest position is specified. Here, underlying components are voxelized in a 3D grid and an implicit surface for the skin is extracted. The skin is anchored to the nearest underlying component. However, some areas of the surface may not be visible and holes must be

covered with generalised tissue. In marching cubes (Lorensen and Cline (1987); Bourke (1994)), an implicit surface is extracted using lookup tables. It relies on the use of a regular grid. This technique, which uses a 3D grid or voxels, frequently generates more vertices than required and needs space partitioning. In Shrinkwrap (Bottino *et al.* (1996); van Overveld and Wyvill (2004)), a technique adaptive to the local behaviour of the surface, a sphere shrinks iteratively to the final shape using Newton-Raphson and curvature is adjusted according to the gradient. The approach can be extended to account for topological changes. However, including topological changes requires reconnection; identification of type of change; and the curvature parameter for the adaptation has to be defined by the user. In active contours (Morse *et al.* (2005)), an initial estimate of the shape is adapted iteratively using radial basis functions and adapts naturally to complex surfaces. However, most of the work on adaptive contours has been done in 2D. Shrinkwrap could be considered an extension of the same idea to 3D. Both approaches rely on iterative processes that converge only under certain conditions and may affect the distribution of large and small triangles.

13.2.1 Interpolation

Our first option was to use a big pre-existing reference shape (Figure 13.1A). Then, we would define characteristic points as in King (2001) (Figure 13.1B). However, these points would be used to fit the skin mesh to the underlying anatomy, not to deform the skin. Next, we would start shrinking a triangulation of the characteristic points inspired in the idea by Bottino *et al.* (1996); van Overveld and Wyvill (2004). However, shrinking a mesh that already has the desired topology should be simpler than shrinking a sphere that has to be adapted to the underlying topology. The idea was that every characteristic point in the facial mesh would have a counterpart in the underlying layers (Figure 13.1C). This way, the characteristic points in the facial mesh would be interpolated to their counterparts and the remaining vertices would be adjusted through their barycentric coordinates (figures 13.1D and E). Appendix I introduces barycentric coordinates. Figure 13.1F shows the final result using this idea. The result looks promising but the fitting is not perfect. We decided to abandon this approach for the following reasons:

- Better fitting requires the definition of more characteristic points and their counterparts. The interactive definition of these is tedious especially in the skin mesh (we found that the semi automatic generation of feature points from the under-

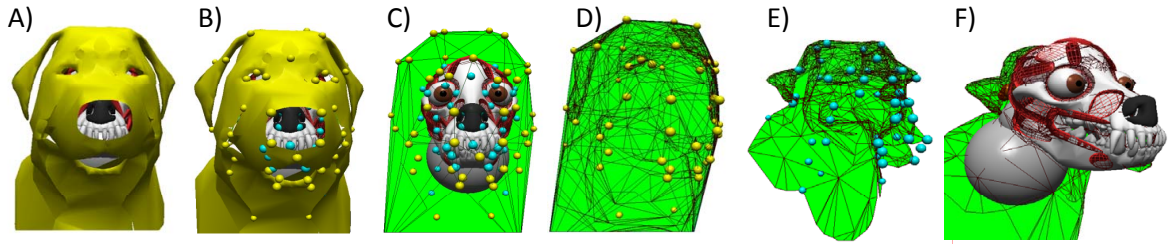


Figure 13.1: Skin interpolation. A) A big mesh inscribes the underlying anatomy. B) Characteristic points in the facial mesh. C) Blue points are counterparts of yellow characteristic points. D) Triangulation of characteristic points in the facial mesh. Remaining vertices are interpolated with barycentric coordinates. E) Facial mesh shrunk to make characteristic points coincide with their counterparts. Remaining vertices are interpolated with barycentric coordinates. F) Interpolated skin.

lying anatomy was feasible).

- The skin mesh (obtained from Artist-3D (2008)) does not belong to the skull used. They were obtained from different sources.
- This approach does not agree with our pure bottom up approach. We did not want to rely on a pre-existing facial mesh. Instead, we decided to generate it.

13.2.2 Bottom up generation of the skin

Skin generation was a major challenge in our bottom up approach. We simplified the problem and took advantage of head symmetry as follows:

- Using the underlying anatomy (Figure 13.2A), we generate feature points on one side of the head semi-automatically (see section 13.2.4).
- Then, we project the feature points on a mirror plane which cuts the head in the middle. As the points representing the ear can cause topological distortions only the root of the ear is projected.
- Once on the plane, using 2D Delaunay (Cheng *et al.* (2007)), we triangulate the points (Figure 13.2B).

- To agree with the desired topology, resulting triangles are filtered using pre-programmed topological anatomical restrictions such as: more than two points belonging to a region with a hole cannot be connected in the same triangle (e.g. nose, ear root, and eye); points from the lower neck cannot connect with points not belonging to the neck.
- Once the one side of the mesh is generated, we mirror and smooth it with $\sqrt{3}$ subdivision to obtain a skin mesh. At this stage, the underlying anatomy overlaps this mesh.
- Inspired by Bottino *et al.* (1996) and by the way a warm towel is put on our face when we go to the barber, the skin mesh is inflated in the direction of the normal of each vertex so that every part of the underlying anatomy is inside it (Figure 13.2C). Then, the 'warm towel' algorithm starts deflating iteratively the skin mesh in direction opposite to each vertex normal. Deflation stops when all skin vertices are within some threshold of the underlying anatomy (Figure 13.2D).

Figure 13.3C shows the dialog box components to generate Londra's skin. Here, we added buttons for optional interactive editing of vertices and triangles and one additional optional smoothing.

13.2.3 Lips

In HFAMs lips have to be shaped and coloured. For example, Kähler *et al.* (2003) determines the thickness of the lips by examining the upper and lower frontal teeth. Tarini *et al.* (2002) identify the lip in a scanned facial mesh region and colour it. Breton *et al.* (2001) implements lips made of a single separate mesh which is moved by muscles. Lips convey the most information during speech (King (2001)). King (2001) introduces a separate and highly deformable lips models. He uses a B-spline surface which allows specifying most useful position and shapes. His model includes an advanced lighting model.

Dog lips can be seen as an extension of the skin. In some breeds lips are firmer than in others. Lips are speechless and follow the motion of the deformation caused on the skin by the action of the orbicularis oris (Sisson *et al.* (1975)) . In Londra, lips are a consequence of the skin mesh and follow the movement of the vertices in the mouth boundary. We generate Londra's lips from the skin (Figure 13.2E). Using the 3D parametric line equation (Figure 8.2A) we generate textured spheres along the

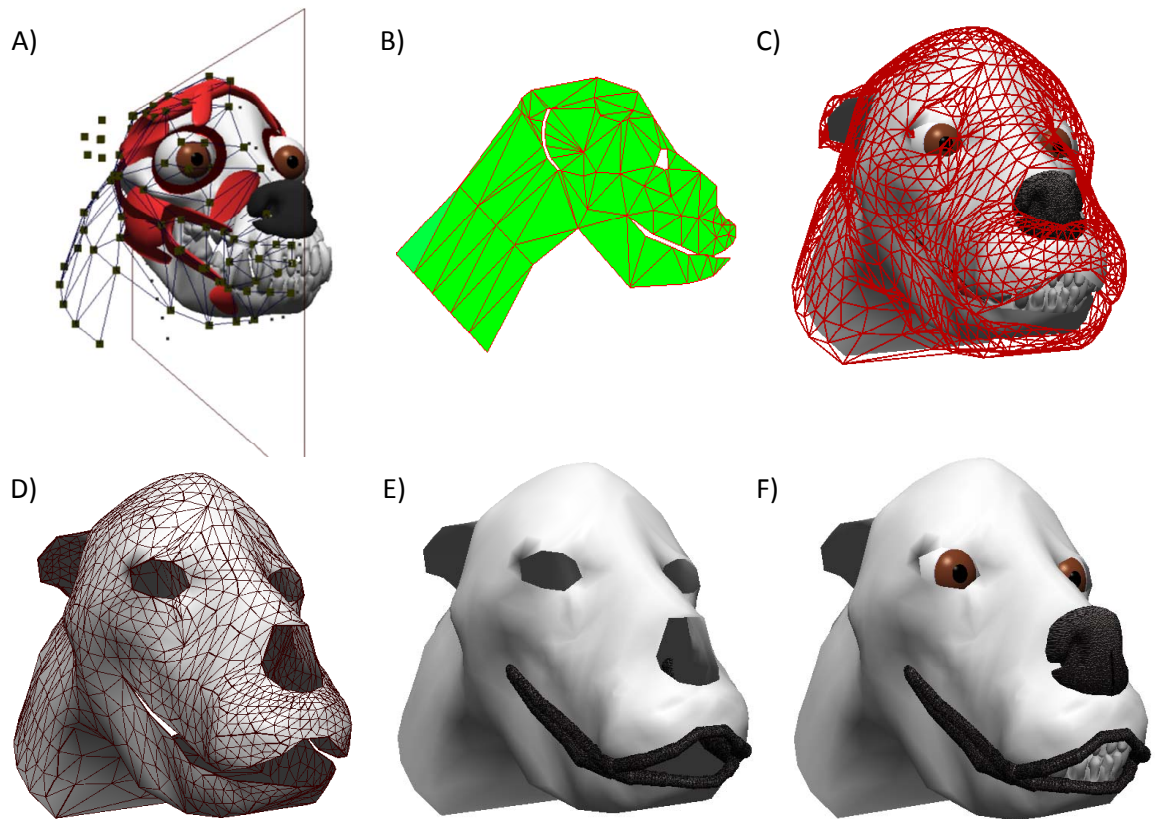


Figure 13.2: Skin generation. A) Feature point generation. B) 2D triangulation. C) Inflating the skin. D) Deflating the skin. E) Skin with lips. F) Bone, muscle, complementary and skin layers.

lines between boundary vertices in the mouth (lip region). We use different radii along different boundary regions of the mouth. For example, the lateral lower lips are thicker than the frontal upper lips (as in real dogs). Figure 13.2F shows the bone, muscle, complementary and skin layers.

13.2.4 About feature point generation

We state that our feature point generation is semi-automatic because it was programmed with our anatomical knowledge. However, once programmed, feature point generation is automatic. The points were generated as follows:

- At a threshold along the path of some muscles (e.g. Zygomatics, Frontalis, Masseter, etc.).
- Sometimes, finding the leftmost, rightmost, lowest and upper most vertex of some muscle or bone and adding a threshold.
- Mirroring half of the points.
- For points around the nose, we detected the nose's boundary (taking advantage of the direct edges data structure).
- For the eyelids, we generate points around the centre of the spheres representing the eyeball at a distance slightly greater than the radius, using an inclination angle (α) (Figure 13.3A). For AU4 and AU15 we change α accordingly.
- For neck and ears we generate points along the main axis of the spheres used as markers. The radii (D_0, D_1, D_2) are defined accordingly (Figure 13.3A). Cropped ears are simpler to generate. However, the idea can be extended by using more spheres as underlying ear markers.
- Some other points are obtained from displacements of others calculated with the above methods.

13.3 Skin deformation

Deformable objects have been represented in many ways (Müller *et al.* (2005)). From finite difference approaches and mass spring systems to finite element methods and particle systems.

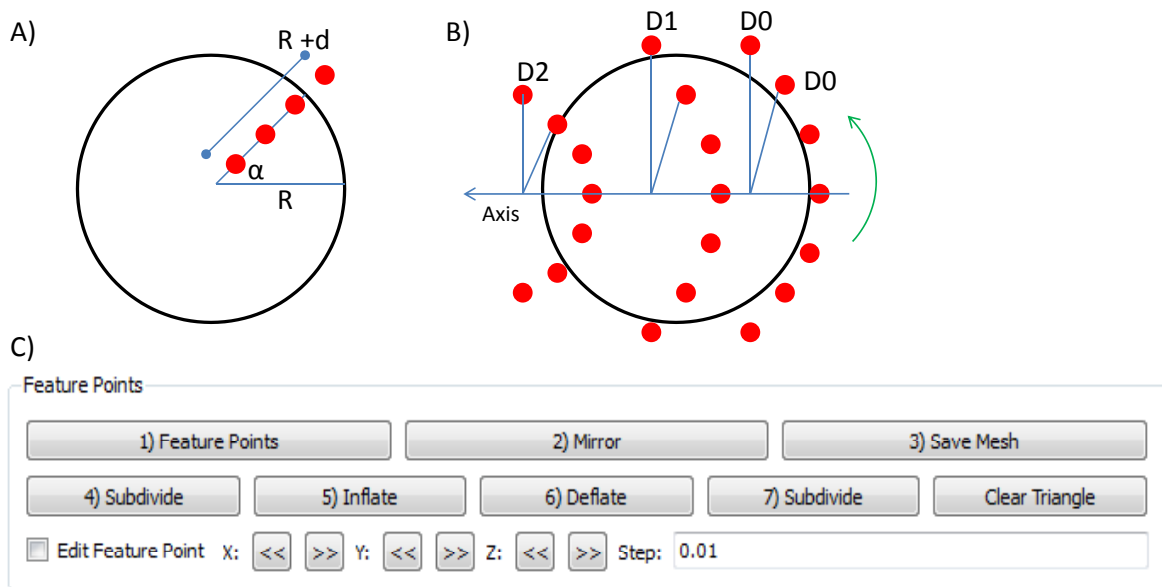


Figure 13.3: Feature points generation. A) Generating feature points at a distance $R + d$ from the centre of a sphere at an angle α . R is the radius of the sphere. B) Generating points along the main axis of a sphere. $D_0 \neq D_1 \neq D_2$ are distances from the main axis. C) Dialog box for skin generation.

Müller *et al.* (2005) use an underlying geometrically motivated model. Here, geometric constraints account for energy and distances of current positions to goal positions account for forces. The approach uses deformation modes, geometrically motivated, related to modal analysis and shape matching with a priori known correspondences. The main contributions of this model are: elasticity is based on shape matching and on pulling a deformed geometry to a goal configuration; representation details can be changed according to the model used (e.g. linear, quadric, clusters); a large variety of objects can be handled; the technique uses simple and intuitive parameters and does not require large data structures; the technique is stable under all circumstances; and is an efficient and simple to implement approach. King (2001) uses a few characteristic points stating that they can be used to reduce complexity of the geometry and that can be placed in areas that move in unison.

We adapted ideas from these two approaches. Particularly, we borrowed from Müller *et al.* (2005) the idea of representing forces with distances and that of keeping the original un-deformed shape in sight. Also, as in King (2001) we believe that characteristic points can be used to reduce the complexity of the geometry. However, our approach is different. Our tissue model, which is explained in the next sections, was implemented taking into account the following requirements:

- Manage a connected mesh structure.
- Approximate skin's elastic properties.
- Control the deformation with a subset of vertices.
- Have potential to maintain skin's anisotropy.
- Allow interaction with other underlying layers through the use of spheres.
- Allow some underlying thickness (not necessarily constant thickness).
- Allow the application of independent forces to each particle.
- Simplify vertex-vertex interaction.
- Allow simple rendering.
- Be able to manage instant and constant forces.
- Use small time steps or make time step size independent from Euler integration. Skin interaction requires small time steps anyway.

- Simplify wrinkles.
- Have the potential to allow some sub-regions behave differently.
- Be simple.

As real particle to particle interaction is not considered, we simulate it by assuming the original unchanged mesh is in equilibrium. For instance, the original position of a particle is its equilibrium position. Any deformation causes an elastic reaction force towards the original position in the original mesh. A control mesh (subset of characteristic points) is deformed and used to create a refined subdivision surface suitable for rendering. In this way we avoid exhaustive elastic calculations while still producing visually appealing results.

13.3.1 Keeping track of the original shape

After deformation, if force is no longer applied, a particle should be able to return to its original position (goal position in Müller *et al.* (2005)). The original method (Müller *et al.* (2005)) claims that no big additional data structures are required. However, in our case we decided to keep a copy of the original skin model in an additional mesh structure. This eases calculations and does not consume too much additional memory because the technique is used for the skin only. The values in the original shape are only updated if the mesh representing the tissue is transformed with respect to the world coordinates. In contrast, the original shape remains unchanged under the action of forces. It is assumed to be in equilibrium.

13.3.2 Obtaining forces

There are three kinds of forces in our model: instant forces applied by the muscles; reaction forces; gravitational force.

In Figure 13.4A, N_m is the normal at the muscle; N_s is the normal at the skin; R is the vector from the centre of the sphere at the muscle to the centre of the sphere at the skin; D is the displacement of the muscle. Here, the force F is obtained as $F = R + D$. In real skin, one factor affecting skin's tensile strength is proximity of muscle attachment. In our case, intensity of the force can be increased (or decreased) having a much bigger (smaller) sphere on the muscle interacting with a smaller (bigger) one on the skin.

In Figure 13.4B, a group of particles is interconnected (connections are represented with dotted lines). Here, one particle has been moved from its equilibrium position P to a deformed position P' by a force F . This causes an elastic reaction force R towards the equilibrium. We had two options to obtain R :

- We could calculate the reaction force from the neighbours (as suggested by the blue dotted arrows in Figure 13.4C).
- We could return the particle to its original position elastically, using the original unchanged mesh as a reference (Section 13.3.1).

The problem of reaching equilibrium in a system with several particles adds complexity and instability. For instance, we decided to calculate the reaction force as the distance between the current (deformed) position and the original (goal) position and we multiply it, according to Hooke's law, by an elastic constant. This brought visually appealing results and a solution which is easier to control.

Gravitational force can be added as a constant to the affected particles. It points towards the negative direction of the Y axis.

Figures 13.5A, B and C show a piece of tissue where the particles are under the action of gravitational force. Figures 13.5B, C, D and F show some instant deformation caused by a muscle.

13.3.3 Particle-particle interaction

King (2001) stated that characteristic points can be used to reduce complexity of the geometry and that they can be placed in areas that move in unison. We took advantage of this idea. Here, a skin control layer interacts with other layers and on deformation it generates a $\sqrt{3}$ smoothed mesh (Chapter 6). Subdivision can be general to the whole mesh (Figure 13.5G) or can be performed in the neighbourhood of the deformed particle (Figure 13.5H).

Real particle to particle (vertex-vertex) interaction is not considered. However, as we assumed the original unchanged mesh is in equilibrium, the original position of a particle is its equilibrium position. Any deformation causes an elastic reaction force towards the original position in the original mesh. Here, a control mesh (that could be seen as a subset of characteristic points) is deformed and used to create a $\sqrt{3}$ subdivision surface suitable for rendering. Figures 13.5D shows the deformation caused by an instant force in the control mesh. Figures 13.5E shows the $\sqrt{3}$ smoothed

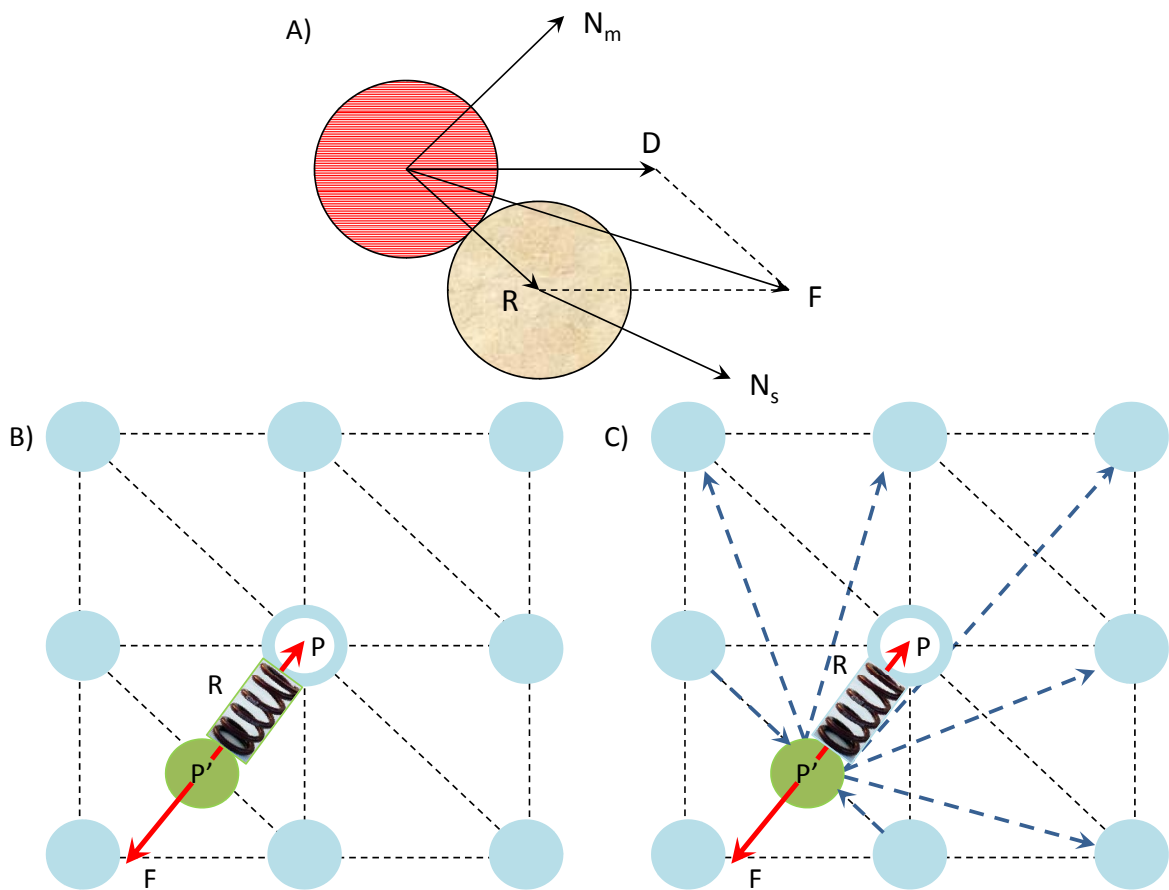


Figure 13.4: Forces calculation. A) Instant forces applied by the muscles. B) Reaction force. C) Reaction force from neighbours.

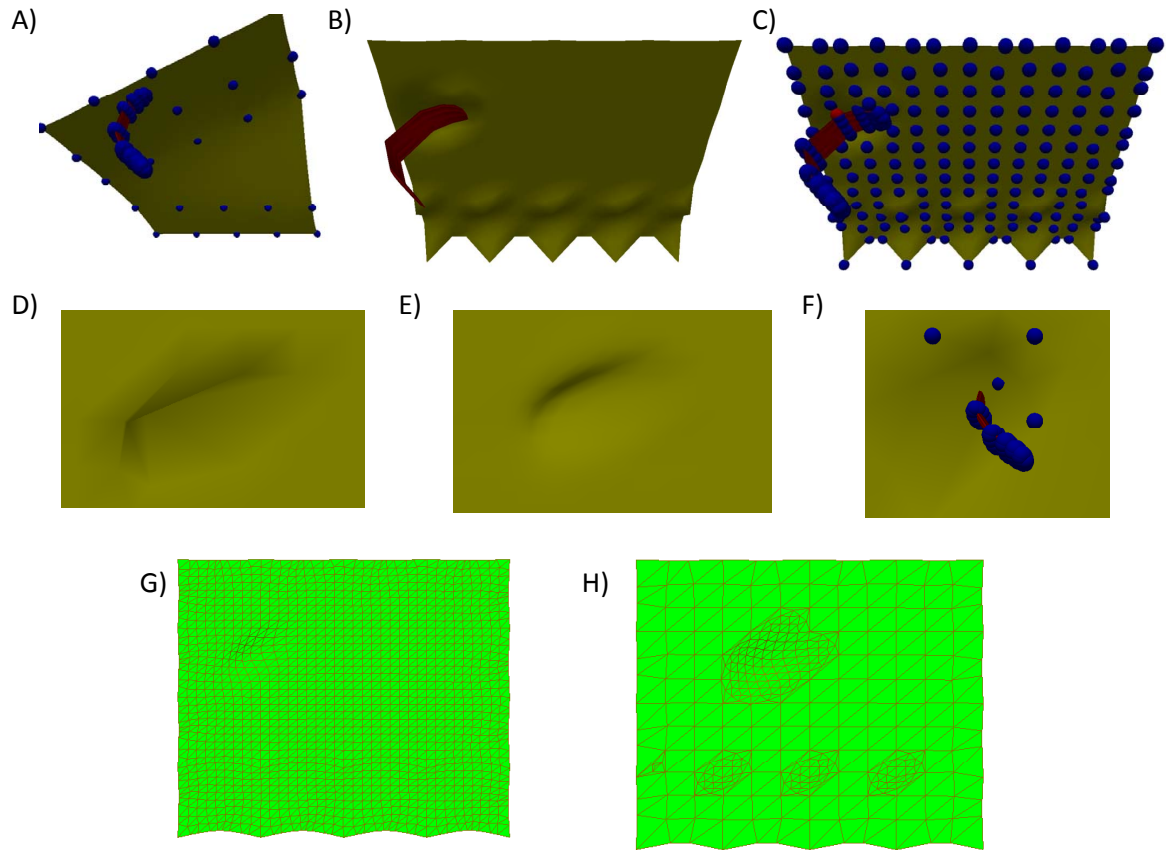


Figure 13.5: An elastic piece of skin. Vertices have spheres associated. A) 5×5 patch with the back region under the action of gravity. B) 13×13 patch under the action of an instant force applied by the superquadric muscle. Some regions are under the action of gravity. C) 13×13 patch under the action of an instant force. Related spheres are displayed. D) Deformation caused by an instant force in the control mesh. E) Smoothed limit surface obtained from the control mesh in Figure D. F) Lower resolution deformation (Appendix K, LowDeform.avi). G) Full smoothing of deformation. H) Localised smoothing of deformation.

version of this deformation. Figures 13.5G shows the deformation caused in a less dense network of control (characteristic) vertices. The result differs from that of figures 13.5D and E.

13.3.4 Elasticity, viscosity and plasticity

Purely elastic materials have stress and strain in phase, so that the response caused is immediate. Plastic materials maintain the deformation. Viscosity is somewhere in the middle. For instance, visco-elastic materials have a time dependent strain, meaning that they do not return to the equilibrium immediately. Viscosity can be linear for small deformations. We did not consider plasticity as it is useful only when permanent tissue deformation is required (e.g. aging). Elasticity is simulated by producing a reaction force that moves particles back to their equilibrium state. This force follows Hooke's law which states that the extension of a spring is in direct proportion with the load added to it as long as this load does not exceed the elastic limit (Eberly and Shoemake (2005)). Here, force for a particle in position P_0 which has been moved to P is obtained as (13.1). Tissue is more or less plastic (elastic) depending on the elasticity (viscosity) coefficient.

$$F = -elasticity \times |P_0 - P| \quad (13.1)$$

We implemented a linear model for a visco-elastic skin. Linear systems are a mathematical idealisation and are simpler to solve. We are assuming a young skin where plastic and viscous behaviour are less evident. Videos *Elasticity1.avi* and *Elasticity2.avi* (Appendix K) show our elastic patch.

13.3.5 Integration and stability

In order to obtain the new positions we use Euler integration because it is intuitive and fast. Here, m is the particle mass.

- In a time step an instant force F is applied, integration is done using (13.2).
- During the next time steps, integration under the action of the reaction force R is done using (13.3).
- If the particle is under the action of gravity, we add a constant to account for the gravitational force.

- If the particle is still under the action of the muscular force, instead of integrating, we use sphere-sphere interaction to avoid tissue returning to its equilibrium state.

$$v_{t+\delta t} = v_t + \left(\delta t \times \frac{F}{m} \right); x_{t+\delta t} = x_t + (\delta t \times v_{t+\delta t}) \quad (13.2)$$

$$v_{t+\delta t} = v_t + \left(\delta t \times \frac{R}{m} \right); x_{t+\delta t} = x_t + (\delta t \times v_{t+\delta t}) \quad (13.3)$$

It is well known that Euler integration is unstable when the time step is too big. A good explanation of this can be found in Müller *et al.* (2005); Voigt *et al.* (2005). We used small steps with visually appealing results. Moreover, our simplification of particle-particle interaction and the use of spheres to prevent a return to an equilibrium state (when required) avoids further instability and complexity.

13.4 Muscles-skin interaction with TSSs

Note: some of the text of this section comes from my own published work at Navarro Newball *et al.* (2009c). Some information was updated.

We believe in the simplicity of the sphere-sphere intersection test (figures 13.5A and C illustrate the concept at different resolutions). For instance, we extended the TSSs to allow skin interaction with muscles. Here, we:

- Generated an approximation of the surface of the interacting meshes (e.g. muscles' super ellipsoids and skin) using spheres (surface TSSs, Figure 8.1E). In surface TSSs M_s we associate each vertex of a mesh with a sphere.
- Once the surfaces were full of spheres, we performed all the basic AUs involving muscles (AU1 to 8 and counter actions) in order to identify the spheres that really collide.
- Finally, we optimised the sphere selection in a TSS.

To validate the concept, we started with the AUs involving the Frontalis (AU5,6 and counter actions). We generated the surface spheres, one at each vertex. To start, the skin had 1426 spheres (Figure 13.6A) and the Frontalis had 280 spheres (Figure 13.6B). After the TSSs were created, the number of spheres was lowered to 70 in the skin (Figure 13.6C) and 190 in the Frontalis (Figure 13.6D) and the required number of tests per

time step was 268, which is much better than an exhaustive test of $70 \times 190 = 13300$ tests per time step.

We used bent ellipsoids for representing the muscles. For instance, an alternative method for skin-Frontalis interaction could be solving the characteristic polynomial described by Wang *et al.* (2001) for at least each one of the 70 selected spheres on the skin (Figure 13.6C). Using TSSs we required 268 tests with 4 products each, for a total of 1072 product computations. With sphere-ellipsoid intersection (with 70 spheres) we require an unbending operation for the ellipsoid plus 2870 product and division computations (70×41). Figure 13.6E shows the localised smoothing and Figure 13.6F shows the deformation produced using the TSS (Appendix K, Frontalis1.avi, Frontalis2.avi).

Using DFACS, the skin and the muscles, we generated the TSSs required for muscle-skin interaction. Figure 13.7A shows the interface for muscle-skin TSSs generation. Here, the matrix of parameters control the density of the spheres on the muscles' surface. Sphere generation is done according to the bent ellipsoid equation. Spheres are initially generated on the surface, mainly facing the skin. This allows us to discard about half of the spheres quickly and easily. Also, there is a button to apply the action units (AUs) that help to find the colliding spheres.

For the final version we had a skin control mesh with 1506 vertices (and spheres). Table 13.1 shows the number of spheres and tests for each muscle pair and the Frontalis using TSSs for muscle skin interaction. Here, the column 'Total' shows the number of sphere-sphere intersection tests with TSSs. 'Exhaustive' shows the number of tests required if TSSs are not used ('Skin spheres' multiplied by 'Muscle spheres'). 'Worst' shows the number of tests required if no subset of spheres is found ('1506 multiplied by Full muscle'). 'Skin spheres' shows the number of spheres on the skin interacting with a muscle pair. 'Muscle spheres' shows the number of chosen spheres for each muscle pair. 'Full muscle' shows the original number of spheres per muscle pair. In practice, the use of the elastic model described before slightly increases the number of tests. Here, if a vertex on the skin has been affected and is not under the action of a sphere from a muscle anymore it will tend to go back to its original position. Thus, while deforming a few more collision tests are required if the sphere is not under the action of a muscle but still conserves some force. This test does not require the use of the whole TSS but only the row related to the particular vertex.

Table 13.2 shows the number of sphere-sphere tests per time step required per AU. In AU7 and AU8 we ignore the Orbicularis Oris. AUs 9 to 15 are based on kinematics

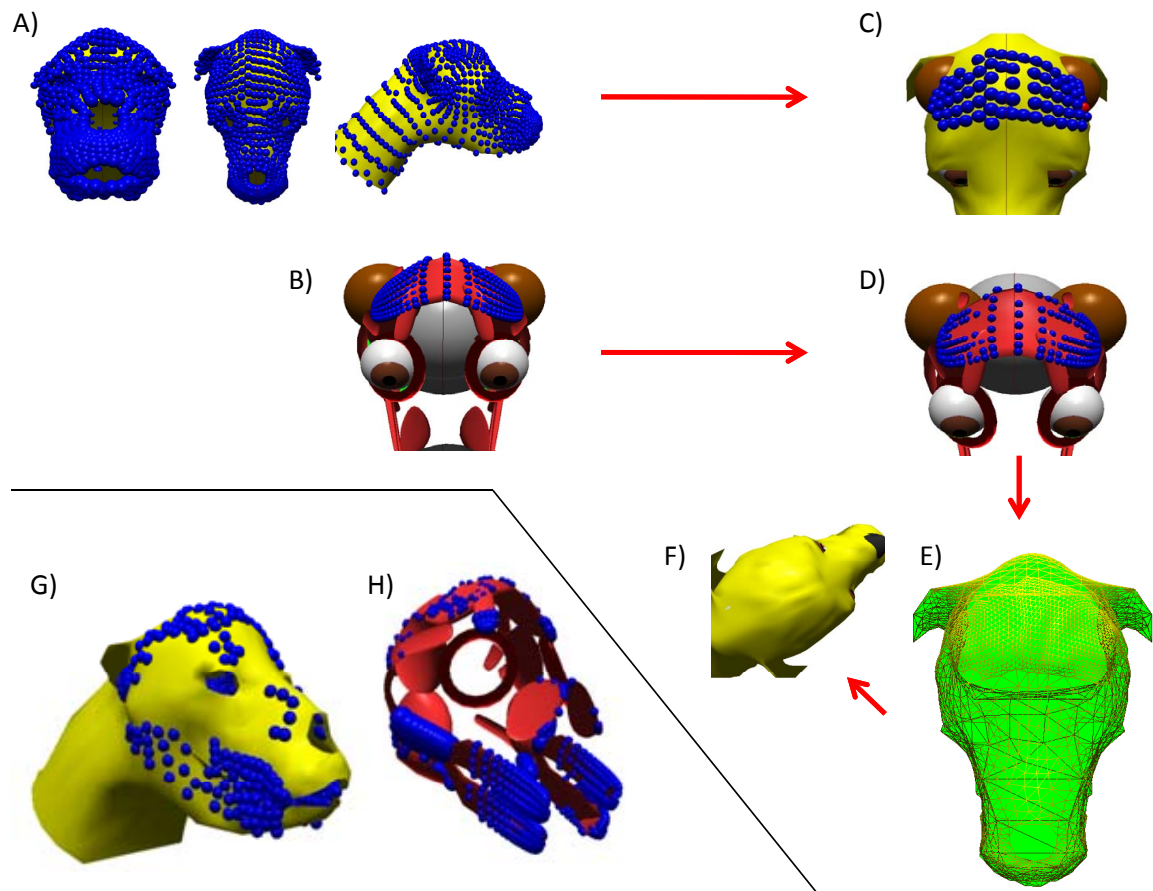


Figure 13.6: Muscle-skin interaction with TSSs. A) Skin surface approximated with 1426 spheres. B) Frontalis approximated with 280 spheres. C) 70 spheres chosen in the skin. D) 190 chosen spheres in the Frontalis. E) $\sqrt{3}$ smoothing localised on the region affected by the Frontalis. F) Sample deformation show some wrinkles between the ears. G) Final selection of spheres in Londra's skin. H) Final selection of spheres in Londra's muscles.

Table 13.1: Tests and spheres per muscle pair per time step

	Total	Exhaustive	Worst	Skin spheres	Muscle spheres	Full muscle
Zygomaticus	145	1640	168672	20	82	112
Orbicularis oris	976	57974	1084320	101	574	720
Mentalis	15	22	361440	7	15	240
Levator oculis	59	336	36144	14	24	24
Levator	60	580	722880	10	58	480
Frontalis	186	11972	316260	73	164	210
Auriculares rostrales	142	3906	271080	42	93	180
Auriculares dorsales	42	798	240960	19	42	160
Digastricus	82	416	180720	8	52	120
Masseter	41	600	156624	20	30	104
Temporalis	22	360	156624	20	18	104
Total	1770	78604	3695724	334	1152	2454
Reduction	$1 - \frac{1770}{3695724}$ 99.9%	$1 - \frac{78604}{3695724}$ 98%		$1 - \frac{334}{1506}$ 78%	$1 - \frac{1152}{2454}$ 53%	

Table 13.2: Total tests per AU

AU	1	2	3	4	5	6	7	8
Tests	1051	145	60	245	370	328	145	145

Table 13.3: Basic operations required

Technique	Operations
TSSs	$1770 \times 4 = 9956$
Ellipsoid-sphere intersection	$334 \times 21 \times 41$ (Wang <i>et al.</i> (2001))
Exhaustive sphere-sphere tests	$334 \times 1152 \times 4 = 1539072$
Worst case	$1506 \times 2454 \times 4 = 14782896$

and do not require TSSs. AUs 16 to 19 are solved with tongue TSSs. Table 13.3 shows the decrease of basic operations using TSSs in AUs 1 to 8 and the chosen 21 muscles (Orbicularis Oris are used for skin generation only) compared other mechanisms (we supposed that all muscles move at the same time. In practice, only a subset of muscles move in each AU). Here, TSSs outperform other options. Figure 13.6G shows the skin's chosen spheres. 13.6H shows the muscles' chosen spheres.

13.5 Regions

Some skin regions first follow kinematics. With skin region detection we determine to which region a portion of skin mesh belongs. Here, we automatically measure in 3D space to which part of the underlying anatomy a portion of the skin is closest. Optionally, the skin region detection mechanism can identify additional regions to display different fur orientation in different skin regions. Figure 13.7B shows 7 regions in our facial mesh: ears; eyelids; mandible; upper lip; neck; region of the Frontalis; front face.

13.6 Thickness

We do not use a multi-layered skin. Thickness is related to the radii of the spheres used for the approximation with spheres and to the distance of the control points to the underlying layers. Additionally, the visible thickness of the skin is modelled with lips along the boundary vertices in the mouth.

A)

Tabulated Sphere Subsets

Muscle:	Frontalis	Au. Dor.	Au. Ros.	Or. Oris	Lev. Ocul	Mentalis	Zygomat	Levator	Masseter	Temporalis	Digastric	
Low muscle:	<input type="text" value="2"/>	<input type="text" value="2"/>	<input type="text" value="2"/>	<input type="text" value="2"/>	<input type="text" value="2"/>	<input type="text" value="2"/>	<input type="text" value="1"/>	<input type="text" value="2"/>	<input type="text" value="2"/>	<input type="text" value="2"/>	<input type="text" value="2"/>	<input type="button" value="Apply AUs"/>
High muscle:	<input type="text" value="2"/>	<input type="text" value="2"/>	<input type="text" value="2"/>	<input type="text" value="2"/>	<input type="text" value="2"/>	<input type="text" value="2"/>	<input type="text" value="1"/>	<input type="text" value="2"/>	<input type="text" value="2"/>	<input type="text" value="2"/>	<input type="text" value="2"/>	<input type="button" value="1) Regions"/>
vSegs:	<input type="text" value="4"/>	<input type="text" value="4"/>	<input type="text" value="4"/>	<input type="text" value="4"/>	<input type="text" value="4"/>	<input type="text" value="3"/>	<input type="text" value="4"/>	<input type="text" value="4"/>	<input type="text" value="4"/>	<input type="text" value="4"/>	<input type="text" value="2"/>	<input type="button" value="2) Divide"/>
uSegs:	<input type="text" value="4"/>	<input type="text" value="4"/>	<input type="text" value="4"/>	<input type="text" value="1"/>	<input type="text" value="4"/>	<input type="text" value="3"/>	<input type="text" value="4"/>	<input type="text" value="4"/>	<input type="text" value="4"/>	<input type="text" value="4"/>	<input type="text" value="2"/>	<input type="button" value="2a) Fur Reg."/>
X Step:	<input type="text" value="2"/>	<input type="text" value="4"/>	<input type="text" value="5"/>	<input type="text" value="4"/>	<input type="text" value="4"/>	<input type="text" value="2"/>	<input type="text" value="4"/>	<input type="text" value="2"/>	<input type="text" value="6"/>	<input type="text" value="6"/>	<input type="text" value="2"/>	<input type="button" value="3) Save"/>
Y Step:	<input type="text" value="4"/>	<input type="text" value="4"/>	<input type="text" value="4"/>	<input type="text" value="2"/>	<input type="text" value="6"/>	<input type="text" value="2"/>	<input type="text" value="4"/>	<input type="text" value="2"/>	<input type="text" value="6"/>	<input type="text" value="6"/>	<input type="text" value="2"/>	

B)

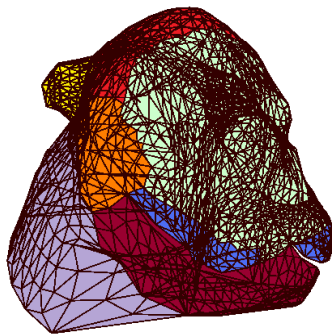


Figure 13.7: TSSs generation and regions. A) Dialog box for muscle-skin TSSs generation. The numbers shown are related to the parameters of the superellipsoids representing the muscles. B) Skin regions.

13.7 Discussion

Feature point generation and automatic facial mesh generation strongly rely on the anatomical knowledge provided to the algorithm. Still, it is much easier than manual editing. One of the reasons for automatic point generation was that interactively placed feature points did not provide enough detail to make a good barycentric interpolation. Anatomical topology is implicit in the triangulation. Instead of using integration, we fix curvature by inflating and deflating at some step size. The existence of more feature points eliminated the need for interpolation of a pre-existing mesh. As a consequence, a new and more anatomically consistent mesh was generated. We believe the mesh is more consistent because it was produced from the underlying anatomy and used more points. In contrast, the pre-existing facial mesh did not belong to the original skull.

The problem of reaching equilibrium in a system with several particles adds complexity and instability. We decided to calculate the reaction force of a vertex as the distance between the current (deformed) position and the original (goal) position multiplied by an elastic constant. Our simplification avoids exhaustive elastic calculations while still producing visually appealing results. Localised $\sqrt{3}$ smoothing gives a more natural look to the deformed skin and simulates the effect of affecting neighbouring vertices.

Our thickness approach simplifies the skin model. It can be enhanced by adding volume and more layers to the skin mesh. Then, as the interacting objects become closer we would switch to volumetric TSSs. However, we believe that our model is good enough to show the advantages of TSSs and to produce basic dog expressions.

TSSs reduced the number of collision tests required for muscle-skin interaction and allowed us to relate the geometry of the muscular shape to skin deformation.

The position and geometry of the underlying muscles and resolution of the approximation to spheres affects the final result. Indeed, a key step in our model is the proper anatomical creation and location of underlying muscles so that they deform the skin adequately.

In dogs, the auriculares affect the shape of the skin next to the ear root and the auricular cartilage is moved by the ear articulation (which is made of cartilage). For instance, we applied TSSs to the region influenced by the Auriculares only, and ears move with kinematics. However, our ear model is a natural part of the skin and helps support some Londra expressions. Further work could include the development of a full dog ear model which also could include several dog ear types (our model only considers

cropped ears). This is out of the scope of this thesis.

Skin is anisotropic. For instance, there may be some slight changes in thickness and elasticity in different regions. We provide the potential to simulate that behaviour. For example:

- Different thickness could be simulated by assigning different radii to the spheres approximating the surfaces.
- Different elasticity values could be assigned so that different regions have different elasticity.

We identified and used a preliminary set of skin parameters:

- Conformational: Underlying feature points and topological restrictions; α orientation of the eyelids; threshold between skin and underlying anatomy; radii of spheres in different regions of the lips.
- Expressive AUs 1 to 15 and their counter actions are higher level parameters used in expression synthesis. AUs 1 to 8 involve muscles and some of them involve kinematics and regions too. AUs 9 to 15 use regions, kinematics and do not involve muscles.

Chapter 14

Fur layer

14.1 Previous work

Human hair modelling has been studied for several years and the hair generation pipeline has had several changes throughout. Here, the challenge is to provide a representation for accurate simulation. Old HFAMs such as Lee *et al.* (1995) included rigid polygonal models for hair. More recent approaches include oriented strands and super helices (Hadap *et al.* (2007)); generalised cylinders (Ward *et al.* (2007)); and, mass-spring models which can capture torsion (Selle *et al.* (2008)). There are three main tasks in hair modelling (Ward *et al.* (2007)):

- Hair styling: long, short, curly, wavy, straight.
- Hair simulation and animation: this is the mechanics of hair. Dynamic grouping, splitting, hair to hair collisions.
- Hair rendering: the way hair fibres are illuminated and the way fibres cast shadows on each other and effects such as wet hair.

Hadap *et al.* (2007); Ward *et al.* (2007); Bertails *et al.* (2008) give more details on human hair technologies.

On the other hand, there are two major issues in the creation of animal visual attributes:

- Coat pattern.
- Fur.

14.1.1 Coat pattern for mammalian models

There are three approaches for pattern generation (Walter *et al.* (1998)):

- Reaction diffusion: the chemical interaction of two substances, under some conditions, produce spatial patterns (Turing (1952); Witkin and Kass (1991); Turk (1991)). Here, the patterns appear when the concentration of the substances is visualised.
- Mechano chemical: A pattern is formed by mechanical forces acting on cells (Walter *et al.* (1998)). Here, forces are chemically induced.
- Cellular automata: Walter *et al.* (1998, 2001) present a better realistic pattern generation model to create striped and spotted mammalian coats. Their approach, the Clonal Mosaic Model (CMM), consistently develops from an embryo to an adult mammal and was tested in giraffes and big cats. Here, the geometry of the model drives the pattern generation mechanism. The CMM states that the yellow-black striped and spotted patterns in mammals are spatially arranged like a mosaic of epithelial cells which derive (clone) from a single progenitor. It uses a small number of parameters. It is based on cell division and cell to cell interaction and is based on experimental evidence on pigment cells (e.g. dark cells split faster). Epithelial cells are represented with Voronoi polygons.

14.1.2 Fur

Animal fur is very stiff and moves in clumps due to hair to hair interaction (Hadap *et al.* (2007)). It includes (Kajiya and Kay (1989)):

- Overcoat: sparser distribution of long hair.
- Undercoat: dense cover of short fur.

Fur generation in creatures is common in the film industry. For example, Preston and Hill (2006) use a dependency graph to deform fur grown on a subdivision surface for King Kong. van Swaaij (2006) ray traces fur using volume texturing and splines for the Ice Age. Previous fur models include:

- Kajiya and Kay (1989) use texels and anisotropic lighting models to render fur. Texels are composed of a scalar density (relative projected area of a micro surface

contained within a volume cell); a field of frames (local orientation of the micro surface); and a field of lighting models.

- Goldman (1997) uses a probabilistic value for the expected reflected light over a small surface area of the skin. The furry effect is emulated with a lighting model and the geometry of individual strands is ignored. Fur is not rendered directly but is used to affect the lighting model. The geometry of the hair on the skin is parameterised with: hair length, hair radius, density of hair and hair tangents at the root and the tip.
- Lengyel *et al.* (2001) simulate real time virtual fur with a particle system which is sampled to a volume texture. Then, the texture is parameterised over a surface of arbitrary topology. They introduce the idea of shell texturing. Here, a geometric model of a patch of hair is sampled into a shell and a fin texture. The shell texture is created based on the geometry of the hair strands. The shell method 'creates a four channel (RGBA) image for each layer of the shell model by overlaying a grid on the bounding box containing the hair strands. At each grid point we compute a colour and opacity by intersecting a tall Gaussian filter with the geometric hair. The filter is tall because the inter-shell spacing is much greater than the grid spacing within each shell. For the innermost shell, all samples are assigned full opacity since this layer represents the skin surface' (Lengyel *et al.* (2001), p.228).
- Papaioannou (2002) implements a simple fur rendering technique. This approach simplifies the shell texturing method (Lengyel *et al.* (2001)) by: ignoring geometric representation of each individual hair; relying on texture mapping and alpha values; using only a few parameters (e.g. fur length, number of layers); emulating a simple hair to hair shadow effect; avoiding tiling volume textures patches; using texture slices parallel to the surface
- Isidoro and Mitchell (2002) produce different colour and density variations using vertex shaders, enhancing the system by Lengyel *et al.* (2001).
- Yang *et al.* (2006) represent fur with hierarchical layers of textured slices. Geometric variations of the furry shape are controlled with vector and scalar fields.

14.1.3 Analysis

Dog fur constitutes a whole field of research. An advanced model has challenges similar to those present in human hair. Mixing coat pattern generation with fur growth seems to be a promising field of research for dog breeds such as Dalmatian. However, Londra's fur is only intended to achieve a decent level of realism. It does not require much of the complexity required by human hair. We decided to use the approach of density maps and adapted the code by (Papaioannou (2002)) and generated short fur. Here, the number of layers and the fur length can be changed. Additionally, instead of generating a coat pattern, we tested different texture maps (Figure 14.2A) and chose the one which did not obscure skin deformations.

14.2 Adding fur

Papaioannou (2002) uses multiple layers of concentric textures. This approach simplifies volume texture techniques to texture slices parallel to the surface. The effect of volumetric fur is achieved by stacking one surface above the other (figures 14.1A and B). Here, each fur layer, which is a displaced version of the previous one, is textured and mapped with an opacity map where high intensity pixels correspond to fur locations. Opacity maps are produced by thresholding. Here, maps further from the skin use a lower threshold (Figure 14.1C). For instance, fewer pixels pass the threshold near the tip of the hair creating the effect of a hair thinning. Hair over skin and hair over hair shadows are approximated by generating and displaying a displacement on the layer's texture map (Figure 14.1D)

Usually, the new layer of fur is obtained by displacing in the direction of the normal (figures 14.1A and B). However, it is possible to displace in a slightly different direction to obtain a different fur orientation (Figure 14.2C left). Moreover, different regions can be displaced in different directions (Figure 14.2C right, Section 13.5). Fur length can also be changed (Figure 14.2D). The fewer layers the less resolution (Figure 14.2E). Figure 14.2B shows Londra with all her anatomical layers.

We studied real Londra's fur orientation (Figure 14.3A) and generated according to that (Figure 14.3B). However, we think that the simple displacement in the direction of normal produced a better looking fur (Figure 14.3C). Anyway, changes in fur orientation are not very perceptible unless they are exaggerated (Figure 14.2C).

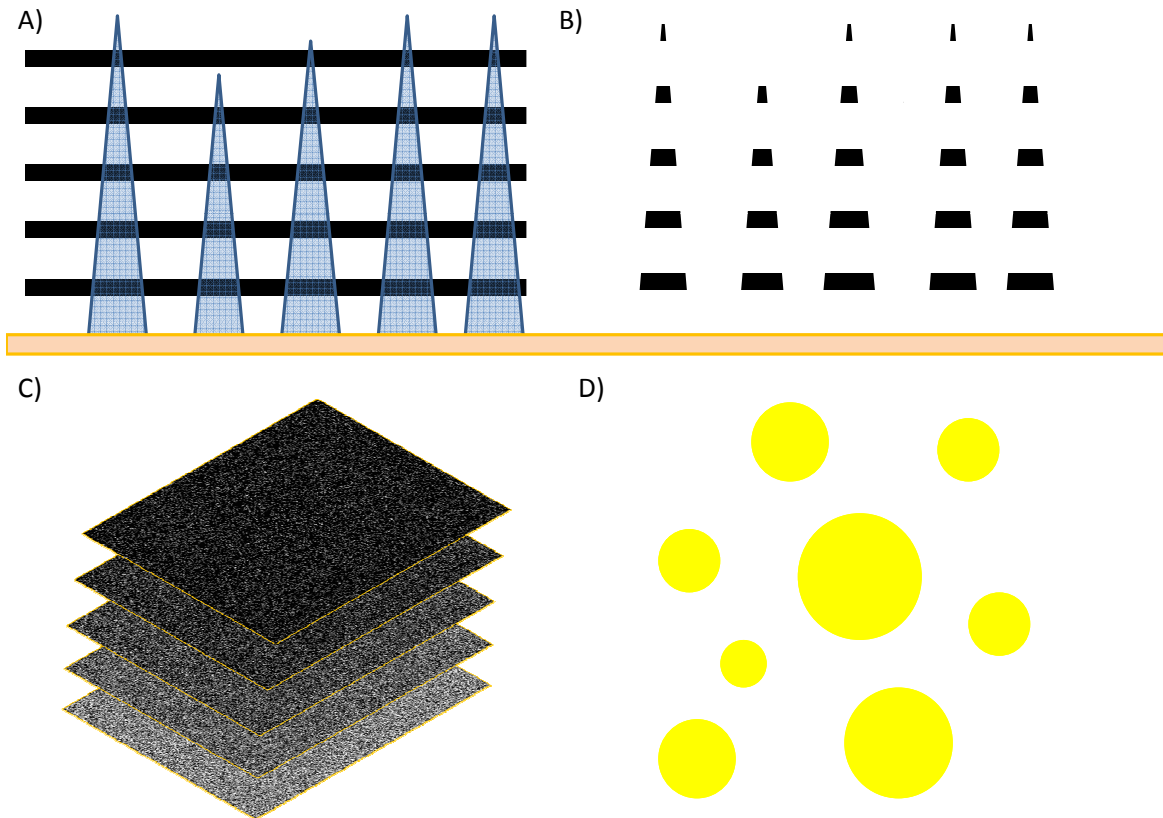


Figure 14.1: Fur Approximation. A) Fur model. B) Parallel displaced layers approximating fur. C) Opacity maps. D) Shadow approximation.

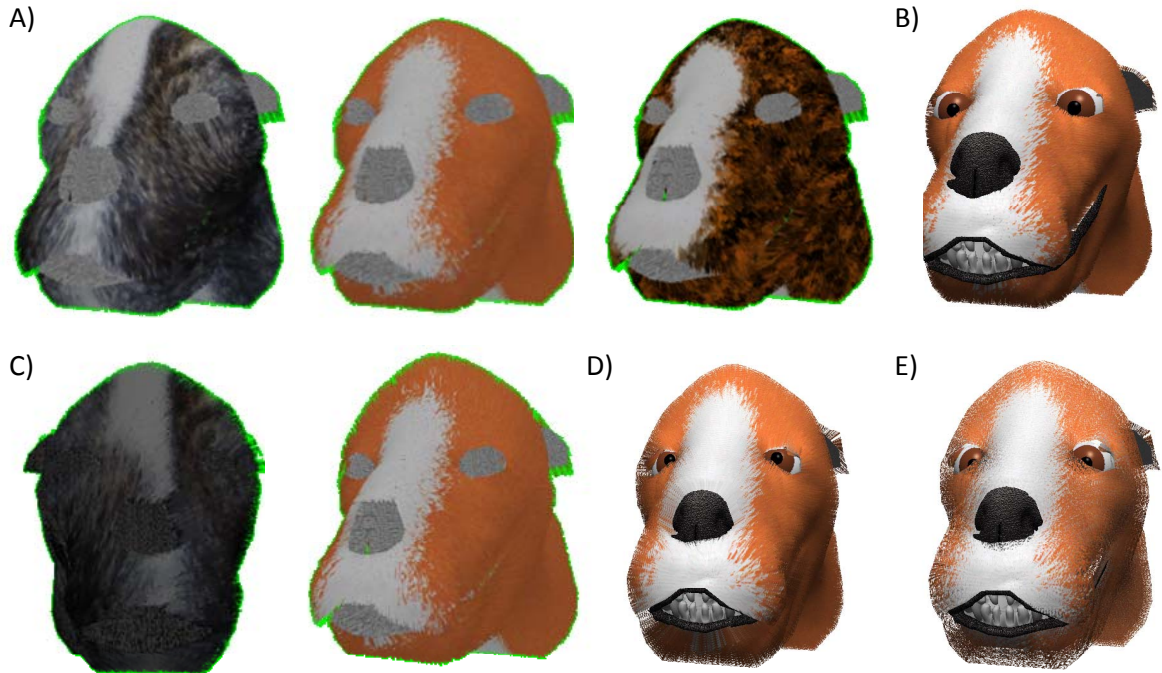
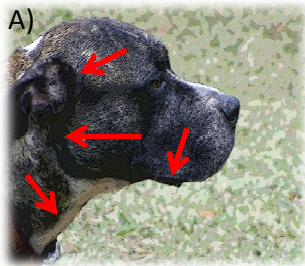


Figure 14.2: Londra's fur. A) Different texture maps. B) Finally, all layers. C) Fur orientation. D) Longer fur. E) Longer fur, fewer layers.

14.3 Discussion

The addition of fur layers enhanced Londra's look. However, it does not constitute an innovation. It is a simple method to achieve a decent level of realism and is not adequate for very close examination. It is mainly based on texture rendering and does not include fur geometry or dynamics. The use of several layers helped simulating fur strands from bottom to top and the effects of the animal undercoat and overcoat. Londra's fur contains three simple parameters: orientation, length and number of layers. Here, the more resolution desired, the more layers required. Further work could involve research on patterned fur generation which includes fur geometry and specialised illumination models.



B)



C)



Figure 14.3: Fur direction. A) Real Londra's fur orientation. B) Approximating fur orientation according to real Londra. C) Fur oriented in the direction of the normal.

Chapter 15

Validation

We tried quantitative (optical flow) and qualitative (surveying and observation) approaches to evaluate Londra's expressions. Our validation is only preliminary but gives some convincing evidence about the accuracy of the expressions.

15.1 optical flow

optical flow computes an approximation to the motion field from time-varying image intensity. In general, optical flow computes a flow field which minimises the difference between two frames (Brox *et al.* (2004)). It performs natural feature tracking and is produced by motion rather than by shape (Chen (2006)). optical flow is sensitive to noise and cannot be applied to rapid motion (Chen (2006)).

Bouguet (2000) implemented a pyramidal version of the Lucas-Kanade optical flow. This is a two-frame differential method. It assumes constant flow around the neighbourhood of the central pixel under consideration (Lucas and Kanade (1981)). It is robust in the presence of noise but does not yield a very high density of flow vectors. For instance, flow information across motion boundaries fades out quickly. Additionally, inner parts of large homogenous areas show little or no motion.

Brox *et al.* (2004) implemented optical flow using warping. Here, the second image is warped towards the first one.

Kharbat (2009) implemented Horn-Schunck optical flow. This method optimises a functional based on brightness and the expected smoothness of the flow field. It yields high density flow vectors but is more sensitive to noise (Horn and Schunck (1981)).

Optical flow can be used to characterise patterns of expressions in HFAMs (Zhang *et al.* (2003b); Chen (2006)) and to quantify subtle expressions. Figure 15.1A shows

the characterisation of a pattern in HFAMs. Here, two frames were taken and the highlighted region in the mixed flow characterises the changes during one expression. We tested optical flow with Londra. For some expressions, we took two frames from a real dog video and two frames from Londra and compared optical flow between pairs. The idea is that regions where changes occurred should be consistent in real and simulated cases.

We downloaded and tested three optical flow packages for MatLab. The package by Bouguet (2000) did not produce clear results. For its characteristics, the flow of information faded and was not displayed properly. The clearest result was produced using the package by Brox *et al.* (2004) in the expression Attention. The package by Kharbat (2009) worked but the arrows were displayed clearly only after zooming. This package helped us characterise flow in the expression Smell. Figure 15.1B shows the characterisation of Attention in real Londra. Figure 15.1C shows the characterisation of Attention in virtual Londra using the same package. The pattern is consistent in Figures 15.1B and C. Here, highlights appear where the ears are moving and under the mandible where there is a twisting motion. 15.2 shows the similarities of flow around the real and virtual nostrils during Smelling.

It can be argued that these results can be verified with plain observation of expressions. Also, if the animations were adapted from accurate observations, the optical flow characterisations should be indeed consistent between the real and virtual Londra. While this is true, our optical flow characterisations of Attention and Smelling successfully quantify the expressions and confirm without relying on the human eye what a good observer should expect. Optical flow tells that the flow of motion is approximately right. However, it has several limitations. For example, the expressions Anger, Affection (two forms), Fear, Yawn and Happiness were not analysed using optical flow for at least one of the following reasons:

- Source videos had low resolution (e.g. anger).
- Source videos were noisy.
- Video background introduced undesired features.
- Filmed dogs moved very fast.
- We did not manage to keep the dog body in the same position relative to the camera.

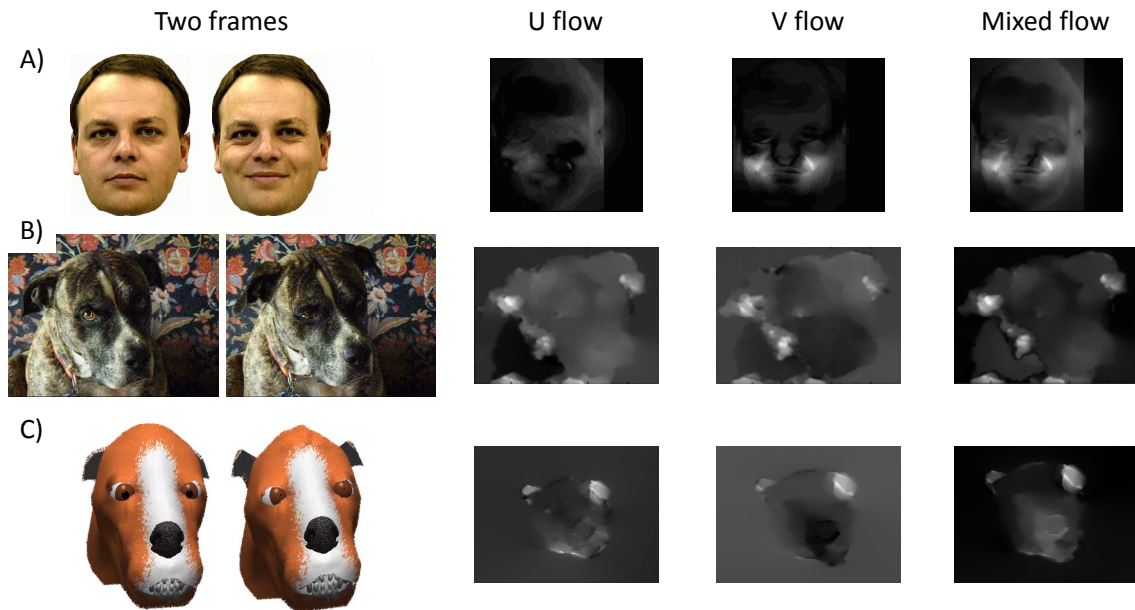


Figure 15.1: optical flow in facial expression. A) optical flow in HFAMs (Prakash (2009), Slide 24). B) optical flow in real Londra (Attention). C) optical flow in virtual Londra (Attention).

- We did not use a tripod to help maintain the camera in the same position.
- Lack of proper illumination conditions and professional photography equipment.
- Filming real dog expressions was a difficult task.
- All packages were affected by noise in all other expressions.
- Results of the characterisation were not conclusive.

15.2 Surveying

Questionnaires are useful for collecting demographic data and opinions and they can be distributed to a large number of people to evidence a wide general opinion. Here, trends and patterns can be identified using spreadsheets. If the number of participants is small, giving actual numbers is better than giving percentages (Preece *et al.* (2002)). In order to validate Londra's expressions:

- We prepared 13 groups of videos (Appendix K, folder 'Chapter15') which included our 8 expressions and some real dog videos. The groups displayed the following

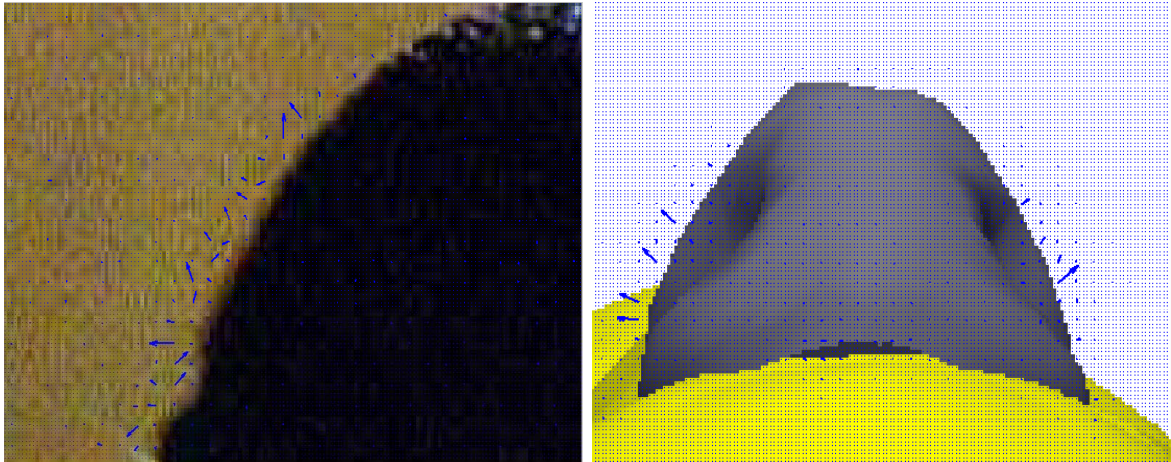


Figure 15.2: optical flow around nostrils. Left, real Londra. Right, virtual Londra.

main expressions: 1) Virtual anger; 2) Virtual affection; 3) Virtual affection; 4) Virtual attention; 5) Virtual fear; 6) Virtual happiness; 7) Virtual smell; 8) Virtual yawn; 9) Real anger (replaced for Virtual anger in sessions 2 and 3); 10) Real fear; 11) Real attention; 12) Real smell; 13) Real affection.

- We applied a questionnaire (Appendix J). Here, we were interested to know if the participants have had dog contact (demography) and what dog expressions were identified from the videos (opinion).
- With this information we evaluated how close the opinions of the participants were to the dog expression descriptions used in Londra.

We did not follow any statistical theory to define the required size of the population. However, the data gathered provided some convincing evidence. We applied the survey to different people in three sessions. Tables 15.1, 15.2, 15.3 show the results from survey sessions 1,2 and 3 and Table 15.4 shows the consolidated result.

15.2.1 Session 1

Held at Abbey College, University of Otago, on November 23, 2009 at 7:30 p.m. 13 people attended, 7 were dog people. For the first group of videos, we only used the videos One1(Old).avi and One2(Old).avi (Appendix K). For the fifth group of videos, we only used the videos Five1(Old).avi and Five2(Old).avi (Appendix K). For the ninth group of videos, we only used the videos Nine1(Old).avi and Nine2(Old).avi (Appendix K). From the first survey, (Table 15.1) we found that:

- From the results in Group 3 we believe that Licking is regarded as a highly positive action. Indeed, affection was well recognized here. Also, it is interesting to see how affection was perceived as mixed with happiness in a few cases. At the end, an affectionate dog is probably a happy dog. Expressions such as attention (Group 4), smell (Group 7) and yawning (Group 8) were correctly identified. In some cases, yawning was associated with tiredness and laziness (which makes sense too). In contrast, affection (Group 2) was evenly confused with attention, smell and tiredness. Fear (Group 5) was identified correctly by some people but was mostly confused with laziness. Happiness (Group 6) was confused with attention. Anger (Group 1) was confused with happiness. This was probably because Londra displayed her tongue at some point and because we did not display a full lateral view of the animation. We believe the tongue is usually assumed to be part of a positive emotion.
- Real videos (groups 9 to 13) were correctly identified by most people. Anger (Group 9), attention (Group 11), and smell (Group 12) were obvious. Fear was confused with attention and affection with happiness. However, this result makes sense as the real dog videos came with mixed emotions and the real Londra was paying attention most of the time.
- Although in our dog observations we observed angry dogs showing the tongue, our main finding from the first survey was the evidence of the fact that the tongue is associated with a positive expression.

15.2.2 Session 2

Held at Abbey College, University of Otago, on November 27, 2009 at 6:40 p.m. 13 people attended, 8 were dog people. In the previous session, anger (Group 1) was not properly recognised. Using the same Londra model and altering some parameter values, for the second survey we made the following changes:

- We included a lateral view to Group 1, (Appendix K, One3.avi).
- As the expressions from real dogs in Group 9 were obvious for all participants, we replaced those videos with Nine1.avi, Nine2.avi and Nine3.avi (Appendix K), which display anger in virtual Londra without showing the tongue (we did not include AU18 in anger).

Table 15.1: Results from session 1. Rows: participants' choice. Columns: video groups. Columns' sub-indices: expression displayed (e.g. An = anger). The number of dog people is indicated in parentheses.

Video group	1 _{An}	2 _{Af}	3 _{Af}	4 _{At}	5 _{Fe}	6 _{Ha}	7 _{Sm}	8 _{Ya}	9 _{An}	10 _{Fe}	11 _{At}	12 _{Sm}	13 _{Af}
Anger (An)	1 (1)	1		3 (1)	1 (1)	1	1		10 (6)				
Affection (Af)	3	3 (3)	12 (6)			2	1 (1)		1	4 (2)	3 (2)		6 (4)
Attention (At)	3 (1)	4 (2)		6 (4)	2 (1)	6 (3)				9 (4)	5 (2)	2 (2)	
Fear (Fe)				1 (1)	3 (2)	4 (3)			2 (1)	2 (2)	1 (1)		
Happiness (Ha)	6 (2)	2 (2)	4 (2)				1 (1)		1	1 (1)	2 (1)	1	9 (5)
Smell (Sm)		4 (1)					12 (6)					9 (4)	
Yawning (Ya)								10 (5)					
Tiredness (Ti)	1 (1)	3 (1)		2	2 (1)			3 (2)		1	2 (2)	1	
Laziness (La)		1 (1)			4 (1)			2 (1)		1	2	1 (1)	

We wanted to know if anger had more recognition and if the successful expressions from Session 1 were still identified. From the second survey, (Table 15.2) we found that:

- Anger (Group 1) was identified by more people. We believe that the lateral view in the video allowed people perceive the effects of AU1 (raise lips) better. However, a few people continued to identify the expression as happiness (probably because of the tongue). Anger (Group 9) without a tongue was identified by most people and sometimes mixed with fear (it makes sense that a scared dog can give some anger in return). Attention (Group 4), smell (Group 7) and yawning (Group 8) continued to be well recognised. In some cases, yawning continued to be associated with tiredness and laziness. In contrast, affection (Group 2) was confused with smell. We believe that moving the head around was associated with smelling on a surface. Affection (Group 3) which was well recognised in the previous survey was now confused with tiredness. For instance, the tongue does not necessarily represent a positive expression among people, as we believed. It can be also associated with the physical expression of exhaustion. Fear (Group 5) and happiness (Group 6) were confused with attention. Probably, slight head and ear movements (in any direction) are associated with the expression of attention.
- There were no important changes in the perception of real dog videos (groups 10 to 13).
- We managed to gain recognition in anger. However, we were not sure if it was because of the lateral view (Group 1) or because of the lack of tongue (Group 9).

15.2.3 Session 3

Held at the Seminar Room from the Computer Science Department, University of Otago, during a Computer Graphics Laboratory meeting on December 4, 2009. 13 people attended, 8 were dog people. In the previous session, anger was properly recognised but we were not sure about the reason why. Also, fear had more recognition in Session 1 than in Session 2. Using the same Londra model and altering some parameter values, for the second survey we made the following changes:

- We emphasised the expression of Fear (Group 5) by assigning a greater intensity value to -AU9 (lower head). We replaced the videos with Five1.avi and Five2.avi (Appendix K).

Table 15.2: Results from session 2. Rows: participants' choice. Columns: video groups. Columns' sub-indices: expression displayed (e.g. An = anger). The number of dog people is indicated in parentheses.

Video group	1 _{An}	2 _{Af}	3 _{Af}	4 _{At}	5 _{Fe}	6 _{Ha}	7 _{Sm}	8 _{Ya}	9 _{An}	10 _{Fe}	11 _{At}	12 _{Sm}	13 _{Af}
Anger (An)	6 (4)	2 (1)		1		2			9 (5)		1 (1)		
Affection (Af)	2 (2)		3 (2)	3 (1)	2 (1)	1 (1)	2 (1)			3 (2)	2		
Attention (At)	2 (1)	2 (1)	2	9 (6)	5 (3)	7 (6)	1	2		9 (6)	6 (5)	4 (3)	2 (1)
Fear (Fe)		1		1		3			4 (3)	1	2 (2)		1 (1)
Happiness (Ha)	2 (1)	1	3 (1)		2 (1)			1 (1)	1 (1)	4 (4)	4 (4)		11 (7)
Smell (Sm)	1 (1)	5 (5)		1 (1)			13 (8)					11 (7)	
Yawning (Ya)				1	1			10 (6)					
Tiredness (Ti)		1 (1)	8 (6)	1	3 (2)		1 (1)	6 (3)		4 (1)	1		
Laziness (La)				1 (1)	2 (1)	1 (1)				1 (1)			

- In anger (Group 9) we did not show Nine3.avi (Appendix K) to verify the effect of the lateral view.

We wanted to differentiate the effect of the tongue and the lateral view in the people's perception of anger (groups 1 and 9). Also, we wanted to know if fear had more recognition and if the successful expressions (attention, smell, yawning) from the previous sessions were still identified. From the third survey, (Table 15.3) we found that:

- Anger (Group 1) was confused with happiness as in Session 1 (despite the lateral view). Affection (Group 3) had a comeback and was correctly recognised by most people. For instance, we have now stronger evidence to believe that the dog tongue is associated with a positive emotion. Attention (Group 4), smell (Group 7) and yawning (Group 8) continued to be well recognised. Affection (Group 2) continued to be confused with smell (probably for the reason explained in the previous section). Despite the parameter intensification, fear was not recognised as such but confused with tiredness (probably because Londra lowers the head). Although, a few people identified happiness (Group 6), it was mainly confused with attention. Now we believe that raising the head and the ears (independent of the intensity) is mostly associated with attention.
- There were no important changes in the perception of real dog videos (groups 10 to 13).
- Anger without tongue (Group 9) was correctly identified by most people even when we did not display a lateral view. That makes us believe that it is the tongue and not the position of the camera that misleads the perception of the expression of anger.

15.2.4 Consolidated result

From the consolidated result, (Table 15.4) we found that:

- Affection with licking (Group 3), attention (Group 4), smell (Group 7), yawning (Group 8) and anger without tongue (Group 9) were successfully displayed expressions. They were correctly recognised by the greatest number of people. For Group 9, we did not take into account the results from Session 1 as these refer

Table 15.3: Results from session 3. Rows: participants' choice. Columns: video groups. Columns' sub-indices: expression displayed (e.g. An = anger). The number of dog people is indicated in parentheses.

Video group	1 _{An}	2 _{Af}	3 _{Af}	4 _{At}	5 _{Fe}	6 _{Ha}	7 _{Sm}	8 _{Ya}	9 _{An}	10 _{Fe}	11 _{At}	12 _{Sm}	13 _{Af}
Anger (An)	4 (4)				1 (1)	1 (1)	1		13 (8)				1
Affection (Af)	4 (2)	4 (3)	11 (8)							5 (4)	1 (1)		8 (6)
Attention (At)	6 (5)	4 (1)	1 (1)	12 (7)	2 (1)	9 (5)	1		1	12 (7)	13 (8)	3 (2)	2 (2)
Fear (Fe)		1 (1)			4 (3)	2 (1)			2 (1)	3 (2)			
Happiness (Ha)	9 (4)	1 (1)	5 (3)	1 (1)		4 (3)		2 (1)		2 (1)	5 (2)		10 (6)
Smell (Sm)		4 (3)	1	1	1 (1)	2 (2)	13 (8)			1		13 (8)	
Yawning (Ya)	1							9 (6)		1 (1)			
Tiredness (Ti)		2 (2)	1		7 (4)			7 (3)			1 (1)		
Laziness (La)			1					2 (1)			2 (2)		

to different videos. Yawning was sometimes perceived as mixed with tiredness (which makes sense too).

- The tongue is mostly associated with a positive expression (e.g. happiness). Indeed when AU18 (show tongue tip) is used with anger, the expression is perceived mostly as happiness. Moreover, affection (Group 3) is many times perceived as mixed with happiness.
- Affection (Group 2) was difficult to perceive. Strong head motions were mostly associated with smell and not with affection. However, Group 2 was also confused with attention and tiredness and correctly identified by some people. The greatest number of people identified it as smell.
- Fear (Group 5) was difficult to perceive. It was understood as attention, fear, tiredness and laziness almost evenly. However, the greatest number of people identified it as tiredness.
- Head and ear raising are mostly perceived as attention as it can be seen in happiness (Group 6) and attention (Group 4).
- Happiness (Group 6) was confused (but consistently) with attention. We believe that results from affection (Group 2) and fear (Group 5) were not conclusive.
- Real videos were correctly identified by most people. Some groups were obvious. Fear was confused with attention and affection with happiness. However, this result makes sense as the real dog videos came with mixed emotions and the real Londra was paying attention most of the time.
- Only when we obtained the consolidated result, had we evidence that dog people recognised dog expressions slightly more accurately. Indeed, all expressions were correctly recognised at least 4 times (in most cases by dog people).

15.2.5 Changing the model

Interaction with people was important to make a preliminary qualitative validation of Londra's expressions. During the sessions we did not alter the Londra model. Instead, we adjusted some parameters using the same model. This way we were able to find evidence for some promising facts. However, during the evaluation sessions a few people suggested that Londra should have better lips. In this sense the sessions were useful

Table 15.4: Final result. Rows: participants' choice. Columns: video groups. Columns' sub-indices: expression displayed (e.g. An = anger). The number of dog people is indicated in parentheses.

<i>Video group</i>	1_{An}	2_{Af}	3_{Af}	4_{At}	5_{Fe}	6_{Ha}	7_{Sm}	8_{Ya}	9_{An}	10_{Fe}	11_{At}	12_{Sm}	13_{Af}
<i>Anger</i> (An)	11 (9)	3 (1)		4 (1)	2 (2)	4 (1)	2		22 (13)		1 (1)		1
<i>Affection</i> (Af)	9 (4)	7 (6)	26 (16)	3 (1)	2 (1)	3 (1)	3 (2)			12 (8)	6 (3)		14 (10)
<i>Attention</i> (At)	11 (7)	10 (4)	3 (1)	27 (17)	9 (5)	22 (14)	2	2	1	30 (17)	24 (15)	9 (7)	4 (3)
<i>Fear</i> (Fe)		2 (1)		2 (1)	7 (5)	9 (4)			6 (4)	6 (4)	3 (3)		1 (1)
<i>Happiness</i> (Ha)	17 (7)	4 (3)	12 (6)	1 (1)	2 (1)	4 (3)	1 (1)	3 (2)	1 (1)	7 (6)	11 (7)	1	30 (18)
<i>Smell</i> (Sm)	1 (1)	13 (9)	1	2 (2)	1 (1)	2 (2)	38 (22)			1		33 (19)	
<i>Yawning</i> (Ya)	1			1	2			29 (17)		1 (1)			
<i>Tiredness</i> (Ti)	1 (1)	6 (4)	9 (6)	3	12 (7)		1 (1)	16 (8)		5 (1)	4 (3)	1	
<i>Laziness</i> (La)		1 (1)	1	2 (1)	6 (2)	1 (1)		4 (2)		2 (1)	4 (2)	1 (1)	

to decide adding lips to Londra (Section 13.2.3). Thus, in that sense user interaction helped enhancing the model. All validation sessions took place with a lipless Londra.

15.3 Visual comparison and sequence of events

Virtual Londra's expressions are valid in the sense that they were built according to the sequence of events described by Darwin (1890) and according to our video observations (Chapter 3). These descriptions produce expressions which approximate real Londra's expressions nicely (figures 5.3, 5.4, 5.5).

The similarities with real dogs are visually evident. Figure 15.3A shows similarities in the lateral view (e.g. cheek region, especially in the yellow dog). Figure 15.3B shows similarities during jaw opening (especially the deformation caused at the cheek). Figure 15.3C shows similarities in the back view. Figure 15.3D shows similarities in the wrinkles produced between the ears. Figure 15.3E shows similarities during the fear expression. Here, the real Londra lowers slightly her head and moves her ears backwards (top row) the same as the virtual Londra (bottom row). Figure 15.3F show similarities in lip contraction. Figure 15.3G shows similarities in the tongue and the nose.

In contrast, virtual Londra is a simplification of a real dog. This simplification is not exact and differences between virtual Londra and real dogs are evident too. For example, the cheek size differs from that of real Londra in Figure 15.3A (the yellow dog cheek is closer in this case). The frontal part of the upper lips is not contracted in 15.3F. The cropped ears are smaller.

Deformations and features shown in Figure 15.3 may vary slightly among breeds making virtual Londra more or less similar to some other breeds (e.g. Figure 15.3A). Still, with virtual Londra we produced visually recognisable dog expressions (based on dog anatomy for the first time) (Section 15.2).

15.4 Beyond real dog expressions

Londra is not aimed at anthropomorphic or cartoonised expressions. It was built considering the important anatomical components required to build a set of recognisable expressions. However, the system comes with some level of flexibility. For example:

- Some cartoonised expressions are possible by exaggerating the parameter value for some AUs. Figure 15.4A shows an exaggerated ear rise and a bigger jaw opening.

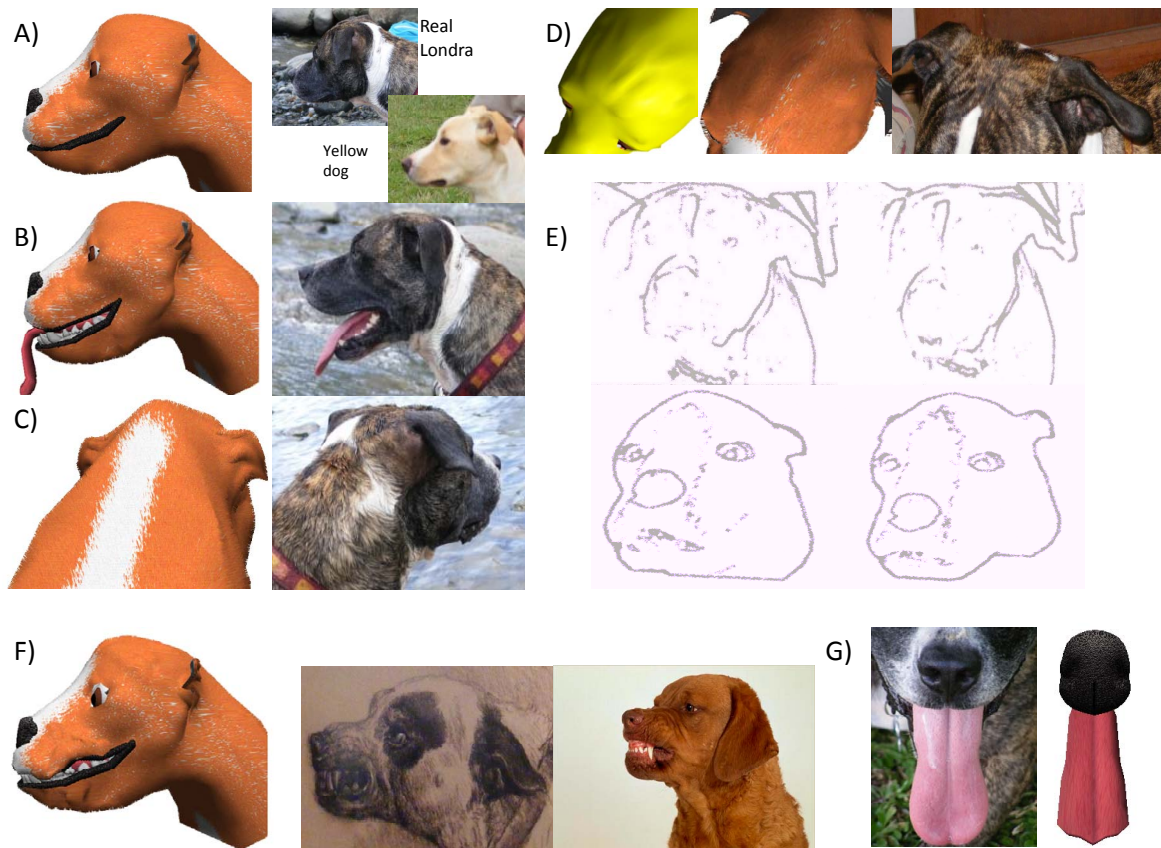


Figure 15.3: Similarities and differences between real and virtual Londra. A) Lateral view. B) Jaw Opening. C) Back view. D) Wrinkles between the ears. E) Expression of fear. F) Lips contraction. G) Tongue and nose.



Figure 15.4: A) Exaggerating AUs. B) A random unknown expression.

A few AUs are easier to exaggerate, but most of them are limited by the underlying anatomy. For instance, we believe that creating cartoonised expressions would be better if we start building the model with a cartoonised skull.

- Expressions were generated according to video observation and Darwin’s descriptions. However, it is possible to mix AUs in many different ways in order to define new expressions. Figure 15.4B shows a random, unnamed expression where AU3: dilate nostril; -AU5: backward ears; AU7: open mandible; AU11: twist head have been applied. This way it is possible to experiment with the way a dog would look if different mixtures of AUs are applied. Video Random.AVI illustrates how a lengthy animation can be produced by randomising the application of the AUs.
- Anthropomorphic animals are very popular. Because Londra was anatomically inspired, creating anthropomorphic expressions needs some work. This would require deep study of human anatomy in order to add the required anatomical components to create a humanised dog. This would include adding more muscles and features that were ignored such as eyebrows. However, if we define the anatomical features of the new creature we could start adding the layers through the use of our system.

Extension to applications such as virtual pets requires the inclusion of a brain capable of deciding Londra’s expression and the ability to interpolate smoothly from one expression to another.

15.5 Model Performance

We measured the number of frames per second (FPS) using a laptop with an Intel processor running at 2 GHz in 32 bit mode with an Intel Graphics Media Card using

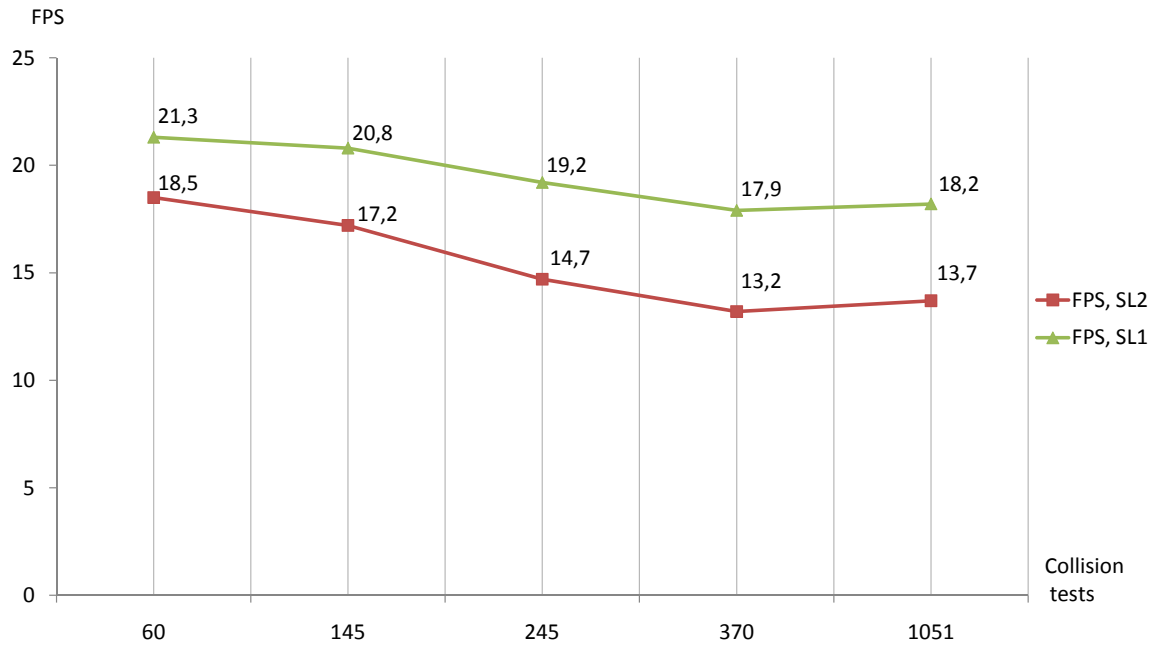


Figure 15.5: Frames per second (FPS) Vs. number of collision tests.
SL= subdivision level.

no acceleration. Figure 15.5 shows the FPS versus number of collision tests per frame using muscle-skin TSSs for AUs: 3, 2, 4, 5, 1 (Table 13.2).

In AUs affecting similar regions, an increase in the number of collision tests lowers the FPS. However, the performance is more affected by the number of polygons on the skin requiring subdivision than by the number of collision tests. For example, the FPS in AU1 which performs 1051 tests is higher than the FPS in AU5 which performs 370 tests. This is because the region of the skin mesh affected by AU5 is larger than that affected by AU1 and because the region affected by AU1 (lips) is next to a boundary which lowers the number of subdivisions.

TSSs not involving posterior subdivision (e.g. jaw and tongue motion) perform at least at 50 FPS. The performance of the model is affected by other factors (e.g. transformations, fur generation). A simple expression such as 'smell' performs at 21.3 FPS while a complex one such as 'anger' performs at 13.3 FPS.

15.6 Discussion

With optical flow we tried to provide an objective evaluation of Londra's expressions. However, we only were able to show the consistency of virtual and real Londra in

attention and smell. Due to practical difficulties related to filming real dogs it was not possible to obtain the optical flow characterization for the other expressions. At the same time, the questionnaire applied to 39 people showed that:

- Anger, affection (with tongue), attention, smell and yawning were identified as such by the greatest number of people. Anger, affection and attention are consistent with the descriptions from Darwin (1890). Smell and yawning are proposed by us.
- Affection (without tongue) was not conclusive, but the greater number of people identified as smell. Fear and Happiness were understood as tiredness and attention.
- Displaying the tongue changed the perception of anger for many participants. It seems that the tongue is associated with a positive expression.

We believe Londra's most successful expression was attention, because it was not obvious and was consistent with the description; was objectively characterised evaluated and was correctly perceived by people. The fact that expressions such as happiness and fear were identified differently does not invalidate the descriptions and the way they were displayed. In fact, we believe that a lot of people misinterpret expressions. Having gained the current level of expression of recognition with the dog head only is somehow a success. Despite the simplifications and assumptions, visual features show similarities between Londra and real dogs. These similarities were good enough to produce visually recognisable expressions. The expressions were created using anatomical and dog expression knowledge.

We claim that Londra's expressions are valid because they were built according to the sequence of events described by Darwin (which were complemented with our observations). But how do we know that Darwin was right? Darwin, a 'keen and astute' (Darwin (1890), p. 2) observer of nature admits that the study of expressions is difficult and imagination can interfere (we expect to see an expression and then imagine its presence). However, in his book, he explains the methodology used to acquire as good a foundation as possible. He includes (among others): observation of the great masters (e.g. painting, sculpture); 'attending as closely as he could, to the expression of the several passions in some of the commoner animals' (p. 12), using them as the safest basis for generalisation on the causes, origin of the movements related to expression. He states that 'in observing animals, we are not likely to be biased by

our imagination; and we may feel safe that their expressions are not conventional ' (p. 12). Also, he defines the chief principles of expressions which are strongly related with his ground breaking evolution theory. Frequently, he explains them with their biological function. Good examples of his descriptions, which are consistent with his theory and methodology are present throughout his book (Darwin (1890)). Moreover, for his observations, Darwin used behavioural patterns and body language (not only the face). Among species, many mental attributes such as anger, happiness, guilt and others could be surmised by behavioural patterns (body language) (p. 6). As good scientists we are free to question the accuracy of the behaviours that Darwin described. However, in this case we prefer to stick to his genius and believe that his descriptions were accurate. Indeed, the fact that several of Londra's expressions were identified correctly gives hints to believe he was right.

Because Londra is anatomically inspired and built layer by layer, creating cartoonised or antropomorphic charaters requires the definition of the creature's features layer by layer using the system. Experimenting different AUs mixtures is straight forward.

Londra performs reasonably well in a basic computer. Our results suggest that mirroring the model has the potential to perform at real time (25 FPS) in all cases if calculations are successfully halved. This is left for further work.

Chapter 16

Conclusions

We have created a virtual model of a dog head which displays facial expressions. Londra is the first anatomically inspired model which focuses on real dog facial expressions.

We demonstrated that the face plays an important rôle in dog expressions. Our demonstration was based on the study of Darwin's descriptions of dog expressions and our own dog and dog's videos observations; and the study of artificial pets. Here, we identified which facial components are used in expressions such as: anger; affection; attention; fear; happiness; smell and yawning.

We understood HFAMs and adapted the layered approach to our dog model by understanding the anatomical differences between humans and dogs. For example, in dogs, ears, tongue and fur are more visible and speech and vascular changes are not important. Anatomical conformation of dog heads is complex and varies amongst breeds. Anatomical information was used to identify several animation parameters.

We followed a new, purely bottom up approach which starts with a skull and does not require a pre-existing facial mesh.

We introduced DFACS, a selective model used to synthesise expressions. It was built theoretically from the knowledge gained from dog anatomy books. It was built upon AUs and is specialised for dogs. Here, we proposed new AUs for the ears and the tongue.

We implemented $\sqrt{3}$ subdivision using counting and the direct edges data structure. Subdivision is used for skin smoothing after skin generation and deformation. Here, counting was essential in memory allocation and indexing at each new face. It allowed the effective implementation of the basic operations required by the subdivision algorithm.

We proposed a muscle model based on superquadrics. Here, we used superellipsoids

and supertoroids as simplifications of generalised cylinders. In that way we reduced the required parameters; and, provided simpler muscle geometry representation, contraction, stretching and bending.

We introduced TSSs, a fast and appropriate method for constrained object interaction. Applications included: articulated bodies (e.g. jaw motion), relatively fixed deformable bodies (e.g. muscle-skin interaction, tongue motion). They rely on a simple test; only consider spheres and regions of the mesh which will collide and only test a sphere with the spheres with which it is most likely to collide. In our sample applications our TSSs outperformed standard techniques (e.g. sphere trees; ellipsoid intersection tests).

Londra's control system is somewhere in between pure geometric parametric models and physically based models. It is anatomically inspired and uses geometrically based modelling with some physics. It reduces the use of complex elements and requires fewer calculations than physical models and less user interaction than pure geometric parameterisations.

With Londra, we prove that a dog face with some basic expressions can be modelled following some basic anatomical principles (e.g. the model is created taking as starting point the inner layer; face anatomy is layered; muscles affect shape and skin behaviour) and simplified anatomical models. We have created a working bone layer for Londra. Our skull model includes: teeth and a movable jaw; a parametric triangular mesh representation with $\sqrt{3}$ subdivision surfaces capability; a kinematics model; a mechanism to allow basic reshaping (still with cartoonish results); TSSs for jaw motion. Our TSSs adapt to the existing skull-mandible shape and spheres appear in their points of contact.

We identified the 23 most important muscles affecting dog's facial shape and expression. Our selection was adequate for Londra. Superquadrics worked fine for the chosen muscles. One advantage of our muscle model is the reduced number of parameters which facilitates their construction, deformation and their interaction with the skin.

We proposed a tongue model which approximates volume preservation. We identified typical dog expressive shapes (e.g. licking) and focused our modelling on those. Our implemented tongue shapes give ideas on how to implement human expressions such as 'sticking the tongue' which are not common in current HFAMs.

We implemented an eye model using layered spheres. It includes a transparent cornea; a gaze formula and a dilatible pupil. Londra's eyes anticipate the expression

where they are important. For example, in attention, they move first towards the object of interest.

We introduced a nose model with dilatable nostrils and rotation.

We generated a new and more anatomically consistent skin mesh using feature points. Anatomic topology was implicit in the triangulation. Feature points generation and automatic facial mesh generation strongly relied on the anatomical knowledge provided to the algorithm.

The problem of reaching equilibrium in a system with several vertices (e.g. skin) adds complexity and instability. We decided to calculate the reaction force of a vertex as the distance between the current (deformed) position and the original (goal) position multiplied by an elastic constant. Our simplification avoids exhaustive elastic calculations while still producing visually appealing results. Localised $\sqrt{3}$ smoothing gives a more natural look to the deformed skin and simulates the effect of affecting neighbouring vertices. TSSs reduced the number of collisions test required for muscle-skin interaction and allowed us to relate the geometry of the muscular shape with skin deformation. Skin deformations use kinematics, muscles or both.

The addition of fur layers enhanced Londra's look. We used a simple method to achieve a decent level of realism although it is not adequate for very close examination. It is mainly based on texture rendering and does not include fur geometry or dynamics. The use of several layers helped simulating fur strands from bottom to top and the effects of the animal undercoat and overcoat.

We validated eight of Londra's expressions successfully. Most of them were identified correctly among the users. Additionally, we characterised two of them using optical flow. Our animations are consistent with Darwin's descriptions and our own dog observations. Despite the simplifications and assumptions, visual features show similarities between Londra and real dogs. These similarities were good enough to produce visually recognisable expressions. The expressions were created using anatomical and dog expression knowledge.

We identified a set of animation parameters (Table 16.1):

Londra's model could be further enhanced by:

- Creating an anatomically accurate skull reshaping method in conjunction with zoology
- Automating muscle placement giving generality to the muscle layer to other skull shapes.

Table 16.1: Animation parameters for Londra

Layer	Conformational	Expressive
Bone	Position of: Nuchal crest Insicive suture Frontonasal suture Zigomatics	AUs 7,8,9,10,11 and counter actions
Muscle	Closed or open Radii a_1, a_2, a_3 Squaredness north-south Squaredness east-west Torus inner radius Latitude, longitude Bending angle, rate, range Position, rotation	Length AUs 1, 2, 3, 4, 5, 6, 7, 8 and counter actions
Complementary (tongue)	Lengths MT, MTM Bending angles: α, β	AUs 16, 17, 18, 19 and counter actions
Complementary (eyes)	Radii Pupil position	Gaze AUs 13, 14, 15 and counter actions
Complementary (nose)	Nostril's spheres radii	Rotation around X AU3 and counter action
Skin	Underlying feature points Topological restrictions α Orientation of eyelids Lips' spheres radii Threshold skin-underlying anatomy	AUs 1 to 15 and counter actions
Fur	Orientation, length Number of layers	



Figure 16.1: Left, Londra as a puppet. Right, rendering with Blender.

- Including more facial muscles to add more fine detail to some deformations
- Creating separate ears models.
- Adding more degrees of freedom to the tongue to allow more asymmetric expression.
- Mixing coat pattern generation with fur generation.
- Adding an expressive dog body.
- Mirroring calculations during expression synthesis.
- Creating a surrounding realistic environment or a full character situation. For example, Figure 16.1 shows a Londra puppet interacting with the real Londra in London's South Bank and Londra rendered in Blender (Appendix K, Blender.avi).
- Additionally, our TSSs open a full field of research for constrained object interaction.
- The Londra model could be expanded to other real or non real non human creatures. And some of the techniques could be used in human systems.

References

- African Art Museum (2009). On-line reference to the artistic styles of Africa. <http://www.zyama.com>.
- Aguado, A. S., Montiel, E., and Zaluska, E. (1999). Modeling generalized cylinders via Fourier morphing. *ACM Trans. Graph.*, 18(4), 293–315.
- Allen, K. D. and Athanasiou, K. A. (2006). Viscoelastic characterization of the porcine temporomandibular joint disc under unconfined compression. *Journal of Biomechanics*, 39, 312–322.
- Allison, A. (2006). *Millennial Monsters: Japanese Toys and the Global Imagination*. University of California Press.
- Amanatides, J. (1987). Realism in Computer Graphics: A Survey. *IEEE Computer Graphics and Applications*, 7(1), 44–56.
- Angelidis, A. (2004). *Shape Modeling by Swept Space Deformation*. Ph. D. thesis.
- Angelidis, A., Cani, M.-P., Wyvill, G., and King, S. (2004). Swirling-sweepers: constant volume modeling. In *SIGGRAPH '04: ACM SIGGRAPH 2004 Sketches*, New York, NY, USA, 40. ACM.
- Archer, K. M. (1997). *Craniofacial Reconstruction using hierarchical B-Spline Interpolation*. University of British Columbia, Department of Electrical and Computer Engineering.
- Artist-3D (2008). Free 3D models download. <http://artist-3d.com/>.
- Ashman, R., Rosinia, G., Cowin, S., and Fontenot, M. (1985). The bone tissue of the canine mandible is elastically isotropic. *Journal of Biomechanics*, 18(9), 717–721.
- Barr, A. H. (1981). Superquadrics and Angle-Preserving Transformations. *IEEE Comput. Graph. Appl.*, 1(1), 11–23.

- Barr, A. H. (1987). Global and Local Deformations of Solid Primitives. In M. A. Fischler and O. Firschein (Eds.), *Readings in Computer Vision: Issues, Problems, Principles, and Paradigms*, 661–670. Los Altos, CA.: Kaufmann.
- Bartneck, C. and Okada, M. (2001a). Emuu - An Emotional Robot. Demonstration at Robo Festa, Osaka, www.bartneck.de/work/.
- Bartneck, C. and Okada, M. (2001b). Robotic User Interfaces. In *Proceedings of the Human and Computer Conference (HC-2001)*, Aizu, 130–140.
- Bertails, F., Hadap, S., Cani, M.-P., Lin, M. C., Ward, K., Marschner, S. R., Kim, T.-Y., and Kacic-Alesic, Z. (2008). Realistic Hair Simulation: Animation and Rendering. In *ACM SIGGRAPH Class Notes, August, 2008*, Los Angeles, Etats-Unis.
- Bickel, B., Botsch, M., Angst, R., Matusik, W., Otaduy, M., Pfister, H., and Gross, M. (2007). Multi-scale capture of facial geometry and motion. In *SIGGRAPH '07: ACM SIGGRAPH 2007 papers*, New York, NY, USA, 33. ACM.
- Blanz, V. and Vetter, T. (1999). A morphable model for the synthesis of 3D faces. In *SIGGRAPH '99: Proceedings of the 26th annual conference on Computer graphics and interactive techniques*, New York, NY, USA, 187–194. ACM Press/Addison-Wesley Publishing Co.
- Blinn, J. F. (1978). Simulation of wrinkled surfaces. In *SIGGRAPH '78: Proceedings of the 5th annual conference on Computer graphics and interactive techniques*, New York, NY, USA, 286–292. ACM.
- Bloomenthal, J. (1985). Modeling the mighty maple. In *SIGGRAPH '85: Proceedings of the 12th annual conference on Computer graphics and interactive techniques*, New York, NY, USA, 305–311. ACM.
- Bondy, M. D., Georganas, N. D., Petriu, E. M., Petriu, D. C., Cordea, M. D., and Whalen, T. E. (2001). Model-based face and lip animation for interactive virtual reality applications. In *MULTIMEDIA '01: Proceedings of the ninth ACM international conference on Multimedia*, New York, NY, USA, 559–563. ACM.
- Borshukov, G., Piponi, D., Larsen, O., Lewis, J. P., and Tempelaar-Lietz, C. (2005). Universal capture - image-based facial animation for "The Matrix Reloaded". In *SIGGRAPH '05: ACM SIGGRAPH 2005 Courses*, New York, NY, USA, 16. ACM.

- Botsch, M., Pauly, M., Kobbelt, L., Alliez, P., Lévy, B., Bischoff, S., and Rössl, C. (2007). Geometric modeling based on polygonal meshes. In *SIGGRAPH '07: ACM SIGGRAPH 2007 courses*, New York, NY, USA, 1. ACM.
- Bottino, A., Nuij, W., and Overveld, K. V. (1996). How to shrinkwrap through a critical point: an algorithm for the adaptive triangulation of iso-surfaces with arbitrary topology. In *In Proc. Implicit Surfaces 96*, 53–72.
- Bouguet, J. (2000). Pyramidal Implementation of the Lucas Kanade Feature Tracker Description of the Algorithm. Technical report.
- Bourke, P. (1994). Polygonising a scalar field. <http://local.wasp.uwa.edu.au/~pbourke/geometry/polygonise/>.
- Bradshaw, G. and O’Sullivan, C. (2002). Sphere-tree construction using dynamic medial axis approximation. In *SCA '02: Proceedings of the 2002 ACM SIGGRAPH/Eurographics symposium on Computer animation*, New York, NY, USA, 33–40. ACM.
- Brennan, S. E. (1984). Caricatures from images. In *ACM 84: Proceedings of the 1984 annual conference of the ACM on The fifth generation challenge*, New York, NY, USA, 228–229. ACM.
- Breton, G., Bouville, C., and Pelé, D. (2001). FaceEngine a 3D facial animation engine for real time applications. In *Web3D '01: Proceedings of the sixth international conference on 3D Web technology*, New York, NY, USA, 15–22. ACM.
- Brox, T., Bruhn, A., and Papenber, N. and Weickert, J. (2004). High accuracy optical flow estimation based on a theory for warping. In T. Pajdla and J. Matas (Eds.), *European Conference on Computer Vision (ECCV)*, Volume 3024 of *LNCS*, Prague, Czech Republic, 25–36. Springer.
- Buss, S. R. (2003). *3D computer graphics: a mathematical introduction with OpenGL*. Cambridge: England: Cambridge University Press.
- Byun, M. and Badler, N. I. (2002). FacEMOTE: qualitative parametric modifiers for facial animations. In *SCA '02: Proceedings of the 2002 ACM SIGGRAPH/Eurographics symposium on Computer animation*, New York, NY, USA, 65–71. ACM.

- Caulkin, S. (2009). Face Modelling and Animation (Industry Presentation). In *Workshop on Face Behaviour and Interaction FBI 2009 Proceedings*, 2. Computing and Mathematics Department, Manchester Metropolitan University.
- Cazedevals, A., Magnenat-Thalmann, N., and Thalmann, D. (1993). Modeling Facial Communication Between an Animator and a Synthetic Actor in Real Time. In *Proc. IFIP Conf. on Modeling in Computer Graphics, Genova*, 378–396.
- Chen, C. (2006). *Design of Novel Algorithms for 3D Human Head Modeling and Expression Synthesis*. Ph. D. thesis, School of Computer Engineering, Nanyang Technological University, Singapore.
- Chen, C. and Prakash, E. C. (2006). Physically based facial expression synthesizer with performance analysis and GPU-aided simulation. In *CyberGames '06: Proceedings of the 2006 international conference on Game research and development*, Murdoch University, Australia, Australia, 171–176. Murdoch University.
- Cheng, S.-W., Dey, T. K., and Ramos, E. A. (2007). Delaunay refinement for piecewise smooth complexes. In *SODA '07: Proceedings of the eighteenth annual ACM-SIAM symposium on Discrete algorithms*, Philadelphia, PA, USA, 1096–1105. Society for Industrial and Applied Mathematics.
- Chernoff, H. (1973). The Use of Faces to Represent Points in K-Dimensional Space Graphically. *Journal of the American Statistical Association*, 68(342), 361–368.
- Curio, C., Breidt, M., Kleiner, M., Vuong, Q. C., Giese, M. A., and Bühlhoff, H. H. (2006). Semantic 3D motion retargeting for facial animation. In *APGV '06: Proceedings of the 3rd symposium on Applied perception in graphics and visualization*, New York, NY, USA, 77–84. ACM.
- Darwin, C. (1890). *The Expression of the Emotions in Man and Animals*. London: Francis Darwin ed.
- Däuber, S., Wörn, H., Univ. of Karlsruhe, Eggers, G., Krempien, R., Mende, U., Welzel, T., and S. (2003). Creating high quality models of the skull using iterative modelling and area of interests. *Computer Assisted Radiology and Surgery (CARS) 2003*, 747–751.
- Davis, T. A. and Kundert-Gibbs, J. (2006). The role of computer science in digital production arts. In *ITICSE '06: Proceedings of the 11th annual SIGCSE conference*

- on Innovation and technology in computer science education*, New York, NY, USA, 73–77. ACM.
- De Jongh, H., Dantuma, R., and Sluijsmans, H. (1989). The shape of the mandible in the domestic sheep: a biomechanical analysis using EMG as an estimator of muscle force. *Acta Morphologica Netherlands- Scandinavia*, 27, 63–73.
- Deng, Z., Neumann, U., Lewis, J., Kim, T.-Y., Bulut, M., and Narayanan, S. (2006). Expressive Facial Animation Synthesis by Learning Speech Coarticulation and Expression Spaces. *IEEE Transactions on Visualization and Computer Graphics*, 12(6), 1523–1534.
- DeRose, T., Kass, M., and Truong, T. (1998). Subdivision surfaces in character animation. In *SIGGRAPH '98: Proceedings of the 25th annual conference on Computer graphics and interactive techniques*, New York, NY, USA, 85–94. ACM.
- Dobai, I., Rothkrantz, L., and van der Mast, C. (2005). Personality model for a companion AIBO. In *ACE '05: Proceedings of the 2005 ACM SIGCHI International Conference on Advances in computer entertainment technology*, New York, NY, USA, 438–441. ACM.
- Donath, J. (2004). Artificial pets: Simple Behaviours Elicit Complex Attachments. *Encyclopaedia of Animal Behaviour*.
- Doo, D. (1978). A subdivision algorithm for smoothing down irregularly shaped polyhedrons. In *in Proceedings on Interactive Techniques in Computer Aided Design*, 157–165. IEEE.
- Doo, D. and Sabin, M. (1978). Behavior of recursive division surfaces near extraordinary points. *Computer-Aided Design*, 10(6), 356–360.
- Dreamworks (2009). <http://www.dreamworks.com>.
- Eberly, D. H. and Shoemake, K. (2005). *Game physics*. Elsevier/Morgan Kaufmann, Amsterdam.
- Ekman, P. and Friesen, W. v. (1978). *Facial Action Coding System: Investigators Guide*. Consulting Psychologists Press. Palo alto, California.

- Ekman, P. and Rosenberg, E. L. (1998). *What the Face Reveals: Basic and Applied Studies of Spontaneous Expression Using the Facial Action Coding System (FACS) (Series in Affective Science)* (1 ed.). Oxford University Press, USA.
- Engwall, O. (2000). A 3D tongue model based on MRI data. In *Sixth International Conference on Spoken Language Processing 2000*, Volume 3, Beijing, China, 901–904.
- Engwall, O. (2004). From real-time MRI to 3D tongue movements. In S. H. Kim and D. H. Young (Eds.), *Proc ICSLP 2004*, Volume 2, Jeju Island, Korea, 1109–1112.
- Falk, R., Minter, D., Vernon, C., Aretos, G., Modesto, L., Lamorlette, A., Walker, N., Cheung, T., Rentel-Lavin, J., and Max, H. (2004). Art-directed technology: anatomy of a Shrek2 sequence. In *SIGGRAPH '04: ACM SIGGRAPH 2004 Course Notes*, New York, NY, USA, 13. ACM.
- Fischer, K. and Gartner, B. (2003). The smallest enclosing ball of balls: combinatorial structure and algorithms. In *SCG '03: Proceedings of the nineteenth annual symposium on Computational geometry*, New York, NY, USA, 292–301. ACM.
- FreeDigitalPhotos.net (2009). Greyhound. <http://www.freedigitalphotos.net/>.
- Friedman, B., Kahn, Jr., P. H., and Hagman, J. (2003). Hardware companions?: what online AIBO discussion forums reveal about the human-robotic relationship. In *CHI '03: Proceedings of the SIGCHI conference on Human factors in computing systems*, New York, NY, USA, 273–280. ACM.
- Furry Paws LLC (2007). Furry Paws. www.furry-paws.com.
- Gal, J., Gallo, L., Palla, S., Murray, G., and Klineberg, I. (2004). Analysis of human mandibular mechanics based on screw theory and in vivo data. *Journal of Biomechanics*, 37, 1405–1412.
- Gerard, J.-M., Wilhelms-Tricarico, R., Perrier, P., and Payan, Y. (2003). A 3D dynamical biomechanical tongue model to study speech motor control. *Research Developments in Biomechanics*, 1, 49–64.
- Gillenson, M. (1974). *The interactive generation of facial images on a CRT using a heuristic strategy*. Ph. D. thesis, Ohio State University, Computer Graphics Research Group.

- Goldman, D. B. (1997). Fake fur rendering. In *SIGGRAPH '97: Proceedings of the 24th annual conference on Computer graphics and interactive techniques*, New York, NY, USA, 127–134. ACM Press/Addison-Wesley Publishing Co.
- Gottschalk, S., Lin, M. C., and Manocha, D. (1996). OBBTree: a hierarchical structure for rapid interference detection. In *SIGGRAPH '96: Proceedings of the 23rd annual conference on Computer graphics and interactive techniques*, New York, NY, USA, 171–180. ACM.
- Guenther, B., Grimm, C., Wood, D., Malvar, H., and Pighin, F. (1998). Making faces. In *SIGGRAPH '98: Proceedings of the 25th annual conference on Computer graphics and interactive techniques*, New York, NY, USA, 55–66. ACM.
- Haber, J. and Terzopoulos, D. (2004). Facial modeling and animation. In *SIGGRAPH '04: ACM SIGGRAPH 2004 Course Notes*, New York, NY, USA, 6. ACM.
- Hadap, S., Cani, M.-P., Lin, M., Kim, T.-Y., Bertails, F., Marschner, S., Ward, K., and Kačić-Alesić, Z. (2007). Strands and hair: modeling, animation, and rendering. In *SIGGRAPH '07: ACM SIGGRAPH 2007 courses*, New York, NY, USA, 1–150. ACM.
- Hadap, S., Eberle, D., Volino, P., Lin, M. C., Redon, S., and Ericson, C. (2004). Collision detection and proximity queries. In *SIGGRAPH '04: ACM SIGGRAPH 2004 Course Notes*, New York, NY, USA, 15. ACM.
- Hannam, A.G., e. a. (2008). A dynamic model of jaw and hyoid biomechanics during chewing. *Journal of Biomechanics*, 41, 1069–1076.
- Hansford, D. (2007). Barycentric Coordinates Introduction to Computer Graphics Arizona State University. <http://www.farinhansford.com/dianne/teaching/cse470/materials/BarycentricCoords.pdf>.
- Henne, M. and Hickel, H. (1996). The Making of "Toy Story". *Computer Conference, IEEE International*, 0, 463.
- Hill, D. R., Pearce, A., and Wyvill, B. (1988). Animating speech: an automated approach using speech synthesised by rules. *The Visual Computer*, 3(5), 277–289.
- Hill, F. (1994). *Graphics Gems IV*, Chapter The Pleasures of Perp Dot Products, 138–148. Paul S. Heckbert, ed.

- Horn, B. and Schunck, B. (1981). Determining optical flow. *Artificial Intelligence*, 17, 185–203.
- Hubbard, P. M. (1996). Approximating polyhedra with spheres for time-critical collision detection. *ACM Trans. Graph.*, 15(3), 179–210.
- Hyneman, W., Itokazu, H., Williams, L., and Zhao, X. (2005). Human face project. In *SIGGRAPH '05: ACM SIGGRAPH 2005 Courses*, New York, NY, USA, 5. ACM.
- Isidoro, J. and Mitchell, J. L. (2002). User customizable real-time fur. In *SIGGRAPH '02: ACM SIGGRAPH 2002 conference abstracts and applications*, New York, NY, USA, 273–273. ACM.
- Iwatsuka, K., Yamamoto, K., and Kato, K. (2004). Development of a Guide Dog System for the Blind People with Character Recognition Ability. *Pattern Recognition, International Conference on*, 1, 453–456.
- James, D. L. and Twigg, C. D. (2005). Skinning mesh animations. In *SIGGRAPH '05: ACM SIGGRAPH 2005 Papers*, New York, NY, USA, 399–407. ACM.
- Kähler, K., Haber, J., and Seidel, H.-P. (2003). Reanimating the dead: reconstruction of expressive faces from skull data. In *SIGGRAPH '03: ACM SIGGRAPH 2003 Papers*, New York, NY, USA, 554–561. ACM.
- Kähler, K., Haber, J., Yamauchi, H., and Seidel, H.-P. (2002). Head shop: generating animated head models with anatomical structure. In *SCA '02: Proceedings of the 2002 ACM SIGGRAPH/Eurographics symposium on Computer animation*, New York, NY, USA, 55–63. ACM.
- Kajiya, J. T. and Kay, T. L. (1989). Rendering fur with three dimensional textures. In *SIGGRAPH '89: Proceedings of the 16th annual conference on Computer graphics and interactive techniques*, New York, NY, USA, 271–280. ACM.
- Kaplan, F. (2000). Free creatures: The role of uselessness in the design of artificial pets. In T. Christaller, G. Indiveri, and A. Poigne (Eds.), *Proceedings of the 1st Edutainment Robotics Workshop*. GMD-AiS.
- Karabassi, E.-A., Papaioannou, G., and Theoharis, T. (1999). A fast depth-buffer-based voxelization algorithm. *J. Graph. Tools*, 4(4), 5–10.

- Kavan, L., Collins, S., Žára, J., and O’Sullivan, C. (2007). Skinning with dual quaternions. In *I3D ’07: Proceedings of the 2007 symposium on Interactive 3D graphics and games*, New York, NY, USA, 39–46. ACM.
- Kharbat, M. (2009). Horn-Schunck optical flow method Implementation. <http://creativecommons.org/licenses/by-nc-sa/3.0/>.
- King, S. A. (2001). *A facial model and animation techniques for animated speech*. Ph. D. thesis, The Ohio State University.
- King, S. A. and Parent, R. E. (2000). A Parametric Tongue Model for Animated Speech. In *Computer Animation and Simulation ’00*, SpringerComputerScience, 3–13. Proceedings of the Eurographics Workshop in Interlaken, Switzerland, August 21–22, 2000.
- Kleiser, J. (1989). A fast, efficient, accurate way to represent the human face. In *SIGGRAPH ’89 Course Notes 22: State of the Art in Facial Animation*, New York, NY, USA, 36–40. ACM.
- Knudsen, M. W., Martin, J.-C., Dybkjr, L., Machuca Ayuso, M. J., Bernsen, N. O., Carletta, J., Heid, U., Kita, S., Llisterri, J., Pelachaud, C., Poggi, I., Reithinger, N., van Elswijk, G., and Wittenburg, P. (2002). ISLE Natural Interactivity and Multimodality Working Group Deliverable D9.1: Survey of Multimodal Coding Schemes and Best Practice. <http://isle.nis.sdu.dk/reports/wp9/>.
- Kobbelt, L. (2000). $\sqrt{3}$ -subdivision. In *SIGGRAPH ’00: Proceedings of the 27th annual conference on Computer graphics and interactive techniques*, New York, NY, USA, 103–112. ACM Press/Addison-Wesley Publishing Co.
- Koolstra, J. and van Eijden, T. (1997). Dynamics of the human masticatory muscles during a jaw open-close movement. *Journal of Biomechanics*, 30(9), 883–889.
- Koolstra, J. and van Eijden, T. (2001). A method to predict muscle control in the kinematically and mechanically indeterminate human masticatory system. *Journal of Biomechanics*, 34, 1179–1188.
- Koolstra, J. and van Eijden, T. (2004). Functional significance of the coupling between head and jaw movements. *Journal of Biomechanics*, 37, 1387–1392.

- Kriglstein, S. and Wallner, G. (2005). HOMIE: an artificial companion for elderly people. In *CHI '05: CHI '05 extended abstracts on Human factors in computing systems*, New York, NY, USA, 2094–2098. ACM.
- Kubo, H., Yanagisawa, H., Maejima, A., Terzopoulos, D., and Morishima, S. (2006). Facial animation by the manipulation of a few control points subject to muscle constraints. In *SIGGRAPH '06: ACM SIGGRAPH 2006 Research posters*, New York, NY, USA, 65. ACM.
- Kumar, P., Mitchell, J. S. B., and Yildirim, E. A. (2003). Approximate minimum enclosing balls in high dimensions using core-sets. *J. Exp. Algorithmics*, 8, 1.1.
- Lachapelle, P., Bergeron, P., Langlois, D., and Robidoux, P. (1985). Tony de Peltrie. 12 SIGGRAPH Film and Video Show de San Francisco.
- Leader, J. K., Boston, R. J., Debski, R. E., and Rudy, T. E. (2003). Mandibular kinematics represented by a nonorthogonal floating axis joint coordinate system. *Journal of Biomechanics*, 36, 275–281.
- Lee, A., Moreton, H., and Hoppe, H. (2000). Displaced subdivision surfaces. In *SIGGRAPH '00: Proceedings of the 27th annual conference on Computer graphics and interactive techniques*, New York, NY, USA, 85–94. ACM Press/Addison-Wesley Publishing Co.
- Lee, A. W. F., Sweldens, W., Schröder, P., Cowsar, L., and Dobkin, D. (1998). MAPS: Multiresolution Adaptive Parameterization of Surfaces. In *Proceedings of SIGGRAPH 98*, 95–104.
- Lee, Y., Terzopoulos, D., and Walters, K. (1995). Realistic modeling for facial animation. In *SIGGRAPH '95: Proceedings of the 22nd annual conference on Computer graphics and interactive techniques*, New York, NY, USA, 55–62. ACM.
- Lengyel, J., Praun, E., Finkelstein, A., and Hoppe, H. (2001). Real-time fur over arbitrary surfaces. In *I3D '01: Proceedings of the 2001 symposium on Interactive 3D graphics*, New York, NY, USA, 227–232. ACM.
- Lewis, J. P. and Parke, F. I. (1987). Automated lip-synch and speech synthesis for character animation. *SIGCHI Bull.*, 17(SI), 143–147.

- Liu, L. and Ma, H. (2006). Wireless sensor network based mobile pet game. In *NetGames '06: Proceedings of 5th ACM SIGCOMM workshop on Network and system support for games*, New York, NY, USA, 30. ACM.
- Longshaw, S., Turner, M., Finch, E., and Gawthorpe, R. (2009). Discrete Element Modelling Using a Parallelised Physics Engine. In *Theory and Practice of Computer Graphics: Eurographics UK chapter proceedings 2009*, 207–214. Eurographics.
- Loop, C. T. (1987). Smooth Subdivision Surfaces Based on Triangles. Master's thesis, Department of Mathematics, The University of Utah.
- Loop, C. T. (2002). Smooth Ternary Subdivision. In *Curve and Surface Fitting, Saint-Malo*, 3–6. Nashboro Press.
- Lorensen, W. E. and Cline, H. E. (1987). Marching cubes: A high resolution 3D surface construction algorithm. In *SIGGRAPH '87: Proceedings of the 14th annual conference on Computer graphics and interactive techniques*, New York, NY, USA, 163–169. ACM.
- Lucas, B. D. and Kanade, T. (1981). An iterative image registration technique with an application to stereo vision. *Proceedings of Imaging understanding workshop*, 121–130.
- Magenat-Thalmann, N., Primeau, E., and Thalmann, D. (1988). Abstract muscle action procedures for human face animation. *Visual Computer*, 3(5), 290–7.
- Mealing, S. (1998). *The art and science of computer animation*. Exeter: England: Intellect.
- Metzgar, J. (2000). SuperQuadric Ellipsoids and Toroids, OpenGL Lighting, and Timing. <http://www.gamedev.net/reference/articles/article1172.asp>.
- Michael, S. and Chen, M. (1996). The 3D reconstruction of facial features using volume distortion. In *Proc. 14th Eurographics UK Conference*, 297–306.
- Mohr, A. and Gleicher, M. (2003). Building efficient, accurate character skins from examples. In *SIGGRAPH '03: ACM SIGGRAPH 2003 Papers*, New York, NY, USA, 562–568. ACM.

- Morse, B. S., Liu, W., Yoo, T. S., and Subramanian, K. (2005). Active Contours Using a Constraint-Based Implicit Representation. *Computer Vision and Pattern Recognition, IEEE Computer Society Conference on*, 1, 285–292.
- Mouroux, O. (2010). Walt Disney’s ALICE IN WONDERLAND Fun Facts. www.euroinvestor.co.uk.
- Müller, M., Heidelberger, B., Teschner, M., and Gross, M. (2005). Meshless deformations based on shape matching. In *SIGGRAPH ’05: ACM SIGGRAPH 2005 Papers*, New York, NY, USA, 471–478. ACM.
- Navarro Newball, A. A., Vélez Beltrán, J. A., Satizabal, J. E., Múnica Salazar, L. E., and García, G. B. (2003). Virtual surgical tele-simulations in ophthalmology. In *CARS*, 145–150.
- Navarro Newball, A. A., Wyvill, G., and McCane, B. (2008a). Efficient Mesh Generation Using Subdivision Surfaces. *Sistemas & Telemática*, 6(12), 111–126.
- Navarro Newball, A. A., Wyvill, G., and McCane, B. (2008b). Towards the creation of Londra: A virtual expressive animated dog. In *New Zealand Computer Science Research Student Conference. NZCSRSC 2008 Proceedings*, 238–241.
- Navarro Newball, A. A., Wyvill, G., and McCane, B. (2009a). Facial animation in dogs. In *British Machine Vision Association and Society for Pattern Recognition. Facial Analysis and Animation Symposium*, 18. University of Edinburgh, UK.
- Navarro Newball, A. A., Wyvill, G., and McCane, B. (2009b). A Model for a Dog Facial Animation System. In *Workshop on Face Behaviour and Interaction FBI 2009 Proceedings*, 6. Computing and Mathematics Department, Manchester Metropolitan University.
- Navarro Newball, A. A., Wyvill, G., and McCane, B. (2009c). Object Interaction Using Tabulated Spheres Subsets. In *Theory and Practice of Computer Graphics: Eurographics UK chapter proceedings 2009*, 57–60. Eurographics.
- New Zealand’s National Education Monitoring (2009). <http://nemp.otago.ac.nz>.
- Nintendo (2005). Nintendogs. <http://www.nintendo.com.au/gamesites/nintendogs/>.

- Noh, J. Y. and Neumann, U. (1998). A Survey of Facial Modeling and Animation Techniques. Technical report. University of Southern California. http://graphics.ucsd.edu/courses/cse169_w04.
- Noldus Information Technology (2009). The Observer XT. <http://www.noldus.com/human-behavior-research/products/the-observer-xt>.
- O'Brien, J. F., Hodgins, J. K., and Bodenheimer, R. (2000). Computer animation. *Encyclopedia of Computer Science, Nature Publishing Group*, 301–304.
- O'Rourke, J. and Badler, N. I. (1979). Decomposition of three-dimensional objects into spheres. *IEEE Trans. Pattern Anal. Mach. Intell., PAMI-1*, 295–305.
- Osborn, J. (1996). Features of human jaw design which maximize the bite force. *Journal of Biomechanics*, 29(5).
- Papaioannou, G. (2002). A simple and fast technique for fur rendering. <http://www.aueb.gr/users/gepap/>.
- Parke, F. I. (1972). Computer generated animation of faces. In *ACM'72: Proceedings of the ACM annual conference*, New York, NY, USA, 451–457. ACM.
- Parke, F. I. (1974). A parametric model for human faces. Technical report, UTEC-CSc-75-047 Salt Lake City: University of Utah.
- Patel, M. (1995). Colouration Issues in Computer Generated Facial Animation. *Computer Graphics Forum*, 14(2), 117–126.
- Pelachaud, C., van Overveld, C., and Seah, C. (1994). Modeling and Animating the Human Tongue during Speech Production. In *Computer Animation 94*, 40–49. Springer-Verlag.
- Pet Comfort Newsletter (2009). Secrets of the dog tongue are revealed below... <http://www.pet-comfort-products.com/dog-tongue.html>.
- Pighin, F., Hecker, J., Lischinski, D., Szeliski, R., and Salesin, D. H. (2005). Synthesizing realistic facial expressions from photographs. In *SIGGRAPH '05: ACM SIGGRAPH 2005 Courses*, New York, NY, USA, 9. ACM.
- Platt, S. M. and Badler, N. I. (1981). Animating facial expressions. In *SIGGRAPH '81: Proceedings of the 8th annual conference on Computer graphics and interactive techniques*, New York, NY, USA, 245–252. ACM.

- Prakash, E. (2009). Facial Expressions - Modeling and Animation. Power Point presentation at the Manchester Metropolitan University, UK.
- Preece, J., Rogers, Y., and Sharp, H. (2002). *Interaction Design: beyond human-computer interaction*. New York: John Wiley and Sons, Inc.
- Preston, M. and Hill, M. (2006). Grooming, animating & rendering fur for "King Kong". In *SIGGRAPH '06: ACM SIGGRAPH 2006 Sketches*, New York, NY, USA, 43. ACM.
- Radford, J. (2006). Virtual history: the secret plot to kill Hitler. In *SIGGRAPH '06: ACM SIGGRAPH 2006 Courses*, New York, NY, USA, 6. ACM.
- Radovan, M. and Pretorius, L. (2006). Facial animation in a nutshell: past, present and future. In *SAICSIT '06: Proceedings of the 2006 annual research conference of the South African institute of computer scientists and information technologists on IT research in developing countries*, Republic of South Africa, 71–79. South African Institute for Computer Scientists and Information Technologists.
- Reeves, W. T. (1990). Simple and complex facial animation: Case studies. In *State Of The Art In Facial Animation, SIGGRAPH course 26*, New York, NY, USA, 90–106. ACM.
- Roble, D. (2000). Vision in film and special effects. *SIGGRAPH Comput. Graph.*, 33(4), 58–60.
- Sagar, M. (2006). Facial performance capture and expressive translation for King Kong. In *SIGGRAPH '06: ACM SIGGRAPH 2006 Sketches*, New York, NY, USA, 26. ACM.
- Selle, A., Lentine, M., and Fedkiw, R. (2008). A mass spring model for hair simulation. *ACM Trans. Graph.*, 27(3), 1–11.
- Semwal, S., Watson, B., and McCullough, D. (Visited 2008). Human Muscle Modeling using Generalized Cylinders for Volume Considerations (Presentation). http://www.cs.uccs.edu/~semwal/Semwal_Debra_Bill.ppt.
- Sifakis, E., Selle, A., Robinson-Mosher, A., and Fedkiw, R. (2006). Simulating speech with a physics-based facial muscle model. In *SCA '06: Proceedings of the 2006 ACM SIGGRAPH Eurographics symposium on Computer animation*, Aire-la-Ville, Switzerland, Switzerland, 261–270. Eurographics Association.

- Simmons, M., Wilhelms, J., and Van Gelder, A. (2002). Model-based reconstruction for creature animation. In *SCA '02: Proceedings of the 2002 ACM SIGGRAPH/Eurographics symposium on Computer animation*, New York, NY, USA, 139–146. ACM.
- Sims, K. (1994). Evolving virtual creatures. In *SIGGRAPH '94: Proceedings of the 21st annual conference on Computer graphics and interactive techniques*, New York, NY, USA, 15–22. ACM.
- Sisson, S., Getty, R., and Grossman, J. D. (1975). *The Anatomy of the Domestic Animals*. London: W.B. Saunders Company.
- Stam, J. (1998). Evaluation of Loop Subdivision Surfaces.
- Stern, A. (1999). Virtual Babyz: Believable Agents with Narrative Intelligence. In *Proceedings of the 1999 AAAI Fall Symposium, Narrative Intelligence*.
- Stern, A., Frank, A., and Resner, B. (1998). Virtual petz (video session): a hybrid approach to creating autonomous, lifelike dogz and catz. In *AGENTS '98: Proceedings of the second international conference on Autonomous agents*, New York, NY, USA, 334–335. ACM.
- Stone, M. (1991). Toward a Model of Three-Dimensional Tongue Movement. *Journal of Phonetics*, 19, 309–320.
- Sud, A., Foskey, M., and Manocha, D. (2005). Homotopy-preserving medial axis simplification. In *SPM '05: Proceedings of the 2005 ACM symposium on Solid and physical modeling*, New York, NY, USA, 39–50. ACM.
- Sunday, D. (2006). Geometry Algorithms. <http://softsurfer.com/>.
- Tarini, M., Yamauchi, H., Haber, J., and Seidel, H.-P. (2002). Texturing Faces. In *Graphics Interface*, 89–98.
- Terzopoulos, D., Mones-Hattal, B., Hofer, B., Parke, F., Sweetland, D., and Waters, K. (1997). Facial animation (panel): past, present and future. In *SIGGRAPH '97: Proceedings of the 24th annual conference on Computer graphics and interactive techniques*, New York, NY, USA, 434–436. ACM Press/Addison-Wesley Publishing Co.

- Terzopoulos, D. and Waters, K. (1990). Physically-based facial modelling, analysis, and animation. *The Journal of Visualization and Computer Animation*, 1, 73–80.
- Thalmann, D. (1996). A New Generation of Synthetic Actors: the Real-time and Interactive Perceptive Actors. In *In Proc. Pacific Graphics 96*, 200–219.
- Thalmann, N. M. and Thalmann, D. (2002). A Taxonomy of Complex Models for Visualizing Humans. http://vrlab.epfl.ch/Publications/pdf/Magenat_Thalmann_Thalmann_CGA_91.pdf.
- Tomlinson, B., Downie, M., Berlin, M., Gray, J., Lyons, D., Cochran, J., and Blumberg, B. (2002). Leashing the AlphaWolves: mixing user direction with autonomous emotion in a pack of semi-autonomous virtual characters. In *SCA '02: Proceedings of the 2002 ACM SIGGRAPH/Eurographics symposium on Computer animation*, New York, NY, USA, 7–14. ACM.
- Turbo Squid, Inc (2008). Dog_Skull_3ds. <http://www.turbosquid.com>.
- Turing, A. M. (1952). The Chemical Basis of Morphogenesis. *Philosophical Transactions of the Royal Society of London. Series B, Biological Sciences*, 237(641), 37–72.
- Turk, G. (1991). Generating textures on arbitrary surfaces using reaction-diffusion. In *SIGGRAPH '91: Proceedings of the 18th annual conference on Computer graphics and interactive techniques*, New York, NY, USA, 289–298. ACM.
- van Overveld, K. and Wyvill, B. (2004). Shrinkwrap: An efficient adaptive algorithm for triangulating an iso-surface. *Vis. Comput.*, 20(6), 362–379.
- van Swaaij, M. (2006). Ray-tracing fur for Ice Age: the Melt Down. In *SIGGRAPH '06: ACM SIGGRAPH 2006 Sketches*, New York, NY, USA, 44. ACM.
- Vitulli, D. (2005). Spacesimulator.net. <http://www.spacesimulator.net/>.
- Voigt, H., Flower, D., and Weisser, D. (2005). COMP-SCI 715 S2 C - Advanced Computer Graphics Report. <http://www.scribd.com/doc/18742507/12155MeshlessDeformationsReport>.
- Walter, M., Fournier, A., and Menevaux, D. (2001). Integrating shape and pattern in mammalian models. In *SIGGRAPH '01: Proceedings of the 28th annual conference on Computer graphics and interactive techniques*, New York, NY, USA, 317–326. ACM.

- Walter, M., Fournier, A., and Reimers, M. (1998). Clonal Mosaic Model for the Synthesis of Mammalian Coat Patterns. In *Proceedings of Graphics Interface*, Vancouver, BC, Canada, 82–91.
- Wampler, K., Sasaki, D., Zhang, L., and Popović, Z. (2007). Dynamic, expressive speech animation from a single mesh. In *SCA '07: Proceedings of the 2007 ACM SIGGRAPH/Eurographics symposium on Computer animation*, Aire-la-Ville, Switzerland, Switzerland, 53–62. Eurographics Association.
- Wang, W., Wang, J., and Kim, M.-S. (2001). An algebraic condition for the separation of two ellipsoids. *Comput. Aided Geom. Des.*, 18(6), 531–539.
- Ward, K., Bertails, F., Kim, T.-Y., Marschner, S. R., Cani, M.-P., and Lin, M. C. (2007). A Survey on Hair Modeling: Styling, Simulation, and Rendering. *IEEE Transactions on Visualization and Computer Graphics*, 13(2), 213–234.
- Warren, A. (2004). CyPet 2: The Virtual Pet For Windows. Axe Software. www.axeuk.com/cypet.htm.
- Watanabe, H., Fukano, A., Takahei, T., and Saito, T. (2004). NetAIBO project. In *SIGGRAPH '04: ACM SIGGRAPH 2004 Web graphics*, New York, NY, USA, 7. ACM.
- Waters, K. (1987). A muscle model for animation three-dimensional facial expression. In *SIGGRAPH '87: Proceedings of the 14th annual conference on Computer graphics and interactive techniques*, New York, NY, USA, 17–24. ACM.
- Watt, A. and Policarpo, F. (2001). *3D Games: Real time rendering and software technology*. Addison Wesley, London.
- Weijts, W. (1989). The functional significance of morphological variation of the human mandible and masticatory muscles. *Acta Morphologica Netherlands- Scandinavia*, 27, 149–162.
- Weisstein, E. (2008). Wolfram Mathworld. <http://mathworld.wolfram.com/>.
- Welzl, E. (1991). Smallest Enclosing Disks (Balls and Ellipsoids). *Lecture Notes in Computer Science*, 555, 359–370.

- Weyrich, T. (2009). Modeling the appearance of human skin. In *British Machine Vision Association and Society for Pattern Recognition. Facial Analysis and Animation Symposium*, 4. University of Edinburgh, UK.
- Wikimedia Foundation (2009a). Beatrix Potter. http://en.wikipedia.org/wiki/Beatrix_Potter.
- Wikimedia Foundation (2009b). Boxer (dog). [http://en.wikipedia.org/wiki/Boxer_\(dog\)](http://en.wikipedia.org/wiki/Boxer_(dog)).
- Wikimedia Foundation (2009c). Canine terminology. http://en.wikipedia.org/wiki/Canine_terminology.
- Wikimedia Foundation (2009d). Facial Action Coding System. http://en.wikipedia.org/wiki/Facial_Action_Coding_System.
- Wikimedia Foundation (2009e). Faunus. <http://en.wikipedia.org/wiki/Faunus>.
- Wikimedia Foundation (2009f). Felix the cat. http://en.wikipedia.org/wiki/Felix_the_cat.
- Wikimedia Foundation (2009g). Horus. <http://en.wikipedia.org/wiki/Horus>.
- Wikimedia Foundation (2009h). Nintendogs. <http://en.wikipedia.org/wiki/Nintendogs>.
- Wikimedia Foundation (2009i). Noh. http://en.wikipedia.org/wiki/Noh_theatre.
- Wikimedia Foundation (2009j). Petz. <http://en.wikipedia.org/wiki/Petz>.
- Wikimedia Foundation (2009k). Quetzalcoatl. <http://en.wikipedia.org/wiki/Quetzalcoatl>.
- Wikimedia Foundation (2009l). Rin Rin the tadpole. http://en.wikipedia.org/wiki/Rin_Rin_the_tadpole.
- Wikimedia Foundation (2009m). The Oregon Duck. http://en.wikipedia.org/wiki/The_Oregon_Duck.
- Wikimedia Foundation (2009n). Tongue. <http://en.wikipedia.org/wiki/Tongue>.
- Wilhelms, J. and Van Gelder, A. (1997). Anatomically based modeling. In *SIGGRAPH '97: Proceedings of the 24th annual conference on Computer graphics and interactive techniques*, New York, NY, USA, 173–180. ACM Press/Addison-Wesley Publishing Co.

- Will (2008). Dogs: *Canis Familiaris*. <http://www.skullsite.co.uk/Dog/dog.htm>.
- Williams, L. (1990). Performance-driven facial animation. In *SIGGRAPH '90: Proceedings of the 17th annual conference on Computer graphics and interactive techniques*, New York, NY, USA, 235–242. ACM.
- Witkin, A. and Kass, M. (1991). Reaction-diffusion textures. In *SIGGRAPH '91: Proceedings of the 18th annual conference on Computer graphics and interactive techniques*, New York, NY, USA, 299–308. ACM.
- Wixon, D. (2006). What is a game? *interactions*, 13(2), 37–ff.
- Wu, Y., Magnenat Thalmann, N., and Thalmann, D. (1994). A plastic-visco-elastic model for wrinkles in facial animation and skin aging. In *Pacific Graphics '94: Proceedings of the second Pacific conference on Fundamentals of computer graphics*, River Edge, NJ, USA, 201–213. World Scientific Publishing Co., Inc.
- Xiang, G., Ju, X., Holt, P. O., and Shang, L. (2009). Facial Expression Transferring with a Deformable Model. In *Theory and Practice of Computer Graphics: Eurographics UK chapter proceedings 2009*, 117–123. Eurographics.
- Yang, G., Sun, H., Wang, W., and Wu, E. (2006). Interactive fur modeling based on hierarchical texture layers. In *VRCIA '06: Proceedings of the 2006 ACM international conference on Virtual reality continuum and its applications*, New York, NY, USA, 343–346. ACM.
- Yao, J., Zhang, M., Zeng, X., and Wang, Y. (2005). Fast Individual Facial Animation. *Computer Graphics, Imaging and Visualization, International Conference on*, 0, 278–281.
- YouTube LLC (2009). YouTube: Broadcast Yourself. <http://www.youtube.com/>.
- Yurany, A. (2008). Gitana. <http://www.gitana1984.blogspot.com>.
- Zachow, S., Gladilin, E., Sader, R., and Zeilhofer, H.-F. (2003). Draw and cut: intuitive 3D osteotomy planning on polygonal bone models. In *CARS*, 362–369.
- Zalewski, L. and Gong, S. (2005). 2D Statistical Models of Facial Expressions for Realistic 3D Avatar Animation. *Computer Vision and Pattern Recognition, IEEE Computer Society Conference on*, 2, 217–222.

- Zehmeister, M. S., Kim, Y. S., and Kang, B. H. (2007). An Illumination Identification System for the AIBO Robot. *Multimedia and Ubiquitous Engineering, International Conference on, 0*, 837–842.
- Zhang, Y. and Prakash, E. C. (2009). Face to face: anthropometry-based interactive face shape modeling using model priors. *Int. J. Comput. Games Technol.*, 2009, 1–15.
- Zhang, Y., Prakash, E. C., and Sung, E. (2003a). Efficient Modeling of an Anatomy-Based Face and Fast 3D Facial Expression Synthesis. In D. Duke and R. Scopigno (Eds.), *Computer Graphics Forum*, Volume 22(2), 159–169. Oxford, UK and Boston, USA: Blackwell Publishing Inc.
- Zhang, Y., Prakash, E. C., and Sung, E. (2003b). Hierarchical facial data modeling for visual expression synthesis. *Journal of Visualization*, 6(2), 313–320.
- Zhang, Y., Prakash, E. C., and Sung, E. (2004a). Face alive. *Journal of Visual Languages and Computing*, 15, 125–160.
- Zhang, Y., Prakash, E. C., and Sung, E. (2004b). A New Physical Model with Multi-layer Architecture for Facial Expression Animation Using Dynamic Adaptive Mesh. *IEEE Transactions on Visualization and Computer Graphics*, 10(3), 339–352.
- Zhang, Y., Sim, T., and Tan, C. L. (2004). Rapid modeling of 3D faces for animation using an efficient adaptation algorithm. In *GRAPHITE '04: Proceedings of the 2nd international conference on Computer graphics and interactive techniques in Australasia and South East Asia*, New York, NY, USA, 173–181. ACM.
- Zorin, D. N. (1998). *Stationary subdivision and multiresolution surface representations*. Ph. D. thesis.

Appendix A

Artificial Pets

An artificial pet is a robotic or software toy intended to provide a companion to its owner and to behave like a pet. It is internally motivated and has own goals. It survives with the help of its user. It occupies the user in tasks such as feeding, cleaning and playing. Finally, it develops according to its owner's treatment (Allison (2006); Donath (2004)). In (Donath (2004)) it is stated that a good artificial pet must have at least the characteristics described next:

- **Autonomy:** The pet needs to look internally motivated and having its own goals
- **Dependence:** They are designed to survive with the help of their users.
- **Interaction:** Compromises the user in tasks like feeding, cleaning and playing.
- **Development:** The pets must be designed to develop according to their owners treatment.

Robotic pets are one particular approach (Bartneck and Okada (2001b)). Here, it is stated that pets can rely on reactive loops to interact with humans and that an event starts some kind of reaction. Additionally, there have been many other advances in artificial pets. For example, pets designed for wireless mobile devices (Liu and Ma (2006)) and; approaches to brain modelling and evolution (Sims (1994)).

Most of the pets are pieces of useless software or devices. However, some artificial pets are useful working artificial pets just like some real pets (Kriglstein and Wallner (2005); Iwatsuka *et al.* (2004)). Indeed, companionship itself is one form of usefulness. In many cases, the technology underlying a specific artificial pet is in general evident but not clearly explained. That is the case of commercial pet games like PETZ (Stern

et al. (1998)) and NintenDogs (Nintendo (2005)). In consequence, many times, the exact developments and particular issues were not found.

Several author's state that the success of a pet does not rely on its realism (Kaplan (2000); Allison (2006)). However, it can be argued that sometimes realism is not only implemented with the graphics but with a successful behaviour.

Some popular artificial pets are explained below:

A.0.1 Tamagotchi (Allison (2006))

Portable pet contained in a liquid crystal screen key chain with a sketchy likeness (Figure A.1A). The objective is to keep the pet alive and socially well behaved. It uses 2D low resolution computer graphics, randomic behaviour algorithms, Simple maths and basic artificial intelligence.

It grows up assuming 1 of 14 possible personalities as an adult. Figure A.1B show variations from 4 personalities as a child. Approved characteristics are: intelligence, alertness, cheerfulness, independenc. Disapproved characteristics are: laziness, mysteriousness, dullness, weirdness.

It interacts through buttons and icons manipulation. Icons exists for food, light, play medicine, cleaning, discipline, attention and a health meter which displays 4 hearts for the status of health, fed, happiness, age and discipline. Tamagotchi beeps for attention.

A.0.2 Cypet (Warren (2004))

Virtual pet for windows. It can be saved in a file (Figure A.1C). It uses 2D low resolution computer graphics, randomic behaviour algorithms, simple maths and basic artificial intelligence. It displays basic facial expressions based mainly on the shape of the mouth.

The owner interacts by clicking iconic buttons. Status is shown with meters for hunger, happiness, boredom, health, dirtiness and behaviour. Icons exist for feeding, playing, vaccinating, disciplining and cleaning

A.0.3 Furry Paws (Furry Paws LLC (2007))

Web based virtual pet. Here, a whole virtual scenario is provided with places such as a market, a kennel and a clinic. It is possible to participate in an online exhibition and contest with the online pet owner community (Figure A.1D). It uses web low resolution

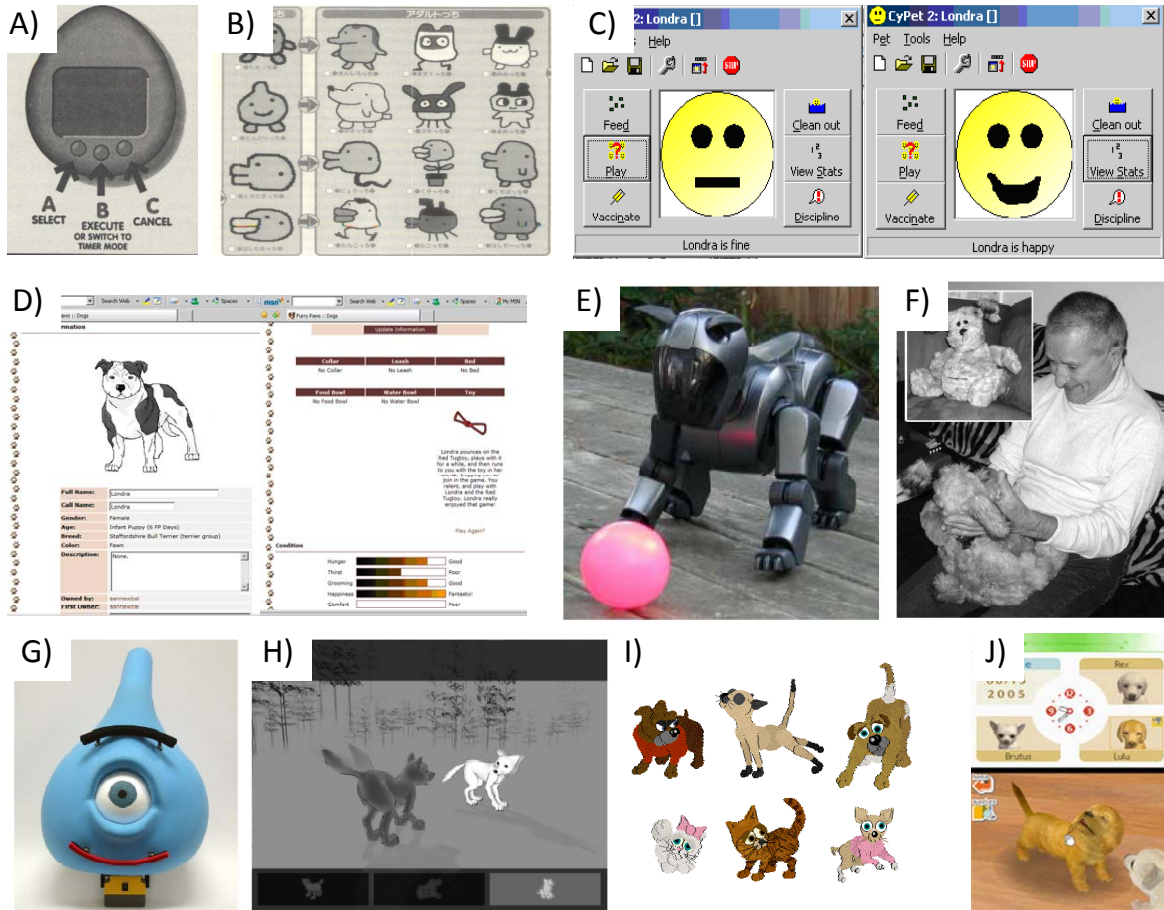


Figure A.1: artificial Pets. A) Tamagotchy (Allison (2006), p. 171). B) Tamagotchy personalities (Allison (2006), p. 173). C) Cypet (Warren (2004)). D) Furry Paws (Furry Paws LLC (2007)). E) AIBO (Friedman *et al.* (2003), p. 274). F) HOMIE (Kriglstein and Wallner (2005), p. 2097). G) eMuu (Bartneck and Okada (2001b), p. 1). H) Alpha wolves (Tomlinson *et al.* (2002), p. 7). I) PETZ (Wikimedia Foundation (2009j)). J) Nintendogs (Wikimedia Foundation (2009h)).

graphics and simple web forms, randomic events and basic artificial intelligence. It displays 2D static images, text messages and condition indicators.

Interaction is done via a web page and there are meters to show hunger, thirst, grooming, happiness and comfort. It shows always the same dog image that is assigned when the breed is chosen.

A.0.4 AIBO (Allison (2006))

Artificial Intelligence robot from Sony. It is a walking, talking computer robot with motors and sensors. It develops its own character and behaviour (Figure A.1E). Several groups are developing features for AIBO. For example, artificial vision technologies (Zehmeister *et al.* (2007)). Network and 3D computer graphics (WEB 3D) technologies (Watanave *et al.* (2004)). Advanced artificial intelligence and software architecture concepts for the development of personality (Dobai *et al.* (2005)).

It responds to a range of emotions and uses software to mimic body language. Standard behaviours come from a manually designed database, but they have been extended in some projects (Dobai *et al.* (2005)). It displays postures from its moveable parts and LED colours.

AIBO recognises 40 voice commands. It has touch sensors. It is equipped with speaker on its chest, LED Lights (on face, ears and back) and a series of movable parts.

A.0.5 HOMIE (Kriglstein and Wallner (2005))

Artificial companion for elderly people (Figure A.1F). It consists on a console plugged to a TV, a dog bed and a collar /bracelet.

It uses speech synthesis; artificial intelligence for learning habits; networking, since it can receive messages from TV; robotics; information management; text recognition. Also, it transfers medical data captured through his collar /bracelet.

It features facial expression and gesture. Particularly, happiness, interest, hopefulness, relaxation, sadness, anger and alertness. It can move ears, eyebrows, mouth, tongue, head, arms, legs and tail.

For interaction, movement and audio sensors react to the user. It produces speech and bark. It has pressure sensors.

A.0.6 eMuu (Bartneck and Okada (2001a,b))

Emotional robot (Figure A.1G). A game engine negotiates, a character engine controls behaviour and runs on a PC and an emotional engine runs inside the robot and controls facial expressions.

It uses advanced artificial intelligence and software architecture; robotics; speech recognition; complex computational. representation of emotion.

It is aimed to the communication of emotions. It moves the eyelids, the eyebrows and the mouth.

It interacts through speech.

A.0.7 Alpha wolves (Tomlinson *et al.* (2002))

Expressive virtual wolves highly controllable but with strong autonomy. It allows multiple wolves (Figure A.1H).

They use sound processing; complex computational representation of emotions; advanced artificial intelligence; 3D computer graphics and animation; autonomous agents.

Expression and feeling are shown through wolf icons that show wolf's mind. Also, through gestures and postures of the wolves, tail, ears, legs and body movement. Also, through motor action.

The user takes the place of a wolf and starts barking, howling, growling or whining. Each wolf can sleep, stand, walk, dominate, submit, or howl and the actions are triggered according to context.

A.0.8 PETZ (Stern *et al.* (1998); Stern (1999))

No goal orientated pet experience, where the user has to raise a number of petz (dogz or catz), (Figure A.1I).

They use 3D computer graphics and animation; autonomous agents; advanced artificial intelligence. They are rendered in non photorealistic cartoon style and built as a set of balls joined by lines. They use colours and textures (Wikimedia Foundation (2009j)).

Facial expressions use head, eyebrows, mouth and ears and body language. They communicate desires through their actions. Expressions include, barking, licking, smiling, laughing, talking. Emotions include excitement, love, boredom, happiness, aggressiveness, timidity, laziness and jealousy.

Interaction is mouse iconic based. The owner can show affection, nurture, play and train. No bar graph displaying emotions, only actions.

A.0.9 Nintendogs (Wixon (2006); Wikimedia Foundation (2009h))

Autonomous pet poppy simulation game developed by Nintendo; here, users can train, pet, play with their puppies. A whole virtual world contextualises the game. The goal is to gain trainer points (Figure A.1J).

They use speech recognition; 3D computer graphics and animation; texturing; some form of artificial intelligence; networking, for remote playing with other pet owners.

They display ears, mouth, head, eyes movements and body movements and postures. Interaction mechanisms are touchscreen, voice, iconic buttons and meters.

Appendix B

Special Effects

Special effects provide the ability to produce complex images. They enhance the realism of characters, scenes or situations such as dynamic hair and deformations in advanced character setup (Buss (2003); Davis and Kundert-Gibbs (2006)).

Special effects replicate phenomena from the real or imaginary world. They are widely used in the entertainment industry and may include disparate events made for a visually seamless scene. In many cases, they require the invention of new techniques or the extension of old ones when a tool does not achieve what is needed. Among the tasks related with special effects are:

- New pipelines (e.g. crowd, hair, advance character setup).
- Developing character setup technology and standards.
- Integrating character setup system which includes motion system, facial animation, body deformations and, hair setup and dynamics.
- The creation of a complete range of movements and, minimizing problems and inefficiencies.

The result constitutes a basis which is complemented with special effects. For example, in the development of Shrek's scene 1350 the animation controls and the spine of the feather in Puss n' Boots hat were provided by the character's developers, while de feather strands were provided by a special effects team (Falk *et al.* (2004)).

Special effects require accuracy, elaboration and technical skills. They are used to enhance realism or the atmosphere of a particular situation and help to develop scenes that cannot be achieved by live action (Roble (2000); Amanatides (1987); Davis and Kundert-Gibbs (2006)). To provide a simple definition, in animation, a special effect is

anything that moves in an animated film and is not a character handled by an animator. They include animating objects and non - character entities and phenomena (Mealing (1998)). Special effects are also seen as an application of computer animation and provide the ability to produce realistic impossible visions such as: complex illumination; multiple camera views; putting together a number of pieces of image in each frame even when the complexity is not evident (Mealing (1998); Buss (2003)).

Appendix C

Original Parke and Waters parameters

Table C.1 shows Parke's Facial Animation Parameters. Here, he presents expression parameters which control expression for a given face and conformation parameters which specify a particular face. He states that expression and conformation parameters must be orthogonal in the sense that manipulating one kind should not interfere or affect the other kind (Haber and Terzopoulos (2004)). Table C.2. shows Water's muscle based parameterisation. Here, he represented muscles by muscle vectors which describe the effect of muscle contraction on the geometry of the skin surface. His muscles induce displacement with geometric distortion functions based on first order elastic tissue properties and have regions of influence defined (Haber and Terzopoulos (2004)).

Table C.1: Parke's Facial Animation Parameters

	Eyes	Mouth	Additional
Expressive	Pupils dilation Open-close eyelids Eyebrows position, shape Viewing direction Eyebrow arch, separation Eyelid opening Eyeball size Eye gaze Pupil size iris size	Mandible rotation Mouth width, shape Upper lip position Mouth corners position Jaw rotation Mouth expression, width Upper lip position	Head rotation Nostrils size
Conformational	Eyelids size Eyeballs size Iris size Eyes position Eyes colour	Lips colour Teeth colour	Face aspect ratio Neck shape, lenght Forehead shape Chin, cheeks shape Nose lenght Nose width Bridge and nostril Skin colour Head, eyelid scaling Relative size of face parts

Table C.2: Water's muscle based parameterisation.

Muscles	Additional
10 muscles: 9 linear: composed by a point of attachment and a direction 1 sphincter: a centre point and two semi axes defining an ellipse	Jaw rotation Viewing direction Eyelids opening

Appendix D

Additional Observations

Figure D.1A shows that at the beginning Londra spend more time closing the nostrils. However, by the end of the video, time slots used to open and close the nostrils tended to be similar, having an almost linear behaviour at the end (Figure D.1B). Additionally, there was one eye blinking. Time slots lengths used for nostril closure / opening tend to be similar. Eye blinking is independent of nostril motion and can occur anytime.

Figure D.2 shows that in attention ears are raised before anything else and all the time. Indeed, raising the ears is the main and can be the only way to express attention (Figure D.2B). However, it is common to have long periods of head twisting that can be followed by short periods of head untwisting (Figure D.2A). Depending on the location of the object of attention there can be a previous lateral head movement (Figure D.2C). Eye blinking may occur any time and seems to be independent of other movements (Figure D.2B and C). The second most common action in attention is head twisting. Note that the degree of head twisting and raising ears could vary. These charts could be complemented adding an intensity value through time.

Figure D.3B shows that a common action in fear is moving the ears backward. This action can be followed by moving the ears forward during short periods of time. Eye blinking may occur anytime. Figure D.3A show the pattern of the time slot values of consecutive forward - backward ears movements and close open mouth movements. The patterns seem to be random and give no additional hint. However, it can be said that while in fear, the dog is most of the time with the ears backward, sometimes lowering the head and opening the mouth slightly almost in parallel. These actions may occur in different intensities through time. The charts could be complemented adding such values. Note that we did not want to cause extreme panic in Londra while filming these videos.

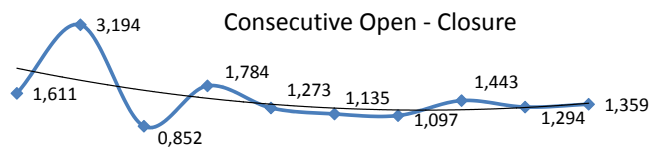
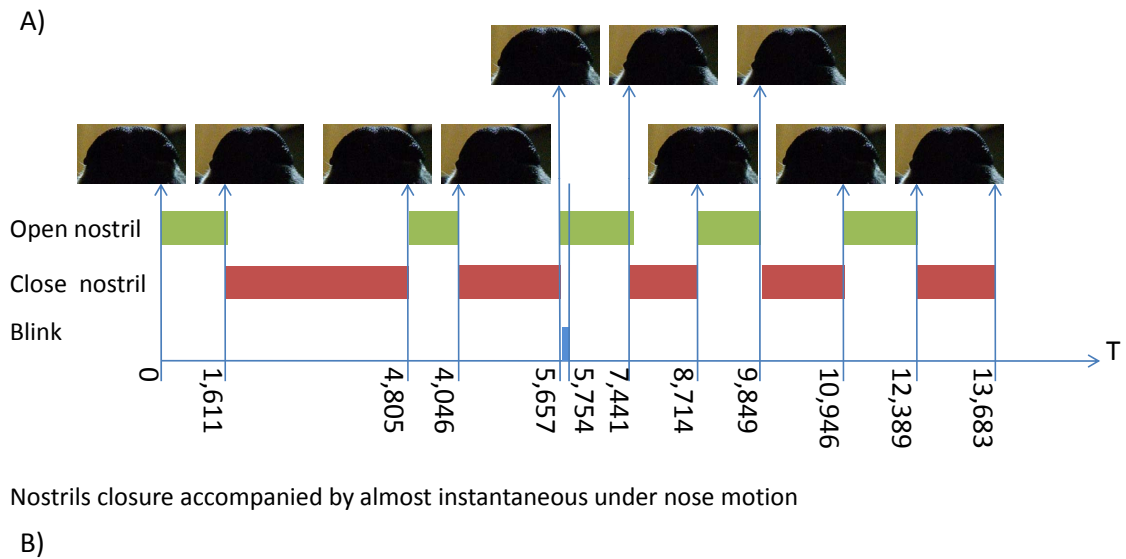


Figure D.1: Nostril movement. Appendix K, ONostril1.avi

Figure D.4 shows another way to reach anger. Here, the dog raises and lowers the lips consecutively. The intensity (not shown in chart) of lips rising becomes stronger as time goes, while the intensity of lips lowering seems to remain similar throughout. The mouth can be slightly opened and the tongue displayed for a short period of time. It can be seen that at the moment of most anger, the dog spent more time (3,217) keeping the lips raised. During that time slot the dog displayed the tongue. Eye blinking was independent from the rest of the actions.

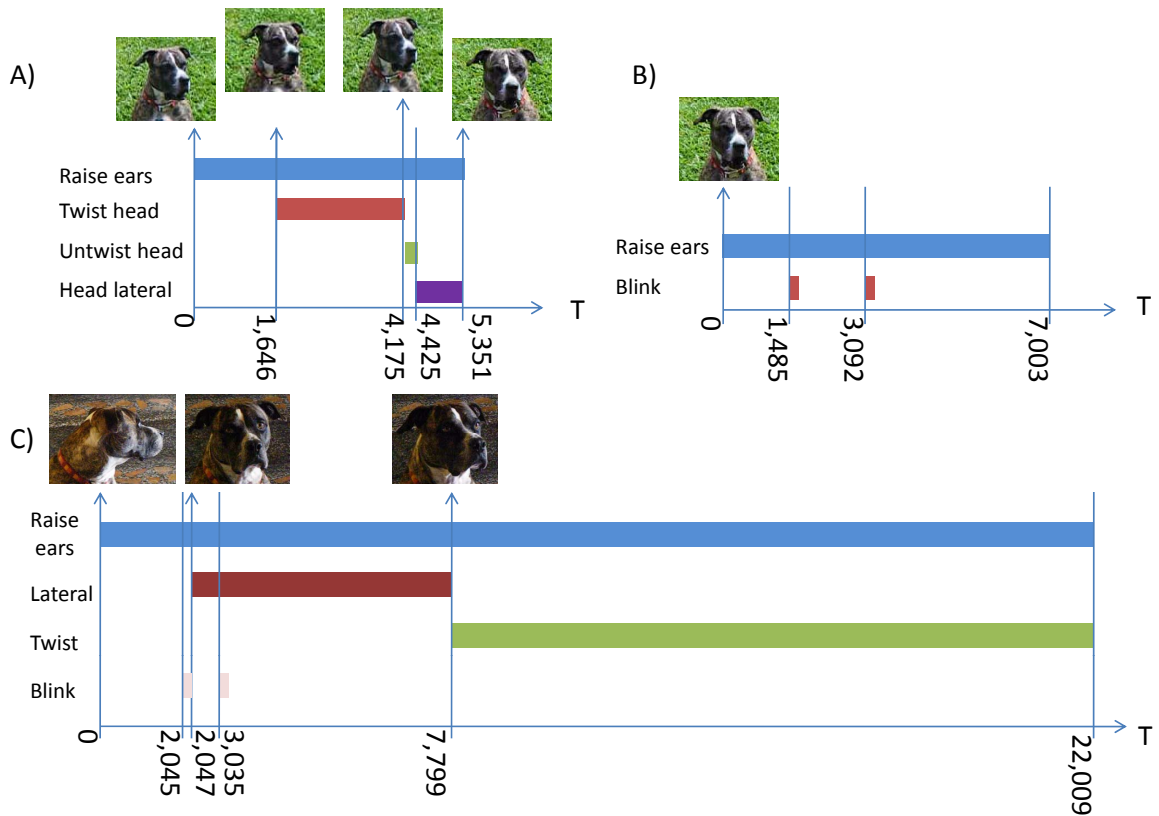


Figure D.2: Attention. A) Common attention (Appendix K, OAttention1a.avi). B) Attention with ears (Appendix K, OAttention1b.avi). C) Attention with previous lateral head motion (Appendix K, OAttention1c.avi)

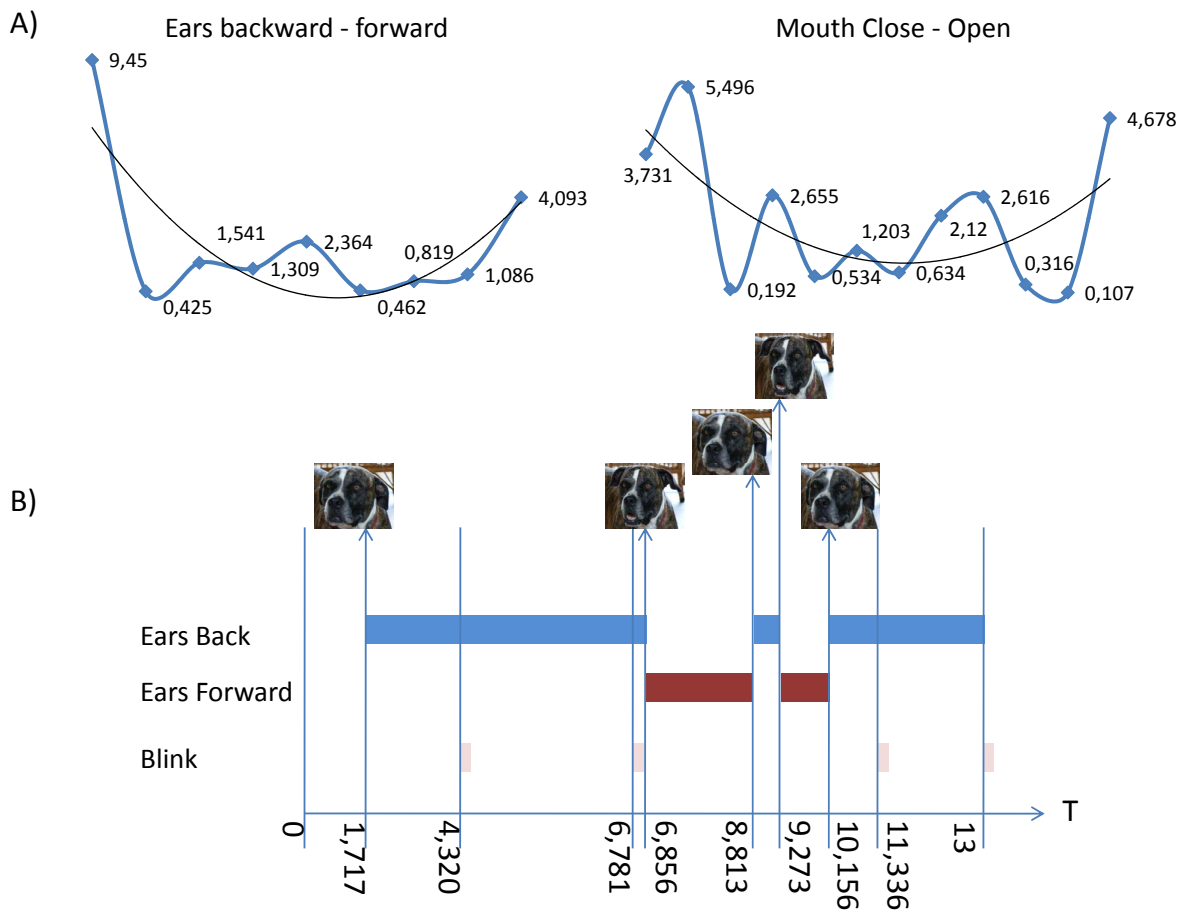


Figure D.3: Fear. A) forward - backward ear and open close mouth patterns (Appendix K, OFear.avi). B) Light fear (Appendix K, OFear1.avi)

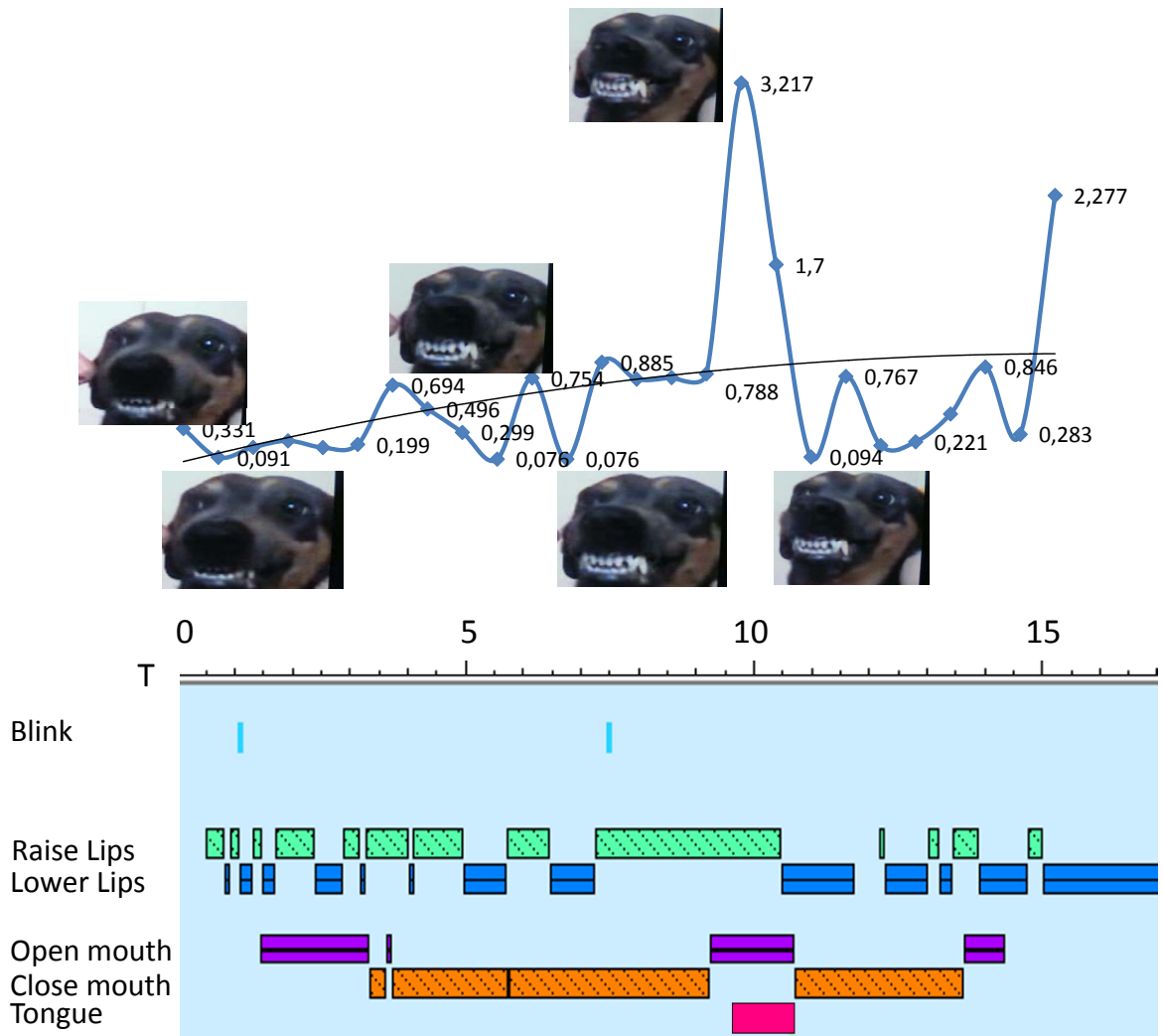


Figure D.4: Another form of anger. (Appendix K, OAnger1.avi)

Appendix E

Subdivision algorithms

E.1 Step1: finding new vertices

```
. For AllFaces
.   If FaceNotAtBoundary
.     If Face Subdividable
.       ComputeMidPoint and Split
.     Else
.       RecreateFace
.   Else
.     If FaceAtBoundary
.       If EvenLevel
.         If Subdividable
.           ComputeMidPoint and Split
.         Else
.           RecreateFace
.       Else
.         If Subdividable
.           CreateFacesAtBoundary
.         Else
.           RecreateFace
```

E.2 Step2: flipping edges

- . For AllFaces
 - . If FaceNotAtBoundary
 - . If Face Subdividable
 - . SwapFace
 - . Else
 - . RecreateFace
 - . Else
 - . If OddLevel
 - . If Subdividable
 - . SwapAtBoundary

E.3 Step 3: old vertices re positioning

- . For AllFaces
 - . If VertexNotAtBoundary
 - . CalculateNeighbourhod
 - . RePosition According to 6.2

E.4 Neighbourhood calculation

- . Find OutgoingHalfedge
- . AverageFirstVertex
- . Increment Neighbourhood size
- . Repeat
 - . Get OppositeHalfEdge
 - . Get NextHalfedgeInRing adding 1
 - . Add vertex to average
 - . Increment Neighbourhood size
- . Until RingComplete or Boundary or Distortion

Appendix F

Halfedge elements implementation

Table F.1 shows the number of bytes per element in our Direct Edges data structure implementation.

Table F.1: Halfedge elements implementation

Vertex (160 bits)	Float x, y, z Int Outgoing Int Boundary	3D position. Index of outgoing halfedge per vertex. Indicate if it is a boundary vertex.
Polygon (224 bits)	Int a, b, c, mate Int subdividable Int iBoundFace Int iNonSubFaces	Vertex indices and mate per face. 1 when subdividable. Boundary faces before this. Non subdividable face before this.
Halfedge (64 bits)	Int oppositeHalfedge Int toVertex	Index of opposite halfedge. Index of vertex the halfedge points to.

Appendix G

The 3DS file format

'The data structure for a complex object can't be written by hand. There are a lot of programs that help to create 3D meshes in a very quick way' (Vitulli (2005)). A 3DS file is formed by a series of blocks called chunks which contain all the information necessary to describe a scene; for example, the name of the object, the vertices coordinates and the list of polygons. Chunks are dependent on others creating a tree structure and their relative parents have to be read first; only the chunks required by the user or application have to be read. Table G.1 shows the typical fields on a chunk, (Vitulli (2005)).

The chunks used for getting the course mesh information (e.g. vertices, faces, mapping coordinates) are described in Table G.2, (Vitulli (2005)). The process of reading the 3DS file involves, (Vitulli (2005)):

- Loop until the end of the file.
- Analyse chunk content.

Table G.1: Fields of a 3DS chunk

Field	Offset (bytes)	Length (bytes)	Description
Identifier	0	2	Identifies chunk. Tells user if it is useful
Length	2	4	Chunk length and length of every sub-chunk
Data	6	n	Has variable length and contains scene data
Sub-chunks	6+n	m	

- If it is a not needed chunk, jump the whole length and reach the next branch of the chunk tree.
- If the chunk allows to reach another needed chunk; read the required data and read the next chunk.

Table G.2: Important 3DS chunks

Chunk	Identifier	Length	Father	Sub-chunks	Data
Main	0x4d4d	0 + sub-chunks	None	3D Editor	None
3D Editor	0x3D3D	0 + sub-chunks	Main	Object, Material, Keyframer	None
Object	0x4000	Name + sub-chunks	3D Editor	Triangular mesh, light, camera	Object name
Triangular mesh	0x4100	0 + sub-chunks	Object	Vertices list, Face descr., Mapping coord. list	None
Vertices list	0x4110	varying + sub-chunks	Triangular mesh	None	Vertices number (unsigned short) Vertices list: x1,y1,z1... (3 floats × vtx)
Face description	0x4120	varying + sub-chunks	Triangular mesh	Faces material	Polygons number (unsigned short) Polygons list: a1,b1,c1... (3 unsigned short × point) Face flag: face options, (unsigned short)
Mapping coord. list	0x4140	varying + sub-chunks	Triangular mesh	Smoothing group list	Vertices number (unsigned short) Mapping coord, list: u1,v1... (2 floats × vtx)

Appendix H

Applying subdivision surfaces to Londra's skull.

We applied $\sqrt{3}$ subdivision to three versions of a 3DS model of a virtual dog skull. The three versions were obtained simplifying the original mesh using 3D Studio Max.

Figure H.1, shows levels 0, 1 and 2 of subdivision for 3 versions of the control mesh in Londra. Here, the relationship of the number of elements can be described as:

- $A < B, C, D, E, F, G, H, I$;
- $B < C, D, E, F, G, H, I$;
- $C < E, F, G, H, I$;
- $D < \underline{C}, E, F, G, H, I$;
- $E < F, H, I$; $F < I$;
- $G < \underline{C}, \underline{E}, \underline{F}, H, I$;
- $H < \underline{E}, I$.

Here, $[A...I]$ represent the number of vertices and faces for each case. The underlined letters refer to a surface produced from a simpler control mesh. It is evident that the 2 level subdivided simplest control mesh (Figure H.1C) looks worse than the original one (Figure H.1G) and has more polygons. Even though our implementation of subdivision surfaces produces fewer elements than the one in 3D Studio max, $\sqrt{3}$ subdivision is only useful if a smaller or better control mesh is obtained.

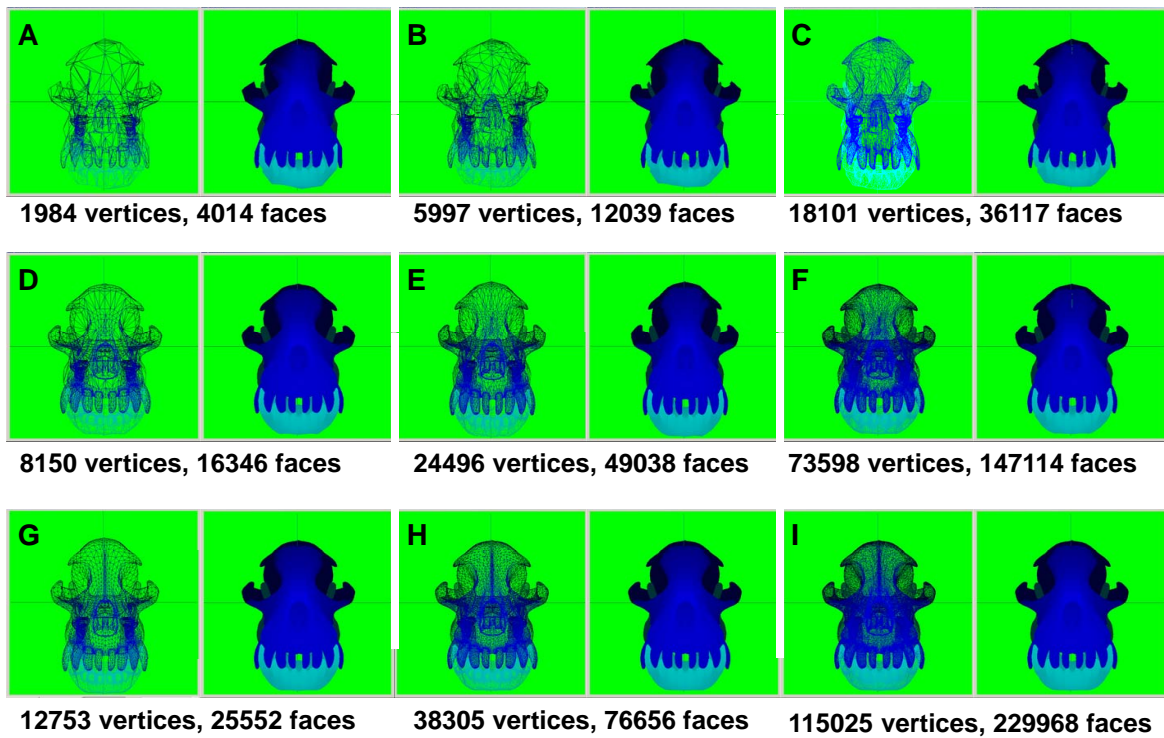


Figure H.1: Subdivision of the skull in Londra. A) B) C) Levels 0, 1, 2 of subdivision for the simplest control mesh. D) E) F) Levels 0, 1, 2 of subdivision for the intermediate control mesh. G) H) I) Levels 0, 1, 2 of subdivision for the original control mesh.

Appendix I

Barycentric coordinates

Barycentric coordinates are ratios of triangle areas representing an alternate coordinate system for the plane. They are triplets (b_0, b_1, b_2) corresponding to weights placed at the vertices of a reference triangle, (Hansford (2007); Weisstein (2008)). These weights determine the geometric centroid P which is identified by the triplet, (Figure I.1). The barycentric combination for an arbitrary point P_a lying on the plane of a triangle would take the form of (I.1); the combinations for the vertices are shown in Table I.1, (Hansford (2007)).

$$P_a = b_0A_0 + b_1A_1 + b_2A_2; \text{ with } b_0 + b_1 + b_2 = 1 \quad (\text{I.1})$$

To find barycentric coordinates of a 3D point $P_a(x, y, z)$ relative to a triangle $T(A_0, A_1, A_2)$ we, (Sunday (2006)):

First, find vectors u , v and w as in (I.2).

$$u = A_1 - A_0; \quad v = A_2 - A_0; \quad w = P_a - A_0 \quad (\text{I.2})$$

Second, we find the parametric coordinates (s, t) of P_a as the solution of (I.3). (Sunday (2006)) propose a solution for (I.3) which leads to a set of equations which are easily solved using dot product only (I.4). Their solution is based on Hill's per dot

Table I.1: Barycentric coordinates for the vertices in a triangle

Vertex	b_0	b_1	b_2
A_0	1	0	0
A_1	0	1	0
A_2	0	0	1

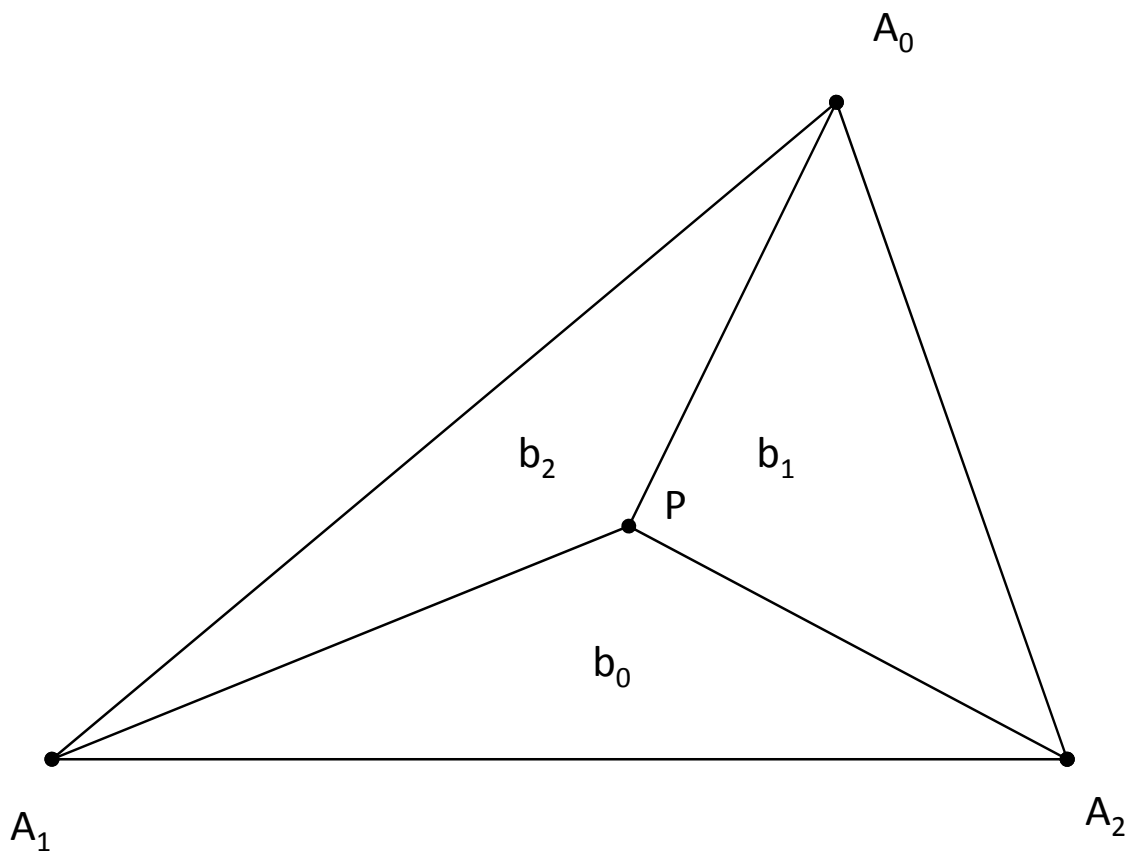


Figure I.1: Barycentric coordinates.

product, (Hill (1994)).

$$w = su + tv \tag{I.3}$$

$$\begin{aligned} d &= (uv)^2 - (uw)(vw) \\ s &= \frac{(uv)(vw) - (vw)(wu)}{d} \\ t &= \frac{uv(wu) - (uw)(vw)}{d} \end{aligned} \tag{I.4}$$

Third, we can obtain the barycentric coordinates of a point from its parametric ones (I.5).

$$b_0 = 1 - s - t; \quad b_1 = s; \quad b_2 = t \tag{I.5}$$

For points outside the plane of a triangle, it is possible to use the idea introduced by King (2001). Here, a point P_a is projected on the plane of the triangle as P'_a . Then, the barycentric coordinates for P'_a are obtained. Finally, a displacement D_a (distance from P_a to the plane of the triangle) is added to the barycentric coordinates as (I.6). D_a allows the definition of any point in R^3 in terms of a triangle.

$$P_a = \sum_{j=0}^2 b_j A_j + D_a; \quad \text{with } D_a = P_a - P'_a \tag{I.6}$$

Appendix J

Survey format

We approached the public with a brief explanation of the project and the following statement:

'Computer facial animation is an area of relevance to computer graphics. It has a wide range of applications such as movies and games. Here, we will show the 3D model of a dog head created to display dog facial expressions. During the presentation we will show 13 groups of videos to validate our system. For each group of videos you will be asked to tick the expression you think the dog is displaying. If expression seems mixed, tick up to three expressions per column. If expression is not clear (or is not named), leave the column empty. '

Then, we applied the questionnaire below (we introduced some noise in the answers by including Tiredness and Laziness):

Are you a dog person? (Y / N) (e.g. you have owned, been a friend to, have had contact with, or trained a dog for a reasonable period of time).

In the Table J.1 tick the expression you think the dog is displaying in each video group.

Table J.1: Dog expression survey

Video group	1	2	3	4	5	6	7	8	9	10	11	12	13
Anger													
Affection													
Attention													
Fear													
Happiness													
Smell													
Yawning													
Tiredness													
Laziness													

Appendix K

Videos

This is a companion DVD which contains all referred videos from chapters 3, 5, 7, 10, 13, 15 and 16. Also, it contains an electronic version of the document.

Please read the additional explanation in the Readme file.

Appendix L

Glossary

- Artificial pet: robotic or software toy intended to provide a companion to its owner and to behave like a pet.
- Auricularis (Dorsales, Rostrales): facial muscles. Move ears, (Figure 4.5B).
- AUs: acronym for Action Units. Constitutive components of facial coding systems.
- Brachycephalic: broad, short skulls.
- Cephalic index: a dog head proportion measure, (4.1).
- Characteristic point: feature point.
- Conformational parameters: lower level parameters which alter shape.
- Cornea: eye anatomy component, (Figure 4.7A).
- Craniofacial index: a dog head proportion measure, (4.2).
- DFACS: acronym for Dog Facial Action Coding System. Our anatomically inspired coding system for dog facial expression synthesis.
- Digastricus: facial muscles. Depress mandible, (Figure 4.5B).
- Direct Edges: data structure for triangular meshes, (Figure 6.1A).
- Dolichocephalic: long , narrow skull.
- EMFACS: acronym for emotional FACS: It is a selective subset of FACS and scoring the expression of simple human emotions only.

- Expressive parameters: higher level parameters which allow specifications and control of expression.
- Facial animation model: a computerised model capable to display typical facial expressions.
- FACS: acronym for Facial Action Coding System. A human facial expression measurement system.
- Feature point: point of anatomical interest within the model. Anatomical landmark.
- Frontalis: facial muscle. Fixes and pulls skin of upper head, (Figure 4.5B).
- Frontonasal suture: facial bones suture, (Figure 4.2).
- Gaze: sum of head and eye position.
- Half edge: oriented indexing component of the direct edges data structure, (Figure 6.1A).
- HFAMs: acronym for Human Facial Animation Models.
- Inisicive suture: facial bones suture, (Figure 4.2).
- Iris: eye anatomy component, (Figure 4.7A).
- Joints in the vertebrae: articulation of the head and the neck.
- Layered model: representation of an anatomical structure with several connected layers.
- Levators: facial muscles. Dilate nostril and raise upper lip, (Figure 4.5B).
- Levator oculis: facial muscles. Lifts medial portion of upper eyelid, (Figure 4.5B).
- Londra: our dog facial animation model, (unless named as real Londra which is the real dog).
- Masseters: facial muscles. Close jaw, (Figure 4.5B).
- Mentalis: facial muscles. Stiffens the lower lip, (Figure 4.5B).

- *MT*: our acronym for the maximum allowable expansion for the tongue tip, (Figure Fig:tongue1C).
- *MTM*: our acronym for the maximum allowable expansion for the tongue back, (Figure Fig:tongue1D).
- Nasal Notch: anatomical location for the dog nose, (Figure 4.2).
- Nuchal crest: head bones prominence, (Figure 4.2).
- Optic flow: technique to compute a flow field which minimises the difference between two frames.
- Orbicularis oculis: facial muscles. Sphincters of the eyelids, (Figure 4.5B).
- Orbicularis Oris: facial muscles. Sphincters muscle of the mouth, (Figure 4.5B).
- Sclera: eye anatomy component, (Figure 4.7A).
- Shell texturing: fur generation method which uses multiple layers of concentric textures and opacity maps.
- Skinning: skin generation around a skeleton.
- Subdivision surfaces: mesh smoothing and generation technique. An object can be modelled as a low resolution control mesh from which we can generate new meshes by refining the previous one.
- Superellipsoid: type of superquadric, (Figure 7.2A).
- Superquadrics: set of smooth parametric objects which can be altered with a few parameters.
- Supertoroid: type of superquadric, (Figure 7.2B).
- Temporalis: facial muscles. Close jaw, (Figure 4.5B).
- Temporomandibular articulation: articulation of the mandible and skull.
- TSSs: acronym for Tabulated Spheres Subsets. Tabulated selection of the colliding spheres from the spheres' approximation of two interacting meshes with constrained degrees of freedom. A TSS indicates which spheres from one mesh must be tested for collision with which spheres from another mesh

- Valence: number of vertices in the neighbourhood of a vertex.
- Zygomaticus (bone): facial bones, (Figure 4.2).
- Zygomaticus (muscle): facial muscles. Move mouth corner, (Figure 4.5B).